

2021 Annual Workshop Proceedings of the CORI WP in EURAD

M. Altmaier (Ed.)

INE SCIENTIFIC WORKING DOCUMENTS 07



This document provides scientific and technical reports related to the presentations given at the 2021 Annual Workshop of the EURAD WP on Cement-Organics-Radionuclide-Interactions (CORI)



Acknowledgement: This project has received funding from the European Union's Horizon 2020 research and innovation programme under grant agreement No 847593.

Institut für Nukleare Entsorgung (INE)

Hermann-von-Helmholtz-Platz 1
76344 Eggenstein-Leopoldshafen
www.ine.kit.edu

Impressum

Karlsruher Institut für Technologie (KIT)
www.kit.edu



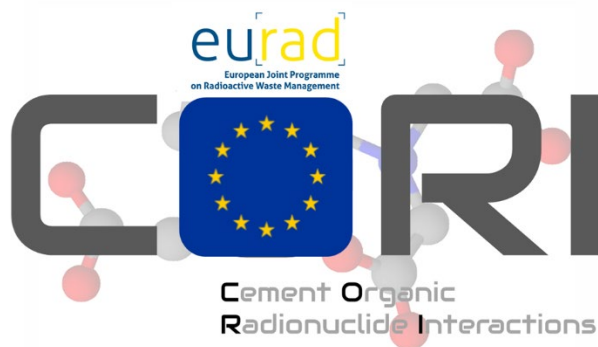
This document is licensed under the Creative Commons Attribution – Share Alike 4.0 International License (CC BY-SA 4.0): <https://creativecommons.org/licenses/by-sa/4.0/deed.en>

2024

URL: <http://www.ine.kit.edu/53.php>

ISSN: 2701-262X

DOI: 10.5445/IR/1000173343



This document provides scientific and technical reports related to the presentations given at the 2021 Annual Workshop of the EURAD WP on Cement-Organics-Radionuclide-Interactions (CORI)

The Annual CORI Workshop in 2021 was held during four days as a video meeting between Thursday 25.11.2021 and Monday 29.11.2021. During this CORI event, several groups involved in CORI provided presentations on the technical progress related to the work in the respective Tasks. The S&T contributions summarized in this documents capture the status of the studies in CORI at that time. They have been reviewed at the WP CORI level, including input from the End Users in CORI.

The CORI (Cement-Organic-Radionuclide-Interactions) Workpackage integrated into EURAD (EURAD – European Joint Programme on Radioactive Waste Management, <https://www.ejp-eurad.eu>) performs research to improve the knowledge on the organic release issues which can accelerate the radionuclide migration in the context of the post closure phase of geological repositories for ILW and LLW/VLLW including surface/shallow disposal. The R&D in CORI extends the current state-of-the-art and will contribute to optimize disposal solutions and consider questions of regulatory concern. CORI results will help member states to further develop their national R&D programs and support programs at an early implementation stage.

CORI research addresses topics in the context of cement-organics-radionuclides-interactions. Organic materials are present in some nuclear waste and as admixtures in cement-based materials and can potentially influence the performance of a geological disposal system, especially in the context of low and intermediate level waste disposal. The potential effect of organic molecules is related to the formation of complexes in solution with some radionuclides of interest (actinides and lanthanides) which can (i) increase radionuclide solubility and (ii) decrease radionuclide sorption. Organic substances require special attention since a significant quantity exists in the waste and in the cementitious materials, with a large degree of chemical diversity. Cement-based materials will be degraded with time, leading to specific alkaline pH conditions under which the organics can degrade, thus increasing their impact on repository performance.

The three R&D Tasks in CORI in which the contributions in this proceedings are integrated are:

- *Organic Degradation.* Focus is on the characterization of soluble organic species generated by radiolytic and hydrolytic degradation of selected organics (PVC, cellulose, resins, superplasticizers). Studies also include the analysis of degradation and stability of small organic molecules such as carboxylic acids and the determination of degradation rates.
- *Organic-Cement-Interactions.* Studies focus on investigating the mobility of selected organic molecules in cement-based materials. Mobility of organic molecules includes sorption and transport properties. Organics also include small ¹⁴C bearing molecules as identified in the EC EURATOM project CAST. Both retention on individual cement phases and cementitious systems are investigated.
- *Radionuclide-Organic-Cement-Interactions.* Radionuclide migration processes are studied in the ternary system. The role of organic molecules on the transfer properties of radionuclides are investigated through sorption and transport experiments. Selected radionuclides cover a range of chemical characteristics and redox states relevant for conditions in L/ILW disposal.

CORI has produced a state-of-the-art document, which gives additional technical background information on the topics investigated in the project. This may provide complementary information to the technical R&D studies summarized here. The SOTA document from CORI (Deliverable D3.1) is available for download via the EURAD homepage at:

<https://www.ejp-urad.eu/publications/eurad-d31-cori-sota-cement-organic-radionuclide-interactions-content-lilw-disposal>

Karlsruhe, 20th Dec 2023,

Marcus Altmaier

(WP CORI Leader on behalf of the CORI team)

Acknowledgement: This project has received funding from Euratom research and training programme 2014-2018 under grant agreement No [847593]

Table of content (listed in alphabetical order of first author)

A	<p>Effect of phthalates on the uptake of Am(III) and Eu(III) by cementitious materials</p> <p><i>N. Ait-Mouheb^{1*}, G. Deissmann¹, P. Henocq², N. Macé³, D. Bosbach¹</i></p> <p>¹ Institute of Energy and Climate Research (IEK-6): Nuclear Waste Management, Forschungszentrum Jülich GmbH, 52425 Jülich (Germany)</p> <p>² Research and Development Division, Andra, 1-7 Rue Jean Monnet, Parc de la Croix Blanche, 92298 Chatenay-Malabry Cedex (France)</p> <p>³ Université Paris-Saclay, CEA, Service d'Étude du Comportement des Radionucléides, 91191, Gif-sur-Yvette (France)</p>
B	<p>Role of the main aqueous cations on cellulose degradation under alkaline conditions and effects on Ni retention in cement.</p> <p><i>O. Almendros Ginestá, M. García-Gutiérrez, T. Missana</i></p> <p>CIEMAT – Physical Chemistry of Actinides and Fission Products Avenida Complutense 40, 28040 MADRID (Spain)</p>
C	<p>Interactions of Adipate, Phthalate, ISA and Uranium with Calcium Aluminum Silicate Hydrates</p> <p><i>J. Begg, M. López-García, D. García</i></p> <p>Amphos21, Carrer Vençuela, 103, Planta 2, 08019, Barcelona (Spain)</p>
D	<p>ISA production during hydrolytic degradation of irradiated cellulosic tissues and its sorption on degraded Ordinary Portland Cement: first set of results</p> <p><i>N. Bleyen, D. Durce, S. Smets, M. Van Gompel, V. Van Gompel, D. Verhaegen, W. Verwimp, K. Wouters, E. Valcke</i></p> <p>W&D Expert Group, SCK CEN, Boeretang 200, 2400 Mol, Belgium</p>
E	<p>Influence of gluconate on the retention of Eu(III), Th(IV), and U(VI) by C-S-H</p> <p><i>S. Dettmann¹, N. Huittinen², J. Kretzschmar², M.U. Kumke¹, T. Reich³, K. Schmeide², L. Spittler³, J. Stietz³</i></p> <p>¹ University of Potsdam, Institute of Chemistry, Karl-Liebknecht-Str. 24-25, 14476 Potsdam (Germany)</p> <p>² Helmholtz-Zentrum Dresden - Rossendorf, Institute of Resource Ecology, Bautzner Landstraße 400, 01328 Dresden (Germany)</p> <p>³ Johannes Gutenberg-Universität Mainz, Department of Chemistry, Fritz-Strassmann-Weg 2, 55128 Mainz (Germany)</p>
F	<p>Influence of selected organic substances on uptake of uranium and europium on cementitious materials – The Czech contribution</p> <p><i>B. Drtinová¹, J. Kittnerová¹, M. Burešová¹, L. Švamberová¹, A. Čejková¹, P. Večerník²</i></p> <p>¹ Czech Technical University in Prague, Faculty of Nuclear Sciences and Physical Engineering, Břehová 7, 115 19 Prague 1 (Czech Republic)</p> <p>² ÚJV Řež, a. s., Hlavní 130, 25068 Řež (Czech Republic)</p>

G	<p align="center">Sorption of Am(III) /Pu (III/IV) on hardened cement paste in the presence of organics</p> <p align="center"><i>R. Druteikienė, R. Gvozdaite, A. Gudelis</i></p> <p align="center">Center for Physical Sciences and Technology, Savanorių ave. 231, LT-02300 Vilnius, Lithuania</p>
H	<p align="center">Radiolytic Degradation of SUBATECH Homemade Ether PolyCarboxylate Superplasticizer</p> <p align="center"><i>V. Fiegel, G. Blain, C. Landesman, J. Vandenborre</i></p> <p align="center">SUBATECH, UMR 6457, Institut Mines-Télécom Atlantique, CNRS/IN2P3, Nantes Université, 4, Rue Alfred Kastler, La Chantrerie BP 20722, 44307 Nantes cedex 3, France</p>
I	<p align="center">Preliminary results on the interactions of organic compounds (ISA, EDTA and Polycarboxylate-based additive) on cement paste</p> <p align="center"><i>M. Grande M. Castellote</i></p> <p align="center">1 Institute of Construction Science Eduardo Torroja, IETcc-CSIC, Serrano Galvache 33, 28033, Madrid, Spain.</p>
J	<p align="center">Sorption study of selected organic ligands on C-S-H phases and their impact on the retention of plutonium</p> <p align="center"><i>R. E. Guidone^{1,2}, B. Lothenbach², A. Tasi¹, X. Gaona¹, M. Altmaier¹, H. Geckeis¹</i></p> <p>¹ KIT-INE, Karlsruhe Institute of Technology, Institute for Nuclear Waste Disposal, Hermann-von-Helmholtz-Platz 1, 76344 Eggenstein-Leopoldshafen, Germany ² Empa, Swiss Federal Laboratories for Materials Science and Technology, Laboratory for Concrete and Construction Chemistry, Überlandstrasse 129, 8600 Dübendorf, CH.</p>
K	<p align="center">Ni-63 uptake on CEM I hardened cement paste – preliminary experimental results</p> <p align="center"><i>C. Ichim, C. Bucur, M. Olteanu</i></p> <p align="center">Institute for Nuclear Research Pitesti, Romania (RATEN ICN)</p>
L	<p align="center">Chemical and physical characteristics of commercial cement superplasticizer based on polymelamine sulphonate</p> <p align="center"><i>A. Judžentienė, A. Zdaniauskienė</i></p> <p align="center">Center for Physical Sciences and Technology, Department of Organic Chemistry; Sauletekio Av. 3, LT-10257 Vilnius, Lithuania</p>
M	<p align="center">Effect of ISA on the uptake of U(VI) on CEM V HCP</p> <p align="center"><i>C. Landesman, N. Bessagnet, V. Baty, S. Ribet, K. David</i></p> <p align="center">SUBATECH, UMR 6457, Institut Mines-Télécom Atlantique, CNRS/IN2P3, Nantes Université, 4, Rue Alfred Kastler, La Chantrerie BP 20722, 44307 Nantes cedex 3, France</p>
N	<p align="center">Investigations on the Interaction of U(VI) with C-S-H in the Presence of EDTA</p> <p align="center"><i>E. Maragkou¹, I. Pashalidis^{1*}</i></p> <p>¹ Department of Chemistry, University of Cyprus, P.O. Box 20537, Cy-1678 Nicosia, (Cyprus)</p>

O	<p align="center">Analysis of superplasticizers adsorption on cement minerals.</p> <p align="center"><i>T. Missana, M. García-Gutiérrez, O. Almendros Ginestá</i></p> <p align="center">CIEMAT – Physical Chemistry of Actinides and Fission Products Avenida Complutense 40, 28040 MADRID (Spain)</p>
P	<p align="center">Radiolytic and hydrolytic degradation of PolyCarboxylate as superplasticizer</p> <p align="center"><i>M. Štrok^{1*}, T. Gajšt¹, E. Heath¹, D. Heath¹, S. Rupnik¹, V. Radulović¹, E. Žagar², D. Pahovnik²</i></p> <p align="center">¹ Jožef Stefan Institute, Jamova cesta 39, 1000 Ljubljana, Slovenia ² National Institute of Chemistry Slovenia, Hajdrihova ulica 19, 1000 Ljubljana, Slovenia</p>
Q	<p align="center">Impact of the degradation products of UP2 on the uptake of Ni(II), Ln(III) and Pu(III/IV): solubility and sorption studies</p> <p align="center"><i>P. Szabo, A. Tasi, X. Gaona, M. Altmaier, H. Geckeis</i></p> <p align="center">Karlsruhe Institute of Technology, Institute for Nuclear Waste Disposal, Karlsruhe (Germany)</p>
R	<p align="center">The stability of α-isosaccharinate under highly alkaline, reducing conditions</p> <p align="center"><i>J. Tits, D. Kunz, T. Guillemot⁺, E. Wieland</i></p> <p align="center">Laboratory for Waste Management, Paul Scherrer Institut, Villigen-PSI, (Switzerland) + present: National Cooperative for the Disposal of Radioactive Waste (Nagra), Wettingen, CH</p>
S	<p align="center">The effect of gamma irradiation on cementitious materials with superplasticizers – The Czech contribution</p> <p align="center"><i>R. Vašíček¹, Z. Hlaváč², P. Večerník³, B. Drtinová⁴, M. Vlk⁴, M. Kučerová¹</i></p> <p align="center">¹ Czech Technical University in Prague, Faculty of Civil Engineering, Thákurova 7, 166 29 Prague 6 (Czech Republic) ² Research Centre Řež, s.r.o.; Hlavní 130, Řež, 250 68 Husinec (Czech Republic) ³ ÚJV Řež, a. s., Hlavní 130, Řež, 25068 Husinec (Czech Republic) ⁴ Czech Technical University in Prague, Faculty of Nuclear Sciences and Physical Engineering, Břehová 7, 115 19 Prague 1 (Czech Republic)</p>
T	<p align="center">An effect of radiolysis and hydrolysis on superplasticizers and organic sorbents – The Czech contribution</p> <p align="center"><i>P. Večerník¹, J. Kozempel², M. Vlk², Z. Hlaváč³, M. Hybášková¹, B. Drtinová²</i></p> <p align="center">¹ÚJV Řež, a. s.; Hlavní 130, Řež, 25068 Husinec (Czech Republic) ²Czech Technical University in Prague, Faculty of Nuclear Sciences and Physical Engineering; Břehová 7, 115 19 Prague 1 (Czech Republic) ³Research Centre Řež, s.r.o.; Hlavní 130, Řež, 250 68 Husinec (Czech Republic)</p>

Effect of phthalates on the uptake of Am(III) and Eu(III) by cementitious materials

N. Ait-Mouheb^{1*}, G. Deissmann¹, P. Henocq², N. Macé³, D. Bosbach¹

¹ Institute of Energy and Climate Research (IEK-6): Nuclear Waste Management, Forschungszentrum Jülich GmbH, 52425 Jülich (Germany)

² Research and Development Division, Andra, 1-7 Rue Jean Monnet, Parc de la Croix Blanche, 92298 Chatenay-Malabry Cedex (France)

³ Université Paris-Saclay, CEA, Service d'Etude du Comportement des Radionucléides, 91191, Gif-sur-Yvette (France)

* Corresponding authors: n.ait.mouheb@fz-juelich.de

Abstract

In this study the role and significance of phthalates as organic degradation products of waste constituents or cement additives on the migration behaviour of ²⁴¹Am and ¹⁵²Eu in a cementitious repository environment were investigated. The sorption of ²⁴¹Am and ¹⁵²Eu at tracer concentration on hardened cement pastes (HCP) prepared from a CEM V/A 42.5N was studied in batch experiments under anoxic conditions in the presence and absence of phthalate. Preparatory solubility tests showed that phthalic acid concentrations up to 1 mM have no impact on the dissolved and colloidal fractions of ²⁴¹Am and ¹⁵²Eu in cementitious waters. In the absence of organics, a strong uptake of ²⁴¹Am and ¹⁵²Eu on the CEM V/A HCP was observed with distribution ratios, R_d , in the order of 10^5 to 10^6 L kg⁻¹. The uptake of ²⁴¹Am and ¹⁵²Eu uptake was found to be dependent on the aqueous phthalic acid concentration, leading to a decrease of the R_d values of several orders of magnitude at phthalic acid concentrations of 100 mM. The reduction of the ²⁴¹Am and ¹⁵²Eu uptake in the presence of phthalic acid is attributed to the destabilisation/dissolution of C-S-H/C-A-S-H due to increasing Ca-complexation by phthalate in solution.

1 Introduction

The safety concept for deep geological disposal of nuclear waste is based on the confinement of the radioactive material over a long period of time by the combination of natural and engineered barriers (multibarrier system). The geological barrier is provided by the surrounding host rock and its inherent isolating properties. The engineered barrier system isolates or retards radionuclide migration towards the geological barrier and further stabilizes the repository system. Many disposal concepts for radioactive wastes developed internationally make extensive use of cementitious materials for example for solidification and stabilisation of low and intermediate level wastes, or as construction materials and backfill in near surface and deep geological disposal facilities (e.g., ANDRA, 2005; Drace and Ojovan, 2013; ENRESA, 1995; Jantzen *et al.*, 2010). This is due to the general radionuclide fixation and immobilisation properties of cementitious materials and their low permeability and diffusivity. However, the impact of organic degradation products, derived either from waste constituents or from

cement additives, on radionuclide solubility and sorption in cementitious environments is not completely understood. In alkaline media, short-chained organic compounds such as phthalate ions ($C_8H_4O_4^{2-}$) have been confirmed as possible degradation products of superplasticizers used as additives to enhance the workability of concrete or as degradation products from PVC plasticizers such as diisononyl phthalate (DINP) or diisodecyl phthalate (DIDP) (*cf.*, Garcia *et al.*, 2018; Colombani *et al.*, 2009; Smith *et al.*, 2013). Here, we investigate the potential effect of phthalates on the solubility and sorption of trivalent actinides and lanthanides in cementitious environments. First, preliminary solubility tests were performed to assess i) the effects of the phthalate on the solubility of ^{241}Am and ^{152}Eu , ii) the sorption of ^{241}Am and ^{152}Eu to the walls of the centrifuge tubes used in sorption experiments, and (iii) the potential binding of ^{241}Am and ^{152}Eu to colloids, which can be generated in cementitious waters. Moreover, batch sorption experiments were performed to quantify the ^{241}Am and ^{152}Eu uptake in cementitious materials and assess the effects of phthalates on their sorption behaviour.

2 Materials and methods

2.1 Preparation of HCP

The hardened cement paste (HCP) was manufactured by the Commissariat à l'énergie atomique et aux énergies alternatives (CEA) in February 2016 from a CEM V/A cement (CEM V/A (S-V) 42.5N CE PM-ES-CP1 NF, Calcia, Rombas) with a cement/water ratio of 0.40 as described by Macé *et al.* (2019). The CEM V/A is a ternary blended cement consisting of 54% Ordinary Portland cement, 23% blast furnace slag (BFS), and 23% fly ash (FA), and is expected to be used in the French nuclear waste disposal program (*cf.* Bildstein and Claret, 2015; Claret *et al.*, 2018). The HCP cylinders (diameter = 5 cm and height = 5 cm) were stored at room temperature in a glove box under controlled atmosphere (Ar) to avoid carbonation. The HCP was mechanically crushed for use in batch sorption experiments.

CEM V/A water was prepared by immersing crushed HCP in Milli-Q® water (Millipore, 18.2 $M\Omega\ cm^{-1}$ at 25 °C and total organic carbon TOC content = 2 ppb) at a solid-to-liquid ratio of 12 g L^{-1} (Pointeau *et al.*, 2004a). The degradation state III free of portlandite was obtained with a resulting pH of 12.2, which is regulated by the dissolution of C-S-H phases. Table 1 shows the chemical composition of the equilibrated solution used in the preliminary solubility tests and the batch sorption experiments.

Table 1: Chemical composition (in mol L^{-1}) and pH of the solution equilibrated with HCP CEM V/A used in the preliminary solubility tests and the batch sorption experiments.

CEM V/A water	Na	K	Si	Ca	pH
	$5.04\ 10^{-4}$	$1.22\ 10^{-3}$	$9.24\ 10^{-5}$	$6.46\ 10^{-3}$	12.2

2.1 Solubility tests

The solubility tests were carried out in a glove box under a controlled Ar atmosphere (O_2 and CO_2 concentrations < 5 ppm) following the experimental procedure of Tits and Wieland (2018). The batch solubility tests were carried out in 40 mL polypropylene centrifuge tubes, which were thoroughly washed and left overnight in a solution of 0.1 M HCl, then rinsed with Milli-Q® water. For the solubility

tests three different concentrations of ²⁴¹Am and ¹⁵²Eu (between ~10⁻⁸ M and ~10⁻¹⁰ M; stock solutions of the radionuclides were obtained from Eckert & Ziegler Nuclitec GmbH) were employed in CEM V/A water in the presence and absence of phthalic acid. Phthalic acid (99.5%, Sigma-Aldrich) stock solutions of 0.1 M were prepared and diluted to obtain the required initial concentrations in the experiments. The concentration of phthalic acid in the solubility tests ranged between 10⁻³ and 10⁻⁵ M. After selected times, aliquots were withdrawn from the solutions before and after centrifugation (6,000 rpm, 1 hour) and analysed for ²⁴¹Am and ¹⁵²Eu with liquid scintillation counting (TriCarb 3100 TR, Perkin Elmer, Freiburg, Germany) using Ultima Gold (Perkin Elmer) as scintillation cocktail.

2.2 Batch sorption experiments

Batch sorption studies with ²⁴¹Am and ¹⁵²Eu on CEM V/A HCP were carried out in a glove box under Ar atmosphere (O₂ and CO₂ levels < 5 ppm) at different concentrations of phthalic acid (concentration range 10⁻¹ M to 10⁵ M) and in absence of phthalic acid; initial ²⁴¹Am and ¹⁵²Eu concentrations in the experiments were 10⁻⁸ to 10⁻¹⁰ M and 3.0·10⁻⁸ to 5.0·10⁻¹¹ M, respectively. The centrifuge tubes (polypropylene) were thoroughly washed and left overnight in a solution of 0.1 M HCl before rinsing with Milli-Q® water. The experiments were performed with a fixed solid/liquid ratio of 5·10⁻⁴ kg L⁻¹. Before adding the radionuclides, the suspensions which consisted of the powdered HCP, CEM V/A water, and phthalic acid, were equilibrated for at least 5 months and the pH was adjusted to reach 12.2 after phthalic acid addition. Aliquots from the ²⁴¹Am and ¹⁵²Eu labelled solutions were added to each of the polypropylene centrifuge tubes which remained static for 7 days; based on literature data, this time is sufficient to reach steady state conditions in the system, due to the fast uptake kinetics of An(III)/Ln(III) on cementitious materials (*cf.* Tits and Wieland, 2018). After one week equilibration time, the suspensions were centrifuged (6,000 rpm, 1 hour). The activities of the tracers in the supernatant solution were determined by liquid scintillation counting as described above. The results of the sorption tests were expressed in form of the distribution ratio R_d [L kg⁻¹] (Equation 1). The results generated in the solubility tests are used in the calculations of the distribution ratios R_d , by considering the wall sorption effects and the formation of ²⁴¹Am and ¹⁵²Eu colloids as described in Tits and Wieland (2018), *i.e.*,

$$R_d = \frac{A_s}{A_l} = \left(\frac{A_{input} - A_{wall} - A_l}{A_l} \right) \cdot \left(\frac{V}{m} \right) = \left(\frac{A_{susp} - A_l}{A_l} \right) \cdot \left(\frac{V}{m} \right) \quad \text{Equation 1}$$

where

A_s [Bq kg⁻¹] is tracer activity on the solid phase,

A_l [Bq L⁻¹] is the tracer activity in solution at the end of the experiment,

A_{input} [Bq L⁻¹] is the initial tracer activity in solution,

A_{wall} [Bq L⁻¹] is the tracer activity sorbed on the wall of the centrifuge tubes,

A_{susp} [Bq L⁻¹] is the tracer activity determined in suspension,

V [L] is the volume of the liquid phase, and

m [kg] is the mass of solid phase used in the experiment.

2.3 Thermodynamic modelling

To aid interpreting the batch sorption experiments in presence of phthalate, the aqueous speciation of the components in solution and saturation indices of relevant phases were calculated using the geochemical code PhreeqC Ver. 3.5.0 (Parkhurst and Appelo, 2013) and GeoChemist's Workbench (GWB) Ver. 11.0.8 (Bethke, 2008). The ThermoChimie v.10d thermodynamic database (Consortium Andra – Ondraf/Niras – RWM; Giffaut *et al.*, 2014; Grivé *et al.*, 2015) was used for the thermodynamic modelling. The activities of aqueous species were calculated using the specific ion interaction (SIT) approach (PhreeqC; *cf.* Brønsted, 1922; Guggenheim, 1935; Scatchard, 1936) or the B-dot equation (GWB; *cf.* Bethke, 2008).

3 Results and discussion

As illustrative examples of the solubility tests, the ²⁴¹Am and ¹⁵²Eu concentrations in the CEM V/A water are shown in Figure 1 as a function of the phthalic acid concentration for different initial radionuclide concentrations. Already a first decrease of ²⁴¹Am and ¹⁵²Eu concentrations in comparison with the input concentrations can be observed before the centrifugation. This decrease of the concentrations of ²⁴¹Am and ¹⁵²Eu is due to the sorption on the walls of the centrifuge tubes. After centrifugation, a further decrease in the activity of ²⁴¹Am and ¹⁵²Eu is observed, which can be explained by the presence of ²⁴¹Am and ¹⁵²Eu colloids generated in CEM V/A water and settled during centrifugation. The presence of phthalate at different concentrations shows no influence on the input and output concentrations of ²⁴¹Am and ¹⁵²Eu in CEM V/A water, *i.e.*, do not influence the solubility of the radionuclides and their sorption to the centrifugation tubes and colloids, respectively. Though phthalates are strong complexing ligands at near neutral conditions, under cementitious conditions their impact on the speciation and solubility of ²⁴¹Am and ¹⁵²Eu is negligible (Figure 2). Assuming amorphous Am(OH)₃ and Eu(OH)₃ as solubility limiting phases, the calculated concentrations under the experimental conditions (*cf.* Table 1) remain unaffected by addition of phthalate up to concentrations of 0.1 mol kg⁻¹, with Am and Eu concentrations of 5.5·10⁻¹⁰ and 2.6·10⁻⁹ M, respectively. The contributions of the aqueous Am- and Eu-phthalate complexes to the total radionuclide concentrations were less than 10⁻⁴ % even at the highest phthalate addition. Based on the PhreeqC calculations, major radionuclide and organic species in solution are Eu(OH)₃(aq) or Am(OH)₃(aq), respectively, as well as phthalate (C₈H₄O₄²⁻) and Ca-phthalate ((Ca(C₈H₄O₄)⁰)).

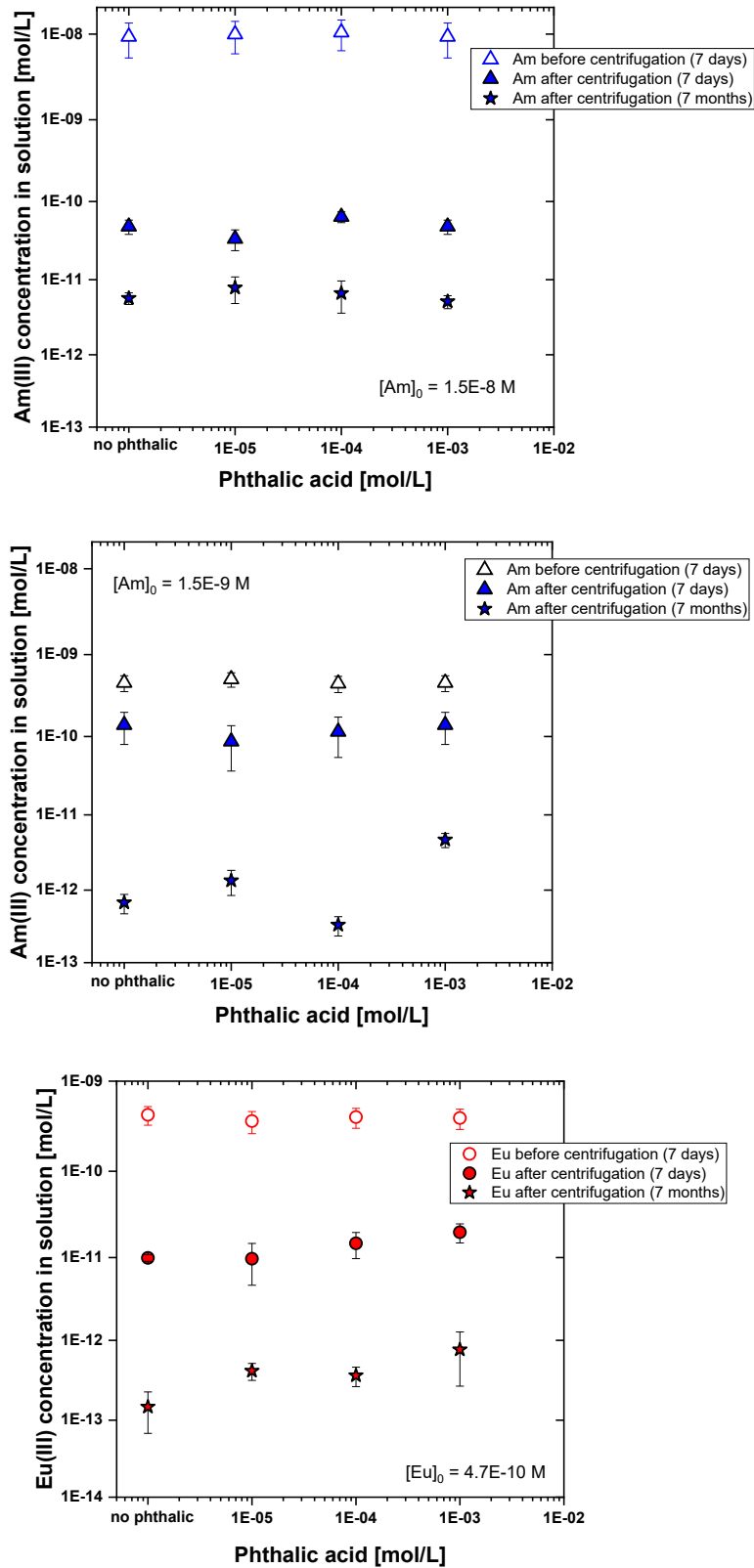


Figure 1: ^{241}Am and ^{152}Eu concentration in HCP CEM V/A equilibrated water as a function of the phthalic acid concentrations after 7 days and 7 months equilibration, at different initial concentration of ^{241}Am and ^{152}Eu . Background electrolyte is the CEM V/A water at equilibrium with the HCP at degradation state III.

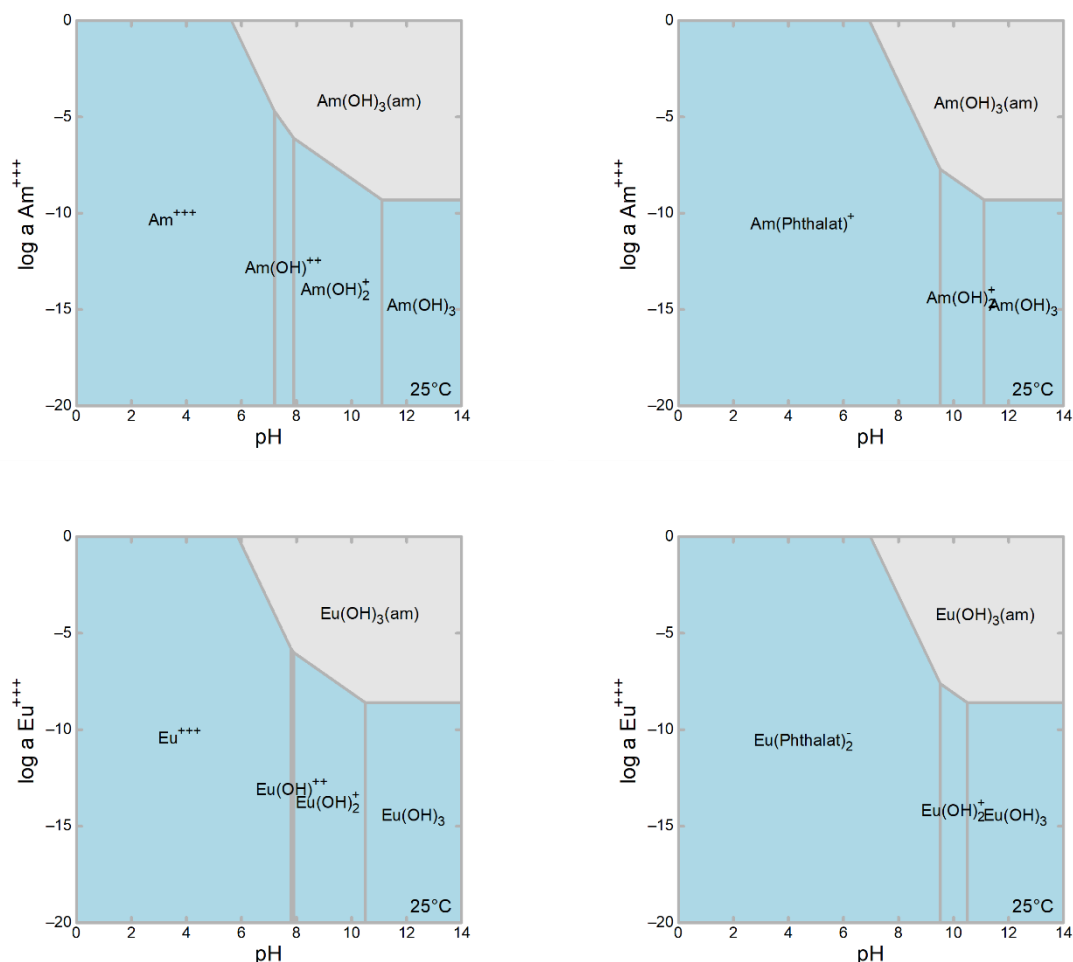


Figure 2: Solubility of Am (top) and Eu (bottom) in the absence (left) and presence (right) of 10 mmol kg⁻¹ phthalate in a solution containing 5·10⁻³ mol kg⁻¹ Ca as function of pH (Thermodynamic database: ThermoChimie V10d).

The results of ²⁴¹Am and ¹⁵²Eu batch sorption experiments with CEM V/A HCP are shown in Figure 3. In the absence of phthalate, R_d values of ²⁴¹Am and ¹⁵²Eu are in the range $10^5 \text{ L kg}^{-1} < R_d < 10^6 \text{ L kg}^{-1}$. These values are in good agreement with the results obtained in the literature (cf. Tits and Wieland, 2018; Pointeau *et al.*, 2004b; Pointeau *et al.*, 2001; Ochs *et al.*, 2016), considering that in absence of organics, the mentioned authors did not observe a distinct effect of the degradation state on An(III)/Ln(III) sorption. The uptake of ²⁴¹Am and ¹⁵²Eu is associated with their incorporation into the C-S-H structure, substituting for Ca²⁺ in the C-S-H interlayer and in the Ca-octahedral layer (cf. Tits *et al.*, 2003; Tits and Wieland, 2018). In the investigated systems, ²⁴¹Am and ¹⁵²Eu uptake by HCP CEM V/A was found to be strongly dependent on the aqueous phthalate concentration. The results in Figure 3 show a plateau of the uptake at low phthalate concentrations ($< 10^3 \text{ M}$), where the R_d values are similar to those in absence of phthalate, followed by a distinct decrease in the R_d values above a so-called “concentration edge” (Tits *et al.*, 2005). Above the “concentration edge” the R_d values of ²⁴¹Am and ¹⁵²Eu decrease by several orders of magnitude to values of about $10^3 \text{ L kg}^{-1} < R_d < 10^4 \text{ L kg}^{-1}$. Due to the negligible presence of phthalate complexes of ²⁴¹Am and ¹⁵²Eu under cementitious conditions, this “concentration edge” cannot be explained by complexation with the organic compound but rather suggests an effect of the phthalate addition on the cementitious material used in the sorption experiments.

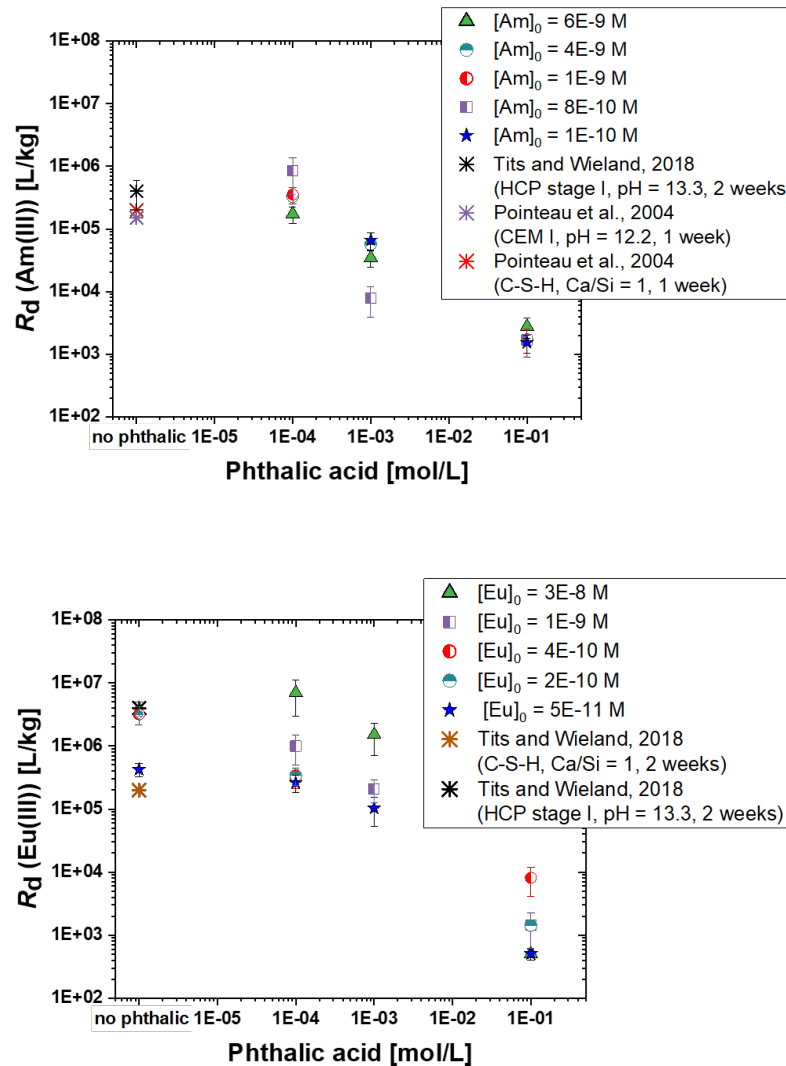


Figure 3: Effect of phthalate on ^{241}Am and ^{152}Eu uptake by CEM V/A HCP (solid/liquid ratio = $5 \cdot 10^{-4} \text{ kg L}^{-1}$, $\text{pH} = 12.2$, 1 week of equilibration, $c_0(^{241}\text{Am}) = 10^{-8} - 10^{-10} \text{ M}$, and $c_0(^{152}\text{Eu}) = 3.0 \cdot 10^{-8} - 5.0 \cdot 10^{-11} \text{ M}$).

In Figure 4, the calculated aqueous speciation of Ca in the solution equilibrated with HCP CEM V/A is shown as function of the phthalate concentration. At phthalate additions above approximately $10^{-3} \text{ mol kg}^{-1}$ the contribution of the aqueous Ca-phthalate complex ($\text{Ca}(\text{C}_8\text{H}_4\text{O}_4)^0$) to the total Ca concentration increases sharply, becoming the dominant Ca-complex at phthalate concentrations above about $10^{-2} \text{ mol kg}^{-1}$. The increasing organic complexation of Ca in solution causes the dissolution/destabilisation of Ca-bearing phases in the cementitious material, leading in particular to a decalcification of C-S-H/C-A-S-H phases, which are the main sorbing phases for $\text{An(III)}/\text{Ln(III)}$ in cementitious materials. The destabilisation of C-S-H is indicated by the calculated saturation indices. As expected in the absence of the organic complexant and at low phthalate concentrations ($\leq 10^{-3} \text{ mol kg}^{-1}$), the solution equilibrated with CEM V/A is practically in equilibrium with C-S-H with low Ca/Si ratio (CSH0.8 ; saturation index $\text{SI} \approx 0$). With increasing phthalate addition, the SI for CSH0.8 decreases to about -0.8 (at $10^{-1} \text{ mol kg}^{-1}$ phthalate), indicating the increasing destabilisation of this phase.

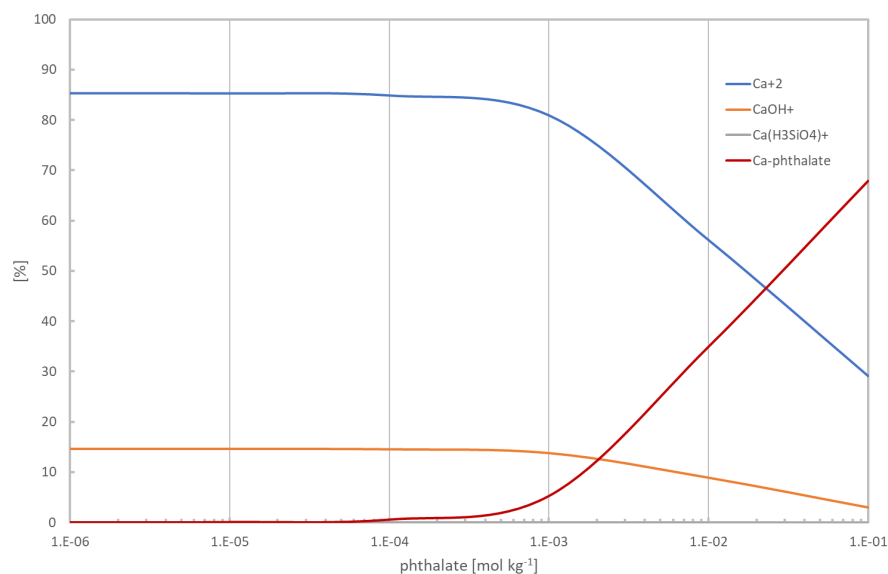


Figure 4: Calculated Ca-speciation in the solution equilibrated with HCP CEM V/A as function of the phthalate concentration ($[Ca]_{tot} = 6.5 \text{ mM}$ and $pH = 12.2$).

5 Concluding perspective

In this study, the impact of phthalates, which might be present in a cementitious repository as degradation products of superplasticizers or PVC additives, on the migration behaviour of trivalent actinides and lanthanides was investigated. Batch sorption experiments on HCP CEM V/A, intended for use in the French repository program, confirmed the strong uptake of *An(III)/Ln(III)* on cementitious materials. The results indicate that above a no-effect level of about 1 mM, the presence of phthalate ions will lead to a strong sorption reduction of trivalent actinides and lanthanides in a cementitious repository, increasing their mobility within the engineered barrier system. However, this sorption reduction is not caused by the complexation of the radionuclides by the organic ligand but is rather due to the decalcification of C-S-H/C-A-S-H as sorbing phases as consequence of the increasing formation of Ca-phthalate complexes. The role and significance of phthalates on the migration behaviour of ²⁴¹Am and ¹⁵²Eu in a cementitious repository will be further explored in diffusion experiments using CEM V/A monoliths as well as in bottom-up studies using C-S-H/C-A-S-H phases synthesised according to the method of L'Hôpital *et al.* (2015).

Acknowledgement

The EURAD-CORI project leading to this application has received funding from the European Union's Horizon 2020 research and innovation programme under grant agreement No 847593.

References

- ANDRA, 2005. Andra Research on the Geological Disposal of High level Long-Lived Radioactive Waste—Results and Perspectives, France.
- Bethke. C.M., 2008. Geochemical and biogeochemical reaction modelling, 2nd edition. Cambridge University Press.

- Bildstein, O., Claret, F., 2015. Stability of clay barriers under chemical perturbations Chapter 5 in: Tournassat, C., Steefel, C.I., Bourg, I.C., Bergaya, F. (eds.) Natural and engineered clay barriers. Developments in Clay Science, 6, Elsevier, Amsterdam.
- Brønsted, J.N., 1922. Studies of solubility: IV. The principle of specific interaction of ions. *J. Am. Chem. Soc.* 44, 877–898.
- Claret, F., Grangeon, S., Loschetter, A., Tournassat, C., De Nolf, W., Harker, N., Boulahya, F., Gaboreau, S., Linard, Y., Bourbon, X., Fernandez-Martinez, A., Wright, J., 2018. Deciphering mineralogical changes and carbonation development during hydration and ageing of a consolidated ternary blended cement paste. *IUCrJ* 5, 150–157.
- Colombani, J., Herbette, G., Rossi, C., Jousot-Dubien, C., Labed, V., Gilardi, T., 2009. Leaching of plasticized PVC: Effect of irradiation. *J. Appl. Polym. Sci.* 112, 1372–1377.
- Drace, Z., Ojovan, M.I., 2013. A summary of IAEA coordinated research project on cementitious materials for radioactive waste management. In: Bart, F., Cau-dit-Coumes, C., Frizon, F., Lorente, S. (eds.), *Cement-based Materials for Nuclear Waste Storage*. Springer, pp. 3–11.
- ENRESA., 1995. Almacenamiento Geológico Profundo de Residuos Radiactivos de Alta Actividad (AGP). Diseños Conceptuales Genéricos. Publicación Técnica ENRESA, 11/95.
- García, D., Grivé, M., Duro, L., Brassinnes, S., de Pablo, J., 2018. The potential role of the degradation products of cement superplasticizers on the mobility of radionuclides. *Appl. Geochem.* 98, 1–9.
- Giffaut, E., Grivé, M., Blanc, Ph., Vieillard, Ph., Colàs, E., Gailhanou, H., Gaboreau, S., Marty, N., Madé, B., Duro, L., 2014. Andra thermodynamic database for performance assessment: *ThermoChimie. Appl. Geochem.* 49, 225–236.
- Grivé, M., Duro, L., Colàs, E., Giffaut, E., 2015. Thermodynamic data selection applied to radionuclides and chemotoxic elements: An overview of the *ThermoChimie-TDB. Appl. Geochem.* 55, 85–94.
- Guggenheim, E.A., 1935. The specific thermodynamic properties of aqueous solutions of strong electrolytes. *Philos. Mag. A* 19, 588–643.
- Jantzen, C., Johnson, A., Read, D., Stegemann, J., 2010. Cements in waste management. *Adv. Cement Res.* 22, 225–231.
- L'Hôpital, E., Lothenbach, B., Le Saout, G., Kulik, D., Scrivener, K., 2015. Incorporation of aluminium in calcium-silicate-hydrates. *Cem. Concr. Res.* 75, 91–103.
- Macé, N., Fichet, P., Savoye, S., Radwan, J., Lim, C., Lefèvre, S., Page, J., Henocq, P., 2019. Use of quantitative digital autoradiography technique to investigate the chlorine-36-labelled radiotracer transport in concrete. *Appl. Geochem.* 100, 326–334.
- Ochs, M., Mallants, D., Wang, L., 2016. *Radionuclide and metal sorption on cement and concrete*, Springer.
- Parkhurst, D.L., Appelo, C.A.J., 2013. Description of input and examples for PHREEQC Version 3 - A computer program for speciation, batch-reaction, one-dimensional transport, and inverse geochemical calculations. U.S. Geological Survey Techniques and Methods, book 6, chapter A43.
- Poiteau, I., Piriou, B., Fedoroff, M., Barthes, M.-G., Marmier, N., Fromage, F., 2001. Sorption mechanisms of Eu^{3+} on CSH phases of hydrated cements. *J. Colloid Interface Sci.* 236, 252–259.
- Poiteau, I., Landesman, C., Giffaut, E., Reiller, P.E., 2004a. Reproducibility of the uptake of U(VI) onto degraded cement pastes and calcium silicate hydrate phases. *Radiochim. Acta* 92, 645–650.
- Poiteau, I., Landesman, C., Coreau, N., Moisan, C., Reiller, P., 2004b. Etude de la rétention chimique des radionucléides Cs(I), Am(III), Zr(IV), Pu(IV), Nb(V), U(VI) et Tc(IV) par les matériaux cimentaires dégradés, CEA report 2004, RT DPC/SECR 03-037 indice A.
- Scatchard, G., 1936. Concentrated solutions of strong electrolytes. *Chem. Rev.* 19, 309–327. Smith, V., Magalhaes, S., Schneider, S., 2013. The role of PVC additives in the potential formation of NAPLs, Report AMEC/PPE/2834/001, AMEC, Didcot, UK.
- Tits, J., Wieland, E., 2018. Actinide sorption by cementitious materials, PSI Report 18–02. Paul Scherrer Institut, Villigen, Switzerland.
- Tits, J., Stumpf, T., Rabung, T., Wieland, E., Fanghänel, T., 2003. Uptake of Cm(III) and Eu(III) by calcium silicate hydrates: A solution chemistry and time-resolved laser fluorescence spectroscopy study. *Environ. Sci. Technol.* 37, 3568–3573.
- Tits, J., Wieland, E., Bradbury, M.H., 2005. The effect of isosaccharinic acid and gluconic acid on the retention of Eu(III), Am(III) and Th(IV) by calcite. *Appl. Geochem.* 20, 2082–2096.

Role of the main aqueous cations on cellulose degradation under alkaline conditions and effects on Ni retention in cement.

O. Almendros Ginestá, M. García-Gutiérrez, T. Missana *

CIEMAT – Physical Chemistry of Actinides and Fission Products
Avenida Complutense 40, 28040 MADRID (Spain)

* Corresponding author: tiziana.missana@ciemat.es

Abstract

One of the objectives of CIEMAT in CORI was to analyse the effects of cellulose degradation products on the mobility of different radionuclides (RN) in cement. The isosaccharinic acid is reported to be the main important degradation products of the cellulose under alkaline conditions and it has been widely studied. However, the chemistry of the environment may affect both the final degradation products and the effects that they may have on RN migration.

In this study we analysed the degradation of pure cellulose under alkaline conditions, under different chemical conditions (dominated either by Ca or Na/K), to compare the extent of degradation and the effects of the degradation products formed on the adsorption of Ni in cement.

The degradation of cellulose was more effective in solutions where alkali ions dominated and according to that, Ni adsorption in cement was lessened more under the “fresh” than in degradation Stage (II) conditions.

Introduction

In the context of low-intermediate level radioactive waste disposals, cements are widely used for the containment of the waste. Many different types of organic materials like, paper, plastic, tissues etc., can be co-stored with the radioactive waste, that can undergo to alkaline and radiolitic degradation. The formation of organic ligands is of concern because they may form very stable aqueous complexes with radionuclides and affect their mobility by increasing their overall solubility.

Cellulose (C₆H₁₀O₅)_n, with n>200 is the main constituent of paper, wood and other textile product; many studies recognised that the most important degradation product of the cellulose under alkaline conditions is the isosaccharinic acid (ISA) (Glaus et al. 1999; Pavasars et al, 2003), which has been widely studied in the frame of low-medium waste radioactive waste repositories, in which the principal containment material is cement. The methodology to produce ISA is standardized, and in most of the cases, the soluble Na-(αISA) is used in the experiments.

Degradation of cellulose in different chemical environments may be different from a kinetic point of view or lead to different degradation products (Knill & Kennedy, 2003). These variations could have

possible implications on radionuclide behaviour in the system, and it is interesting to analyse them more in detail using degradation products obtained under different chemical conditions.

Materials and methods

Cellulose

The cellulose used for the experiments was a chemical from Sigma-Aldrich (CAS: 9004-34-6), a microcrystalline powder of 20 µm. The carbon in cellulose is around 44% of the solid. This pure cellulose was suspended in five different alkaline solutions, at a solid to liquid ratio of 1 g·L⁻¹, to analyse the extent of degradation in each case. The suspensions were prepared and maintained under N₂ atmosphere during all the test duration.

Aqueous solutions

The aging of the cellulose has been carried out in different alkaline solutions, namely: a) 1.4 M NaOH (pH=13.95); b) 0.046 M NaOH (pH=12.64); c) 0.016 M Ca(OH)₂ (pH=12.45); d) synthetic water representative of fresh cement, and e) synthetic water representative of Stage(II) of cement degradation, Deg(II). The initial composition of the two synthetic waters is summarised in Table 1.

Table 1: Initial composition of the synthetic waters used in the experiments.

[mg·L ⁻¹]	Fresh	Deg(II)
Al	1.2	<0.03
Ca	3.9	450
K	6100	240
Na	2100	67
Si	19	1
TOC	<2	<2
pH	13.3	12.4

To determine the progressive degree of degradation, the total organic carbon, TOC, leached in solution, was periodically measured. All the samples were filtered by 0.1-0.2 µm syringe filters (Millipore). Apart from TOC measurements, the analysis of the different suspensions was carried out by UV-Vis. The initial cellulose powder and the degraded cellulose were analysed by ATR FTIR. Preliminary analyses on the supernatant solutions were carried out also by high performance anion-exchange chromatography with pulsed amperometric detection, HPAEC/PAD.

Cement

The cement used in these tests is the reference CEM I provided to the CORI participants by the Czech team. The hardened cement paste was prepared in the laboratory and after 28 days curing, it was crushed and sieved to <0.1 mm. Part of the powder was degraded to Stage (II), washing with deionised water (DW) and synthetic Deg(II) water, using a standard procedure. The solids were characterised by XRD and ATR-FTIR. The natural content of Ni in the initial cement powder was 32 ppm. As reported in Wieland et al. (2006), Ni can be in the form of Ni-Al hydrotalcite-like solids.

Sorption tests

For the adsorption tests the isotope ^{63}Ni was used. The distribution coefficient for ^{63}Ni was determined in fresh and Stage (II) degraded cement ($1\text{g}\cdot\text{L}^{-1}$) without and with the presence of the cellulose degraded in the respective waters. The contact time was 7 days.

The distribution coefficient for ^{63}Ni was determined using the following formula:

$$K_d(^{63}\text{Ni}) = \frac{C_{\text{Ni},\text{ini}} - C_{\text{Ni},\text{fin}}}{C_{\text{Ni},\text{fin}}} \cdot \frac{V}{m}$$

being $C_{\text{Ni},\text{ini}}$ and $C_{\text{Ni},\text{fin}}$ the initial and final ^{63}Ni concentration in solution [$\text{Bq}\cdot\text{mL}^{-1}$], V the volume of the solution [mL] and m the mass of the solid [g]. The activity of ^{63}Ni was measured by liquid scintillation counting (LSC) with a TriCarb 4910TR counter. The non-negligible presence of Ni in the cement, indicates that isotopic exchange can be a relevant process in this system (Wieland et al., 2006), but this aspect will not be discussed here.

Results and Discussion

Cellulose degradation

Figure 1 shows the TOC leached as a function of time from the cellulose suspended in the different alkaline solution and, in particular, from fresh and Deg(II) water. All the measurements were carried out upon filtering by $0.2\ \mu\text{m}$.

Results indicate that in the fresh water (and $1.4\ \text{M}\ \text{Na}(\text{OH})$) the degree of degradation, estimated by measuring the TOC, is significantly higher than in other solutions. In particular, cellulose degradation in fresh water is approximately ten times higher than that observed, under the same time span, in Deg(II) water.

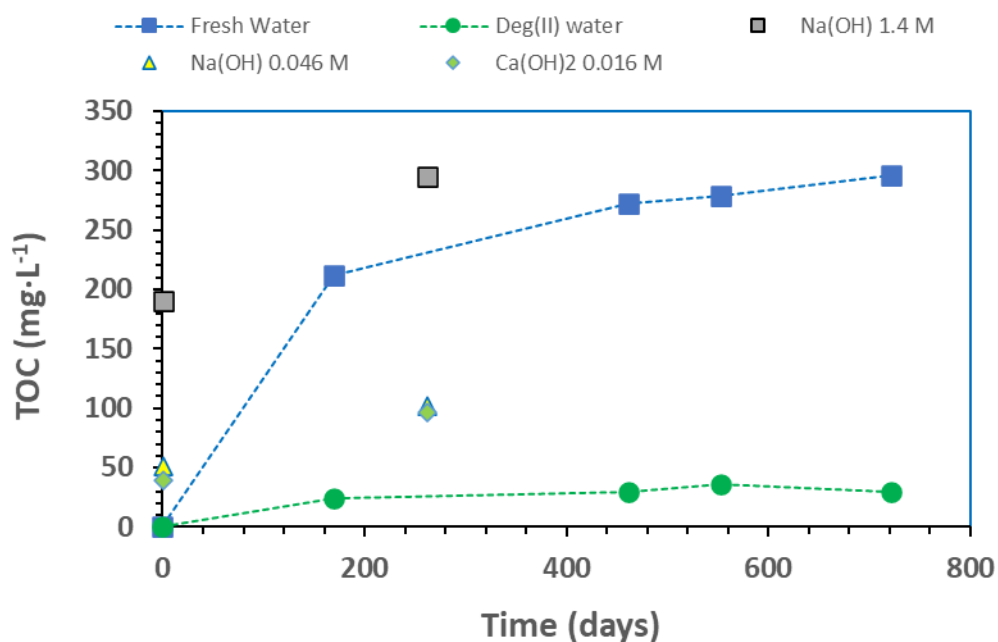


Figure 1: TOC leached in solution from cellulose ($1\ \text{g}\cdot\text{L}^{-1}$) suspended in different alkaline solutions.

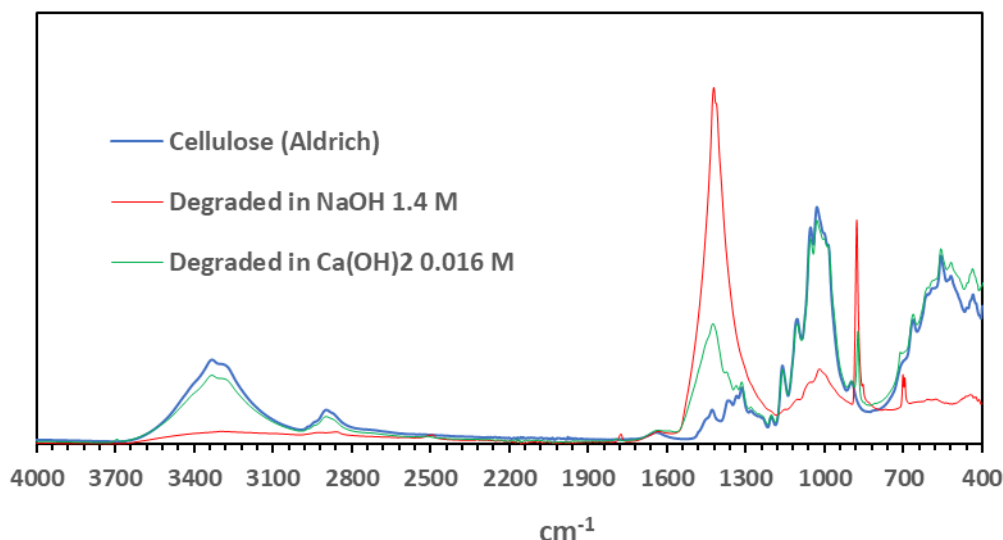


Figure 2: ATR FTIR spectra of the initial cellulose and cellulose degraded in different solutions.

The initial solid and the degraded solid (upon centrifuging and drying) were analysed by ATR-FTIR. Figure 2 shows the spectra of the initial cellulose, compared to the spectra of the material degraded in Na(OH) 1.4 M or Ca(OH)₂ 0.016 M. It can be observed that the mayor changes in the cellulose are observed when it is treated in the sodium hydroxide solution.

In part, this effect can be related to the higher pH of the mentioned solutions, but the dominating ion in solution may also have a role on the degradation (Li et al., 2017) and the different chemical environment may be the responsible of the formation of different final degradation products.

Additionally, we observed that the suspensions of cellulose in Na-solutions and in fresh water (in which alkali ions dominate), acquired a yellowish tone, whereas the others remained clear. The formation of chromophores during cellulose degradation, has been already observed (Ahn et al., 2019), even the reason why this can occur is not totally clear. The spectra obtained by UV-Vis spectroscopy of the different supernatant are shown in Figure 3, where it could be confirmed that, in effect, only those solutions in which the alkali ions are predominant, show a clear UV-Vis adsorption peak. Apart the different colour acquired during the test, preliminary tests showed that the aqueous solutions are not the same.

The analysis by HPAEC/PAD of fresh and Deg(II) waters upon the contact with the cellulose showed that the main peak identified, by comparison with the reference sample, was that of isosaccharinate (Figure4). However, in the case of Deg(II) water one additional (unidentified) peak was observed, but in the case of fresh water two additional peaks were present. These samples were compared with other references (lactic, formic, acetic, levulinic, propionic acid) which presence was not detected.

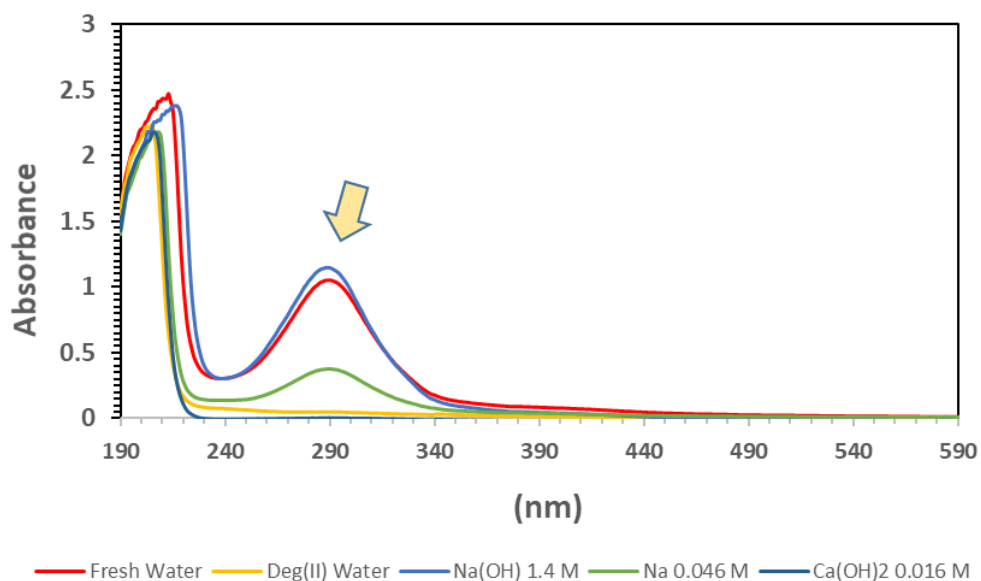


Figure 3: UV-Vis spectra of the different solutions in contact with cellulose.

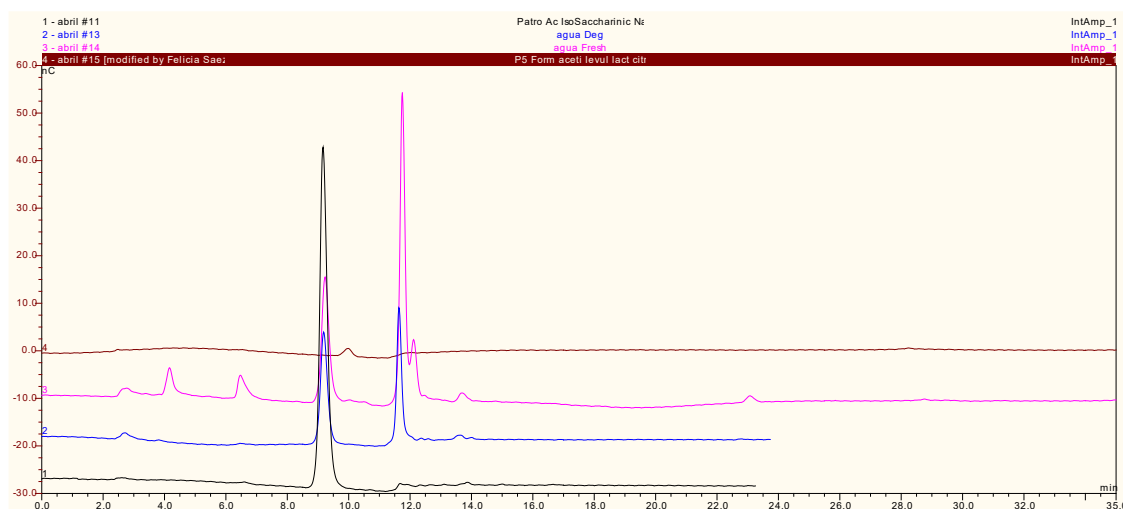


Figure 4 Chromatogram spectra of isosaccharinic acid (black); supernatant of degraded cellulose in fresh water (pink); ; supernatant of degraded cellulose in Deg (II) water (blue).

Effect of cellulose degradation products on Ni retention

Batch sorption experiments to determine the effects of these “real” cellulose degradation products on Ni retention were carried out with fresh and Deg(II) cement (CEM I), in their respective fresh and Deg(II) waters and also in fresh and Deg(II) water in which cellulose was degrading during 722 days.

The distribution coefficients obtained in without and with the cellulose degradation products (CDP) are summarised in Table 2.

Table 2: Distribution coefficients (⁶³Ni) obtained for CEM I in the different waters (with and without cellulose degradation products, CDP) in mL·g⁻¹. [⁶³Ni]=1.1·10⁻⁹ M

	Fresh Water	Deg(II) Water	Fresh Water + CDP	Deg(II) Water + CDP
CEM I (Czech)	1370± 167	7646± 1550	556± 55	7000± 970

The calculated distribution coefficients are higher in Deg(II) water than in fresh water (a factor of 5.6). This agrees with the considerations made by Ochs et al. (2016), which estimated higher K_d values for Ni in degraded State (II) than for fresh conditions, but the values determined here are slightly of higher than those proposed in Ochs et al. (2016).

In respect to the variation K_d values in the presence of the cellulose degradation products, in the case of fresh water a decrease was observed (almost a 60 % of the initial value), which was not so clear in the case of the Deg(II) cement, considering the experimental errors (near the 8 %). This agrees with the higher degradation of the cellulose in the presence of alkalis that has been observed in Figure 1. Other factors may play a role in the difference observed such as ISA sorption on cement (probably higher in Deg-II water) and eventually, sorption of Ni-ISA complexes on cement.

Conclusions

The degradation of pure cellulose has been analysed in different alkaline solutions. It has been shown that the presence of alkalis induces a higher degradation of the material: particularly in a “fresh” cement water the degradation was 10 times more efficient than in Stage (II) cement water. The main degradation product that could be identified in both waters was isosaccharinate, but was not the only organic formed.

The distribution coefficients of Ni in CEM (I) were determined in fresh and Stage (II) degraded cement in the presence of the degradation products of cellulose. The effect of these degradation products was especially evident in the “fresh” system with a reduction of the distribution of approximately a 60 % of the initial value.

Future studies are necessary to understand whether this effect is produced only by the higher quantity of organic formed in the “fresh” system or if differences in the cellulose degradation products obtained under different chemical conditions, may be also relevant. Other factors such as sorption of ISA and sorption of Ni-ISA complexes may also play a role.

Acknowledgement

The EURAD-CORI project leading to this application has received funding from the European Union’s Horizon 2020 research and innovation programme under grant agreement No 847593.

References

- Ahn K., Zaccaron S., Zwirchmayr N.S., Hettenger H., Hofinger A., Bacger M., Henniges U., Hosoya T., Potthast A., Rosenau T. (2019) Yellowing and brightness reversion of celluloses: CO or COOH, who is the culprit? *Cellulose*, 26, 429-244.
- Glaus, M. A., Van Loon, L. R., Achatz, S., Chodura, A., & Fischer, K. (1999). Degradation of cellulosic materials under the alkaline conditions of a cementitious repository for low and intermediate level radioactive waste, part 1: Identification of degradation products. *Analytica Chimica Acta*, 398, 111–122
- Knill C.J., Kennedy J.F (2003). Degradation of cellulose under alkaline conditions. *Carbohydrate Polymers*, 51, 281-300.
- Li Q., Wang A., Ding W., Zhang Y (2017). Influencing factors for alkaline degradation of cellulose. *BioResources* 12(1), 1263-1272.
- Ochs M., Mallant D., Wang L. (2016) Radionuclide and metal sorption on cement and concrete. 322p. Springer
- Pavasars I., Hagberg J., Borén H., Allard B. (2003) Alkaline degradation of cellulose: mechanisms and kinetics. *Journal of polymers and the environment*, 11 (2), 39-46.
- Wieland E., Tits J., Ulrich A., Bradbury M (2006). Experimental evidence for solubility limitations of the aqueous Ni limitations and isotopic exchange of Ni(II) in cementitious system. *Radiochim. Acta*, 94, 29-36.

Interactions of Adipate, Phthalate, ISA and Uranium with Calcium Aluminum Silicate Hydrates

J. Begg^{1*}, M. López-García¹, D. García¹

¹ Amphos21, Carrer Veneçuela, 103, Planta 2, 08019, Barcelona (Spain)

* Corresponding author: james.begg@amphos21.com

Abstract

Understanding the interaction of radionuclides and organic molecules with cementitious materials is a key component of nuclear waste repository safety cases. In this work we examine the adsorption of adipate, phthalate, isosaccharinate (ISA), and uranium to calcium aluminium silicate hydrates (CASH) with different aluminium contents as representative cement hydration products. Our results show no significant sorption of adipate and phthalate to the solid phases. For ISA, there was measurable sorption to low aluminium content CASH but little to no sorption to the high aluminium content CASH. The sorption affinity of uranium for all CASH phases was extremely high, with solution concentrations largely being below the instrument detection limit. The presence of ISA increased the measured concentration of uranium in solid-free experiments. However, in parallel sorption experiments, its effect on sorption was only detectable in experiments performed with very low solid:solution ratios.

1 Introduction

Nuclear energy contributed 10.3% to global electricity production in 2019 (IEA, 2019). As the urgency to combat the climate crisis grows, nuclear energy has been identified by some countries as a key low carbon technology for achieving ambitious and urgent climate change mitigation. (IAEA, 2020; IEA, 2019a). Deep geological repositories (DGR) are considered the most practical and effective way to safely isolate the associated radioactive waste for the long timeframes needed, relying on both engineered and natural barriers (Birkholzer et al., 2012). Cements feature extensively in waste repository scenarios being used as structural materials for construction of vaults and tunnels as well as backfill materials and as encapsulants for storage and transport of active wastes (Glasser and Atkins, 1994). Importantly, they can affect the behavior of dissolved species and may act as significant sorbents for organics and radionuclides (Li and Pang, 2014; Ochs et al., 2015; Wieland et al., 2016; García et al., 2020).

Calcium silicate hydrate (C-S-H) is the main hydration product in cement, constituting 60-70% of a fully hydrated paste. When fly ash is added as a supplementary cementitious material to improve the properties of the cement, the aluminium from this additive can become incorporated into C-S-H structures producing C-A-S-H (calcium-aluminate-silicate-hydrate) phases with different structures and higher chain lengths than those of C-S-H (Kalousek, 1957; Faucon et al., 1998; Sun et al., 2006; Lothenbach et al., 2011; L'Hôpital, 2014; Haas and Nonat, 2015). The sorption properties of CASH in

the context of radionuclides have received only minimal attention (Li and Pang, 2014; Olmeda et al., 2019).

Given the multitude of operations in nuclear energy production, there are a variety of waste matrices with complex compositions. In this context, organic materials are of special relevance as they have the potential to affect radionuclide behavior. The sources of the organics include cellulose materials, spent ion exchange resins, and PVC tubes (IAEA, 2009; Gaona et al., 2008; Felipe-Sotelo et al., 2012; Boggs et al., 2013; Ochs et al., 2014; González-Siso et al., 2018; Keith-Roach, 2008; Tasi et al., 2018; Brinkmann et al., 2019;).

The work presented here describes ongoing research into the interaction of three organic molecules (adipate, phthalate, and ISA) and uranium with calcium aluminium silicate hydrates. Adipate and phthalate were selected as commonly used additives in plastics manufacturing while isosaccharinic acid (ISA) is a product of the alkaline hydrolysis of cellulose (Rahman and Brazel, 2004).

2 Material and Methods

2.1 Calcium Aluminium Silicate Hydrates

In this text, solid cementitious phases are referred to as CASH x1-x2 where x1 refers to the theoretical Ca/Si ratio and x2 refers to the theoretical Al/Si ratio. For CASH phases, the ratios 1.2-0.05 and 1.2-0.02 were chosen based on previous work looking at sorption of radium to CASH (Olmeda et al., 2019). Synthesis was performed in an anaerobic chamber under a N₂ atmosphere (CO₂ < 10 ppm and O₂ < 10 ppm) to prevent carbonation based on the procedure reported in Olmeda et al. (2019). Samples were prepared by adding deoxygenated deionized water (DDW) to weighed amounts of reagent grade CaO, SiO₂, and Al(NO₃)₃·9H₂O. The mass of each solid was chosen to achieve both the desired Ca:Si and Al:Si ratios and a solid:liquid ratio of 10 g·L⁻¹. The pH and conductivity of the solution phase were monitored periodically during equilibration. Synthesis was considered complete when there was no significant change in these values, typically a period of 28 days.

After the synthesis period, aliquots of the suspension were transferred to 15 mL centrifuge tubes. The tubes were removed from the glovebox for centrifugation (2600 g, 10 minutes: nominal particle size cut-off 0.5 µm) then returned to the glovebox, and the supernatant passed through a 0.22 µm nylon syringe filter. The filtrate was acidified as necessary, and the solid phase left to dry inside the glovebox for 72 h before characterization. The concentration of Ca in the filtrate was determined with ion chromatography (ICS-2000 system, Dionex), Si and Al were measured with ICP-MS (model 7500cx, Agilent Technologies Inc.)

For solid phase characterization, scanning electron microscopy (SEM; FE-SEM - ZEISS Ultraplus) was used to obtain images of the sample surfaces. Energy Dispersive X-ray Spectroscopy (EDX; X-Max EDX detector, OXFORD Instruments) was used to obtain semi-quantitative chemical composition analysis of the solid. The crystalline and semi-crystalline phase composition of solid samples was determined via XRD (PANalytical X'Pert PRO MPD). The zeta potential of the CASH 1.2-0.05 suspension was determined with a Zetasizer Nano ZS (Malvern Panalytical). The results of the aqueous, solid, and suspension characterization are summarized in Table 1. The characterization of the samples was broadly consistent with that observed in a previous study with CASH solids (Olmeda et al., 2019). Particularly, we note that the CASH 1.2-0.2 samples had a lower pH value (10.2) than that reported by Olmeda et al. (11.0).

Table 1: Representative aqueous and solid phase characterization of CASH suspensions used in experiments. Reported Ca:Si and Si:Al molar ratios are taken from semi-quantitative EDX measurements.

Sample	Ca (mol/L)	Al (mol/L)	Si (mol/L)	pH	Ca:Si	Si:Al	ζ potential (mV)
CASH 1.2-0.05	6.40×10^{-3}	9.44×10^{-6}	2.73×10^{-4}	11.24	1.13	0.04	-2.35 ± 0.73
CASH 1.2-0.2	1.38×10^{-2}	6.06×10^{-7}	1.77×10^{-3}	10.24	0.74	0.41	-

2.2 Organics

Na-(ISA)(s) was obtained following a 2-step reaction based on the methods described in Vercammen (2000), Evans (2003), and Colàs (2014) in which the calcium salt of isosaccharinic acid was prepared from the alkaline degradation of α - lactose hydrate and then converted to the sodium form with an ion exchange resin. The major crystalline phase identified in the X-ray powder diffraction diagram of the dried solid was sodium isosaccharinate monohydrate, $\text{NaC}_6\text{H}_{11}\text{O}_6 \cdot \text{H}_2\text{O}$ (Cambridge Structural Database reference BERJAK). Semi-quantitative phase analysis by means of the Rietveld method showed 99.7% sodium isosaccharinate. Stock solutions of ISA were prepared by dissolution of the solid in DDW inside the glovebox.

Adipate and phthalate were obtained from commercial adipic (Sigma-Aldrich, BioXtra) and phthalic (Sigma-Aldrich, ACS reagent) acids. Given the low solubilities of adipic and phthalic acid in water, to achieve the higher concentrations in our experiments, stocks were made by dissolving solids in ethanol (96%, Pharmpur, Scharlab).

Uranium stock solutions were prepared from a standard solution (PerkinElmer Pure Plus). Dilutions were performed volumetrically using 2 % ultrapure HNO_3 .

2.3 Sorption Experiments

Sorption experiments were performed in an anoxic glove box under a N_2 atmosphere using the suspensions from the original solid synthesis. Experiments were carried out in duplicate. Aliquots of the respective suspensions were added to 15 mL propylene centrifuge tubes and then spiked with the appropriate stock solution. Binary organic sorption experiments were performed with CASH 1.2-0.05 and CASH 1.2-0.2 at initial adipate, phthalate, or ISA concentrations of 1×10^{-4} to 1×10^{-2} M. Solid-free experiments were performed using the solution from the relevant equilibrating suspension that had been phase separated via filtration ($0.22 \mu\text{m}$). To assess the solubility of uranium in our systems, initial uranium experiments were performed with solid-free CASH 1.2-0.05 and CASH 1.2-0.2 porewaters. Samples were spiked with initial concentrations of 1×10^{-9} to 1×10^{-6} M uranium. Sorption experiments were performed with initial uranium concentrations of 1×10^{-8} to 1×10^{-6} M. Following spiking, the samples were left to equilibrate on an orbital shaker inside the glovebox.

Experiments were sampled at 14 days after spiking. For organic experiments, to ensure that this equilibration period was sufficient, a subset of samples was also sampled sacrificially at 1 and 7 days after spiking. At the sampling timepoint, the tubes were removed from the glovebox for centrifugation (2600 g, 10 minutes: nominal particle size cut-off $0.5 \mu\text{m}$). The samples were returned to the glovebox, and the supernatant passed through a $0.22 \mu\text{m}$ nylon syringe filter. The pH of a portion of filtrate was measured in representative samples. For CASH 1.2-0.05 experiments, pH values were 11.3 ± 0.2 , for

CASH 1.2-0.2 they were 10.2 ± 0.1 . For organic experiments, an aliquot of selected samples was acidified with concentrated HNO_3 to be analysed for major ions in solution. The remainder of the filtrate was stored inside the glovebox until it was analysed for organic determination in solution via ion chromatography. For uranium samples, the filtrate was acidified with ultrapure HNO_3 and the concentration determined with ICP-MS.

3 Results and Discussion

3.1 Sorption of adipate, phthalate and ISA to CASH

The sorption of adipate, phthalate, and ISA to CASH 1.2-0.05 and CASH 1.2-0.2 was studied at initial concentrations of 1×10^{-4} to 1×10^{-2} M. For adipate and phthalate, after 14 d equilibration, there was no appreciable sorption to either CASH phase with measured concentrations in solid-free experiments matching those in the presence of the solid (Figure 1 A-D). There currently exists little published experimental data for the adsorption of phthalate and adipate on cementitious solids however, our results suggest that sorption will likely be limited under repository conditions.

In the case of ISA, there was a small but significant amount of sorption observed at all initial concentrations for solid containing CASH 1.2-0.05 experiments compared to the solid-free experiments (Figure 1E). For the ISA CASH 1.2-0.2 experiments, there was no appreciable sorption at initial organic concentrations of 1×10^{-2} M and 1×10^{-3} M and only a very small amount of sorption at 1×10^{-4} M (< 10%).

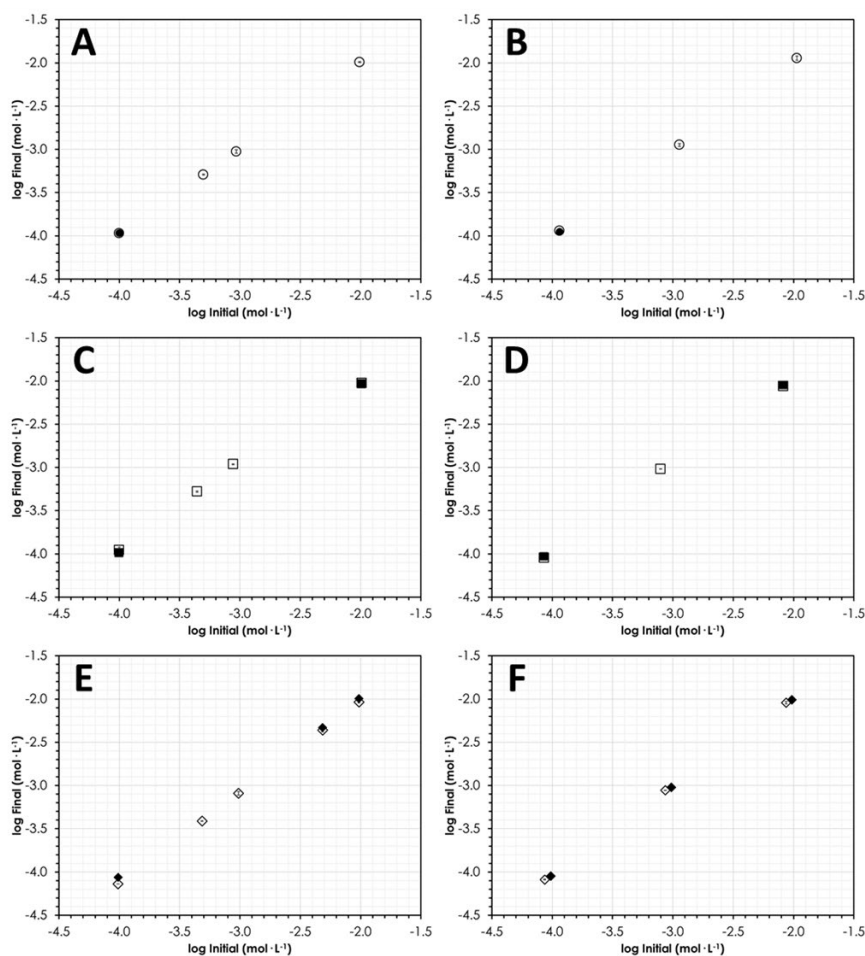


Figure 1. 14 day sorption of: adipate to (A) CASH 1.2-0.05 and (B) CASH 1.2-0.2; phthalate to (C) CASH 1.2-0.05 and (D) CASH 1.2-0.2; ISA to (E) CASH 1.2-0.05 and (F) CASH 1.2-0.2. Closed symbols are for solid-free experiments. Data plotted as calculated initial concentration in experiments against measured solution concentration. Error bars are the standard deviation of duplicate measurements.

Calculation of the speciation of each organic under the solution conditions of the CASH 1.2-0.05 experiments with initial concentration of 1×10^{-3} M is shown in Figure 2. In the cases of adipate and phthalate, speciation is either negatively charged or neutral. For ISA, approximately 16 % is calculated to be present as the positively charged $\text{Ca}(\text{HISA})^+$ species. Given the negative zeta potential measured for the CASH 1.2-0.05 suspensions (-2.35 ± 0.73 ; Table 1), it appears reasonable that there is electrostatic attraction between the positively charged organic and the solid phase, facilitating the formation of surface complexes. This does not necessarily occur in the case of negatively charged or neutral solution species.

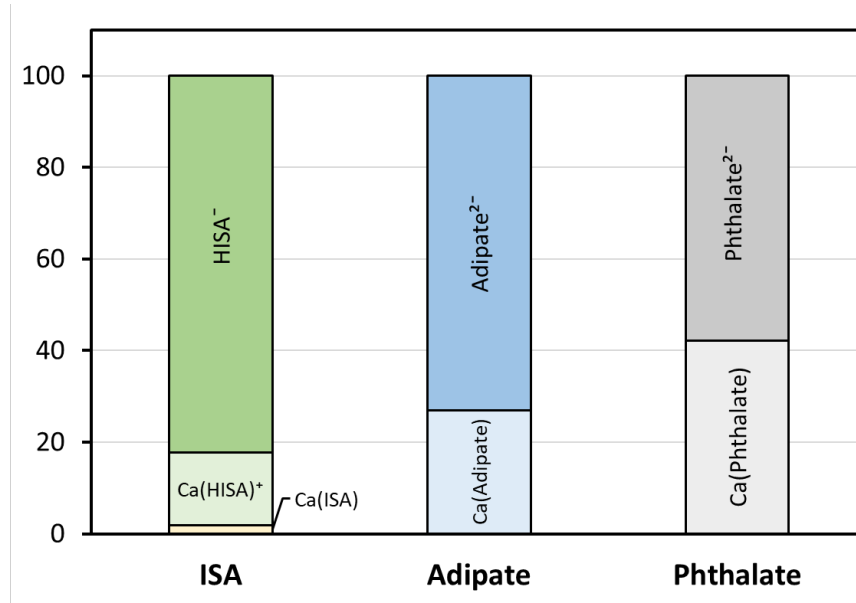


Figure 2 Speciation of ISA, adipate and phthalate under the solution conditions of the experiments with CASH 1.2-0.05 (see Table 1) at concentration $1 \cdot 10^{-3}$ M. Calculations were performed using GibbsStudio code coupled with ThermoChimie v10a database (Nardi A. & de Vries, 2017; Giffaut et al., 2014).

The sorption of ISA to CASH phases in the current experiment is plotted with selected literature data for ISA sorption to CSH 1.2, Hardened Cement Paste (HCP) in degradation state I, HCP in degradation state II, and CEM I (Ordinary Portland Cement) in Figure 3 (Van Loon et al., 1997; García et al., 2020). The trend in our data for CASH 1.2-0.05 follows that previously observed for a range of cementitious material, although the extent of sorption is generally lower. For CASH 1.2-0.2, sorption was only observed at the lowest concentration of ISA investigated (1×10^{-4} M) and the extent of sorption at this concentration is shown to be much lower than for the other solids, including the CASH 1.2-0.05.

We modelled the CASH 1.2-0.05 ISA experimental sorption data with a Langmuir isotherm considering only one adsorption site, with the following form (Eq. 1) (Dagnelie et al., 2014):

$$q_e = q_m \cdot \frac{KL \cdot C_e}{1 + KL \cdot C_e} \quad \text{Eq.1}$$

where q_e stands for the amount of adsorbed organic ($\text{mol} \cdot \text{Kg}^{-1}$), C_e stands for the aqueous equilibrium concentration of the organic ($\text{mol} \cdot \text{L}^{-1}$), q_m stands for the maximum adsorption capacity of the adsorbent ($\text{mol} \cdot \text{Kg}^{-1}$) and KL stands for the sorption affinity of the organic towards the adsorbent. As seen in Figure 3, a one-site Langmuir isotherm could explain the adsorption behaviour of ISA on the CASH phase well, consistent with a previous modelling effort for the sorption of ISA on CSH 1.2 (Garcia et al., 2020).

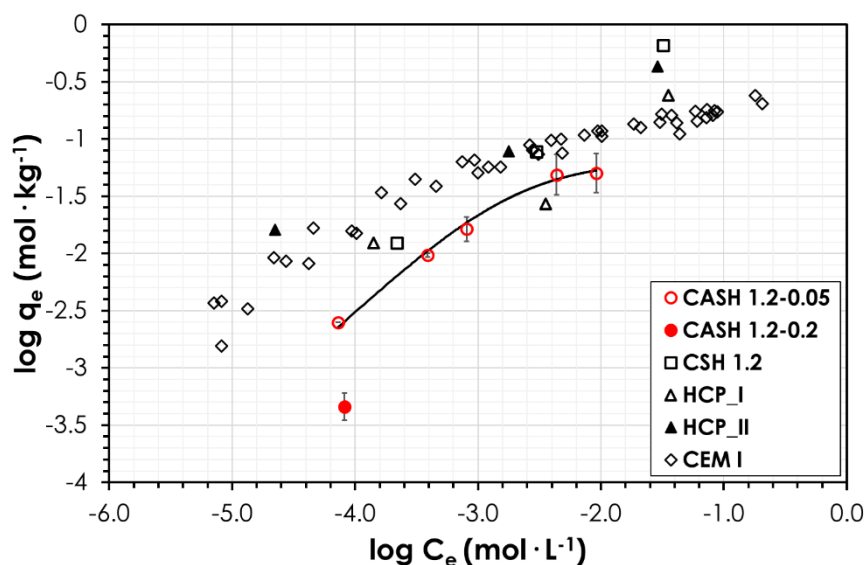


Figure 3 Sorption of ISA to CSH 1.2 (Garcia et al., 2020), CASH 1.2-0.05 and 1.2-0.2 (current work), hardened cement paste degradation state I (HCP_I) and state II (HCP_II) (Garcia et al., 2020), and CEM I (Van Loon et al., 1997). Error bars are the standard deviation of duplicate measurements. For clarity, error bars are not included for literature data. Solid line is the 1-site Langmuir model for the CASH 1.2-0.05 data.

3.2 Solubility of uranium in CASH porewaters

Uranium was spiked into solid-free CASH 1.2-0.05 and CASH 1.2-0.2 porewaters with initial concentrations ranging from 1×10^{-9} to 1×10^{-6} M. For CASH 1.2-0.05, at initial concentrations $\leq 5 \times 10^{-7}$ M, measured concentrations matched the initial concentration (Figure 4). However, at an initial uranium concentration of 1×10^{-6} M, the measured concentration was $4.3 \pm 1.8 \times 10^{-7}$ M, indicating the precipitation of a solid uranium-containing phase. This measured concentration is above that predicted for uranium in these experiments based on modelling of our porewaters. Similarly, for CASH 1.2-0.2, while the measured concentration matched the initial concentration in the 1×10^{-8} M sample, at 1×10^{-6} M the measured concentration was significantly lower than the initial value (Figure 4). Based on the measured solution concentrations, 4×10^{-7} M was taken as the provisional solubility limit for uranium in sorption experiments.

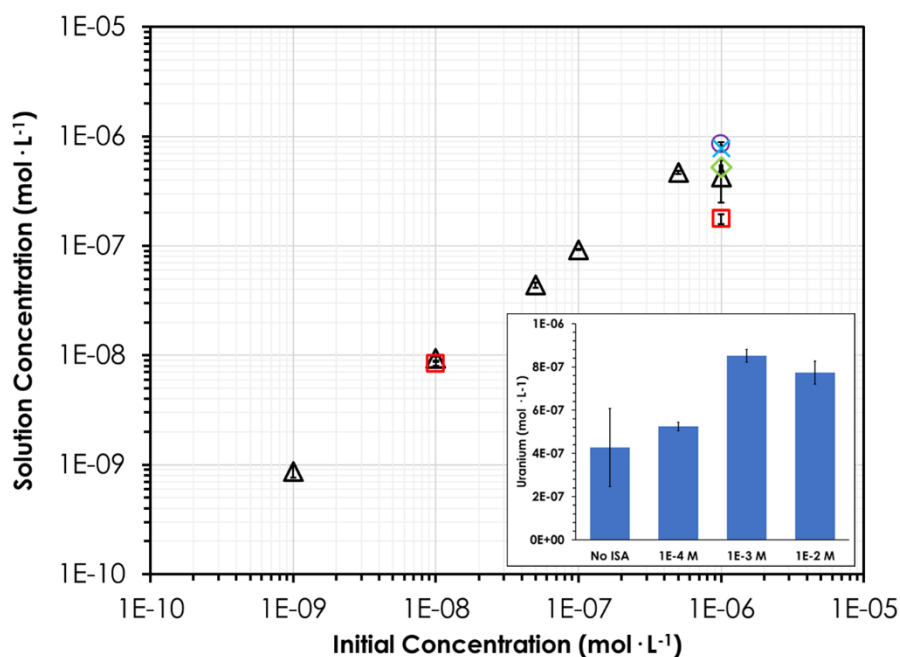


Figure 4 Concentration of uranium in CASH 1.2-0.05 porewater (black triangles), CASH 1.2-0.2 porewater (red squares), and CASH 1.2-0.05 porewater amended with 1×10^{-4} M ISA (green diamond), 1×10^{-3} M ISA (blue cross) and 1×10^{-2} M ISA (purple circle). Inset is bar plot of uranium solution concentration in CASH 1.2-0.05 porewater at initial concentration of 1×10^{-6} M uranium in the absence and presence of ISA. Error bars are the standard deviation of duplicate measurements except for the CASH 1.2-0.05 initial concentration 1×10^{-6} M data point where it is the standard deviation of quadruplicate measurements.

When ISA, at initial concentrations of 1×10^{-3} and 1×10^{-2} M was spiked into experiments with CASH 1.2-0.05 porewater and 1×10^{-6} M uranium, the measured concentration of uranium was higher than in the absence of ISA. The measured concentration in the presence of 1×10^{-3} M ISA was $8.5 \pm 0.3 \times 10^{-7}$ M and $7.7 \pm 0.5 \times 10^{-7}$ M with 1×10^{-2} M ISA, compared to $4.3 \pm 1.8 \times 10^{-7}$ M when ISA was not present. The addition of 1×10^{-4} M ISA did not have a significant effect on the measured concentration of uranium. The modelled speciation of U in these ISA addition experiments is shown in Figure 5. One noticeable change in the speciation of U is the increasing fraction of U present as $\text{UO}_2(\text{OH})_4(\text{HIsa})^{-3}$ at the pH of the experiment (11.2) as the concentration of ISA increases. This suggests that the formation of this species leads to the increased solubility of uranium in our systems.

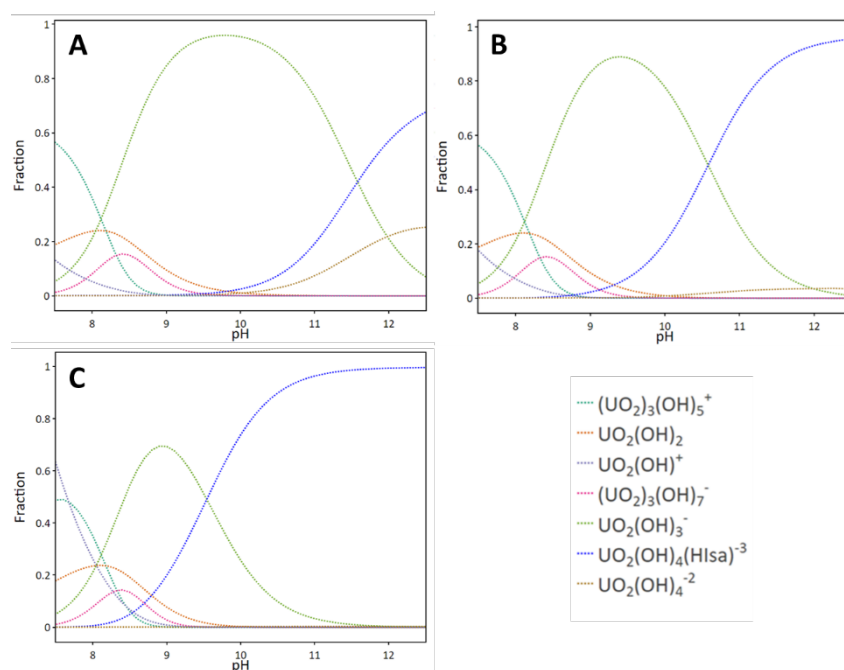


Figure 5 U speciation at $[U] = 1 \cdot 10^{-6} \text{ M}$ under the solution conditions of the experiments with CASH 1.2-0.05 ($\text{pH} = 11.24$). (A) $[ISA] = 1 \times 10^{-4} \text{ M}$, (B) $[ISA] = 1 \times 10^{-3} \text{ M}$, (C) $[ISA] = 1 \times 10^{-2} \text{ M}$. Calculations were performed using GibbsStudio code coupled with ThermoChimie v10a database (Nardi A. & de Vries, 2017; Giffaut et al., 2014). For clarity, species whose contribution never rises above 0.05 are not shown.

3.3 Sorption of uranium to CASH 1.2-0.05 and 1.2-0.2

In sorption experiments with CASH phases at $10 \text{ g} \cdot \text{L}^{-1}$ and initial uranium concentrations ranging from 1×10^{-8} to $1 \times 10^{-6} \text{ M}$, the solution concentration in all samples after 14 days of equilibration was below the instrument detection limit ($4 \times 10^{-10} \text{ M}$). Despite the observation that ISA could increase the measured concentration of uranium in solid-free experiments, its presence, even at $1 \times 10^{-2} \text{ M}$, did not lead to measurable concentrations of U in the sorption experiments. Taking the 10^{-7} M initial U sample (the 10^{-6} M sample was excluded because of potential precipitation of U solids) and the instrument detection limit, at the solid:solution ratios in these experiments ($10 \text{ g} \cdot \text{L}^{-1}$) we estimated a minimum log Rd of 4.8 for uranium sorption to CASH 1.2-0.05 and 1.2-0.2.

Following these results, a set of sorption experiments were performed with CASH 1.2-0.05 at a solid:solution ratio of $0.2 \text{ g} \cdot \text{L}^{-1}$ and uranium at an initial concentration of $4 \times 10^{-7} \text{ M}$. These resulted in measurable uranium solution concentrations and a calculated log Rd of 5.7, which is broadly comparable to previously obtained values for U sorption to CSH at a pH value < 12 (Tits et al., 2014). The addition of $1 \times 10^{-3} \text{ M}$ ISA decreased the log Rd value to 5.3, indicating that its presence can increase the mobility of U in cementitious systems.

4 Conclusions and Future Work

In this work, we examined the sorption of adipate, phthalate and ISA, as well as uranium, to two calcium silicate aluminum hydrates. No sorption of adipate or phthalate was observed while adsorption of ISA was limited. In contrast, uranium sorption to both solid phases was extremely high. Despite evidence for the formation of a uranium-ISA complex in solution, the addition of ISA did not demonstrate a measurable effect on the adsorption of uranium to CASH at solid:solution ratios of $10 \text{ g} \cdot \text{L}^{-1}$ possibly due to a combination of the high sorption affinity of U for CASH solids and the detection limit of the

measurement instrument. At a solid:solution ratio of $0.2 \text{ g}\cdot\text{L}^{-1}$ there was a small but significant reduction in the extent of adsorption caused by the presence of ISA. However, given the extremely low solid:solution ratios, and the relatively low concentration of ISA used (10^{-3} M) it remains unclear how this would affect the mobility of uranium in an actual repository setting.

Acknowledgement

The authors thank Dr. Carlos Rey-Castro from the Environmental Physicochemistry Group at Universitat de Lleida for performing zeta potential measurements and Dr. Xavi Gaona at Karlsruhe Institute of Technology for help performing a portion of the uranium concentration measurements.

The EURAD-CORI project leading to this application has received funding from the European Union's Horizon 2020 research and innovation programme under grant agreement No 847593.

References

- Birkholzer J., Houseworth, J. & Tsang C.-F. (2012) Geologic disposal of high-level radioactive waste: Status, key issues, and trends. *Annual Review of Environment and Resources*, 37, 79-106.
- Boggs M. A., Islam M., Dong, W. & Wall, N. A. (2013) Complexation of Tc(IV) with EDTA at varying ionic strength of NaCl. *Radiochimica Acta*, 101, 13-18.
- Brinkmann H., Patzschke M., Kaden P., Raiwa M., Rossberg A., Kloditz R., Heim K., Moll H. & Stumpf T (2019) Complex formation between UO_2^{2+} and α -isosaccharinic acid: insights on a molecular level. *Dalton Transactions*, 48, 13440-13457.
- Colàs E. (2014) Complexation of Th(IV) and U(VI) with polyhydroxy and polyamino carboxylic acids. PhD thesis, Universitat Politècnica de Catalunya.
- Dagnelie R.V.H., Descostes M., Pointeau I., Klein J., Grenut B., Radwan J., Lebeau D., Georgin D., Giffaut E., 2014. Sorption and diffusion of organic acids through clayrock: Comparison with inorganic anions. *Journal of Hydrology* 511, 619–627.
- Dolado J.S., Griebe M. & Hamaekers J. (2007) A molecular dynamic study of cementitious calcium silicate hydrate (C-S-H) gels. *Journal of the American Ceramic Society*, 90, 3938-3942.
- Faucon P., Charpentier T., Nonat A. & Petit J.C. (1998) Triple-quantum two-dimensional ^{27}Al magic angle nuclear magnetic resonance study of the aluminum incorporation in calcium silicate hydrates. *Journal of the American Chemical Society*, 120, 12075-12082.
- Felipe-Sotelo M., Hinchliff J., Evans N., Warwick P. & Read, D. (2012) Sorption of radionuclides to a cementitious backfill material under near-field conditions. *Mineralogical Magazine*, 76, 3401–3410.
- Gaona X., Montoya V., Colàs E., Grivé M. & Duro L. (2008) Review of the complexation of tetravalent actinides by ISA and gluconate under alkaline to hyperalkaline conditions. *Journal of Contaminant Hydrology*, 102, 217–227.
- García D., Henocq P., Riba, O., López-García, M., Madé B. & Robinet J.-C. (2020) Adsorption behaviour of isosaccharinic acid onto cementitious materials. *Applied Geochemistry*, 118, 104625.
- Giffaut E., Grivé M., Blanc P., Vieillard P., Colàs E., Gailhanou H., Gaboreau S., Marty N., Madé B. & Duro L. (2014) Andra thermodynamic database for performance assessment: ThermoChimie. *Applied Geochemistry* 49, 225–236.
- González-Siso M.R., Gaona X., Duro L., Altmaier M. & Bruno, J. (2018) Thermodynamic model of Ni (II) solubility, hydrolysis and complex formation with ISA. *Radiochimica Acta* 106, 31–45.
- Haas J. & Nonat A. (2015) From C–S–H to C–A–S–H: Experimental study and thermodynamic modelling. *Cement and Concrete Research*, 68, 124-138.
- IAEA (2009) IAEA Safety Standards Classification of Radioactive Waste for protecting people and the Environment. Classification of Radioactive Waste. General Safety Guide No. GSG-1. IAEA, Vienna.
- IAEA (2020) INTERNATIONAL ATOMIC ENERGY AGENCY, Climate Change and Nuclear Power 2020, Non-serial Publications, 2020.

- IEA (2019) World gross electricity production by source, 2019, IEA, Paris <https://www.iea.org/data-and-statistics/charts/world-gross-electricity-production-by-source-2019>.
- IEA (2019a) Nuclear Power in a Clean Energy System, IEA, Paris <https://www.iea.org/reports/nuclear-power-in-a-clean-energy-system>.
- Kalousek, G.L. (1957) Crystal chemistry of hydrous calcium silicates: I. Substitution of aluminum in lattice of tobermorite. *Journal of the American Ceramics Society*, 40, 74-80.
- Keith-Roach, M.J. (2008) The speciation, stability, solubility and biodegradation of organic co-contaminant radionuclide complexes: A review. *Science of The Total Environment* 396, 1–11.
- L'Hôpital E. (2014). Aluminium and alkali uptake in calcium silicate hydrates (C-S-H). PhD thesis, École Polytechnique Fédérale de Lausanne.
- Li K. & Pang, X. (2014) Sorption of radionuclides by cement-based barrier materials. *Cement and Concrete Research*, 65, 52-57
- Lothenbach B., Scrivener K. & Hooton R. D. (2011) Supplementary cementitious materials. *Cement and Concrete Research*, 41, 1244-1256.
- Nardi A. & de Vries L. (2017) GibbsStudio. Barcelona Science Technologies SL, Barcelona, Spain.
- Ochs M., Colàs E., Grivé M., Olmeda J., Campos I. & Bruno, J. (2014) Reduction of radionuclide uptake in hydrated cement systems by organic complexing agents: Selection of reduction factors and speciation calculations (No. SKB R-14-22).
- Olmeda J., Missana T., Grandia F., Grivé M., García-Gutiérrez M., Mingarro M., Alonso U., Colàs E., Henocq P., Munier I. & Robinet J.C. (2019) Radium retention by blended cement pastes and pure phases (C -S -H and C A S -H gels): Experimental assessment and modelling exercises, *Applied Geochemistry*,
- Pacewska B. & Wilińska, I. (2020) Usage of supplementary cementitious materials: advantages and limitations. *Journal of Thermal Analysis and Calorimetry*, 142, 371–393.
- Rahman M. & Brazel C.S. (2004) The plasticizer market: an assessment of traditional plasticizers and research trends to meet new challenges. *Progress in Polymer Science* 29, 1223–1248.
- Sun G.K., Young J.F. & Kirkpatrick R.J. (2006) The role of Al in C-S-H: NMR, XRD, and compositional results for precipitated samples. *Cement and Concrete Research*, 36, 18-29. Glaus M. A., Van Loon L. R., Achatz S., Chodura A. & Fischer K (1999) Degradation of cellulosic materials under the alkaline conditions of a cementitious repository for low and intermediate level radioactive waste. Part I : Identification of degradation products. *Analytica Chimica Acta*, 398, 111 – 122.
- Tasi A., Gaona X., Fellhauer D., Böttle M., Rothe J., Dardenne K., Polly R., Grivé M., Colàs E., Bruno J., Källström K., Altmaier M. & Geckeis, H. (2018) Thermodynamic description of the plutonium – α -D-isosaccharinic acid system I: Solubility, complexation and redox behavior. *Applied Geochemistry*, 98, 247–264.
- Tits J., Fujita T., Harfouche M., Dähn R., Tsukamoto M. & Wieland, E. (2014) Radionuclide uptake by calcium silicate hydrates: case studies with Th(IV) and U(VI). (PSI Bericht, Report No.: 14-03). Paul Scherrer Institut.
- Van Loon L.R., Glaus M.A., Stallone S. & Laube, A., (1997) Sorption of isosaccharinic acid, a cellulose degradation product, on cement. *Environmental Science & Technology*, 31, 1243–1245.

ISA production during hydrolytic degradation of irradiated cellulosic tissues and its sorption on degraded Ordinary Portland Cement: first set of results

N. Bleyen, D. Durce, S. Smets, M. Van Gompel, V. Van Gompel, D. Verhaegen,
W. Verwimp, K. Wouters, E. Valcke

W&D Expert Group, SCK CEN, Boeretang 200, 2400 Mol, Belgium

* Corresponding author: nbleyen@sckcen.be

Abstract

Cellulosic materials are widely used in the nuclear industry, and therefore make up a large quantity of certain waste streams. Both during interim storage and final disposal, cellulose will undergo radiolytic and/or hydrolytic degradation in cement water at highly alkaline pH. Under disposal conditions, the α and β isomers of isosaccharinic acid (α - and β -ISA) are important cellulose degradation products. Especially α -ISA has been shown to form complexes with radionuclides, which may facilitate their migration from the waste to the biosphere. On the other hand, sorption of α -ISA on cementitious material present in a disposal facility could counteract the enhancing effect of α -ISA on radionuclide migration. In this study, the effect of pre-irradiation of cellulosic tissues on the production of soluble degradation products, and more specifically ISA, under alkaline conditions was assessed during 3 months, as well as the sorption of α -ISA on Portland cement degraded to state III.

The results show that pre-irradiation of cellulosic tissues enhances the production of ISA during hydrolytic degradation. The ISA production rates and yield increased with the absorbed dose applied during pre-irradiation, which can be linked to an increased number of radiolytic chain scissions with increased absorbed dose. Under all test conditions of the degradation study, α - and β -ISA isomers were produced equally. The sorption of α -ISA on cement degraded to state III was found to be lower than previously observed on fresh cement. Moreover, it followed a one-site Langmuir sorption isotherm, with a mild sorption showing a maximum solid/liquid distribution ratio of $109 \pm 67 \text{ L kg}^{-1}$.

1 Introduction

Cellulose is an unbranched linear homopolymer of $\beta(1,4)$ -linked D-glucopyranose monomeric units and is broadly present in nature. Cellulosic materials are widely used in the nuclear industry, *e.g.* as paper, tissues, filters, wood and textiles, and therefore make up a large quantity of certain waste streams. In Belgium, cellulose-containing waste forms are proposed to be disposed of in either a surface facility (for low- and intermediate-level short-lived waste) or in a deep geological disposal facility (for

intermediate-level long-lived waste). Both Belgian disposal concepts foresee the emplacement of the waste drums in thick-walled concrete containers or monoliths that will be placed inside concrete-lined galleries. Due to the presence of large amounts of cement and concrete, water infiltrating the disposal facilities and reaching the waste drums will have a highly alkaline pH, at least as long as the advective water flow remains limited (Bleyen, 2020; ONDRAF/NIRAS, 2013, 2019).

During interim storage, but also under disposal conditions, cellulose is susceptible to degradation. Indeed, due to the presence of radionuclides in the waste, radiolytic degradation will occur during storage and disposal, under either oxic (storage) or anoxic (disposal) conditions. Radiation-induced degradation of cellulose is known to lead to reactions in the polymer such as chain scission, gas production, and formation of carbonyl and carboxyl groups (Arthur, 1958; Arthur, 1971; Charlesby, 1955; Ershov, 1998). Nevertheless, detailed information on the effect of the irradiation conditions on the cellulose structure and properties is scarce.

Furthermore, under the anoxic and alkaline conditions imposed by the excess of cementitious materials in disposal facilities, hydrolysis of cellulose will occur, resulting in the production of water-soluble cellulose degradation products that may form strong complexes with radionuclides. This may result in an increased radionuclide solubility and a reduced radionuclide sorption, which may facilitate radionuclide migration (Allard and Ekberg, 2006; Gaona et al., 2008; Vercammen et al., 1999). Under disposal conditions, the α and β isomers of isosaccharinic acid (ISA) are the most important cellulose degradation products (Bleyen, 2020; Glaus and Van Loon, 2008; Van Loon and Glaus, 1998; Van Loon et al., 1999), in terms of both degradation yield and solubility enhancement, with the α isomer showing a stronger complexation capacity towards key radionuclides (Van Loon and Glaus, 1998).

Several properties of cellulose influence its hydrolytic degradation reactions and rates under alkaline conditions, *e.g.* morphological structure, crystallinity and degree of polymerisation (Gentile et al., 1987; Haas et al., 1967; Ioelovich, 2009; Lai and Sarkanen, 1967; Mittal et al., 2011; Van Loon and Glaus, 1998). Changes made to these cellulose properties during radiolysis prior to hydrolytic degradation could thus have a significant effect on the overall production of radionuclide complexing molecules in the waste, such as α -ISA.

In addition, it has been demonstrated previously that α -ISA can sorb on cement phases, especially on the calcium-silicate-hydrate (C-S-H) phases. Such sorption could counteract the enhancing effect of α -ISA on radionuclide migration. ISA sorption was shown to depend on the degradation state of the cement phases (Bruno et al., 2018; García et al., 2020; Pointeau et al., 2008; Van Loon et al., 1997). From a nuclear waste disposal point of view, fresh cement and cement in degradation state II are often considered as the most relevant (Jacques et al., 2014) and are consequently most commonly used in sorption experiments. They are indeed assumed to cover most of the critical time period for radionuclide release. However, cement degradation is not expected to be homogeneous over the full repository and higher degradation states could occur locally within shorter time frames. As leaching of the cement crystalline phases during cement degradation and the concomitant decalcification can affect the sorption properties of the cement (García et al., 2020; Pointeau et al., 2006), sorption of α -ISA should also be assessed on cement in higher degradation states.

The sorption of α -ISA onto the cement material used as structural reinforcement or as immobilisation matrix is thus an important process. Together with the cellulose degradation rates and mechanisms, and the α -ISA complexation properties, it defines the capacity of α -ISA to enhance the migration of key radionuclides. Increasing the knowledge of cellulose degradation (radiolytic and

hydrolytic) and assessing the α -ISA sorption over the full lifetime of the cement materials is therefore of high interest for safety assessment calculations for the disposal facilities of radioactive waste.

In the present study, the effect of pre-irradiation on the short- and long-term production of dissolved organic compounds, and more specifically ISA, from cellulosic tissues in contact with artificially prepared cement water at highly alkaline pH was investigated. Furthermore, sorption of α -ISA was assessed on Portland cement degraded to state III. At that state, the hydrated cement is expected free of portlandite and the decalcification of the C-S-H phases lowers their Ca/Si ratio. Note that this study is ongoing and only the first set of results are shown.

2 Materials and methods

2.1 Materials

2.1.1 Cellulosic tissues

The cellulosic tissues (Extra Soft Tork Facial Tissues) used in the degradation study were all part of the same batch (number 2211191/4), to avoid differences in the composition and cellulose properties between batches. The composition of the tissues was determined by PTS (Papiertechnische Stiftung), according to the standard procedures in Table 1.

Table 1: Overview of the composition of the cellulosic tissues and the procedures used. The average content is derived from two measurements. The indicated uncertainty has been calculated using the Student's *t* test for 95% confidence.

Component	Average content (wt%)	Procedure
Dry content	95.6 ± 1.9	Using an infrared moisture analysis balance
α-cellulose	88.1 ± 0.6 ^a	Adapted from TAPPI standard T203 cm-99 (TAPPI, 2009)
Hemicellulose	11.4 ± 0.4 ^a	Based on alkaline solubility S ₅ (DIN54356) (DIN, 1977)
Lignin	0.5 ± 0 ^a	TAPPI standard T222 om-21 (TAPPI, 2021)
Inorganic additives	0.54 ± 0 ^a	ISO standard 1762 (ISO, 2019)

^a expressed in g per 100 g dry material

2.1.2 CEM I hardened cement paste

The sorption experiments were performed on a CEM I hardened cement paste (HCP) degraded to state III. The cement paste was prepared from a batch of CEM I 52.5 N. The cement powder was mixed with water at a water/cement ratio of 0.5 and transferred to a PVC tube. To avoid the formation of air bubbles, gas was released by vibration before the tube was closed and sealed. Segregation was prevented by rotating the tube for 12 to 24 h after sealing. The tube was then stored in a hydration chamber (95% relative humidity, 20-22 °C) for the entire hydration period, which lasted for a minimum of 3 months.

At the end of the hydration period, the PVC tube was cut with a diamond saw. The CEM I HCP was crushed and sieved to grain sizes smaller than 74 μm under inert atmosphere (in a glovebox with N_2 atmosphere with an O_2 concentration $< 0.0002 \text{ vol}\%$). The cement powder was degraded to state III by dynamic leaching in ultrapure water. In the glovebox, 1.2 g of cement powder was mixed with 220 mL of degassed ultrapure water in a 250 mL centrifuge bottle (Nalgene, Millipore). The mixture was shaken for 3 days on an orbital shaker and centrifuged for 2 h at $20\,000 \times g$. After these 3 days, 200 mL of the supernatant were discarded and replaced by 200 mL of fresh degassed water, inside the glovebox. The solid was resuspended by thorough hand shaking or if needed by use of a vortex, and the whole procedure (shaking, centrifugation, and solution renewal) was repeated five consecutive times. After the last centrifugation step, the supernatant was sampled, filtered at 0.2 μm (through a nylon membrane) and stored under inert atmosphere (N_2) until further use. It is referred to as DCW (Degraded Cement Water). The degraded cement was recovered, freeze dried and also stored under inert atmosphere (N_2) until further use. It is referred to as ACP (Aged Cement Powder). The leaching procedure has a global yield of $\sim 30 \text{ wt}\%$ and was repeated several times to collect enough ACP. The DCW solution is assumed to be in equilibrium with ACP and representative of degradation state III. Its composition, reported in Table 2, was determined by ionic chromatography and inductively coupled plasma atomic emission spectroscopy (ICP-OES), both performed by the Department of Earth and Environmental Science, Section Geology of KU Leuven (Belgium). The composition of ACP, reported in Table 3, was determined by quantitative XRD measurements performed on a Bruker D8 Advance diffractometer with ZnO as internal standard. The data quantification was done with the Rietveld refinement method. The specific surface area of ACP was determined by N_2 adsorption measurements on a Micromeritics Tristar II 3020 Surface Area Analyser and is reported in Table 3.

Table 2. Composition and pH of the Degraded Cement Water (DCW). The values are the average of four different DCW batches and the indicated uncertainty corresponds to the standard deviation. n.m= not measured.

pH	11.4-11.6
Ca (mol L^{-1})	$(1.7 \pm 0.3) \times 10^{-3}$
Si (mol L^{-1})	$(2.5 \pm 0.3) \times 10^{-4}$
Al (mol L^{-1})	$(4.8 \pm 0.4) \times 10^{-5}$
Na (mol L^{-1})	n.m
K (mol L^{-1})	$(4.3 \pm 1.0) \times 10^{-6}$
SO_4^{2-} (mol L^{-1})	$(2.5 \pm 1.0) \times 10^{-4}$

Table 3. XRD Composition and BET surface area of the Aged Cement Powder (ACP).

BET surface area (m² g⁻¹)	36.4
Clinker (wt%)	1.8
Ettringite (wt%)	0.0
AFm (wt%)	0.8
Hydrogarnet (wt%)	4.6
Portlandite (wt%)	0.0
Quartz (wt%)	0.2
Amorphous (wt%)	92.5

2.1.3 Synthesis of α -ISA

Ca-(α -ISA)₂ was synthesised according to the protocol reported by Vercammen *et al.* (1999) and Van Loon and Glaus (1998), with some minor modifications. Only the major steps are reported here. In the glovebox with N₂, a mixture of D-lactose monohydrate (ACS grade, Merck) and Ca(OH)₂ in degassed ultrapure water was stirred for 48 h and then boiled for 6 h with reflux. The hot solution was filtered over a 0.8 μ m nylon filter to filter out the unreacted Ca(OH)₂ and D-lactose. The filtrate was reduced by boiling to ~20 % of its initial volume and was stored overnight at 4 °C to allow the crystallisation of Ca-(α -ISA)₂. The formed precipitate was resuspended in a small volume of ultrapure water and filtered on a 0.8 μ m nylon filter. The recovered solid was further washed twice with ethanol absolute (ACS grade, Merck) and dried overnight at 55 °C. It was then redissolved in ultrapure water by boiling (ca. 1 g per 100 mL of water) and filtered on a 0.8 μ m nylon filter. The volume of solution was reduced to ~10 % and stored overnight at 4 °C. The white precipitate was washed consecutively with ultrapure water, twice with ethanol absolute (ACS grade, Merck) and twice with acetone (HPLC grade, Merck).

The obtained Ca-(α -ISA)₂ was then converted to Na- α -ISA using a Chelex®-100 (BioRad) resin with *ca.* 25 g of resin for 1 g of Ca-(α -ISA)₂. The suspension was filtered with 0.2 μ m nylon filters to remove the resin and the filtrate was evaporated until obtaining a syrup. Finally, the water was removed by washing with di-ethylether (analytical grade, Merck) and drying at 55 °C. The molal yield of the whole procedure is 12-13%.

A stock solution, referred to as ‘Na- α -ISA_0’ and containing 0.96 mol L⁻¹ Na- α -ISA, was prepared in degassed ultrapure water, analysed and stored at -20 °C until further use. The purity of the synthesised Na- α -ISA was assessed by analysis of the Na- α -ISA_0 solution with Electrospray Ionisation Mass Spectrometry (ESI-MS), ionic chromatography (IC) with a CarboPac PA-100 column (Dionex) and Pulse Amperometric detection (PAD), and TOC/TIC analyses with a TOC-L (Shimadzu) carbon analyser and was found to be pure α -ISA.

2.2 Irradiation

Gamma-irradiation was performed at the Geuse II facility of the Belgian Nuclear Research Centre (SCK CEN, Mol, Belgium) in between spent fuel assemblies of the BR2 reactor (Fernandez *et al.*, 2002).

For this, 15 to 100 g of tissues were placed inside gas-tight stainless steel cylindrical containers (inner volume 1.2 L). After filling and closing of the containers, the headspace was replaced by pure argon (99.9997%, Air Products) or compressed air (20.9 vol% O₂ and 79.1 vol% N₂, Air Products) by extensive flushing. Gas pressures at the start of the irradiation were 0.2 – 0.3 MPa.

Mean dose rates and absorbed doses were determined based on the results of four dosimetries performed throughout the irradiation, *i.e.* at the start, after ~2.5 months, after 4 months and at the end of the irradiation (after 5.5 months). This dosimetry was performed with Amber (type 3042) Perspex (polymethylmethachrylate) dosimeters (Harwell Dosimeters), according to the ISO/ASTM standard on the practice for dosimetry in radiation processing (ISO/ASTM, 2013).

The total absorbed doses ranged from 10 kGy to 1.4 MGy (Table 4). For those tissues irradiated with a total absorbed dose of 0.05 MGy and 0.8 MGy, the effect of the dose rate (0.3 vs 0.6 kGy h⁻¹) and of the presence of O₂ during irradiation, was studied as well (Table 4).

Table 4: Gamma irradiation conditions. The uncertainty on the measured weight is 0.08 g (for 95% confidence). The uncertainties on the dose and dose rate are calculated as combined uncertainties, taking into account the uncertainty on the measured dose rates during the dosimetries and uncertainty on the exponential fit of the decay curve.

Test code	Weight tissues (g)	Mean total absorbed dose (kGy)	Mean dose rate (kGy h ⁻¹)	Atmosphere during irradiation
C1	101.2	10 ± 2	0.63 ± 0.14	Ar
C2	100.2	47 ± 11	0.63 ± 0.14	Ar
C3	100.3	47 ± 11	0.63 ± 0.14	Air ^a
C4	101.2	48 ± 7	0.34 ± 0.05	Ar
C5	100.9	48 ± 7	0.34 ± 0.05	Air ^a
C6	101.2	180 ± 40	0.69 ± 0.16	Ar
C7	100.9	352 ± 56	0.67 ± 0.11	Ar
C8	100.9	760 ± 92	0.62 ± 0.08	Ar
C9	15.5	760 ± 92	0.62 ± 0.08	Air ^a
C10	100.0	764 ± 91	0.31 ± 0.04	Ar
C11	15.0	764 ± 91	0.31 ± 0.04	Air ^a
C12	40.4	1368 ± 160	0.55 ± 0.06	Ar

^a compressed air: 20.9 vol% O₂ and 79.1 vol% N₂

2.3 Degradation of cellulose tissues under alkaline conditions

To study the release of organics from non-irradiated and irradiated cellulosic tissues, suspensions of (non-)irradiated cellulose (cut in small pieces of a few cm²) were prepared in artificial young cement water (ACW; 0.114 M NaOH, 0.18 M KOH saturated with Ca(OH)₂, pH >13 (Glaus and Van Loon, 2008; Van Loon and Glaus, 1998)), at a tissue-to-liquid ratio of 100 g L⁻¹. Replicates were prepared for all test conditions, in order to sacrifice one of them at each sampling time. Sampling was performed after 1-2 hours, after 1 week, after 1 month and after 3 months. For each sampling, the suspensions were

filtered using a PTFE filter (0.45 µm pore size) inside a MILLICUP-FLEX™ filtration system (Merck Life Science). Afterwards, DOC (dissolved organic carbon) and ISA concentrations were determined, with a TOC/TIC analyser using the combustion and acidification method, and with IC-PAD, respectively. The analysis method used in IC-PAD allows discriminating and quantifying the two ISA isomers (α and β). pH measurements were performed on each sampled solution using an InLab® Mono pH electrode (Mettler-Toledo), which was calibrated before each use with buffers at pH 7 and pH 13 (Hanna instruments).

To avoid organic leaching from materials other than the tissues, all suspensions were prepared in opaque PTFE bottles (180 mL, Vitlab). Furthermore, blanks (ACW without tissues in PTFE bottles) were prepared as well, confirming no significant leaching of organics up to 3 months. All tests were conducted under anoxic conditions (inside a glovebox with Ar atmosphere with an O₂ concentration < 0.0005 vol%) and at room temperature. In addition, all bottles were kept in the dark to avoid photo-induced reactions. No special precautions were taken to keep the systems sterile, though at each sampling time, additional samples were taken to verify sterility using flow cytometry. Up to 3 months, no microbial growth was observed in the test solutions.

2.4 Sorption of α -ISA on degraded Portland cement

The sorption of Na- α -ISA on ACP was investigated in DCW over a range of concentrations from 2×10^{-5} to 2×10^{-2} mol L⁻¹ at a solid-to-liquid ratio of 25.6 ± 0.5 g L⁻¹. All the experimental steps but the centrifugation were performed under Ar atmosphere (with an O₂ concentration lower than 0.0002 vol%).

Two sub-dilutions of Na- α -ISA_0 were prepared in 0.003 M NaOH to a concentration of $(4.0 \pm 0.6) \times 10^{-2}$ and $(8 \pm 1) \times 10^{-3}$ mol L⁻¹ and referred to as Na- α -ISA_1 and Na- α -ISA_2, respectively. To avoid the presence of potential colloids, DCW was ultrafiltered at 30 kDa (polyether sulfone membranes, Millipore). In 50 mL centrifuge tubes (Nalgene, Millipore), 0.18 g of ACP was suspended in 7 mL of ultrafiltered DCW. The suspensions were allowed to equilibrate under agitation for 24 h and aliquots of Na- α -ISA_1 or Na- α -ISA_2 were added to the suspensions to reach concentrations ranging from 2×10^{-5} to 2×10^{-2} mol L⁻¹. The pH of the suspensions was measured and the average pH was 11.59 ± 0.03 . The suspensions were shaken on an orbital shaker for 21 days before centrifugation for 1 h at $20\,000 \times g$. In agreement with the results of Van Loon et al. (1997), a contact time of 21 days was assumed sufficient to reach an apparent sorption equilibrium. After 21 days, the supernatants were sampled, the pH measured and the solution analysed by IC-PAD for α -ISA concentrations. The average equilibrium pH was 11.89 ± 0.14 . Three blank solutions at a concentration of $(4.0 \pm 0.6) \times 10^{-4}$ Na- α -ISA in ultrafiltered DCW, were run in parallel to the samples to follow the stability of α -ISA throughout the full procedure.

The extent of sorption of α -ISA on degraded cement was quantified by the determination of the solid/liquid distribution coefficient, R_d , calculated according to Equation 1.

$$R_d = \frac{ISA_0 - ISA_{eq}}{ISA_{eq}} \times \frac{V}{m} = \frac{ISA_s}{ISA_{eq}} \quad (1)$$

With ISA_0 (mol L⁻¹) the initial concentration in the suspension, ISA_{eq} (mol L⁻¹) the concentration measured in the supernatant after centrifugation, ISA_s (mol kg⁻¹) the concentration of α -ISA sorbed, V (L) the total volume of solution and m (kg) the mass of cement. The error on the R_d values was calculated by propagation of the experimental errors (confidence limit of 95 %) neglecting correlations.

3 Results and discussion

3.1 Degradation of pre-irradiated cellulosic tissues under alkaline conditions

Within 1 to 2 hours after contact with ACW, significant amounts of organic molecules were released from the (non-)irradiated cellulosic tissues (Figure 1). The concentration of instantaneously released organics (*i.e.* organics released within 1 to 2 hours after submersion in ACW) increased with the absorbed dose applied during pre-irradiation, under both anoxic and oxic conditions, although no additional increase in DOC concentration can be observed above 0.8 MGy. For tissues pre-irradiated at these high doses (≥ 0.8 MGy), the released DOC concentration was ~ 20 times higher compared to suspensions with non-irradiated tissues.

No statistically significant difference is found between the concentrations of DOC instantaneously released from tissues irradiated at the same absorbed dose though with a varying dose rate, *i.e.* no influence of the dose rate on the instantaneous DOC release is observed. Furthermore, although pre-irradiation at ~ 50 kGy under oxic conditions resulted in a higher DOC release ($\sim 60\%$ increase) compared to under anoxic conditions, such increase in instantaneous DOC release due to the presence of oxygen during pre-irradiation was not observed at 0.8 MGy (all DOC values within the 30% uncertainty on the measured values).

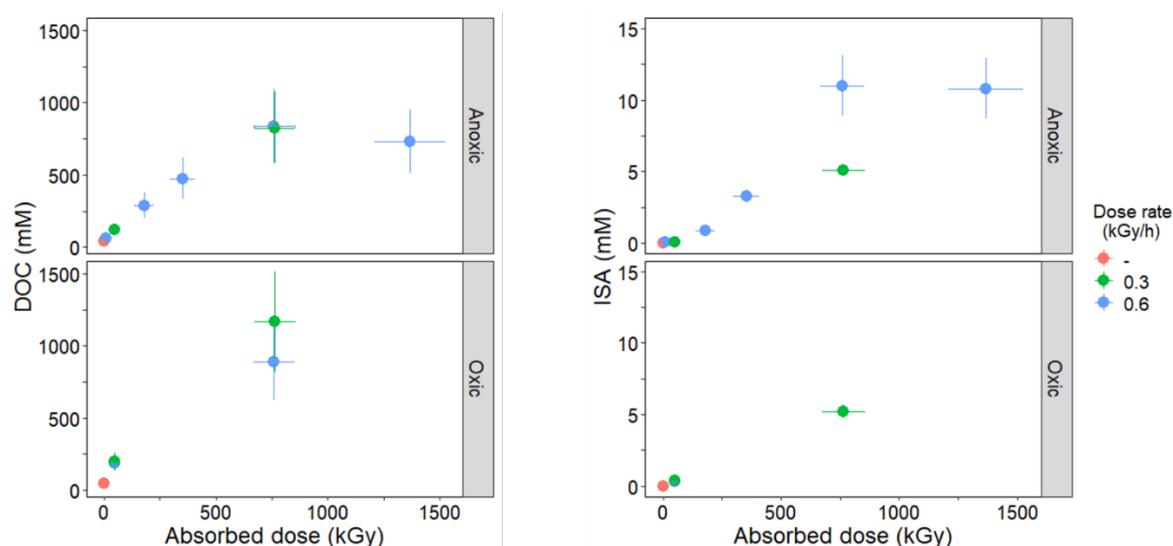


Figure 1: Instant release of dissolved organic carbon compounds (left), including ISA (right), in suspensions of (non-) irradiated cellulose in ACW (sampled after 1-2 h). Concentrations were plotted in function of the absorbed dose and the atmospheric conditions during irradiation. Different colours of the markers indicate differences in the dose rate during irradiation. The error bars represent the uncertainty for a 95% confidence interval.

Similar to the DOC, also the short-term (*i.e.* within 1-2 hours) production of ISA is strongly increased with an increasing absorbed dose (at least up to ~0.8 MGy) during pre-irradiation (Figure 1). The ISA concentration leaching from tissues irradiated at ~0.8 and 1.4 MGy (anoxic conditions; dose rate ~0.6 kGy h⁻¹) was ~620 times higher than the ISA concentration leaching from non-irradiated tissues. A significantly higher ISA concentration can be observed for tissues pre-irradiated at ~50 kGy under oxic compared to under anoxic conditions. Though again, this difference was no longer observed at higher doses. Furthermore, no consistent impact of the dose rates on the ISA production was observed.

After 1 to 2 hours, about 0.2% (non-irradiated cellulose) up to 9% (cellulose irradiated with ~1.4 MGy) of the total organic compounds in solution was ISA, with the short-term produced ISA concentrations ranging from 0.02 to 11 mM respectively (Figure 1). α - and β -ISA each made up about 50% of the total ISA content, independently of the irradiation conditions. This short-term ISA release was not observed in suspensions of irradiated tissues (C8; Table 4) in demineralised water (data not shown), demonstrating that the ISA found in the tissue suspensions in ACW was produced by rapid alkaline hydrolysis rather than radiolysis.

The main factor influencing the instantaneous DOC release and ISA production is thus the absorbed dose, while dose rate and atmospheric conditions during pre-irradiation do not have a consistent effect. Gamma irradiation is expected to result in chain scission and thus in the production of smaller cellulose chains (Ershov, 1998), each with its own reducing end group. The decrease in chain length is proportional to the increase in absorbed dose (Ershov, 1998). Furthermore, based on the mechanism of cellulose hydrolysis under alkaline conditions, a higher number of reducing end groups is expected to result in a higher ISA production rate (Glaus and Van Loon, 2008; Van Loon and Glaus, 1998). Therefore, the observed dependency of the instantaneous ISA production on the absorbed dose during pre-irradiation is in line with the expectations based on previous studies.

The ISA concentrations released from non-irradiated and irradiated cellulose tissues (pre-irradiated under anoxic conditions; dose rate ~0.6 kGy h⁻¹) in ACW were monitored further up to 3 months, as shown in Figure 2. The pH of all suspensions remained above 13 (data not shown).

The results show a clear increase of the ISA concentrations in time for all test cases. In addition, for each sampling time, the ISA concentrations increased with increasing absorbed dose. Again, this can be linked to the decrease in chain length with increasing absorbed dose during irradiation (Ershov, 1998). Similar to the instantaneous release, α - and β -ISA were found in equimolar amounts, independently of the absorbed dose. For the irradiated tissues (especially those irradiated at high absorbed doses), the ISA production started to level off after 3 months. This levelling off is not yet observed for non-irradiated tissues, though also for these tests, this behaviour is expected on the long term, based on literature data available for pure cellulose and cellulosic paper or tissues (Glaus and Van Loon, 2008; Van Loon and Glaus, 1998).

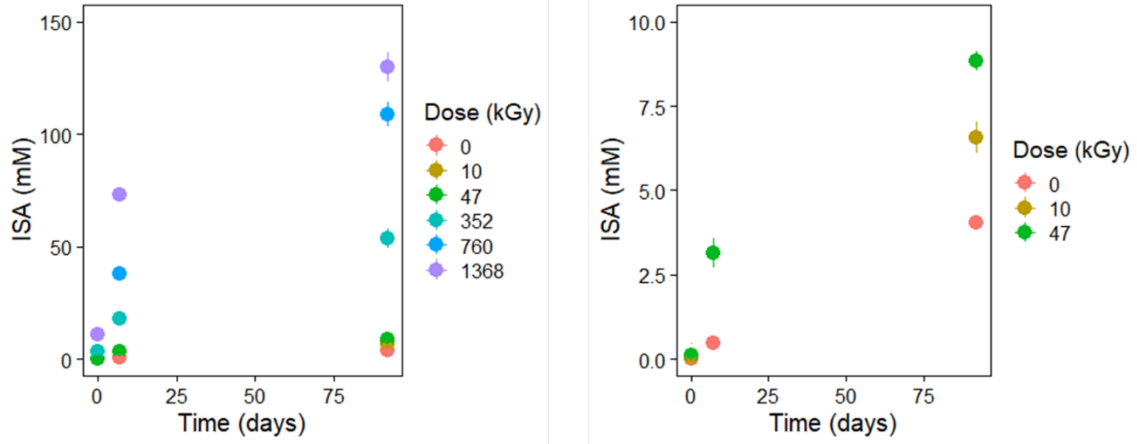


Figure 2: Evolution of ISA concentrations as a function of time, in suspensions of (non-) irradiated cellulose in ACW. Pre-irradiation was performed under anoxic conditions at different absorbed doses (see legend) and at a dose rate of $\sim 0.6 \text{ kGy h}^{-1}$. Left: all test conditions; Right: only tests with non-irradiated tissues or with tissues irradiated at low doses are shown. The error bars represent the uncertainty for a 95% confidence interval.

3.2 Sorption of α -ISA on cement

The sorption isotherm of α -ISA on ACP is reported in Figure 3 together with the evolution of the R_d values in function of the α -ISA equilibrium concentrations. The experimental sorption isotherm shows a stabilisation of the α -ISA uptake at an equilibrium concentration higher than $2 \times 10^{-4} \text{ mol L}^{-1}$, indicating saturation of the sorption sites. The absence of a second inflection point in the sorption isotherm suggests that the uptake of α -ISA in the presently studied concentration range occurs mainly on a single sorption site. However, due to the high uncertainty associated with the highest concentration point, the contribution of a second sorption site cannot be ruled out and extra experimental data are needed to confirm or disprove this. The calculated R_d values reached a maximum value of $109 \pm 67 \text{ L kg}^{-1}$, suggesting a mild α -ISA sorption on CEM I degraded to state III. The sorption isotherm and the R_d evolution are well described with a 1-site Langmuir isotherm (Equation 2):

$$ISA_s = \frac{S_{tot} \times K_L \times ISA_{eq}}{1 + K_L \times ISA_{eq}} \quad (2)$$

with S_{tot} (mol kg^{-1}) the sorption site capacity and K_L (L mol^{-1}) the adsorption affinity constant.

The optimisation of the site capacity and the adsorption affinity constant on the R_d experimental values using the minimisation of least square errors led to values of $(1.2 \pm 0.3) \times 10^{-2} \text{ mol kg}^{-1}$ and $(8.02 \pm 2.34) \times 10^3 \text{ L mol}^{-1}$, respectively.

In Figure 3, the experimental data and modelled Langmuir isotherm are compared with the 2-sites Langmuir isotherm used by Van Loon et al. (1997). The authors investigated the sorption of α -ISA on fresh CEM I HCP at pH 13.3. This comparison reveals a lower sorption of α -ISA on the degraded cement (state III) than on the fresh CEM I. Sorption of α -ISA on C-S-H phases via cation bridging with Ca^{2+} was proposed as the dominant sorption mechanism by several authors (Bruno et al., 2018; García et al., 2020; Pointeau et al., 2008). Pointeau et al. (2008) showed that the sorption of α -ISA was dependent on the pH and calcium concentration of the cement system with the highest sorption observed

at pH 12.5. The concentration of calcium in DCW is sensibly the same as in the solutions of Van Loon et al. (1997), *i.e.* 2 mmol L⁻¹. However, according to the model of Pointeau et al. (2008), the lower pH used in the present study would lead to a lower deprotonation of the C-S-H surface sites, thereby decreasing the sorption of α -ISA via cation bridging, which could explain the difference in sorption observed between our study and Van Loon et al. (1997). On the other hand, the lower sorption observed in our study could also be linked to the partial decalcification of the C-S-H occurring during leaching. Indeed, García et al. (2020) observed a decrease of Rd values with a decrease of the Ca/Si ratio of the investigated C-S-H phases. Due to decalcification, the zeta potential of the C-S-H is expected to decrease, which could limit the sorption of α -ISA as well. Unfortunately, at this stage of the study neither the zeta potential nor the Ca/Si ratio of the C-S-H present in ACP have been measured.

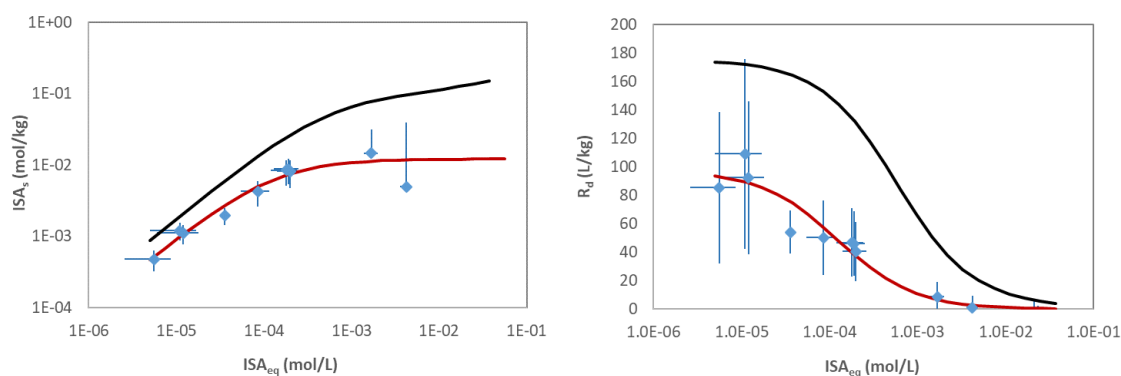


Figure 3. Sorption isotherms of α -ISA (left) and solid-liquid distribution ratio (R_d) as a function of α -ISA concentration (right), on ACP in DCW solution at a solid-liquid ratio of 25.6 ± 0.5 g/L and for 21 days of contact. The red curves correspond to the 1-site Langmuir model optimised on the experimental data points. The black curves correspond to the 2-sites Langmuir model reported by Van Loon et al. (1997).

4 Conclusion

In this study, the effect of pre-irradiation of cellulosic tissues on the production of soluble degradation products, and more specifically ISA, under alkaline conditions was investigated, as well as the sorption of α -ISA on cementitious materials.

The pre-irradiation of cellulosic tissues was shown to enhance the instantaneous release of organic carbon and to favour the production of ISA during hydrolytic degradation at highly alkaline pH. The dose rate applied during irradiation did not affect the short-term degradation rate of the tissues in ACW. On the other hand, the presence of oxygen during irradiation was observed to have an impact on the hydrolytic degradation, but only at low absorbed doses. The effect of pre-irradiation on the short-term hydrolytic degradation can thus mainly be attributed to the absorbed dose applied during irradiation. Over the course of 3 months, the effect of the absorbed dose during pre-irradiation on the ISA production rates was maintained, *i.e.* higher ISA production rates and yields were obtained for tissues pre-irradiated at higher absorbed doses. This effect of pre-irradiation can be attributed to radiolytic chain scission and consequently to the generation of more reducing end groups per gram tissue, each participating in the hydrolytic degradation reactions to produce ISA. Under all test conditions of the degradation study, the isomeric ratio of ISA was constant, *i.e.* α and β -ISA isomers were produced equally. This indicates that pre-irradiation does not favour production of one of the isomers.

The sorption of α -ISA was investigated on Portland cement degraded to state III. At that state, the hydrated cement is free of portlandite and the decalcification of the C-S-H phases lowers their Ca/Si ratio. α -ISA sorption on the degraded cement was found to follow a one-site Langmuir sorption isotherm with a mild uptake showing a maximum solid/liquid distribution ratio of $109 \pm 67 \text{ L kg}^{-1}$. A comparison of the obtained results with the results published on fresh Portland cement highlighted the lower sorption of α -ISA on cement degraded to state III. This can be attributed to both the lowering of the pH and the decalcification of the C-S-H phases at state III, which limits the formation of cation bridging and as such the sorption of α -ISA.

5 Future work

To assess the sorption of α -ISA in a compact system and the resulting α -ISA mobility in degraded Portland cement, the transport of α -ISA is intended to be investigated in lab-scale diffusion experiments on degraded cement discs. Furthermore, the effect of pre-irradiation on the hydrolytic degradation of cellulosic tissues will continue, in order to investigate the degradation rates and yields on the long term.

Acknowledgements

The EURAD-CORI project leading to this application has received funding from the European Union's Horizon 2020 research and innovation programme under grant agreement No 847593. Furthermore, it has been performed in the broader framework of a public-public cooperation between ONDRAF/NIRAS and SCK CEN. The technical and analytical support from the RCA unit and the Geuse II irradiation team at SCK CEN is highly appreciated.

References

- Allard, S. and Ekberg, C. (2006) Complexing properties of alpha-isosaccharinate: Stability constants, enthalpies and entropies of Th-complexation with uncertainty analysis. *J. Solut. Chem.* 35, 1173-1186.
- Arthur, J.C. (1958) Part II: Proposed mechanism of the effects of high energy gamma radiation on some of the molecular properties of purified cotton. *Text. Res. J.* 28, 204-206.
- Arthur, J.C. (1971) Reactions induced by high energy radiation. In: N.M. Bikales and L. Segal (Eds.), *Cellulose and cellulose derivatives*. Wiley Interscience, pp. 937-975.
- Bleyen, N. (2020) Degradation of cellulose under disposal conditions. State-of-the-art report. External Report SCK CEN-ER-0791, SCK CEN, Mol, Belgium.
- Bruno, J., González-Siso, M.R., Duro, L., Gaona, X. and Altmaier, M. (2018) Key master variables affecting the mobility of Ni, Pu, Tc and U in the near field of the SFR repository. Main experimental findings and PA implications of the PhD thesis. SKB Technical Report TR-18-01. Svensk Kärnbränslehantering AB Solna, Sweden.
- Charlesby, J.A. (1955) The degradation of cellulose by ionizing radiation. *J. Polym. Sci.* 15, 263-270.
- DIN (1977) Testing of Pulp - Determination of the alkali solubility of pulp. DIN standard 54356, pp. 4.
- Ershov, B.G. (1998) Radiation-chemical destruction of cellulose and other polysaccharides. *Russ. Chem. Rev.* 67, 353-375.
- Fernandez, A., Ooms, H., Brichard, B., Coeck, M., Coenen, S. and Berghmans, F. (2002) Test facilities at SCK CEN for radiation tolerance assessment: From space applications to fusion environments. *Proceedings of the RADECS 2002 Workshop*, 200-204.

- Gaona, X., Montoya, V., Colàs, E., Grivé, M. and Duro, L. (2008) Review of the complexation of tetravalent actinides by ISA and gluconate under alkaline to hyperalkaline conditions. *J. Contam. Hydrol.* 102, 217-227.
- García, D., Henocq, P., Riba, O., López-García, M., Madé, B. and Robinet, J.-C. (2020) Adsorption behaviour of isosaccharinic acid onto cementitious materials. *Appl. Geochem.* 118, 104625.
- Gentile, V.M., Schroeder, L.R. and Atalla, R.H. (1987) Physical structure and alkaline degradation of hydrocellulose. In: R.H. Atalla (Ed.), *The structures of cellulose*. American Chemical Society, pp. 272-291.
- Glaus, M.A. and Van Loon, L.R. (2008) Degradation of cellulose under alkaline conditions: New insights from a 12 years degradation study. *Environ. Sci. Technol.* 42, 2906-2911.
- Haas, D.W., Hrutford, B.F. and Sarkanen, K.V. (1967) Kinetic study on the alkaline degradation of cotton hydrocellulose. *J. Appl. Polym. Sci.* 11, 587-600.
- Ioelovich, M. (2009) Accessibility and crystallinity of cellulose. *Bioresources* 4, 1168-1177.
- Jacques, D., Perko, J., Seetharam, S.C. and Mallants, D. (2014). A cement degradation model for evaluating the evolution of retardation factors in radionuclide leaching models. *Appl. Geochem.* 49, 143-158.
- ISO (2019) Paper, board, pulps and cellulose nanomaterials - Determination of residue (ash content) on ignition at 525 °C. ISO standard 1762, pp. 9.
- ISO/ASTM (2013) Practice for dosimetry in radiation processing. ISO/ASTM standard 1762, pp. 13.
- Lai, Y.-Z. and Sarkanen, K.V. (1967) Kinetics of alkaline hydrolysis of glycosidic bonds in cotton cellulose. *Cellul. Chem. Technol.* 1, 517-527.
- Mittal, A., Katahira, R., Himmel, M.E. and Johnson, D.K. (2011) Effects of alkaline or liquid-ammonia treatment on crystalline cellulose: Changes in crystalline structure and effects on enzymatic digestibility. *Biotechnol. Biofuels* 4, 41.
- ONDRAF/NIRAS (2013) ONDRAF/NIRAS research, development and demonstration (RD&D) plan for the geological disposal of high-level and/or long-lived radioactive waste including irradiated fuel if considered as waste. NIRAS/ONDRAF Technical Report NIROND-TR-2013-12 E, ONDRAF/NIRAS, Brussels, Belgium.
- ONDRAF/NIRAS (2019) Hoofdstuk 14 uit het veiligheidsrapport voor de oppervlaktebergingsinrichting van categorie A-afval in Dessel: Veiligheidsevaluatie - langetermijnveiligheid. NIRAS/ONDRAF Technical Report NIROND-TR 2011-14N Versie 3, ONDRAF/NIRAS, Brussels, Belgium.
- Pointeau, I., Coreau, N. and Reiller, P.E. (2008) Uptake of anionic radionuclides onto degraded cement pastes and competing effect of organic ligands. *Radiochim. Acta* 96, 367-374.
- Pointeau, I., Reiller, P., Macé, N., Landesman, C. and Coreau, N. (2006) Measurement and modeling of the surface potential evolution of hydrated cement pastes as a function of degradation. *J. Colloid Interface Sci.* 300, 33-44.
- TAPPI (2009) Alpha-, beta- and gamma-cellulose in pulp. TAPPI standard T 203 cm-09, pp. 5.
- TAPPI (2021) Acid-insoluble lignin in wood and pulp. TAPPI standard T 222 om-21, pp. 5.
- Van Loon, L.R. and Glaus, M.A. (1998) Experimental and theoretical studies on alkaline degradation of cellulose and its impact on the sorption of radionuclides. PSI Bericht Nr. 98-07, Paul Scherrer Institut, Villigen, Switzerland.
- Van Loon, L.R., Glaus, M.A., Laube, A. and Stallone, S. (1999) Degradation of cellulosic materials under the alkaline conditions of a cementitious repository for low- and intermediate level radioactive waste. Part III: Effect of degradation products on the sorption of radionuclides on feldspar. *Radiochim. Acta* 86, 183-189.
- Van Loon, L.R., Glaus, M.A., Stallone, S. and Laube, A. (1997) Sorption of isosaccharinic acid, a cellulose degradation product, on cement. *Environ. Sci. Technol.* 31, 1243-1245.
- Vercammen, K., Glaus, M.A. and Van Loon, L.R. (1999) Complexation of calcium by alpha-isosaccharinic acid under alkaline conditions. *Acta Chem. Scand.* 53, 241-246.

Influence of gluconate on the retention of Eu(III), Th(IV), and U(VI) by C-S-H

Sophie Dettmann¹, Nina Huittinen², Jérôme Kretzschmar², Michael U. Kumke^{1*}, Tobias Reich^{3*}, Katja Schmeide^{2*}, Leon Spittler³, Janina Stietz³

¹ University of Potsdam, Institute of Chemistry, Karl-Liebknecht-Str. 24-25, 14476 Potsdam (Germany)

² Helmholtz-Zentrum Dresden - Rossendorf, Institute of Resource Ecology, Bautzner Landstraße 400, 01328 Dresden (Germany)

³ Johannes Gutenberg-Universität Mainz, Department of Chemistry, Fritz-Strassmann-Weg 2, 55128 Mainz (Germany)

* Corresponding authors: kumke@uni-potsdam.de, reich@uni-mainz.de, k.schmeide@hzdr.de

Abstract

The retention of radionuclides in different oxidation states (Rn(X)) by a calcium-silicate-hydrate (C-S-H) phase with a Ca:Si (C:S) ratio of 0.8 in the presence of gluconate (GLU) was investigated. The elements considered were Th(IV), U(VI), as well as Eu(III) as chemical analogue for Cm(III) and Am(III). In addition to the ternary systems Rn(X)/C-S-H/GLU, also binary systems Rn(X)/C-S-H and C-S-H/GLU were studied. Complementary analytical techniques were applied to address the different specific aspects of the ternary systems. Time-resolved laser-induced fluorescence spectroscopy (TRLFS) was applied in combination with PARAFAC analysis to identify retained species and to monitor species-selective sorption kinetics. ²⁹Si magic-angle-spinning (MAS) nuclear magnetic resonance (NMR) spectroscopy and X-ray photoelectron spectroscopy (XPS) were applied to determine the bulk structure and the composition of the C-S-H surface, respectively, in the absence and presence of GLU. The influence of GLU was investigated for a large concentration range up to 10⁻¹ M. The results showed, first, that GLU had little to no effect on Rn(X) retention by C-S-H with C:S of 0.8, regardless of the oxidation state of the radionuclides, and second, that GLU had an effect on Rn(X) speciation in the solid phase, as shown for Eu(III).

1 Introduction

Calcium-silicate-hydrate (C-S-H) phases are the major components in cement and are key players in the retention process of metal ions in general (radionuclides in particular). C-S-H phases are formed in the first weeks of cement hydration and undergo a transition in their composition over time due to pore water exchange. They are nanocrystalline but amorphous on the micro/macro scale. Basic building elements are a CaO layer and an interlayer, in which water and exchangeable Ca(II) ions are located. The retention of radionuclides depends on the specific oxidation state / speciation. The CaO layer as well as the interlayer and the surface of C-S-H phases are involved in sorption processes [1]. Edges, defects and the exchange for Ca(II) in both layers are contributing to the overall sorption, but with differences in the kinetics and in the strength of interaction. In fresh cement the C:S ratio is high with values around 1.6 – 1.8, but with time (years to hundreds of years) pore water is exchanged and the C:S ratio is lowered down to 0.6 – 0.8 due to loss of Ca(II). Accompanied with the decrease of the C:S ratio

is also a drop in the pH value of the pore water from 12.5 down to < 10. The loss of Ca(II) from the interlayer is accompanied by structural changes, which lead to less bridging between the SiO₂ tetrahedra of the C-S-H phases. The decrease of the Ca(II) concentration and the structural changes also alter the sorption of radionuclides. The complexity of the interaction between radionuclides (Rn(X)) and C-S-H is further increased by the presence of organic molecules. Low and high molecular weight organic molecules originate from the waste itself (e.g., tissue paper etc.) or are additives of the cement, which were added to control the physical-chemical properties during the processing. These organic molecules may alter the retention of Rn(X) either by competition (surface complexation vs. complex formation) or by blocking surface groups for radionuclide complexation or by formation of mixed complexes [2-6].

Here, we report results of our joint effort on the investigation of the retention of selected radionuclides (Rn(X): Eu(III), Th(IV), and U(VI)) by C-S-H in the presence of gluconic acid (GLU). The C:S ratio was adjusted to 0.8, representing a situation of aged cement (pH 9.5). GLU was used as a proxy for isosaccharinic acid (ISA) and as a model compound for cement additives [7, 8], respectively. We have investigated the influence of the concentration of GLU in the range of $0 \text{ M} < c_0(\text{GLU}) < 1 \times 10^{-1} \text{ M}$. In our experiments we investigated actinides (or their analogues) in different oxidation states to elucidate differences in the retention. Various experimental techniques, such as time-resolved laser-induced fluorescence spectroscopy (TRLFS), X-ray photoelectron spectroscopy (XPS), ²⁹Si magic-angle-spinning (MAS) nuclear magnetic resonance (NMR) spectroscopy, inductively coupled plasma-mass spectrometry (ICP-MS) and liquid scintillation counting (LSC), were applied to qualitatively and quantitatively monitor the retention of Rn(X) and/or GLU and to characterize the C-S-H phases before and after Rn(X) and/or GLU retention experiments.

2 Experimental section

2.1 Sample preparation

The syntheses and retention experiments were performed in glove boxes under N₂ or Ar atmosphere.

Th(IV) experiments: The "direct reaction method" [9] was used to prepare amorphous C-S-H phases (C:S = 0.8) using CaO (Thermo Fischer GmbH, Kandel, Germany) and SiO₂ (Aerosil 300, Evonik Industries AG, Essen, Germany). Depending on the desired solid to liquid (S/L) ratio, the corresponding amounts of the reactants were weighed into 10 mL polycarbonate centrifuge tubes (Beckman Coulter, Brea, USA). The S/L ratio achieved in the samples was determined from the dry weight of the solids formed. The background solution was MilliQ water (18.2 MΩ cm, Millipore, Billerica, USA) degassed with Ar. The pH values were measured using an inoLab pH/Cond 720 (WTW, Weilheim, Germany), which was connected to a BlueLine 16 pH electrode (Schott Instruments, Schott AG, Mainz, Germany). As an electrolyte, 3 M KCl (Mettler-Toledo AG, Urdorf, Switzerland) was used. Calibration was performed using reference buffer solutions as three-point calibrations with the pH values 6.87 (SI Analytics, Weilheim, Germany), 4.01 and 9.18 (Merck, Darmstadt, Germany).

The C-S-H phases formed during a period of two weeks where the centrifuge tubes were rotated in an end-over-end rotator (Stuart Rotator SB3, Bibby Scientific Limited, Stone, UK). After the C-S-H synthesis, aliquots of the respective stock solutions of GLU and/or Th(IV) were added. A stock solution of 3.7 MBq/mL ¹⁴C-GLU (Hartmann Analytic, Braunschweig, Germany) was diluted in MilliQ water to the various concentrations used in the batch sorption experiments of the binary system. In addition, an inactive GLU stock solution was prepared by weighing the appropriate amount of sodium gluconate (Sigma Aldrich, St. Louis, USA) and dissolving it in MilliQ water. An aliquot of a ²³²Th ICP-MS standard (SPS Science, Baie D'Urfé, Montreal, Quebec, Canada) was diluted in 2% HNO₃ to achieve the initial concentration of $1 \times 10^{-8} \text{ M}$ Th(IV) in the batch experiments. The contact time in the batch

sorption experiments of the binary system was 72 h. In the case of experiments with the ternary system, where the order of reactant addition was varied, the contact time was first 72 h with GLU or with Th(IV), followed by the addition of the remaining component or the simultaneous addition of Th(IV) and GLU, also for a contact time of 72 h. Samples were precentrifuged at $3,770\times g$ (SIGMA 3K30, SIGMA Laborzentrifugen GmbH, Osterode, Germany) for 5 min and ultracentrifuged at $108,800\times g$ (Avanti J-30I, Beckman-Coulter, Brea, USA) for 1 h. The pH of each suspension was then determined.

U(VI) experiments: A U(VI)-doped C-S-H phase with a C/S ratio of 0.8 was prepared directly by suspending 411 mg carbonate-free CaO (anhydrous, 99.99%, Sigma-Aldrich, Missouri, USA) and 550 mg fumed silica (Aerosil 300, Evonik Industries AG, Essen, Germany) in 40 mL degassed deionized water within a 50 mL centrifuge tube (polypropylene, Greiner bio-one, Kremsmünster, Austria). Immediately after that, an aliquot of a $^{238}\text{U(VI)}$ stock solution (1×10^{-3} M UO_2Cl_2 in 0.005 M HCl) was added to the suspension. The initial U(VI) concentration was 2×10^{-5} M, the S/L ratio was 24 g/L. The sample was equilibrated using an end-over-end rotator (Stuart Rotator SB3) for 67 days, during which the U(VI)-doped C-S-H phase formed. The final pH value and U(VI) loading were 10.8 and 198 mg/kg, respectively. The C-S-H phase with a C:S ratio of 1.2, used for NMR studies, was prepared in the same way, but with adjusted amounts of reactants. For further U(VI) and GLU sorption experiments, U(VI)-free C-S-H phases were also prepared by the same procedure. For phase separation, the suspensions were centrifuged at $6,800\times g$ for 30 min (mod. Avanti J-20 XP, Beckman Coulter, Krefeld, Germany), and the solid phases isolated. The powders were left to dry to constant weight under N_2 atmosphere at room temperature (RT) and stored inside the glove box. To study the influence of GLU on U(VI) retention, the U(VI)-doped C-S-H phase was equilibrated in 1×10^{-3} M or 1×10^{-2} M gluconate solutions (sodium gluconate (Sigma Aldrich, St. Louis, USA)) for 4 months. The S/L ratio was 10 g/L. The U(VI) concentration in the supernatant solution was determined by ICP-MS (NexION 350X/Elan 9000, PerkinElmer, USA).

Eu(III) experiments: The C-S-H phases were synthesized by mixing 85.5 mg CaO (nanoparticles ($d < 160$ nm), 98%, Sigma Aldrich, Missouri, USA) and 114.5 mg SiO_2 (nanoparticles ($d = 10 - 20$ nm), 99.5%, Sigma Aldrich, Missouri, USA) with 5 mL of 1×10^{-2} M NaCl solution (99.5%, Carl Roth, Karlsruhe, Germany) in quartz tubes. After constant shaking in an end-over-end rotator (REAX 20/4, Heidolph instruments, Schwabach, Germany) for 14 days, 1 mL of a mixture of $\text{EuCl}_3\cdot 6\text{H}_2\text{O}$ (Sigma-Aldrich, Missouri, USA) and sodium gluconate (Sigma-Aldrich, Missouri, USA, meets USP testing specifications) was added to the C-S-H samples to yield a Eu(III) concentration of 5×10^{-5} M and GLU concentrations in the range of 0 M to 5×10^{-3} M. The final S/L ratio was 33 g/L. After the addition of Eu(III) and GLU, the samples were equilibrated for up to 72 days in an end-over-end rotator under Ar atmosphere.

2.2 Methods

Th(IV) experiments: The liquid phase of the batch sorption experiments in the binary system was analyzed for ^{14}C by liquid scintillation counting (Hidex 300 SL, Hidex, Finland). For this, 1–2 mL of each sample solution were added to 10 mL LSC cocktail Ultima GoldTM XR (PerkinElmer LAS GmbH, Germany). The samples were measured until a 2σ error of 2% was attained. The resulting limit of detection (LOD) was 1×10^{-9} M for ^{14}C . To analyze ^{232}Th in ternary systems, ICP-MS (7900ce Series ICP-MS, Model Nr. G8409A, Agilent Technologies, Santa Clara, USA) was used. The samples were diluted in 2% HNO_3 before ICP-MS analysis. Aliquots of ^{193}Ir in 2% HNO_3 were added as internal standard ($c(\text{Ir}) = 100$ ppt). The LOD for ICP-MS measurements of ^{232}Th was 3×10^{-11} M.

To determine the solids' surface composition of the binary system C-S-H/GLU, XPS measurements were performed. For this, the C-S-H phases were dried under Ar atmosphere at RT for at least 72 h and the powders were milled in an agate mortar. A small amount of the powder was pressed into an indium foil on a copper sample holder. The measurements were performed with a custom-built XPS system

(SPECS GmbH, Berlin, Germany) under a vacuum of 7×10^{-9} mbar and at RT. Non-monochromatic Mg K α radiation (1253.6 eV) from a high intensity double anode X-ray source (Al/Mg) XR-50 was used for photoelectron excitation. Photoelectron detection was conducted with a constant analyzer pass energy of 13 eV using the PHOIBOS 100 hemispherical energy analyzer. The spectra were analyzed using CasaXPS (version 2.3.15).

U(VI) experiments: For TRLFS measurements of U(VI)-containing C-S-H, the sample was transferred as a wet paste pellet into a copper sample holder with a sealable quartz glass lid and measured with a tunable diode pumped solid state (DPSS) laser (Ekspla, NT230, Vilnius, Lithuania) at 10 K. The emitted luminescence light was directed into a spectrograph (Shamrock 303i Andor Oxford Instruments, Abingdon, United Kingdom) equipped with a polychromator with 300, 600, and 1200 lines/mm gratings, and the emission was monitored with an intensified CCD camera (Andor iStar, Oxford Instruments) 10 μ s after the exciting laser pulse in a time window of 10 ms. U(VI) associated with the C-S-H phase was excited at selected wavelengths (330–335 nm, 342 nm, 357 nm).

²⁹Si cross-polarization (CP) and single-pulse (SP) MAS NMR spectra were recorded on a Bruker AvanceTM 400 MHz WB spectrometer operating at a field strength of 9.4 T, with corresponding ²⁹Si and ¹H resonance frequencies of 79.5 and 400.3 MHz, respectively, equipped with a CP/MAS DVT probe. Samples were packed in 7 mm zirconia rotors and spun at 5 kHz rotational frequency. CP spectra were acquired with 5 ms contact time, using a 80% ramp, by accumulating 2048 spectra recorded for 25 ms applying a relaxation delay of 3 s. 200 SP spectra were accumulated by respectively applying 5.6 μ s (30°) excitation pulse, 25 ms acquisition time, and a relaxation delay of 360 s allowing for quantitative measurements. Chemical shifts are reported in ppm relative to external tetramethylsilane (TMS).

X-ray diffractograms of a U(VI)-free and a U(VI)-containing C-S-H sample with C:S of 0.8 were collected with a MiniFlex 600 diffractometer (Rigaku, Tokyo, Japan) equipped with a Cu K α X-ray source (40 keV/15 mA operation for X-ray generation) and the D/teX Ultra 1D silicon strip detector in the Bragg-Brentano θ - 2θ geometry at a scanning speed of 2° per min. For this, the samples were mounted on a low-Si-background sample holder.

Eu(III) experiments: In the TRLFS experiments a tunable pulsed Nd:YAG/OPO laser system operated at 20 Hz was used (Quanta Ray, Spectra Physics, GWU-Lasertechnik Vertriebsges. mbH, $\lambda_{\text{ex}} = 394$ nm). The emission was recorded using an intensified CCD camera (iStar DH720-18V-73, Andor Technology, Oxford Instruments, Abingdon, United Kingdom) combined with a spectrograph (Shamrock 303i, Andor Technology, Oxford Instruments, Abingdon, United Kingdom) equipped with a 600 l/mm grating blazed at 1000 nm. The emission measurements for each sample were carried out for the spectral range covering the ⁵D₀ \rightarrow ⁷F₀ to ⁵D₀ \rightarrow ⁷F₄ luminescence bands of Eu(III) using the box car technique (initial delay = 10 μ s, 50 accumulations per spectrum, 100 steps to record the kinetics, use of a linear increasing gate step). The luminescence spectra were corrected for the spectral emission sensitivity of the detector. The time-resolved emission spectra at different GLU concentrations and after different contact times were deconvoluted to find the species-related emission spectra, luminescence intensities and decay constants. Deconvolution was executed using PARAFAC in Matlab 2019b (The MathWorks, Inc.) with a monoexponential constraint in the time dimension. Based on the emission spectra, the luminescence quantum yields of the different Eu(III) species were determined using the Judd-Ofelt parameters. The concentration of each species was then calculated using the quantum yields and the luminescence intensities obtained by deconvolution.

The TRLFS measurements were performed for C-S-H samples prepared and sealed in quartz tubes and stored under Ar atmosphere. In between measurements, the samples were placed in an end-over-end rotator to achieve a homogenous contact of fluid and solid phase. Before the TRLFS measurements, the samples were allowed to rest for 60 min to have the solid phase settled. TRLFS data were recorded

for the solid as well as for the supernatant solution. The limit of detection for Eu(III) in the solution phase was approximately 5×10^{-8} M.

3 Results and discussion

3.1 Th(IV) / GLU / C-S-H

3.1.1 Binary System

Initially, the sorption of ^{14}C -labelled GLU on the C-S-H phase (C:S = 0.8) was investigated in the binary system. The batch sorption experiments were performed as a function of the S/L ratio ($c_0(\text{GLU}) = 1 \times 10^{-2}$ M; S/L = 0.5 – 50 g/L) and as sorption isotherm of GLU (S/L = 5 g/L; $c_0(\text{GLU}) = 1 \times 10^{-9} - 1 \times 10^{-1}$ M). As shown in Figure 1a, the determined GLU concentration is in the range of the initial concentration. There is a low sorption of GLU on the C-S-H phase of max. 6% up to S/L = 20 g/L and at S/L = 50 g/L to approx. 11%.

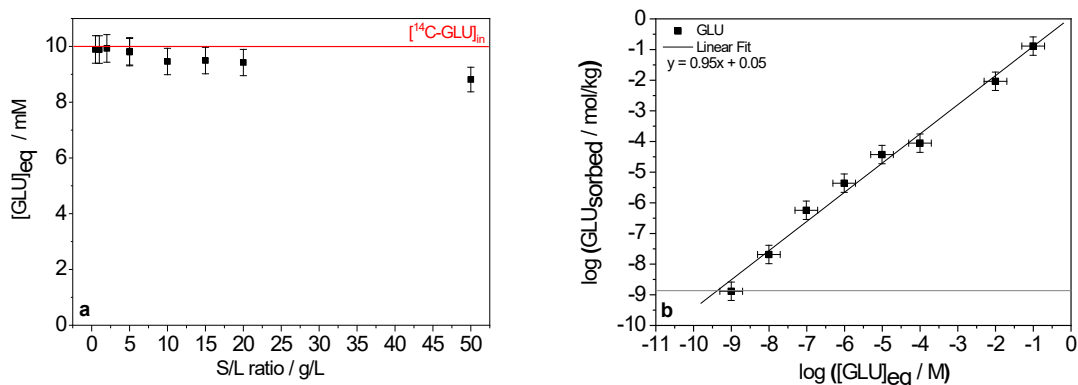


Figure 1: a) Batch sorption experiments at constant GLU concentration ($c_0(\text{GLU}) = 1 \times 10^{-2}$ M) and varying S/L ratio (S/L = 0.5 – 50 g/L, C:S = 0.8, pH 9.8) with a contact time of 72 h. The red line marks the initial concentration of 1×10^{-2} M of GLU. b) The sorption isotherm with initial GLU concentrations from 1×10^{-9} M to 1×10^{-1} M at S/L = 5 g/L (C:S = 0.8, pH 9.8) after a contact time of 3 days shows very low sorption ($S\% < 3\%$) over the whole range. The gray line shows the limit of detection (LOD).

The sorption isotherm of GLU is shown in Figure 1b. An average R_d value of 2.6 ± 1.9 L/kg was determined for the various samples, which agrees well within the uncertainty limits of the value reported by Androniuk et al. ($R_d = 4.5$ L/kg) [10] and confirms that the sorption of GLU on the C-S-H phase is very low at a C:S ratio of 0.8. Therefore, no blocking of sorption sites by GLU on C-S-H phases is assumed.

The XPS measurements of C-S-H samples in the binary system were carried out analogously to the batch sorption experiments described beforehand for an analysis of the C-S-H phases' surfaces in presence and absence of GLU. The overview spectra showed only XPS signals of calcium, oxygen and silicon, but no C 1s signal. The comparison of the spectra of C-S-H samples with and without contact to GLU showed identical signals. From the absence of any C 1s signal in these samples, it can be concluded that a sorption of GLU on the C-S-H phase is unlikely under the experimental conditions. This XPS result for the solid phases agrees with the results of the batch sorption experiments of the liquid phase. The intensities of the Ca 2p and Si 2p signals were used to calculate the corresponding

atomic ratio using equation (1). The experimental sensitivity factor $S_{Ca/Si} = 0.24$ was derived from the XPS measurement of $CaSiO_3$ (Sigma Aldrich, St. Louis, USA).

$$\frac{n_{Ca}}{n_{Si}} = \frac{I_{Ca\ 2p}}{I_{Si\ 2p}} \cdot S_{Ca/Si} \quad (1)$$

The results in Table 1 show that the C:S ratio at the surface of the C-S-H powders is lower than the C:S ratio of 0.8 in the bulk. This effect has been observed previously by Häußler et al. [11], where the Ca content at the surface was somewhat lower than the C:S ratio used in the C-S-H synthesis.

Table 1: C:S target ratios in comparison to the C:S ratios of all samples determined by XPS measurements (the estimated errors are about $\pm 10\%$) and literature data [11].

Solid phase	C:S ratio	pH values
CaSiO ₃ reference	1*	
C-S-H phases (C:S 0.8)	0.56	10.2
C-S-H phases GLU (C:S 0.8)	0.54	10.2
C-S-H phases (C:S 0.75) [11]	0.70	

*) This ratio was assumed to calculate the sensitivity factor $S_{Ca/Si}$.

3.1.2. Ternary System

In experiments of the ternary system, the influence of GLU ($c_0(\text{GLU}) = 1 \times 10^{-2} \text{ M}$) on the sorption of $^{232}\text{Th(IV)}$ ($c_0(\text{Th}) = 1 \times 10^{-8} \text{ M}$) on C-S-H phases ($S/L = 5 \text{ g/L}$, $C:S = 0.8$) was investigated as a function of addition order after a contact time of 72 h: (i) (C-S-H+Th) + GLU, (ii) (C-S-H+GLU) + Th, and (iii) (C-S-H+Th+GLU). GLU and the order of reactant addition had no influence on the sorption of Th(IV) on the C-S-H phase after a contact time of 72 h. As can be seen in Figure 2, a quantitative sorption of $^{232}\text{Th(IV)}$ on the C-S-H phases ($S_{\%} > 99\%$) was observed. The R_d values are in the range of $10^5 - 10^6 \text{ L/kg}$ and are thus in the same order of magnitude ($R_d = 2 \times 10^5 \text{ L/kg}$) as for the sorption of $^{232}\text{Th(IV)}$ on C-S-H phases in the absence of GLU reported in the literature [11].

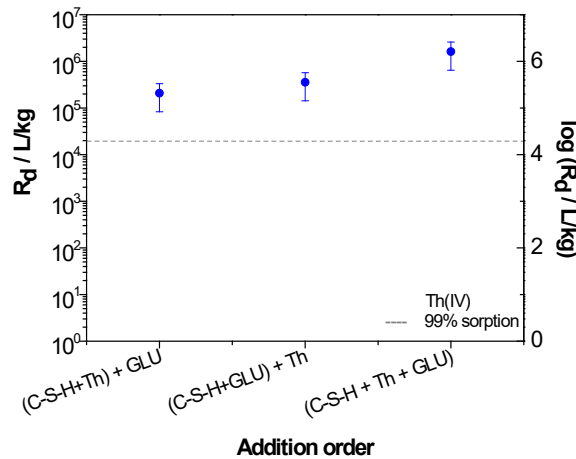


Figure 2: Batch sorption experiments to study the order of addition with $c_0(^{232}\text{Th(IV)}) = 1 \times 10^{-8} \text{ M}$ and $c_0(\text{GLU}) = 1 \times 10^{-2} \text{ M}$ shows no influence on the sorption of $^{232}\text{Th(IV)}$ on C-S-H ($S/L = 5 \text{ g/L}$, $C:S = 0.8$, $\text{pH } 9.8$).

3.2 U(VI) / GLU / C-S-H

The X-ray diffractograms of C-S-H with C:S = 0.8 prepared in the absence and presence of U(VI) ($c_0(\text{U(VI)}) = 2 \times 10^{-5} \text{ M}$, U(VI) loading: 198 mg/kg) are characteristic for C-S-H. U(VI) has no effect on the C-S-H structure (Figure 3a).

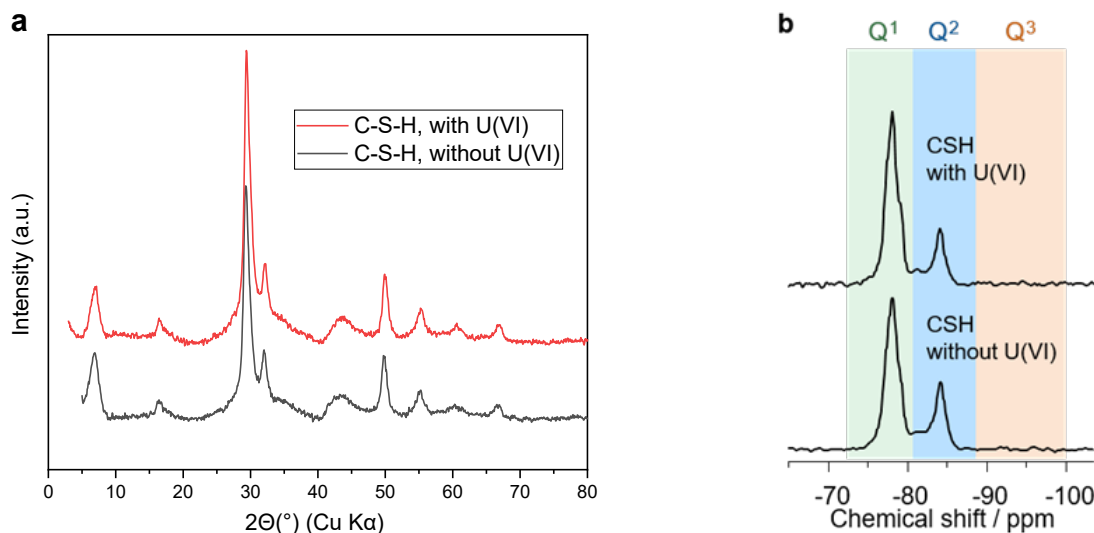


Figure 3: a) Powder X-ray diffractograms of C-S-H (C:S = 0.8) and b) ²⁹Si MAS NMR spectra of C-S-H (C:S = 1.2) prepared in the absence (bottom) and presence of U(VI) ($c_0(\text{U(VI)}) = 2 \times 10^{-5} \text{ M}$) (top).

²⁹Si SP MAS NMR spectra in principle allow for discrimination and quantification of Si(OH)₄ tetrahedra degree of condensation, denoted as Qⁿ groups ($n = 1$ through 4), representing Si(OSi)_n. Accordingly, the mean chain length of the C-S-H dreierketten units can be determined. Upon increasing C:S the Q¹:Q² ratio also increases, according to a decreasing mean chain length. Varying C:S between 0.6 and 1.6 almost inverts the Q¹:Q² ratio from 0.09 to 7.3, associated with mean chain lengths of about 24 and 2.3, respectively [12]. The spectra depicted in Figure 3b, here exemplarily shown for a C-S-H phase with C:S = 1.2, reveal two major results. First, the degree of silicate condensation is low; the integral of the signals associated with Q¹ and Q² groups, respectively, is almost exactly 2:1. Therefore, the mean chain length is 3, corresponding to a high degree of isolated dreierketten units (Q¹-Q²-Q¹). Additionally, some dimeric Q¹-Q¹ and pentameric Q¹-Q²-Q²_b-Q²-Q¹ chains are present as implied by the small shoulders in the Q¹ signal and the minor signal at about $\delta_{\text{Si}} -81 \text{ ppm}$ due to the bridging Q² (Q²_b), respectively. Second, no notable spectral changes upon presence of U(VI) during C-S-H phase synthesis can be detected. Hence, the short-range order of the C-S-H phase remains unaffected by U(VI). Comparable results are expected for the C-S-H phase with C:S = 0.8.

By means of TRLFS (Figure 4), three main U(VI) species have been identified for a U(VI)-loaded C-S-H phase in correspondence with the literature [13, 14]: Two of them have almost identical lifetimes ($(143 \pm 18) \mu\text{s}$) and are assigned to U(VI) sorption complexes on C-S-H surfaces. The third one has a clearly longer lifetime ($(387 \pm 40) \mu\text{s}$), and is assigned to U(VI) sorbed into the interlayer region of C-S-H phases. The latter species is sometimes referred to in the literature as incorporated species. These lifetimes agree very well with previously obtained lifetimes for U(VI) in C-S-H phases [14].

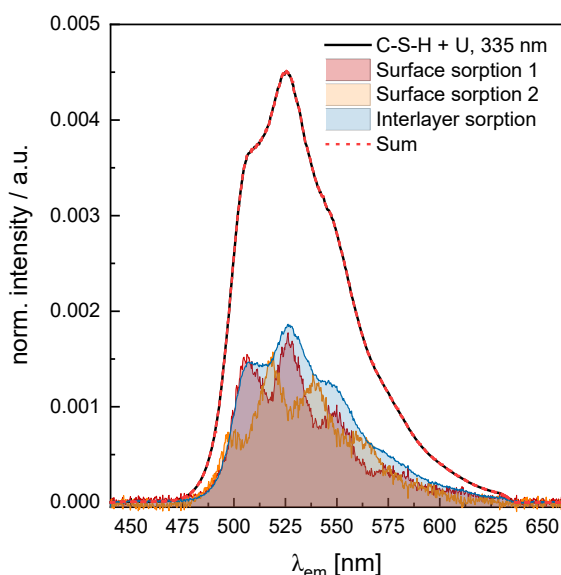


Figure 4: *U(VI) emission spectrum of a U(VI)-loaded C-S-H phase ($c_0(\text{U(VI)}) = 5 \times 10^{-7} \text{ M}$, $S/L = 1 \text{ g/L}$, $C:S = 0.8$, $\text{pH } 10.87$) and extracted pure components from decomposition of the measured spectrum.*

To study the influence of GLU on U(VI) retention by C-S-H, the U(VI)-loaded C-S-H sample was contacted with $1 \times 10^{-3} \text{ M}$ or $1 \times 10^{-2} \text{ M}$ GLU solutions. The results showed that less than 0.1% of the previously retained U(VI) is remobilized in the presence of GLU. This means that GLU has no effect on U(VI) retention by C-S-H under these conditions. Presently, the ternary system is further studied by TRLFS and NMR to identify U(VI) species on the solid phase and in the supernatant.

3.3 Eu(III) / GLU / C-S-H

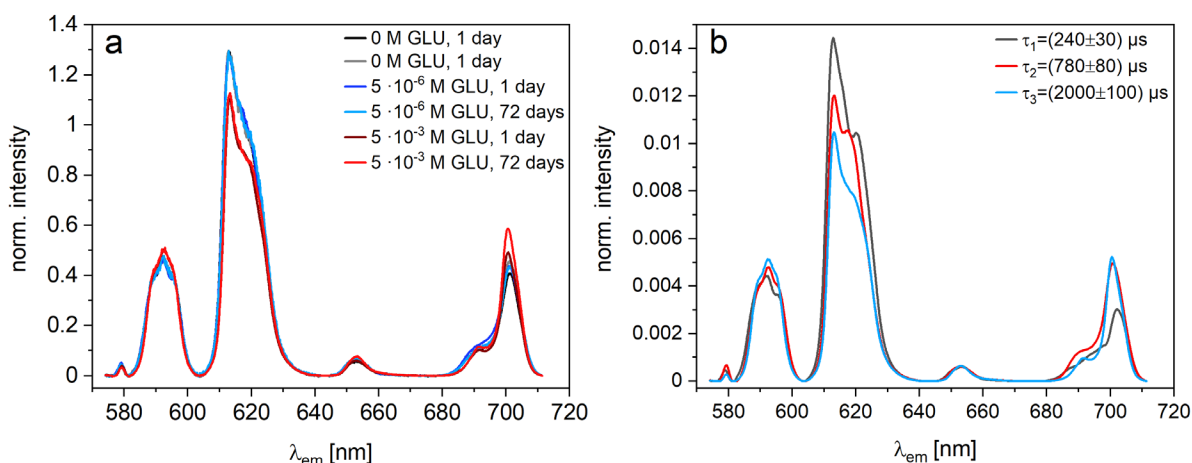


Figure 5: (a) *Luminescence spectra (raw data) of Eu(III) sorbed to C-S-H phases ($S/L = 33.3 \text{ g/L}$) without GLU and in the presence of $5 \times 10^{-6} \text{ M}$ and $5 \times 10^{-3} \text{ M}$ GLU after 1 and 72 days of contact time, recorded after $10 \mu\text{s}$ and (b) deconvoluted luminescence spectra of the three identified Eu(III) species and their respective luminescence decay times. All spectra are normalized to the area of the ${}^5D_0 \rightarrow {}^7F_1$ transition.*

The sorption of Eu(III) ($c_0(\text{Eu}) = 5 \times 10^{-5} \text{ M}$) on C-S-H phases ($S/L = 33.3 \text{ g/L}$) was investigated at a concentration range of $0 \leq c_0(\text{GLU}) \leq 5 \times 10^{-3} \text{ M}$ and up to 72 days contact time. The recorded

emission spectra of the solid phase at a low (5×10^{-6} M) and high (5×10^{-3} M) GLU concentration after a contact time of 1 and 72 days are shown in Figure 5a. Only minor changes can be observed with increasing contact time indicating a fast sorption process. However, more significant differences appear between samples with different GLU concentrations. To further analyze the influence of GLU, a deconvolution of the emission data was carried out to obtain the luminescence characteristics of each Eu(III) species. Three different Eu(III) species were identified with decay constants of (240 ± 30) μ s, (780 ± 80) μ s and (2000 ± 100) μ s, respectively (see Figure 5b). The number of water molecules in the coordination environment of Eu(III) may be estimated using the empirical derived equation (2) proposed by Kimura and Choppin [15]:

$$n_{H_2O} \pm 0.5 = \frac{1.07}{\tau [\text{ms}]} - 0.62 \quad (2)$$

where n_{H_2O} is the number of water molecules and τ is the decay constant in ms. In accordance with previously reported interpretations for the sorption of Eu(III) to C-S-H phases, the Eu(III) species with a decay constant of 240 μ s could be surrounded by approximately four water molecules, which may correspond to a sorption to the C-S-H surface [16]. The decay constant of 780 μ s correlates to approximately one water molecule in the near Eu(III) coordination environment, suggesting an uptake either into the CaO layer or the interlayer of the C-S-H phases. The decay constant of 2000 μ s could correspond to a coordination environment with no water molecules and may indicate an incorporation of Eu(III) into the CaO layer [16-18]. All three Eu(III) species appear both in samples with and without GLU, thus no additional Eu-GLU-complexes were observed. Moreover, the Eu(III) concentration in the aqueous phase remained below the limit of detection of approximately 5×10^{-8} M even in the presence of up to 5×10^{-3} M GLU.

Nevertheless, GLU appears to influence the relative concentrations of the different sorption species. As shown in Figure 6 and Figure 7, without GLU and at a low GLU concentration (up to 5×10^{-5} M GLU) the majority of the Eu(III) is sorbed to the C-S-H surface. However, at higher GLU concentrations an increasing amount of Eu(III) appears to be incorporated into the interlayer or the CaO layer of the C-S-H phases. This might indicate an increasing dissolution and recrystallization rate (or more general speaking the formation of a solid phase) of the C-S-H phases in the presence of GLU, proposedly due to the formation of Ca-GLU-complexes, as a faster recrystallization would favor the incorporation of Eu(III) into the structure of the solid phase. Based on our current data interpretation (*vide supra*), independent of the GLU concentration a slight increase of Eu(III) sorbed into the CaO layer can be observed with increasing contact time, which is in accordance with the literature and indicates that the CaO layer is the thermodynamically most favorable sorption site [16, 18]. However, the observed changes up to a contact time of 72 days were relatively small.

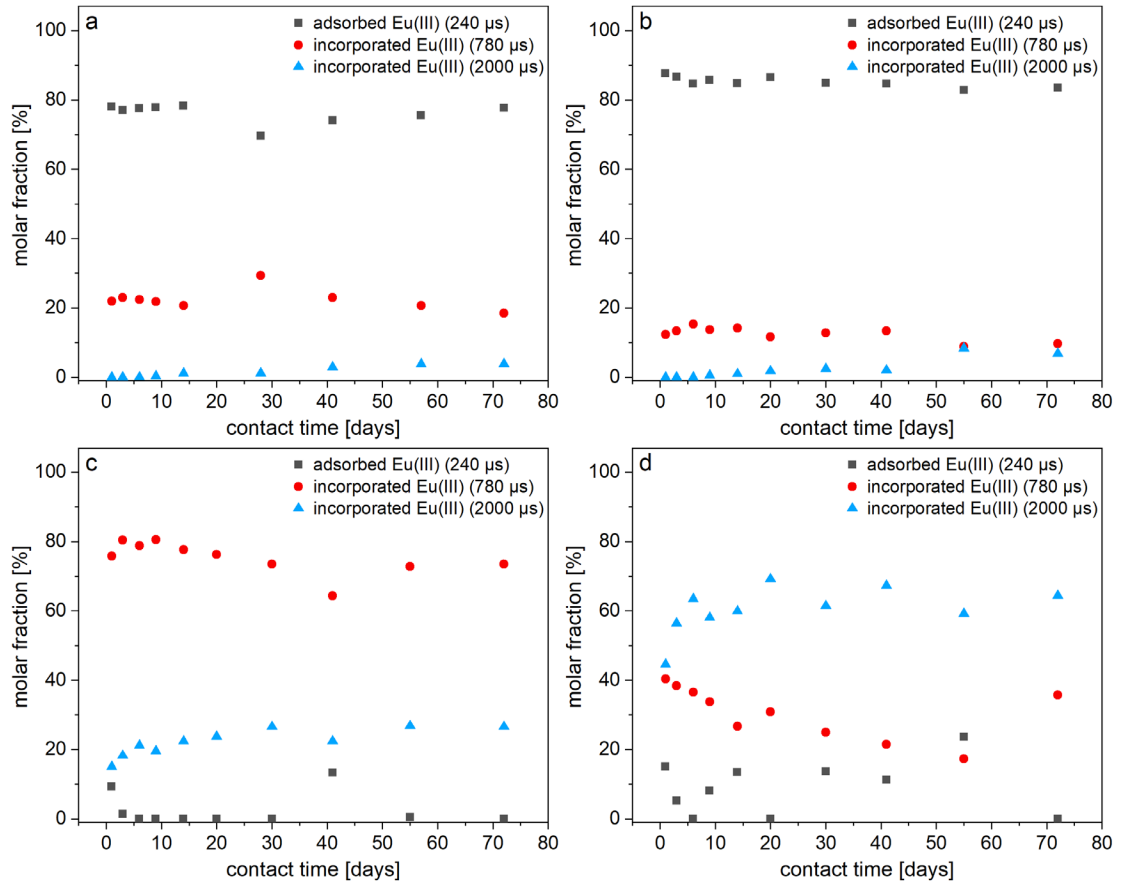


Figure 6: Speciation of Eu(III) sorbed to C-S-H phases ($S/L = 33.3$ g/L) in the presence of (a) 0 M GLU, (b) 5×10^{-6} M GLU, (c) 5×10^{-4} M GLU and (d) 5×10^{-3} M GLU at different contact times. The total Eu(III) concentration was 5×10^{-5} M in all samples.

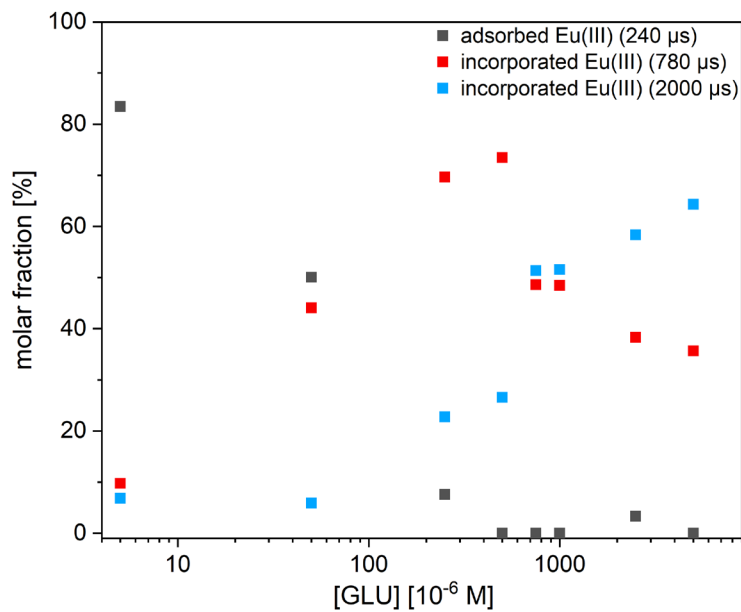


Figure 7: Speciation of Eu(III) sorbed to C-S-H phases ($S/L = 33.3$ g/L) after a contact time of 72 days in dependence of the GLU concentration. The total Eu(III) concentration was 5×10^{-5} M in all samples.

4 Conclusions

The potential influence of GLU on the sorption of actinides and analogues in different oxidation states (tri-, tetra- and hexavalent) on a stage III C-S-H phase (C:S = 0.8) has been investigated. For the binary system of GLU/C-S-H, both GLU sorption and structural alteration of C-S-H surface due to presence of GLU were found to be very low, which may be different for other C-S-H phases with a higher Ca(II) content in the interlayers. In the sorption experiments involving radionuclides, different mixing orders of reactants and contact times were investigated. The strong Eu(III), Th(IV), and U(VI) retention on C-S-H in the absence of organics was found almost unaffected by GLU. Complementary to the binary system, also no significant influence on the principal occurrence of sorption species was found. While the general speciation (surface sorption as well as incorporation of the radionuclides) remained unaffected by the presence of GLU (even at a very high concentration of GLU, no novel sorption species were found for Eu(III)), the relative amount of each species seemed to be altered. For Eu(III), the presence of GLU in concentrations larger than 1×10^{-4} M enhanced the formation of an incorporation species significantly. It is attractive to assume a kinetic effect of GLU on the solubilization and precipitation of the solid phase, e.g., due to complexation of Ca(II) ions. However, the overall concentration of Ca(II) ions in this stage III system is distinctly lower than at earlier stages of the cement alteration process, therefore, due to a different porewater chemistry the presence of GLU might have a more pronounced influence there.

Acknowledgement

The EURAD-CORI project leading to this application has received funding from the European Union's Horizon 2020 research and innovation programme under grant agreement No 847593.

References

1. Tits, J. and Wieland, E. (2018) Actinide sorption by cementitious materials. Villigen PSI, Switzerland, PSI Report 18-02.
2. Ochs, M., Dolder, F., and Tachi, Y. (2022) Decrease of radionuclide sorption in hydrated cement systems by organic ligands: Comparative evaluation using experimental data and thermodynamic calculations for ISA/EDTA-actinide-cement systems. *Appl. Geochem.* 136 105161.
3. Roach, M.K. and Shahkarami, P. (2021) Organic materials with the potential for complexation in SFR, the final repository for short-lived radioactive waste. Investigation of new acceptance criteria. Svensk Kärnbränslehantering AB, SKB R-21-03.
4. Wieland, E., Lothenbach, B., Glaus, M.A., Thoenen, T., and Schwyn, B. (2014) Influence of superplasticizers on the long-term properties of cement pastes and possible impact on radionuclide uptake in a cement-based repository for radioactive waste. *Appl. Geochem.* 49, 126-142.
5. Garcia, D., Grive, M., Duro, L., Brassinnes, S., and de Pablo, J. (2018) The potential role of the degradation products of cement superplasticizers on the mobility of radionuclides. *Appl. Geochem.* 98, 1-9.
6. Gaona, X., Montoya, V., Colas, E., Grive, M., and Duro, L. (2008) Review of the complexation of tetravalent actinides by ISA and gluconate under alkaline to hyperalkaline conditions. *J. Contam. Hydrol.* 102, 217-227.
7. Van Loon, L.R., Glaus, M.A., Laube, A., and Stallone, S. (1999) Degradation of cellulosic materials under the alkaline conditions of a cementitious repository for low- and intermediate level radioactive waste. Part III: Effect of degradation products on the sorption of radionuclides on feldspar. *Radiochim. Acta* 86, 183-189.

8. Altmaier, M., Blin, V., García, D., Henocq, P., Missana, T., Ricard, D., and Vandenberghe, J. (2021) SOTA on cement-organic-radionuclide interactions. Final version as of 19.05.2021 of deliverable D3.1 of the HORIZON 2020 project EURAD. EC Grant agreement no: 847593.
9. Atkins, M., Glasser, F.P., and Kindness, A. (1992) Cement hydrate phases: solubility at 25°C. *Cement Concrete Res.* 22, 241-246.
10. Androniuk, I., Landesman, C., Henocq, P., and Kalinichev, A.G. (2017) Adsorption of gluconate and uranyl on C-S-H phases: Combination of wet chemistry experiments and molecular dynamics simulations for the binary systems. *Phys. Chem. Earth* 99, 194-203.
11. Häußler, V., Amayri, S., Beck, A., Platte, T., Stern, T.A., Vitova, T., and Reich, T. (2018) Uptake of actinides by calcium silicate hydrate (C-S-H) phases. *Appl. Geochem.* 98, 426-434.
12. Roosz, C., Vieillard, P., Blanc, P., Gaboreau, S., Gailhanou, H., Braithwaite, D., Montouillout, V., Denoyel, R., Henocq, P., and Made, B. (2018) Thermodynamic properties of C-S-H, C-A-S-H and M-S-H phases: Results from direct measurements and predictive modelling. *Appl. Geochem.* 92, 140-156.
13. Tits, J., Geipel, G., Macé, N., Eilzer, M., and Wieland, E. (2011) Determination of uranium(VI) sorbed species in calcium silicate hydrate phases: A laser-induced luminescence spectroscopy and batch sorption study. *J. Colloid Interf. Sci.* 359, 248-256.
14. Tits, J., Walther, C., Stumpf, T., Macé, N., and Wieland, E. (2015) A luminescence line-narrowing spectroscopic study of the uranium(VI) interaction with cementitious materials and titanium dioxide. *Dalton Trans.* 44, 966-976.
15. Kimura, T. and Choppin, G.R. (1994) Luminescence study on determination of the hydration number of Cm(III). *J. Alloys Compd.* 213, 313-317.
16. Mandaliyev, P., Stumpf, T., Tits, J., Dähn, R., Walther, C., and Wieland, E. (2011) Uptake of Eu(III) by 11 Å tobermorite and xonotlite: A TRLS and EXAFS study. *Geochim. Cosmochim. Acta* 75, 2017-2029.
17. Pointeau, I., Piriou, B., Fedoroff, M., Barthes, M.G., Marmier, N., and Fromage, F. (2001) Sorption mechanisms of Eu³⁺ on CSH phases of hydrated cements. *J. Colloid Interf. Sci.* 236, 252-259.
18. Tits, J., Stumpf, T., Rabung, T., Wieland, E., and Fanghänel, T. (2003) Uptake of Cm(III) and Eu(III) by calcium silicate hydrates: A solution chemistry and time-resolved laser fluorescence spectroscopy study. *Environ. Sci. Technol.* 37, 3568-3573.

Influence of selected organic substances on uptake of uranium and europium on cementitious materials – The Czech contribution

B. Drtinová^{1*}, J. Kittnerová¹, M. Burešová¹, L. Švamberová¹, A. Čejková¹,
P. Večerník²

¹ Czech Technical University in Prague, Faculty of Nuclear Sciences and Physical Engineering,
Břehová 7, 115 19 Prague 1 (Czech Republic)

² ÚJV Řež, a. s., Hlavní 130, 25068 Řež (Czech Republic)

* Corresponding author: barbora.drtinova@jfifi.cvut.cz

Abstract

The impact of the degraded organic radioactive waste (ion exchangers and sorbents, other organic waste) fixed in the cement matrix on the behavior of radionuclides in the cement/concrete environment was studied. Specifically, the distribution ratios, R_d , for ^{233}U and ^{152}Eu on different cementitious materials (hydrated cement paste CEM I and witness sample of concrete from L/ILW repository Richard, Czech Republic, containing CEM III) in the presence of three organic substances (EDTA, adipate, and phthalate) were determined. Resulting values of R_d were in the range 10^3 - 10^5 L·kg⁻¹ for Eu and 10^3 - 10^4 L·kg⁻¹ for U under experimental conditions.

1 Introduction

The organic materials of interest include model molecules that represent substances previously identified as degradation products arising from the radiolytic or hydrolytic decomposition of some organic materials contained in radioactive waste. From this wide spectrum of substances adipate and phthalate were selected for the study together with EDTA, most likely used as a decontaminating agent, which was chosen for its poor degradability in the environment.

Study of sorption behaviour of U, Eu, and Pb (partly in Burešová et al. 2023, Drtinová et al. 2023, see Table 1 and 2), also in the presence of organic substances, was done on several cementitious matrices: newly prepared hydrated cement paste CEM I (without the addition of plasticizer), test specimens of structural concrete from the Richard repository (15 years old), and pure CSH phase.

The obtained results will support the safety assessment of the operated Richard L/ILW repository (located near Litoměřice, Northern Bohemia, Czech Republic), especially regarding the possible extension of its service life. The data will be also usable for safety assessment and calculations related to other radioactive waste repositories, including the ILW + HLW part of a planned deep geological repository in the Czech Republic (concrete containers, structures, and fillings).

2 Materials and methods

Uranium was acquired 12.1.2021 in the form of uranium-233 ($1 \text{ kBq}\cdot\text{g}^{-1}$). It is an α -emitter with $T_{1/2} = 1.59\cdot 10^5 \text{ y}$. Due to its limited solubility in strongly alkaline media ($\approx 10^{-6} \text{ mol}\cdot\text{L}^{-1}$, e.g., Brownsword et al. 1990), its detection is quite complicated. Therefore, methodical study of uranium activity measurement by liquid scintillation counting, LSC, under the cement water ($\text{pH} > 12.5$) conditions was carried out by scintillation cocktail Ultima Gold AB with the resulting detection limit of $3\cdot 10^{-10} \text{ mol}\cdot\text{L}^{-1}$. As a chemical analogue of trivalent actinides, europium-152 is used (stock solution $1.7 \text{ MBq}/1 \text{ mL}$ as of 13.5.2021, $T_{1/2} = 13.54 \text{ y}$). Eu activity is determined by gamma spectrometry.

In the group of model molecules, these substances are studied at present: EDTA, in the form of disodium salt, Chelaton 3 (Lachema), p.a.; phthalic acid, manufactured by Sigma-Aldrich, with purity $\geq 99.5 \%$; and adipic acid, manufactured by Sigma-Aldrich, purity ≥ 99.5 . The organics working concentrations ($5\cdot 10^{-5} \text{ mol}\cdot\text{L}^{-1}$ and $5\cdot 10^{-3} \text{ mol}\cdot\text{L}^{-1}$) were selected based on (Van Loon & Hummel 1995).

Details on the preparation of cement samples are given in contribution on Task 3 (Vašiček et al. 2023). Simple solutions were selected as a liquid medium simulating leachate from cementitious materials due to its complexity and time variability: a saturated solution of $\text{Ca}(\text{OH})_2$ (portlandite water) with a concentration approximately $0.02 \text{ mol}\cdot\text{L}^{-1}$, and $0.1 \text{ mol}\cdot\text{L}^{-1}$ NaOH solution. Both liquid systems have a pH of approximately 12.5 and were used for experiments with fresh CEM I and Richard concrete (hereinafter also referred to as CEM III, because it contains this type of cement). The ratio of solid and liquid phases L/S in all sorption experiments performed was equal to 100, 250, 500 and $800 \text{ L}\cdot\text{kg}^{-1}$ (in the case of Eu experiments also L/S $10 \text{ L}\cdot\text{kg}^{-1}$ was investigated). The dry matter of the cementitious material was also considered. Moisture was determined for all materials by drying to constant weight for 3 days at 105°C . On average, CEM I cement contains 5.34 % of moisture and CEM III material 3.26 %.

The procedure of sorption experiments was the same for both studied radionuclides. First, the hydrated cement paste was ground into smaller pieces, until they passed through a 0.4 mm sieve. Furthermore, solutions of predetermined concentrations were prepared, containing either only NaOH or $\text{Ca}(\text{OH})_2$, or being mixed with one of the selected organic substances. Each of these solutions also contained enough radionuclide to match the concentration required in the experiment. The liquid phase in its final composition was prepared prior to its contact with cementitious material weighed in individual ampoules. The procedure used does not introduce a significant pipetting error into the system, especially with regard to the activity of the samples.

The amount of cement in the ampoules corresponded to the studied phase ratios with a constant liquid volume of 6 mL, the ampoules were shaken on a shaker during the experiments ($120 \text{ oscillations}\cdot\text{min}^{-1}$). Finally, the ampoules were centrifuged (RCF 900 g for HCP) for 10 minutes on an MPW 350R centrifuge before sampling for activity determination. In the case of uranium, 100, 200 or 500 μL of the solution above the solid phase was carefully taken into a measuring ampoule and mixed with 5 mL of Ultima Gold AB scintillation cocktail. The measurement was performed on a Hidex 300 SL liquid scintillation spectrometer for 12 hours. In experiments with europium, a 2 mL sample was taken and subsequently measured on an HPGe detector (type GEM40P4 with Ortec DSPEC jr 2.0; the analysis of the spectra was done with Maestro software version 7.0.) for 10 minutes.

At the start of the kinetic experiment, ampoules were prepared containing a given liquid phase and a cementitious material. The samples were then removed after a total of 4 weeks for uranium and

4 days for europium at predetermined intervals. In the case of equilibrium experiments, uranium samples were taken after 3 weeks, samples containing europium after 48 hours. The related issue of uranium and europium wall sorption evaluation has been discussed elsewhere (Burešová et al. 2023, Drtinová et al. 2023).

Table 1: Completed sorption experiments with uranium as of November 2021

Experiment	$c_{(U)}$ (mol L ⁻¹)	$c_{(ORG)}$ (mol·L ⁻¹)	Type of cement	Liquid phase	L/S (L·kg ⁻¹)
Kinetics	$7 \cdot 10^{-8}$	×	CEM I, CSH	NaOH Sat. Ca(OH) ₂ CSH solution	100 in NaOH; 100, 500, 800 in Ca(OH) ₂ ; 800 in CSH solution
		EDTA $5 \cdot 10^{-5}$			100 in NaOH; 800 in Ca(OH) ₂ ; 800 in CSH solution
Equilibrium	$1.2 \cdot 10^{-6}$	×	CEM I, CSH	NaOH	100, 250, 500, 800, walls
		EDTA $5 \cdot 10^{-5}$			
		×	CEM I		
		EDTA $5 \cdot 10^{-5}$			
		Phthalate $5 \cdot 10^{-5}$			
Adipate $5 \cdot 10^{-5}$					
EDTA $5 \cdot 10^{-3}$					

Each experimental set-up was performed in two parallel determinations. In case of uranium, a high error rate, around 30 %, occurs, which leads, for the sake of clarity, to the omission of error bars in the graphs and standard deviations in the tables below. On the contrary, but for the same reason, trends in the form of power interpolation for kinetic experiments and linear or exponential trends in the case of equilibrium experiments are added in following figures, which better illustrates the expected course of sorption behavior.

The evaluation of sorption experiments was performed using the distribution ratio R_d , the calculation of which can be found elsewhere (e.g., Kittnerová et al. 2020).

An overview of the completed experiments for uranium and europium is given in Table 1 and Table 2. In this contribution, the results for the systems ²³³U in the presence of CEM I in NaOH solution and ¹⁵²Eu with CEM III in Ca(OH)₂ solution are discussed. Other results have been already published (Burešová et al. 2023).

Table 2: Completed sorption experiments with europium as of November 2021

Experiment	$c_{(\text{Eu})}$ (mol·L ⁻¹)	$c_{(\text{ORG})}$ (mol·L ⁻¹)	Type of cement	Liquid phase	L/S (L·kg ⁻¹)	
Kinetics	2.9·10 ⁻⁹	×	CEM I, CEM III	Sat. Ca(OH) ₂	(100), 500	
		EDTA 5·10 ⁻⁵ , 5·10 ⁻³	CEM I, CEM III		(100), 500	
		Adipate 5·10 ⁻⁵	CEM I, CEM III		500	
		Phthalate 5·10 ⁻⁵	CEM I		500	
Equilibrium		×	CEM I, CEM III			(10), 100, 250, 500, 800, walls
		EDTA 5·10 ⁻⁵ , 5·10 ⁻³	CEM I, CEM III			
		Adipate 5·10 ⁻⁵	CEM I, CEM III			
		Phthalate 5·10 ⁻⁵	CEM I			

3 Results and discussion

Both radionuclides have a low solubility limit under strongly alkaline conditions. In the case of uranium, the solubility limit of approximately 5·10⁻⁶ mol·L⁻¹ in the environment of portlandite water and probably an order of magnitude higher in the system with NaOH makes its determination difficult. On the other hand, europium does not precipitate due to its high sorption (e.g. up to 99.8 % sorption on CSH) which prevents normal precipitation (Pointeau et al. 2001). However, its ability to sorb to many materials, i.e. also to the walls of ampoules, has a negative effect, which greatly complicates the evaluation of experiments.

3.1 Sorption of ²³³U on CEM I in NaOH solution

The sorption of uranium (7·10⁻⁸ and 1.2·10⁻⁶ mol·L⁻¹) on the cementitious material CEM I in an alkaline solution of 0.1 mol·L⁻¹ NaOH simultaneously with the effect of the organic molecules – EDTA, adipate or phthalate was studied (Table 1).

Within the kinetics part of the experiment, the aim was to obtain the information about the time development of the relative concentration of uranium in the liquid phase to find out the time required

to reach equilibrium. In the following equilibrium experiment the dependence of the distribution ratio R_d on the phase ratio L/S , composition of the liquid phase and the rate of uranium sorption on the walls of the ampoules were determined. For a system containing $7 \cdot 10^{-8} \text{ mol} \cdot \text{L}^{-1}$ of uranium, the average wall sorption rate was $(2.8 \pm 1.4) \%$, for uranium with a concentration of $1.2 \cdot 10^{-6} \text{ mol} \cdot \text{L}^{-1}$ then $(2.2 \pm 1.0) \%$ and on average $(2.5 \pm 1.2) \%$, which can be neglected.

Kinetic experiment

Kinetic experiments were performed for two different liquid phase compositions – in the first case the liquid phase contained only $0.1 \text{ mol} \cdot \text{L}^{-1}$ NaOH, in the second case also EDTA with a concentration of $5 \cdot 10^{-5} \text{ mol} \cdot \text{L}^{-1}$ was added to the system. The concentration of uranium in the solution was in both cases $7 \cdot 10^{-8} \text{ mol} \cdot \text{L}^{-1}$ and the phase ratio $100 \text{ L} \cdot \text{kg}^{-1}$.

The resulting insignificant influence of the different liquid phases is shown in Figure 1 (it does not contain values from all samples, as not all samples could be measured due to its very low concentrations in the liquid phase, close to detection limit).

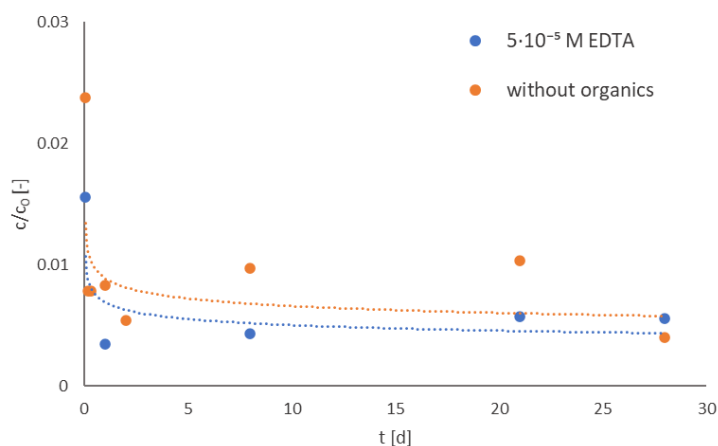


Figure 1: Kinetics of ^{233}U ($7 \cdot 10^{-8} \text{ mol} \cdot \text{L}^{-1}$) sorption on CEM I in NaOH environment with and without EDTA ($5 \cdot 10^{-5} \text{ mol} \cdot \text{L}^{-1}$).

The relative concentration of uranium in the liquid phase decreases with increasing sampling time, until the sorption equilibrium stabilizes, manifested by an approximately constant trend after 3 weeks. In most of samples taken, the relative concentration of uranium in the liquid phase containing only NaOH is approximately twice higher as for the liquid phase containing also EDTA.

The accuracy of the experiment encounters more issues here. Apart from those already mentioned, it can be stated that the consequence of a very low working uranium concentration is that the equilibrium is established very quickly – in about one day. According to (Wieland et al. 2010), however, the time required to establish equilibrium in similar systems is 14 days, according to (Tits et al. 2011) 10 days, according to (Pointeau et al. 2004) 9 days. The short time suggests that the mechanism is based on surface sorption rather than incorporation of uranium into the solid-state chemical structure (Tits et al. 2011).

Equilibrium experiment

Equilibrium experiments with two uranium concentrations ($7 \cdot 10^{-8}$ and $1.2 \cdot 10^{-6}$ mol·L⁻¹) in NaOH environment and in the presence of organic compounds was performed for 3 weeks. For lower uranium concentration EDTA only with concentration $5 \cdot 10^{-5}$ mol·L⁻¹, for higher uranium concentration EDTA with concentrations $5 \cdot 10^{-5}$ mol·L⁻¹ and $5 \cdot 10^{-3}$ mol·L⁻¹ and other organic compounds, specifically adipate and phthalate with a concentration of $5 \cdot 10^{-5}$ mol·L⁻¹ were used.

The following figures (Figure 2 and 3) show the results of the equilibrium experiments as a dependence of the distribution ratio R_d on the phase ratio.

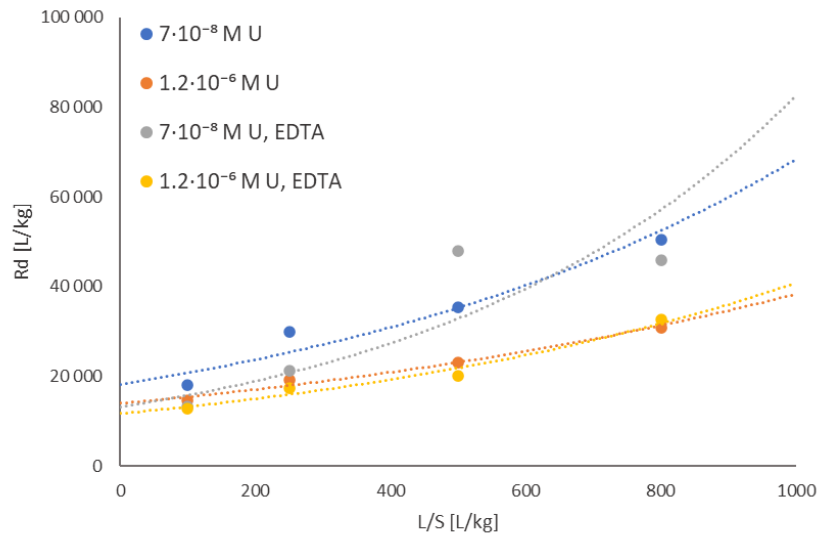


Figure 2: Dependence of R_d ($L \cdot kg^{-1}$) on the phase ratio L/S of ^{233}U ($7 \cdot 10^{-8}$ and $1.2 \cdot 10^{-6}$ mol·L⁻¹) sorption on CEM I in NaOH environment with and without EDTA ($5 \cdot 10^{-5}$ mol·L⁻¹).

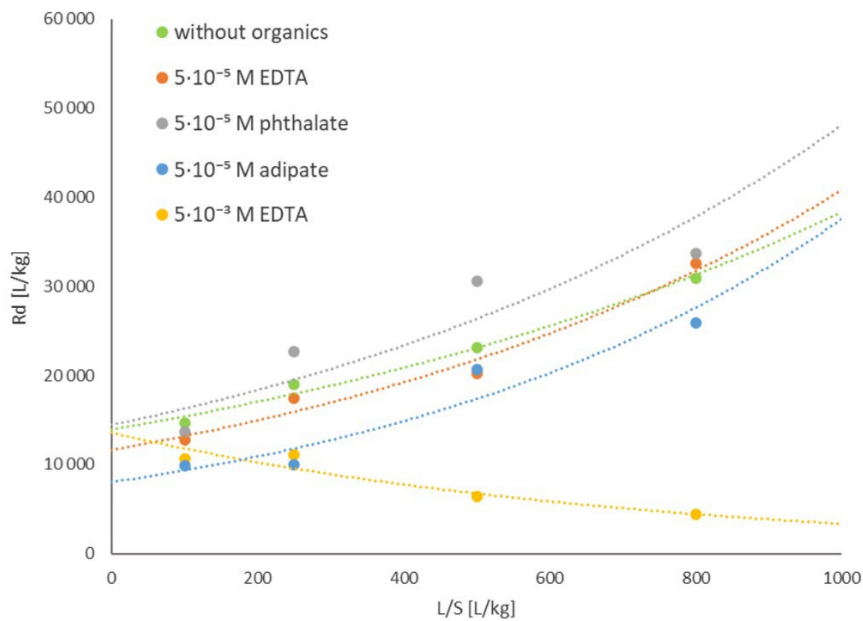


Figure 3: Dependence of R_d ($L \cdot kg^{-1}$) on the phase ratio L/S of ^{233}U ($1.2 \cdot 10^{-6}$ mol·L⁻¹) sorption on CEM I in NaOH environment with and without organics ($5 \cdot 10^{-5}$ and $5 \cdot 10^{-3}$ mol·L⁻¹).

It is evident from Figure 2 and Table 3 that the distribution ratio R_d in all investigated cases reached, at the uranium concentration $7 \cdot 10^{-8} \text{ mol} \cdot \text{L}^{-1}$, the order of $10^4 \text{ L} \cdot \text{kg}^{-1}$. It cannot be clearly determined in which liquid phase the sorption of uranium to the cement material occurs to a greater extent. The comparison of the dependence of the distribution ratio on the phase ratio for different concentrations of uranium shows that for both compositions of the liquid phase the distribution ratio is higher in the case of a lower concentration of uranium - i.e. that a lower concentration of uranium leads to a higher rate of uranium sorption on the cement material.

For the systems containing the higher uranium concentration the distribution ratio was found of the order of 10^3 to $10^4 \text{ L} \cdot \text{kg}^{-1}$ according to the composition of the liquid phase (Figure 3, Table 3). The fact that in the presence of $5 \cdot 10^{-3} \text{ mol} \cdot \text{L}^{-1}$ EDTA a completely opposite trend occurs – with increasing phase ratio R_d decreases, is of particular interest. It can be expected that the trend would be similar for even higher EDTA concentrations in the liquid phase.

Table 3: Distribution ratios R_d ($\text{L} \cdot \text{kg}^{-1}$) of ^{233}U ($7 \cdot 10^{-8}$ and $1.2 \cdot 10^{-6} \text{ mol} \cdot \text{L}^{-1}$) sorption on CEM I in NaOH environment with and without organics ($5 \cdot 10^{-5}$ and $5 \cdot 10^{-3} \text{ mol} \cdot \text{L}^{-1}$)

L/S ($\text{L} \cdot \text{kg}^{-1}$)	Without organics	$5 \cdot 10^{-5} \text{ mol} \cdot \text{L}^{-1}$ EDTA	Without organics	$5 \cdot 10^{-5} \text{ mol} \cdot \text{L}^{-1}$ EDTA	$5 \cdot 10^{-3} \text{ mol} \cdot \text{L}^{-1}$ EDTA	$5 \cdot 10^{-5} \text{ mol} \cdot \text{L}^{-1}$ Adipate	$5 \cdot 10^{-5} \text{ mol} \cdot \text{L}^{-1}$ Phthalate
	$7 \cdot 10^{-8} \text{ mol} \cdot \text{L}^{-1} \text{ U}$			$1.2 \cdot 10^{-6} \text{ mol} \cdot \text{L}^{-1} \text{ U}$			
R_d ($\text{L} \cdot \text{kg}^{-1}$)							
100	18 100	13 200	14 700	12 700	10 700	9 900	13 600
250	30 000	21 000	19 000	17 400	11 200	10 000	23 000
500	36 000	48 000	23 000	20 000	6 500	20 700	31 000
800	50 000	46 000	31 000	33 000	4 400	26 000	34 000

A comparison with our previous results (Burešová et al. 2023) of sorption of ^{233}U ($7 \cdot 10^{-8} \text{ mol} \cdot \text{L}^{-1}$) on CEM I in a saturated $\text{Ca}(\text{OH})_2$ solution shows that the trends in both liquid environments are the same, only with three to ten times lower R_d values in portlandite water. For CSH, higher R_d values are expectedly achieved, up to $1 \cdot 10^5 \text{ L} \cdot \text{kg}^{-1}$.

The obtained values (Table 3) of the distribution ratios are consistent with the data reported in the literature. In the study (Tits et al. 2011), the distribution ratio lay between 10^3 and $10^6 \text{ L} \cdot \text{kg}^{-1}$ for different liquid phase compositions (with the highest values being reached for the alkali-free liquid phase). In the study (Wieland et al. 2010), the average value $R_d = (2.2 \pm 0.5) \cdot 10^3 \text{ L} \cdot \text{kg}^{-1}$ was found. According to (Pointeau et al. 2004), the values of the distribution ratio from $3 \cdot 10^4$ to $1.5 \cdot 10^5 \text{ L} \cdot \text{kg}^{-1}$ was determined according to the degree of degradation of the cement paste – for the least degraded R_d was the lowest. In our previous study of the behavior of natural uranium in the presence of cementitious matrices, the obtained R_d values for hydrated cement paste CEM II in NaOH environment and phase ratios L/S 5, 100 and 400 $\text{L} \cdot \text{kg}^{-1}$ also ranged between 10^2 and $10^4 \text{ L} \cdot \text{kg}^{-1}$ (Večerník et al. 2019).

3.3 Europium

The experiments with uranium were followed by a study (Table 2) of the sorption behavior of ^{152}Eu with an initial concentration of $2.9 \cdot 10^{-9} \text{ mol} \cdot \text{L}^{-1}$ on cement material CEM I (Burešová et al. 2023) and CEM III in a saturated $\text{Ca}(\text{OH})_2$ solution with or without the addition of organic substances (adipate, phthalate acid and EDTA) in different concentrations ($5 \cdot 10^{-5} \text{ mol} \cdot \text{L}^{-1}$ and $5 \cdot 10^{-3} \text{ mol} \cdot \text{L}^{-1}$).

Kinetic experiment

First, it was necessary to verify the time required to attain equilibrium in the system containing CEM III. Kinetic experiments lasted up to 2 days ($\text{L/S } 500 \text{ L} \cdot \text{kg}^{-1}$) without organic matter and with the addition of organic matter in a concentration of $5 \cdot 10^{-5} \text{ mol} \cdot \text{L}^{-1}$ and in the case of EDTA also with a concentration of $5 \cdot 10^{-3} \text{ mol} \cdot \text{L}^{-1}$.

In all kinetic experiments (Figure 4), an initial rapid decrease in activity in solution to equilibrium is evident. Equilibrium is reached within 24 hours.

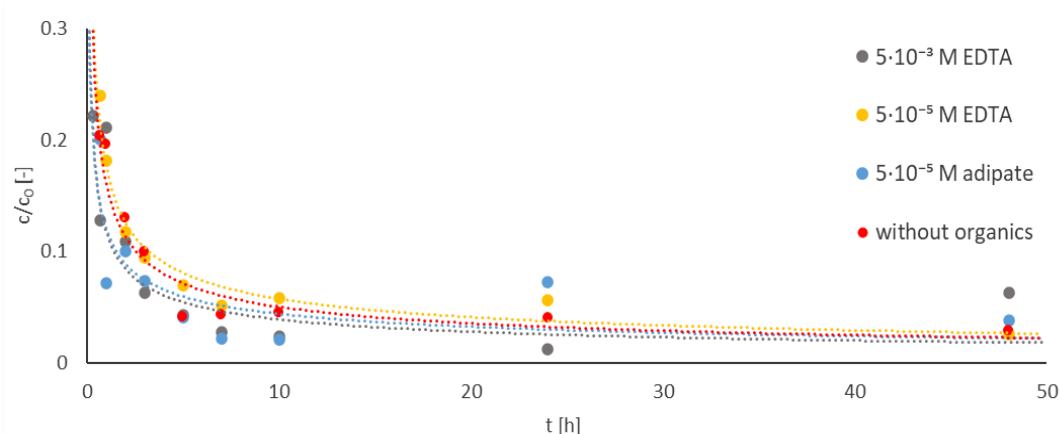


Figure 4: Kinetics of ^{152}Eu ($2.9 \cdot 10^{-9} \text{ mol} \cdot \text{L}^{-1}$) sorption on CEM III in portlandite water with and without organics ($5 \cdot 10^{-5}$ and $5 \cdot 10^{-3} \text{ mol} \cdot \text{L}^{-1}$).

The behavior of a system with CEM III is nearly identical to that of a system containing CEM I, only equilibrium in the currently shown system occurs slower. The effect of organics presence (independently of its concentration in the case of EDTA) on the course of the experiment is not significant (Burešová et al. 2023).

Equilibrium experiment

Equilibrium experiments were performed with sampling after 2 days and in 9 different configurations (Table 2).

The results shown in Table 4 and on Figure 5 indicate the effect of the presence of organic matter on the resulting R_d value. In the presence of studied organic substances, values of R_d are comparable (adipate) or higher (EDTA) than in their absence. EDTA has a larger effect on R_d values in the system containing CEM III than in the case of CEM I (Table 5).

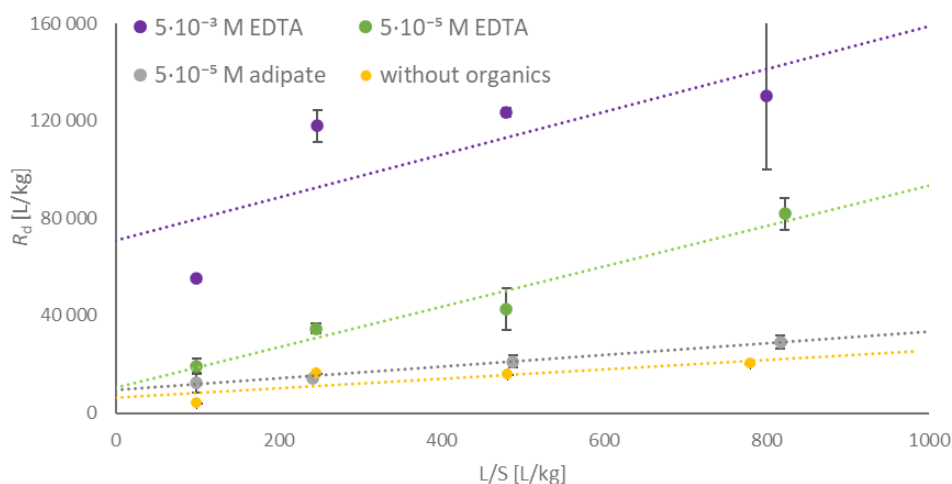


Figure 5: Dependence of R_d ($L \cdot kg^{-1}$) on the phase ratio L/S of ^{152}Eu ($2.9 \cdot 10^{-9} mol \cdot L^{-1}$) sorption on CEM III with and without organics ($5 \cdot 10^{-5}$ and $5 \cdot 10^{-3} mol \cdot L^{-1}$).

Table 4: Distribution ratios R_d ($L \cdot kg^{-1}$) of ^{152}Eu ($2.9 \cdot 10^{-9} mol \cdot L^{-1}$) sorption on CEM III with and without organics ($5 \cdot 10^{-5}$ and $5 \cdot 10^{-3} mol \cdot L^{-1}$)

L/S ($L \cdot kg^{-1}$)	Without organics	$5 \cdot 10^{-5} mol \cdot L^{-1}$ EDTA	$5 \cdot 10^{-3} mol \cdot L^{-1}$ EDTA	$5 \cdot 10^{-5} mol \cdot L^{-1}$ Adipate
	R_d ($L \cdot kg^{-1}$)			
100	4 000	19 300	55 000	12 300
250	16 400	34 600	118 000	14 200
500	15 900	42 600	123 000	21 200
800	20 200	82 000	130 000	29 000

For all experiments performed, the distribution ratios were in the order of 10^3 - $10^5 L \cdot kg^{-1}$ which agrees with the published R_d values for cementitious materials (e.g. Glaus et al. 2020, Wieland et al. 1998) and also for americium (Ochs et al. 2015) for which Eu is an often used analogue.

Sorption on the walls

To supplement the already published issue of sorption of Eu to walls of experimental ampoules (Burešová et al. 2023), an interesting finding from the study of Eu diffusion through compacted, pre-crushed CEM I (material identical to the one used in sorption experiments) was gained (Čejková 2021). An overall mass balance was performed for the diffusion cell experiments where no organic matter was added (with ^{152}Eu only) and for the cell where EDTA was added together with Eu (Figure 6).

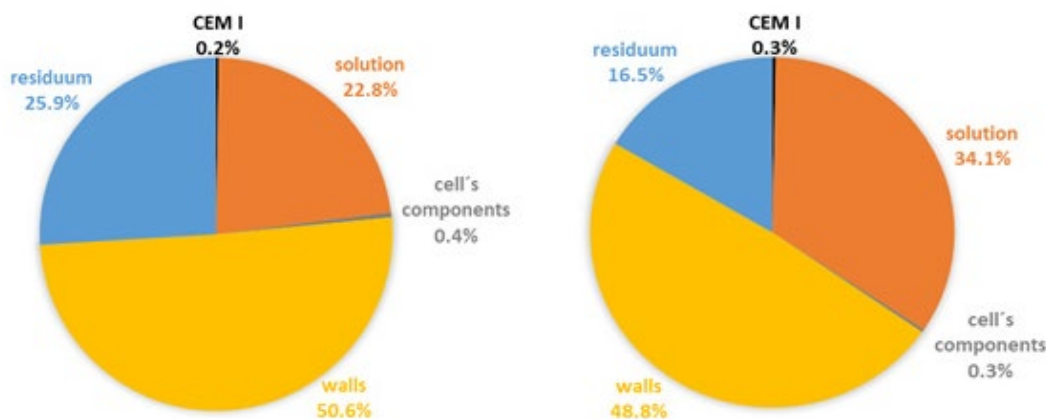


Figure 6: Substance balances for the diffusion cell where EDTA was added (left) and for the cell without organics (right).

A significant part of the radionuclide (around 50 %) was sorbed on the walls of the plexiglass reservoirs. This confirmed the fact that europium is a highly sorbed element (e.g., Glaus et al. 2020), which is therefore not suitable for diffusion experiments, because wall sorption significantly affects the course of the experiment. The presence of EDTA results in a slightly increased sorption on the reservoirs walls as well as on the individual components of the diffusion cell compared to the system without organics.

4 Conclusions

The results obtained so far are summarized in Table 5. Due to experimental errors, it can be only stated that the distribution ratios are of the order 10^3 - 10^5 L·kg⁻¹ for Eu sorption on both CEM I and CEM III materials (the issue with sorption on the walls is still ongoing), and in case of uranium sorption on CEM I in NaOH and in portlandite water environment in the range 10^3 - 10^4 L·kg⁻¹, and up to 10^5 L·kg⁻¹ for uranium on CSH. Distribution ratios increase with increasing phase ratio with the exception of the system containing uranium, CEM I and $5 \cdot 10^{-3}$ mol·L⁻¹ EDTA. Further additions to this direction of research are planned.

5 Future work

In the case of uranium and europium, efforts will be made to supplement missing experiments in the schedule performed (Table 5). It is also necessary to investigate sorption of Eu on CSH, U on CEM III, and also use NaOH solution as a liquid phase in some cases.

The sorption behavior of lead (used in its stable form, determined by means of AAS) of the initial concentration $5 \cdot 10^{-4}$ mol·L⁻¹ in the presence of CEM I or CEM III in a portlandite water environment has been studied. EDTA and phthalate are gradually added to this initial system. Also lead sorption on CSH with a Ca/Si ratio of 1 and 1.2 will be studied. Experiments with EDTA at various concentrations will be completed. Sorption behavior of lead was already published (Drtinová et al. 2023).

For all studied elements it is also planned to perform experiments with irradiated samples of cementitious materials. Organic-free systems and then probably the same systems in the presence of EDTA will be studied.

For the products identified in Task 2, clear results are still not completed and therefore sorption experiments cannot be planned. However, irradiated CEM I and CEM III samples that already contained a plasticizer are available. Therefore, sorption and diffusion experiments on these materials with studied radionuclides are proposed.

Table 5: Distribution ratios R_d ($L \cdot kg^{-1}$) of radionuclides sorption on different cementitious materials in different liquid phase with and without organics ($5 \cdot 10^{-5}$ and $5 \cdot 10^{-3}$ mol·L⁻¹)

Organics			Without organics	$5 \cdot 10^{-5}$ mol·L ⁻¹ EDTA	$5 \cdot 10^{-3}$ mol·L ⁻¹ EDTA	$5 \cdot 10^{-5}$ mol·L ⁻¹ Adipate	$5 \cdot 10^{-5}$ mol·L ⁻¹ Phthalate
RN	CEM	Liquid phase	R_d ($L \cdot kg^{-1}$)				
¹⁵² Eu	CEM I	Ca(OH) ₂	10 000-27 000	44 000-56 000	18 000-80 000	5 500-60 000	21 000-34 000
	CEM III	Ca(OH) ₂	4 000-20 000	19 300-82 000	55 000-130 000	12 300-29 000	×
²³³ U	CEM I	Ca(OH) ₂	2 700-12 500	2 000-13 000	×	×	×
		NaOH	14 700-50 000	12 700-48 000	4 400-11 200	9 900-26 000	13 600-34 000
	CSH	×	11 300-100 000	52 000-90 000	×	×	×

Acknowledgement

The EURAD-CORI project leading to this application has received funding from the European Union's Horizon 2020 research and innovation programme under grant agreement No 847593. The output was created also with the financial participation of SÚRAO (Czech Radioactive Waste Repository Authority) (SO2020-017). This contribution is partially a result of European Regional Development Fund-Project "Centre for Advanced Applied Sciences" (Grant No. CZ.02.1.01/0.0/0.0/16_019/0000778).

References

- Atkins, M., Glasser, F.P., Kindness, A. (1992). Cement hydrate phases: Solubility at 25 °C. *Cem. Concr. Res.* 22, 241–246.
- Brownsword, M., Buchan, A.B., Ewart, F.T., McCrohon, R., Ormerod, G.J., Smith-Briggs, J.L., Thomason, H.P. Oversby, V.M., Brown, P.W. (Eds.). (1990). *The solubility and sorption of uranium(VI) in a cementitious repository*. United States: Materials Research Society.
- Burešová, M., Kittnerová, J., Drtinová, B. (2023). Comparative study of Eu and U sorption on cementitious materials in the presence of organic substances. *J Radioanal Nucl Chem.* <https://doi.org/10.1007/s10967-022-08705-3>
- Čejková, A. (2021). Diffusion of europium in repository barrier materials (bachelor thesis, in Czech). CTU in Prague.
- Drtinová, B., Kittnerová, J., Bergelová, K., Burešová, M., Baborová L. (2023). Sorption of lead on cementitious materials in presence of organics. *Front. Nucl. Eng.* 1:1095233. doi: 10.3389/fnuen.2022.1095233
- Glaus, M. A., Frick, S., Van Loon, L. R. (2020). A coherent approach for cation surface diffusion in clay minerals and cation sorption models: Diffusion of Cs⁺ and Eu³⁺ in compacted illite as case examples. *Geochimica et Cosmochimica Acta*, 274, 79–96. <https://doi.org/10.1016/j.gca.2020.01.054>
- Glaus, M.A., Laube, A., Van Loon, L.R. (2004). A generic procedure for the assessment of the effect of concrete admixtures on the sorption of radionuclides on cement: Concept and selected results. *Mater Res Soc Symp Proc* 807:365–370. <https://doi.org/10.1557/proc-807-365>
- Hummel, W. (1993). *Organic Complexation of Radionuclides in Cement Pore Water: A Case Study*. PSI, Report Number TM-41-93-03/PES-93-617
- KIT (2021). Milestone MS98 – CORI Technical Report - Task 4 (i) Radionuclide transport in HCP in the presence of organics, (ii) Radionuclide speciation under alkaline conditions in presence of organics.
- Kittnerová, J., Drtinová, B., Štamberg, K., Vopálka, D., Evans, N., Deissmann, G., Lange, S. (2020). Comparative study of radium and strontium behaviour in contact with cementitious materials. *Applied Geochemistry*. 122. 104713. [10.1016/j.apgeochem.2020.104713](https://doi.org/10.1016/j.apgeochem.2020.104713).
- Lange, S., Kowalski, P.M., Pšenička, M., Klinkenberg, M., Rohmen, S., Bosbach, D., Deissmann, G. (2018). Uptake of ²²⁶Ra in cementitious systems: A complementary solution chemistry and atomistic simulation study. *Appl. Geochemistry* 96, 204–216. <https://doi.org/10.1016/j.apgeochem.2018.06.015>
- Ochs, M., Mallants, D., Wang, L. (2015). *Radionuclide and Metal Sorption on Cement and Concrete*. Springer, vol. 9999, pp. 171–182.
- Poinreau, I., Landesman, C., Giffaut, E., Reiller, P. (2004). Reproducibility of the uptake of U(VI) onto degraded cement pastes and calcium silicate hydrate phases. *Radiochimica Acta*, 92(9–11), 645–650. <https://doi.org/10.1524/ract.92.9.645.55008>
- Poinreau, I., Piriou, B., Fedoroff, M., Barthes, M. G., Marmier, N., Fromage, F. (2001). Sorption mechanisms of Eu³⁺ on CSH phases of hydrated cements. *Journal of Colloid and Interface Science*, 236(2), 252–259. <https://doi.org/10.1006/jcis.2000.7411>
- Tits, J., Geipel, G., Macé, N., Eilzer, M., Wieland, E. (2011). Determination of uranium(VI) sorbed species in calcium silicate hydrate phases: A laser-induced luminescence spectroscopy and batch sorption study. *Journal of Colloid and Interface Science*, 359(1), 248–256. <https://doi.org/10.1016/j.jcis.2011.03.046>
- Van Loon, L. & Hummel, W. (1995). *The radiolytic and chemical degradation of organic ion exchange resins under alkaline conditions: effect on radionuclide speciation (PSI--95-13)*. Switzerland
- Vašíček, R., Hlaváč, Z., Večerník, P., Drtinová, B., Vlk, M., Kučerová, M. (2023). The effect of gamma irradiation on cementitious materials with superplasticizers – The Czech contribution. *Proceedings Document – CORI 3rd Annual Workpackage Meeting – 25.-29. Nov. 2021*.
- Večerník, P., Drtinová, B., Bárta, J., Brázda, L., Galeková, E., Havlová, V., Hofmanová, E., Kašpar, V., Kittnerová, J., Kolomá, K., Rosendorf, T., Vopálka, D. (2019). *Transport properties of cementitious materials*. Final report. TZ 430/2019/ENG, SÚRAO/ÚJV Řež, a. s., Praha, 103 pp.
- Wieland, E., Macé, N., Dähn, R., Kunz, D., Tits, J. (2010). Macro- and micro-scale studies on U(VI) immobilization in hardened cement paste. *Journal of Radioanalytical and Nuclear Chemistry*, 286(3), 793-800.

Wieland, E., Tits, J., Spieler, P., Dobler, J.P. (1998). Interaction of Eu(III) and Th(IV) with sulphate-resisting Portland cement. Mater Res Soc Symp - Proc 506:. <https://doi.org/10.1557/proc-506-573>

Sorption of Am(III) /Pu (III/IV) on hardened cement paste in the presence of organics

R.Druteikienė*, R.Gvozdaitė, A.Gudelis

Center for Physical Sciences and Technology,
Savanorių ave. 231, LT-02300 Vilnius, Lithuania

* Corresponding author: ruta.druteikiene@ftmc.lt

Abstract

The sorption kinetics of elements in the ternary systems Pu/Am- HCP-adipic acid / dioctyl adipate were investigated using batch-type experiments, and the distribution coefficients K_d , representing the experimental systems, were obtained. The experiments performed in this study demonstrate the high retention capability of hardened cement paste towards the investigated actinides in the presence of organics under alkaline (pH 12.5 -12.56; Eh -323 - -328 mV) conditions. All sorption experiments showed significant uptake of > 90% Pu/Am by HCP and some effect of adipic acid and dioctyl adipate on sorption.

The highest values of Pu K_d 2218-2645 L/Kg and Am (III) K_d 392-996 L/Kg were obtained at 0.1 M adipic acid, indicating a weak effect of adipic acid on the sorption of Pu(III/IV) and Am (III). K_d decreases at 0.2 M adipic acid, indicating the effect of organic ligands concentration on sorption. The K_d values of Pu(III/IV) and Am (III) in the system with DOA indicate that DOA inhibits the uptake of both elements by HCP and the K_d values decrease with increasing DOA concentration.

INTRODUCTION

Solidification of low and intermediate level radioactive waste with cementitious materials is one of the most frequently applied techniques prior to the near-surface or underground disposal (Tits et al, 2006; Harfouche et al, 2006; Gaona et al, 2011; Li and Pang, 2014). Radionuclide interactions with cement-based barrier materials are of great interest to the assessment of the long-term safety of radioactive waste repositories.

The retention of radionuclides in the cement matrix is related to the chemical composition of the sorbent, speciation of sorbate and the interaction mechanism between the sorbent and sorbate (Smith et al, 2015; Evans, 2008; Plecas et al, 2006; Kienzler et al, 2014). A large pH gradient, the redox potential, the electrolyte composition, and the ionic strength, specific to a cementitious backfill are the factors influencing radionuclide retention or transport from the disposal facility (Stockdale and Bryan, 2013).

Several principal mechanisms as precipitation of insoluble phase, co-precipitation with other phases, and incorporation into lattice, chemisorption/physical adsorption, and complex/colloid formation in the aqueous phase are decisive factors in the retention of radionuclides in cement (Smith et al, 2015; Evans, 2008; Isaacs et al, 2020). Because of a chemical composition of a fresh cement paste in equilibrium with the cement pore water dominated by Na⁺, K⁺ hydroxides and saturated with Ca(OH)₂, the cement generates a hyperalkaline environment (10 < pH <13) for a long period of time (Jacques et al, 2010).

The cement matrix of radioactive waste packages, depending on the type of waste, may contain various organic compounds: some of them are polymeric additives as plasticizers, and others are hydrolysed and radio-oxidized polymers formed during the operation of nuclear fuel cycle facilities.

It is known that hyperalkaline conditions in cementitious medium can cause aging and degradation of polymeric additives with the production of new organics with new chemical properties (Tasi et al, 2018).

The capability of a cement engineered barrier to ensure retention of any given radionuclide is directly connected to the properties of the cement. The backfill mixture must provide a high pH environment and sufficient surfaces for sorption (Evans et al, 2012). Superplasticizers, (polymeric additives) improve the plasticity of the cement and act as a water reducer, affecting the solubility and migration of radionuclides. There are some categories of cement additives such as polycarboxylic, amino-sulfonic, naphthalene-sulfonic, lignin-sulfonic and melamine-sulfonic which are basic for cement formulation (Kitamura et al, 2013; Garcia et al, 2018).

The next biggest reservoir of organic contaminants in geological repositories of a radioactive waste, which is affected the behaviour of radionuclides, are the radio-oxidized polymers generated during the exploitation of nuclear fuel cycle facilities. These polymers, as gloves, filters, seals, cables, ion-exchange resins, etc, are stowed in the intermediate-level long-lived repositories in cemented packages where they start to degrade due to hydrolysis and oxidation (Fromentin and Reiller, 2018).

Other organic contaminants in waste packages are cellulose and cellulosic materials (tissues, cotton, paper), which degradation under strongly alkaline conditions generated a strong complexing agent - isosaccharinic acid (Tits et al, 2005), which forms strong complexes with many elements, especially with actinides (Rai and Kitamura, 2017; Tasi et al, 2018).

Significantly progress has recently been made in getting fundamental knowledge on the influence of organic ligands, originating from the degradation of organic materials in cementitious environments, on the chemical behaviour of radionuclides (Fromentin and Reiller, 2018; Tits et al, 2005; Tasi et al, 2018; Garcia et al, 2018; Ma et al, 2019; Vercammen et al, 2001; Wieland et al, 2014). It was found that high concentrations of isosaccharinic acid (above 10^{-5} M) and gluconic acid (above 10^{-7} M) in the cement pore water significantly reduced the uptake of Eu(III), Am(III) and Th(IV) by calcite due to the formation of metal-ligand complexes in solution (Tits et al, 2005; Evans et al, 2012). Evans with co-authors (Evans et al, 2012) investigated the complexation of a radionuclide mixture of ^{60}Co , ^{90}Sr and Eu by α -isosaccharinic, gluconic and picolinic acids. The competition effects of Co and Sr on Eu solubility in the presence of iso-saccharinate, gluconate and picolinate have also been investigated. An increase in the solubility of Eu in the presence of iso-saccharinate and gluconate and an increase in the solubility of Co in the presence of gluconate was determined. However, in the systems, Eu with iso-saccharinate and Sr as a competing ion, as well as Eu with gluconate and either Co or Sr as a competing ion, the solubility of Eu was reduced. Kitamura et al (Kitamura et al, 2013) found that a polycarboxylic acid-type superplasticizer had no significant effect on the solubility of Th and Am in cement pore water squeezed from ordinary Portland cement paste compared to data from cement-equilibrated water without superplasticiser.

Adipic acid is the main hydro-soluble degradation product of polyesterurethane, used in gloves for glove boxes. Adipate ions are able to complex trivalent f-transition elements such as Eu(III)- an analogue of 5f actinides (III) for the complexation by oxygen-containing molecules (Wang et al, 2000; Fromentin and Reiller, 2018).

The formation of the Eu(III) complex with adipic acid in $0.5 \text{ mol kg}_w^{-1} \text{ NaClO}_4$ ionic medium was investigated by (Fromentin and Reiller, 2018). Moreover, the solubility and deprotonation constants of adipic acid, as well as specific interaction theory (SIT) coefficients of aqueous $\text{AdipH}_{2(\text{aq})}$ and adipate ions (AdipH^- and Adip^{2-}) were estimated using available literature data in NaCl and NaClO_4 ionic media. They concluded that an adipic acid would control the Eu(III) speciation from slight

acidic to mildly basic conditions, but would not control in highly basic solutions characteristic for the cement pore water.

Actinides are important category of elements presented in most radioactive waste streams. Investigation of their behaviour in cement backfill under representative chemical conditions is relevant to assessing safe storage in the long term. Organic ligands resulting from the degradation of organic materials in the storage or present as cement additives can affect the retardation of tri- and tetravalent actinides by forming metal-ligand complexes in the solution (Tits et al, 2005) .

This work focuses on the sorption kinetics of Pu and Am (III) on HCP in the presence of adipic acid and dioctyl adipate, with the carboxyl/carboxylate group as a strong complexing moiety. There is a very little data on the complexation of tri- and tetravalent actinides with a dicarboxylic acid and dicarboxylates in strongly alkaline ($10 \leq \text{pH} \leq 13.5$) cement media. Knowledge of the interaction between radionuclides and organic ligands released from degraded polymers resulting from cement additives is crucial for predicting the subsequent geochemical behaviour of actinides. Thus, understanding the solubility and complexation of actinide ions with carboxylic/carboxylate ligands under hyperalkaline conditions is essential.

1.Methods

Preparation of hardened cement paste and sorption kinetics experiments was performed in the air under ambient conditions.

Commercial Portland cement (CEM I 42.5 R, Heidelberg Cement Group, Sweden) cured 3 months with a water to cement ratio (S/L) of 0.5 under ambient conditions (20°C and relative humidity above 70%) in clogged plastic vials. Then the prepared hardened cement paste (HCP) was dried, crushed in a grinding-mill and sieved out through 0.25 mm separator. To achieve the HCP leachate with pH 12.5, the powdered HCP was poured with the deionized water at solid to liquid ratio (S/L) of 0.25 and allowed to shake for 7 days in the air (20°C and relative humidity above 70%). Subsequently, the solution was separated from the solid phase by centrifugation (5000 rpm, 10 min) and the pH of the equilibrium solution was measured. If the pH has not reached the required value, the fresh deionized water was poured into the solid phase and the procedure was repeated under above mentioned ambient conditions until the pH of the equilibrium solution was approximated to ~ 12.50, Eh varied from -323 to -328 (Table 1).

Table 1: pH/Eh of the corresponding equilibrium solutions (S/L 0.25)

Sample	Eh	pH
D1 (3 days)	-325	12,50
D2 (7 days)	-323	12,48
D3 (14 days)	-327	12,54
D4 (30 days)	-327	12,56
D5 (3 days)	-327	12,54
D6 (7 days)	-328	12,56
D7 (14 days)	-325	12,51
D8 (30 days)	-326	12,53

Solid phase was separated by centrifuging the suspension and dried at 105° C. The chemical composition (Table 2) of the obtained hardened cement paste (HCP) was determined using fluorescent X-ray spectrometer with wave dispersion Axios mAX (Pananalytical, Netherlands) and Carbon and Sulphur analyser CS-2000 (Eltra, Germany).

Table 2: Chemical composition of the raw cement (CEM I 42.5 R) and hardened cement paste after 90 days of curing

Compound formula	Raw cement	Hardened cement paste (after 90 days of curing)
	%	%
CO ₂	13.90	16.01
O	5.93	6.66
Na ₂ O	0.10	0.05
MgO	2.13	1.86
Al ₂ O ₃	3.19	3.41
SiO ₂	14.98	13.73
P ₂ O ₅	0.07	0.06
SO ₃	2.98	2.79
Cl	0.02	0.04
K ₂ O	0.97	0.06
CaO	52.51	51.95
TiO ₂	0.25	0.23
MnO	0.04	0.04
Cr ₂ O ₃	0.03	0.02
Fe ₂ O ₃	2.78	2.94
NiO	0.01	0.01
CuO	0.002	0.003
ZnO	0.02	0.01
Rb ₂ O	0.004	-
SrO	0.07	0.05
Y ₂ O ₃	0.004	-
BaO	0.01	0.02

For the sorption experiments, 0.1M and 0.2M adipic acid solutions in deionized water were prepared. The pH of the 0.1M and 0.2M adipic acid solution was adjusted to a value of 12.50 ± 0.02 with 0.1 M sodium hydroxide. The tracer solutions of Pu⁴⁺ (0.5 Bq/mL or $9.1 \cdot 10^{-13}$ M) and Am³⁺ (0.5 Bq/mL or $2.9 \cdot 10^{-13}$ M) in 2M HNO₃ were prepared using ²³⁹Pu and ²⁴³Am stock solutions (Eckert & Ziegler Isotope Products). The oxidation state of Pu (IV) was maintained by adding 0.1 ml of 0.5 M NaNO₂ to the solution.

For sorption kinetics studies, 40 mL of 0.1M/0.2M adipic acid solution (in deionized water) at pH 12.5 were added to 10 g of powdered HCP (S/L ratio 0.25), respectively and the suspension was allowed to equilibrate for 7 days before spiking with the appropriate amounts of ²³⁹Pu (0.3 Bq/sample or $5.50 \cdot 10^{-13}$ M) and ²⁴³Am (0.3 Bq/sample or $1.73 \cdot 10^{-13}$ M). The centrifuge tubes were shaken end-over-end for an appropriate period of time (3, 7, 14, 30 days). After equilibration, the phases were separated by centrifugation and the supernatant was taken for further radiochemical analysis and preparation of ²³⁹Pu sources for alpha spectrometry. The samples were measured with the alpha-spectrometer Octete Plus (Ortec). Counting times ranged from 25 to 75 hours depending on the

activity of the sample. The alpha counting efficiency was 25% and resolution 25–27 keV, the detection limit of ²³⁹Pu for α counting time of 86,400 s is 10^{-3} Bq.

Gamma-spectrometric measurements of ²⁴³Am in the solid phase of HCP were carried out using a HPGe detector with Genie 2000 gamma-spectroscopy analysis software (Canberra Industries, USA). The detector itself was that of GMX series made by Ortec, USA, with relative efficiency of 30%. The detection limit for ²⁴³Am is 12 mBq.

The uptake of plutonium and americium by HCP is quantified in terms of a distribution coefficient K_d [L/Kg], as follows (eq. 1):

$$Kd = \frac{[C]_0 - [C]_{eq}}{[C]_{eq}} \cdot \frac{V}{m} \quad (1),$$

with $[C]_0$ [mol/ L], radionuclide concentration of the suspension; $[C]_{eq}$ [mol/ L], radionuclide concentration in the equilibrium solution; V [L], volume of the solution; m [kg], mass of the solid.

The same set of experiments were carried out in the ternary system of Pu, Am /HCP (CEM I) / dioctyl adipate (DOA). Pure dioctyl adipate (DOA) was used for the sorption experiment because it is sparingly soluble in water. There 2.5 mL, 5 mL and 7.5 mL of DOA corresponding to the molar concentration of 0.006 M, 0.012 M, 0.019 M were added to the HCP suspension, respectively.

The sorption kinetics tests of Pu(IV) and Am(III) without organic matter were performed under the same experimental conditions.

2. Results and Discussion

Evolution of the pH and Eh was controlled at the beginning and at the end of each experiment. The pH ranged between 12.50 and 12.56 throughout the experiment with the adipic acid and dioctyl adipate in all batch systems; the Eh of the suspensions ranges from -323 to -328 mV, and remained relatively stable during the experiment, indicating that the experimental system was maintained under reduction conditions.

Preliminary results of sorption kinetic studies showed a little effect of adipic acid on Pu (III/IV) uptake by HCP at pH ~12.5. This is consistent with the sorption kinetics in the blank system without adipic acid: all these results have shown rapid sorption kinetics during the first 3 days. In the system without organic ligands, the residual amount of plutonium has not exceeded 1% in the solution after 7 days. In the system with 0.1 M adipic acid, a negligible amount (less than 0.5% within uncertainties) of Pu(III/IV) remained in the solution after 3 days and maintained a steady state until the end of the experiment. Within 30 days, an insignificant effect of 0.2 M adipic acid for Pu sorption was obtained within the limits of statistical error (Fig.1). After 30 days of exposure, the amount of residual Pu(III/IV) in the solution remains below 0.5 %. The sorption of Pu(III/IV) onto HCP in the absence of adipic acid showed an inclination to be reversible. The blank test showed that the concentration of plutonium decreased in the solution during the first seven days and then began to increase until day 30. Regarding the quantitative uptake of Pu by HCP in the presence of adipic acid, which was observed in our experiments after 30 days, it is assumed that adipic acid may inhibit the desorption of Pu from the matrix.

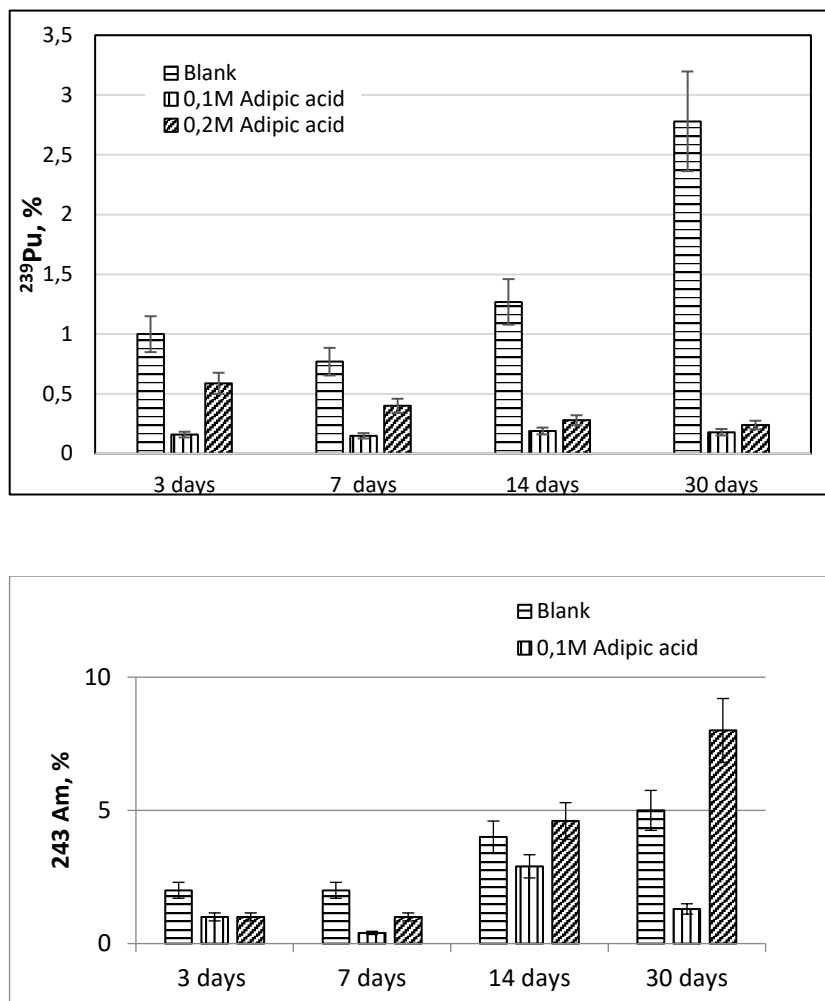


Figure 1 – Sorption of radionuclides on HCP in presence of adipic acid: percentage of Pu(III/IV) and Am(III) remaining in solution

The sorption kinetics of Am(III) to HCP in the presence of the adipic acid showed that the equilibrium of the system was not reached within 30 days. Compared to the blank test, the presence of adipic acid had some effect on the sorption of Am onto hardened cement paste during the first seven days with no more than 2% Am remaining in the solution. During the next 14-30 days, the amount of Am in the solution began to increase indicating the likely reversibility of the sorption reaction. The blank test without adipic acid also showed a quite significant increase of Am in the solution to 8% at day 30. There was no identifiable trend in the sorption of both Pu and Am onto HCP in the presence of dioctyl adipate (DOA). The concentration of DOA in the experimental system had relevant effect on the sorption of Pu and Am (III) to HCP (Fig. 2). Pu(III/IV) sorption was slightly lower when the concentration of DOA in the system was higher (0.019 M), and the percentage of Pu(III/IV) remaining in the solution varied between 10-20%. The lowest effect of DOA on Pu sorption was observed when the concentration of DOA in the system was 0.006 M. In this case, the remaining amount of Pu in the solution did not exceed 5% during 30 days.

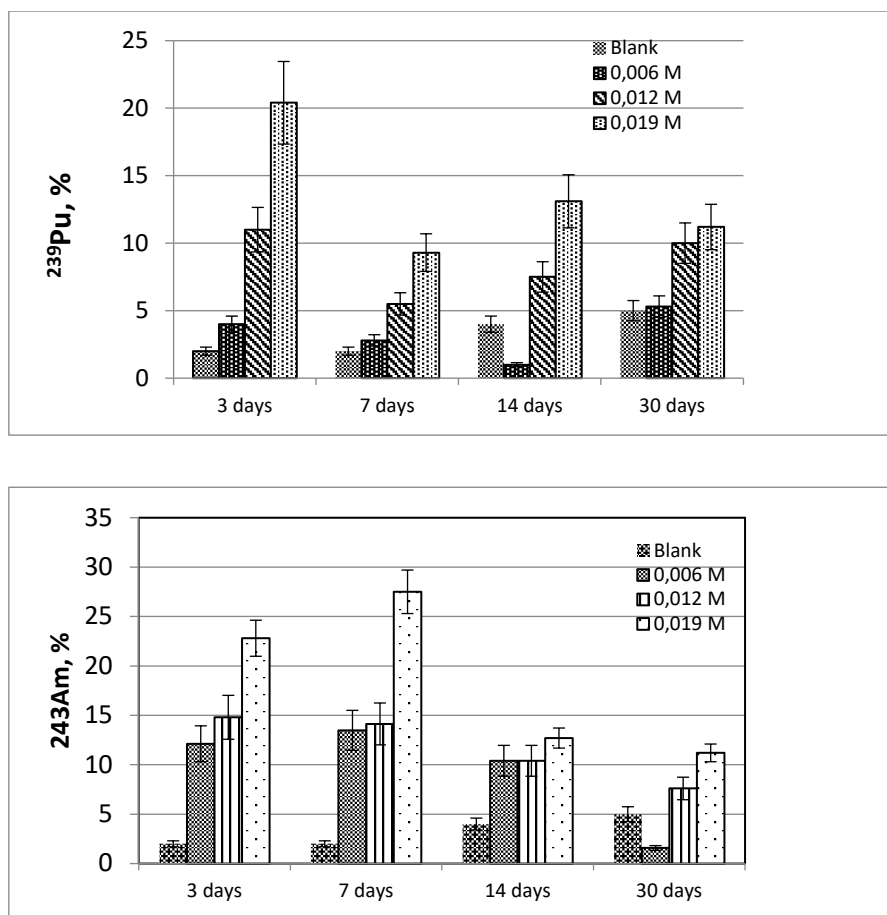


Figure 2 - Sorption of radionuclides on HCP in presence of dioctyl adipate: percentage of Pu(III/IV) and Am(III) remaining in solution

The data show that DOA suppressed the sorption of Am(III) to HCP under given experimental conditions. A marked decrease in Am(III) sorption to HCP was found at 0.019 M DOA. The concentration of Am(III) in solution varied from about 13% after 3 days to about 26% at the end of experiment (30 days). The concentrations of Am(III) in solution at 0.006 M DOA ranged from 3% after 3 days to about 10% on day 7 and about 5-7 % after 14-30 days. The percentage of Am(III) in solution at 0.012 M DOA varied from 5% to 20-25% throughout the experiment.

The distribution coefficients K_d of Pu and Am(III) were calculated. It is known that K_d values are strongly influenced by various environmental conditions and it is representative only for equilibrium conditions of the system (Kaplan et al., 2011). Sorption kinetics results indicated that sorption may not have reached equilibrium, so K_d will be defined as conditional K_d . It should be noted that K_d values usually demonstrate nonlinear sorption with an intense process at the beginning (especially due to organic matter) and slow saturation lasting up to 10 days (Zuo et al., 2010) or even more than 100 days (Begg et al., 2018). Therefore, the resulting conditional K_d values approximate those that would be obtained under equilibrium conditions. The distribution coefficients of Pu and Am(III) in the HCP in the presence of adipic acid and DOA are presented in Table 3.

Table 3. Calculated K_d values for Pu(III/IV) and Am (III) sorption to HCP at pH ~ 12.5 in the presence of 0.1 M and 0.2 M adipic acid and 0.006 M, 0.012 M and 0.019 M dioctyl adipate (DOA)

Days	K_d [L/Kg]						K_d [L/Kg]					
	Pu(III/IV)			Am(III)			Pu(III/IV)			Am(III)		
	Adipic acid						DOA					
	blank	0.1 M	0.2 M	blank	0.1 M	0.2 M	0.006M	0.012M	0.019M	0.006M	0.012M	0.019M
3	396±20	2496±50	675±26	196±14	392±20	393±20	96±10	32±7	16 ± 4	29 ± 5	23 ± 5	13 ± 4
7	496±22	2645±51	996±32	196±14	996±32	392±20	139±12	69 ± 8	39 ± 6	26 ± 5	24 ± 5	10 ± 3
14	311±18	2101±46	1424±38	96±10	134±12	83 ± 9	396±20	49 ± 7	26 ± 5	34 ± 6	34 ± 6	27 ± 5
30	140±12	2218±47	1662±41	76 ± 9	304±17	46 ± 7	71 ± 8	36 ± 6	32 ± 7	249±16	49 ± 7	32 ± 7

The highest values of Pu K_d 2218-2645 L/Kg and Am (III) K_d 392-996 L/Kg were obtained at 0.1 M adipic acid, indicating a weak effect of adipic acid on the sorption of Pu(III/IV) and Am (III). K_d decreases at 0.2 M adipic acid, indicating the effect of organic ligands concentration on sorption. The K_d values of Pu(III/IV) and Am (III) in the system with DOA indicate that DOA inhibits the uptake of both elements by HCP and the K_d values decrease with increasing DOA concentration.

There may be several reasons for the variation of K_d . One of the implicit assumptions regarding K_d is reversibility. It was noted that hydrated cement systems are relatively unique in this sense because the sorbing solid is undergoing alterations while sorption is taking place. The wide dispersion in K_d values may be due to the inhomogeneity of the system caused by the incompatibility of the organic phase with water, especially if it involves DOA. On the other hand, this may be due to the short contact of analytes with cement. For most of the systems the distribution coefficients increased with time, reaching a fairly constant level after several months (Kaplan et al., 2011).

In the scientific literature, there is a complete lack of data on the complexation of tri- and tetravalent actinides with adipic acid or dioctyl adipate in a strongly alkaline (pH about 12.5) medium. Without a consistent and reliable set of thermodynamic data, we could not draw clear conclusions about the effects of these organics on the solubility and complexation of Pu and Am (III) in cement systems under hyper alkaline conditions. The interpretation of the behaviour of Pu under the studied strong alkaline conditions is complicated, because the evolution of oxidation states of Pu was not followed during the experiments.

3. Conclusions

The experiments performed in this study demonstrate the high retention capability of hardened cement paste towards the investigated actinides in the presence of organics under alkaline (pH 12,5 -12.56; Eh -323 - -328 mV) conditions. All batch-type sorption experiments were provided in air under ambient conditions. The obtained results showed that at pH 12.5, in the presence of organic ligands, the hardened cement paste significantly adsorbed Pu(III/IV) and Am (III) by more than 90%. The highest values of Pu K_d 2218-2645 L/Kg and Am (III) K_d 392-996 L/Kg in the presence of adipic acid were obtained. The K_d values of Pu(III/IV) and Am (III) in the system with DOA indicated that DOA inhibits the uptake of both elements by HCP. In addition, the K_d of Pu and Am (III) decreased linearly with increasing of DOA concentration.

These observations can be rationalized by taking into account the actinide speciation in cement water, the formation of surface complexes and the complexing behaviour of the cement additives and their degradation products.

Acknowledgement

The EURAD-CORI project leading to this application has received funding from the European Union's Horizon 2020 research and innovation programme under grant agreement No 847593.

References

1. Tits J, Wieland E, Müller CJ, Landesman C, Bradbury MH (2006) Strontium binding by calcium silicate hydrates. *J Colloid Interface Sci* 300,78–87.
2. Harfouche M, Wieland E, Dähn R, Fujita T, Tits J, Kunz D, Tsukamoto M (2006) EXAFS study of U(VI) uptake by calcium silicate hydrates. *J Colloid Interface Sci* 303,195–204.
3. Gaona X, Dähn R, Tits J, Scheinost AC, Wieland E (2011) Uptake of Np(IV) by C-S-H phases and cement paste: an EXAFS study. *Environ Sci Technol* 45,8765–71.
4. Li K, Pang X (2014) Sorption of radionuclides by cement-based barrier materials. *Cem Concr Res* 65:52–57.
5. Smith KF, Bryan ND, Swinburne AN, Bots P, Shaw S, Natrajan LS, Mosselmans JFW, Livens FR, Morris K (2015) U(VI) behaviour in hyperalkaline calcite systems. *Geochim Cosmochim Acta* 148,343–359.
6. Evans NDM (2008) Binding mechanisms of radionuclides to cement. *Cem Concr Res* 38,543–553.
7. Plecas I, Dimovic S, Smiciklas I (2006) Utilization of bentonite and zeolite in cementation of dry radioactive evaporator concentrate. *Prog Nucl Energy* 48,495–503.
8. Kienzler B, Borkel C, Finck N, Heck S, Hilpp S, Schlieker M, Metz V, Plaschke M, Soballa E, Cron T, Miasoedov A (2014) Characterization and radionuclide retention properties of heat-treated concrete. *Phys Chem Earth, Parts A/B/C* 70-7,45–52.
9. Stockdale A, Bryan ND (2013) The influence of natural organic matter on radionuclide mobility under conditions relevant to cementitious disposal of radioactive wastes: A review of direct evidence. *Earth Sci Rev* 121,1-17.
10. Jacques D, Wang L and Mallants D (2010) Modelling chemical degradation of concrete during leaching with rain and soil water types. *Cem. Concr. Res.* 40, 1306-1313.
11. Isaacs M, Lange S, Deissmann G, Bosbach D, Milodowski A E, Read D (2020) Retention of technetium-99 by grout and backfill cements: Implication for the safe disposal of radioactive waste. *Applied Geochemistry* 116, 104580.
12. Tasi A, Gaona X, Fellhauer D, Böttle M, Rothe J, Dardenne K, Polly R, Grive M, Colas E, Bruno J, Kallstrom K, Altmaier M, Geckeis H (2018) Thermodynamic description of the plutonium – α -D-isosaccharinic acid system I: Solubility, complexation and redox behavior *Applied Geochemistry* 98, 247–264.
13. Evans N, Warwick P, Felipe-Sotelo M, Vines S (2012) Prediction and measurement of complexation of radionuclide mixtures by α -isosaccharinic, gluconic and picolinic acids. *J Radioanal Nucl Chem* 293, 725-730.
14. Kitamura A, Fujiwara K, Mihara M, Cowper M, Kamei G. (2013) Thorium and americium solubility in cement pore water containing superplasticisers compared with thermodynamic calculations *J Radioanal Nucl Chem* 298485-493.
15. Garcia D, Grive M, Duro L, Brassinnes S, de Pablo J. (2018) The potential role of the degradation products of cement superplasticisers on the mobility of radionuclides, *Appl. Geochem.* 98, 1-9.

16. Fromentin E, Reiller PE (2018) Influence of adipic acid on the speciation of Eu(III): Review of thermodynamic data in NaCl and NaClO₄ media, and a new determination of Eu-adipate constant in 0.5 mol·kg⁻¹ NaClO₄ medium by time-resolved luminescence spectroscopy. *Inorganica Chimica Acta* 482, 588-596.
17. Wang Z M , Van de Burg I J, Chopin G R, Spectroscopic study of lanthanide (III) complexes with aliphatic dicarboxylic acids, *Inorg Chem Acta* 310 (2000) 248-256
18. Tits J, Wieland E, Bradbury M H (2005) The effect of isosaccharinic acid and gluconic acid on the retention of Eu(III), Am(III) and Th(IV) by calcite. *Applied Geochemistry* 20 , 2082-2096.
19. Rai D, Kitamura A (2017) Thermodynamic equilibrium constants for important isosaccharinate reactions: A review. *J.Chem. Thermodynamics* 114, 135-143.
20. Kaplan DI, Roberts KA, Schwehr KA, Brinkmeyer R, Denham ME, Diprete D, Li H, Powell BA, Xu C, Yeager C, Zhang S, Santschi PH (2011) Evaluation of a radioiodine plume increasing in concentration at the Savannah River Site. *Environ Sci Technol* 45, 489–495.
21. Begg JD, Edelman C, Zavrín M, Kersting AB (2018) Sorption kinetics of plutonium V/VI to three montmorillonite clays. *Appl Geochem* 96, 131–137.
22. Zuo R, Teng Y, Wang J, Hu Q (2010) Factors influencing plutonium sorption in shale media. *Radiochim Acta* 63, 27–34.
23. Ma B, Charlet L, Fernandez-Martinez A, Kang M, Made B (2019) A review of the retention mechanisms of redox-sensitive radionuclides in multi- barrier systems. *Appl. Geochem.* 100, 414-431.
24. Vercammen K, Glaus MA, van Loon LR (2001) Complexation of Th(IV) and Eu(III) by α -isosaccharinic acid under alkaline conditions. *Radiochim Acta* 89, 393-401.
25. Wieland E, Lothenbach B, Glaus MA, Thoenen T, Schwyn B (2014) Influence of superplasticizers on the long-term properties of cement pastes and possible impact on radionuclide uptake in a cement-based repository for radioactive waste. *Appl. Geochem.* 49, 126-142.
26. Neck V, Altmaier M, Fanghanel T (2007) Solubility of plutonium hydroxides/hydrous oxides under reducing conditions and in the presence of oxygen. *Compt. Rendus Chem.* 10, 959–977.
27. Xiong Y, Leigh C D (2014) Modeling Actinide Compounds Solubilities In Alkaline To Hyperalkaline Solutions: Part Two, Solubility Of Pu(IV) Compounds In NaOH Solutions, International Symposium on Solubility Phenomena (ISSP-16) July 21-25, Karlsruhe, Germany.
28. Vitorge P (1991) Solubility Limits of Radionuclides in Interstitial Water: Americium in Cement, A Series of Final Reports (1985-1989), No. 34, Commission of the European Communities.

Radiolytic Degradation of SUBATECH Homemade Ether PolyCarboxylate Superplasticizer

V. Fiegel¹, G. Blain¹, C. Landesman¹, J. Vandendorre^{1*}

¹ SUBATECH, UMR 6457, Institut Mines-Télécom Atlantique, CNRS/IN2P3, Université de Nantes, 4, Rue Alfred Kastler, La chantrerie BP 20722, 44307 Nantes cedex 3, France

* Corresponding author: johan.vandendorre@subatech.in2p3.fr

Abstract

The degradation of organic products by radiolysis at high pH (> 12.5) is insufficiently known. Consequently, R&D effort has been focused on the radiolytic degradation of selected organics of interest. The key topic is the kinetic study of radiolytic degradation rates measurements vs. irradiation time and the identification of the resulting organic substances with the intention to constitute a source term for relevant organic molecules. Relevant organic molecule chosen in this study is: PolyCarboxylate-Ether (PCE) as an active component of recent cement superplasticizers. PCE polymer will be synthesized following a protocol developed in SUBATECH Lab. Radiolytic degradation rates depend on H⁺, O₂ and any organic/inorganic impurities concentrations in solution. That is the reason why the systems proposed are PCE in Ultrapure Water (Milli-Q) buffered with KOH or a mixture of Ca(OH)₂, KOH, NaOH at pH = 13.5 ± 0.1 under aerated conditions but without CO₂. γ and α radiations produce different radiolytic degradation rates. SUBATECH irradiation facilities will allow studying the alpha (16 < E < 68 MeV, 100 < Dose Rate < 3000 Gy.min⁻¹, ARRONAX cyclotron) and gamma (E = 0.66 MeV, 1 < Dose Rate < 10 Gy.min⁻¹, Cs-137 source) impact on organics degradation under controlled conditions. The release of dissolved organic products are measured by Ion Chromatography and the radiolytic Gas production (H₂, CO₂, C_xH_y) by μgas-Chromatography. The results show the high dihydrogen gas production during the few days gamma irradiation of PCE and the second one is the identification of the degradation products of PCE (formate, acetate, oxalate) and G-yield associated to these measurements.

1 Introduction

In geological disposal facilities, low- and intermediate-level radioactive waste are conditioned in cementitious materials as confinement and stabilisation barrier. Superplasticizers (SPs) are widely used as organic chemical admixtures in the cement to improve the mechanical strength and workability of concrete or the dispersion and hydration of cement particles.[1] Among the SPs, ether polycarboxylate based compound (PCE) is the last generation of polymer used by cement manufacturers. The chemical structure of PCE investigated in this study is represented in Figure 1. Addition of PCE improves the dispersion of cement particles by electro-steric repulsions due to the carboxylate and sulfonate moieties and the long ether hydrophobic sidechains.

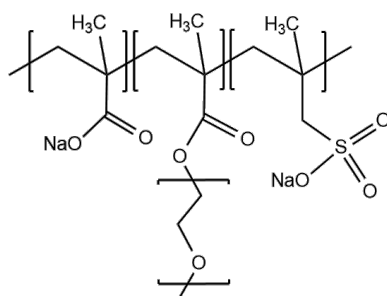


Figure 1: Ether Polycarboxylate (PCE) chemical structure.

During storage of nuclear waste, PCE undergoes degradation by the radiation emitted by material nearby. The resulting radiolytic degradation products can affect the radionuclide sorption and migration behaviour in the waste package. In order to improve knowledge of degradation of organic wastes in conditions representative of disposal facilities, degradation of homemade synthesized PCE (Figure 1) is proposed by alpha and gamma irradiation. Gaseous and soluble organic degradation products will be characterized and quantified using micro-gas chromatography, ion chromatography, UV-visible spectrophotometry. It is worth noting that no data in the literature was found about the radiolytic degradation of PCE superplasticizer polymer.

2 Material and methods

2.1 Synthesis and characterization of homemade PCE

Since the exact composition of commercial PCE superplasticizer (i.e. Glenium 27 from BASF) is not always known and often masked with other compounds, it was decided to synthesize pure PCE to be sure only PCE is irradiated leading to a better comprehension of its degradation mechanisms. The homemade PCE synthesis (Figure 2) is based on a previous work in the laboratory [2] and originally adapted from Plank *et al.*[3]

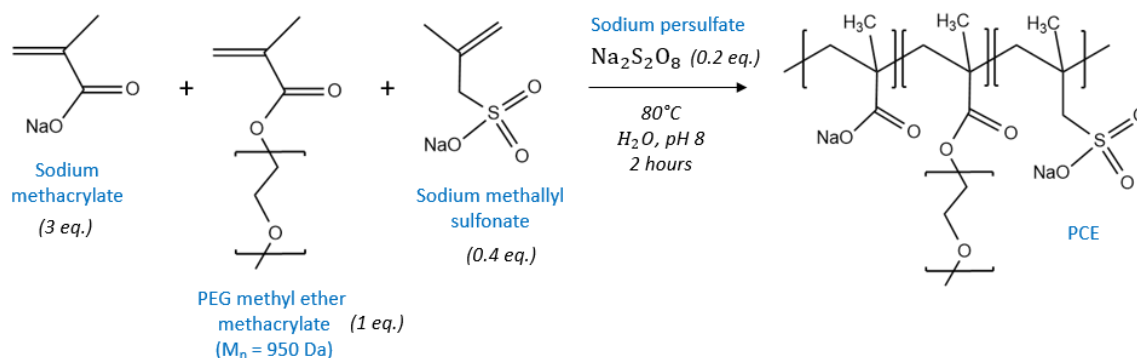


Figure 2: Reaction scheme of the PCE synthesis.

The synthesized PCE batches have been characterized by size exclusion chromatography (SEC) by Dr. Mélanie Legros from the Institut Charles Sadron (ICS, Strasbourg, France) specialized in polymer science. SEC was performed on a DIONEX Ultimate 3000 chromatograph with four Shodex OH-pak 30 cm columns (802.5HQ, 804HQ, 806HQ, 807HQ) and two types of detection: a refractometer (OPTILAB rEX, Wyatt Technology) and a multiangle light scattering MALS detector (DAWN HELIOS II, Wyatt Technology). Mobile phase is composed of ultrapure water with 0.1M NaNO₃, 200ppm NaN₃, pH 9 (adjusted with 0.3M NaOH) at a flow rate of 0.5 mL.min⁻¹. SEC characterization is represented in Table 1. A polymer can be characterized with two notions, the number-average molecular mass (M_n) and the mass-average molecular mass (M_w) to access to the polydispersity (M_w/M_n) of the polymer. If the polydispersity equals to 1, all polymer molecules in the sample have the same size and mass. For the two PCE synthesis batches used in this study (Table 1), the polydispersity is quite high, between 5,8 and 7.4. For example in a previous work [2], another PCE batch made with this synthesis was characterized at ICS giving a M_n of 33 700 g.mol⁻¹ and a M_w of 92 500 g.mol⁻¹ corresponding to a polydispersity (M_w/M_n) of 2.75.² Nevertheless, a high polydispersity is not a problem in this type of study: quantification of gaseous and soluble polymer degradation products.

Table 1: SEC characterization of homemade PCE synthesis. M_w = mass-average molecular mass and M_n = number-average molecular mass.

Synthesis	Mass (g)	M _w (g.mol ⁻¹)	M _n (g.mol ⁻¹)	Polydispersity (M _w /M _n)
PCE2	0.9	98 350	16 980	5.8
PCE5	3.9	73 560	9 940	7.4

In addition to the SEC characterization, the refractive index increment, also written dn/dc, has been determined for the PCE polymer. Dn/dc represents the difference in refractive index between the sample and the solvent, and is useful to convert the refractometer output into sample concentration. The same refractometer and same mobile phase as for SEC analysis was used but a flow rate of 0.3 mL/min. Dn/dc determination was done on PCE5 synthesis with 5 different concentrations (0.954, 1.928, 2.862, 3.816, 4.658 mg.mL⁻¹) and gave a dn/dc of 0.151 ± 0.02 mL.g⁻¹.

2.2 Irradiation experiments

The radiolytic degradation of the homemade PCE superplasticizer was performed both by alpha radiolysis using a helium ion beam ${}^4_2\text{He}$ delivered by the ARRONAX cyclotron ($E = 60.7$ MeV, dose rate = 844 and 887 Gy.min⁻¹) and by gamma irradiation with a ${}^{137}\text{Cs}$ source ($E = 0.66$ MeV, dose rate = 6 – 8 Gy.min⁻¹). The aim was to study the influence of different medium on the degradation of PCE, getting closer to conditions representative of disposal facilities and compare alpha and gamma radiolysis in term of production of gaseous and organic soluble degradation products. Three medium have been tested, detailed in Table 2, with a PCE concentration of 1 g.L⁻¹. First PCE is simply dissolved in ultrapure water (pH 8.5) as reference, compared to PCE in alkaline solutions (pH 13.7). PCE in ACW medium corresponds to Artificial Cement pore Water with different cations (K^+ , Na^+ , Ca^{2+}) representative to the chemical conditions in concrete waste packages. PCE in K^+ medium is a simplified version of the ACW one where only K^+ cation is present. All PCE samples are irradiated under synthetic air atmosphere containing only 80% N_2 and 20% O_2 . Very alkaline solutions have the property to dissolve a lot of carbon dioxide in the form of carbonate ions CO_3^{2-} . As carbon dioxide can be a radiolytic degradation product interesting to follow (originating from PCE carboxylate function), synthetic air is used to avoid the 400 ppm of atmospheric CO_2 in the experiments. In the same idea, all solutions used to dissolve PCE polymer (H_2O , K^+ and ACW) are initially degassed and decarbonated by heating the solution to 50°C under vacuum during 2 hours, that a minimum amount of CO_2 is present in the solutions.

Table 2: PCE systems studied by alpha and gamma irradiation.

Medium	Medium composition	Atmosphere
PCE 1 g.L ⁻¹ H_2O	PCE 1 g.L ⁻¹ Ultrapure water pH 8.5	Synthetic Air (80% N_2 , 20% O_2)
PCE 1 g.L ⁻¹ K^+	PCE 1 g.L ⁻¹ [K^+] = 370 mM pH 13.7	Synthetic Air (80% N_2 , 20% O_2)
PCE 1 g.L ⁻¹ ACW	PCE 1 g.L ⁻¹ [K^+] = 291 mM [Na^+] = 79 mM [Ca^{2+}] = 0.8 mM pH 13.7	Synthetic Air (80% N_2 , 20% O_2)

2.3 Analytical procedures

Directly after irradiation, gaseous products were characterized by micro gas-chromatography (μGC). Molecular hydrogen and carbon dioxide were measured using a 490-GC micro gas-chromatograph (VARIAN). Two columns were used: a 5 Å molecular sieve for H_2 and a poraplot Q for CO_2 detection. Before analyses, the injection system and the column were purged with argon gas.

PCE aqueous degraded solutions were analyzed on two ion chromatography devices. Carbonates anions concentration was determined using a DIONEX chromatograph with a DIONEX IonPac AS18 column and 30 mmol.L⁻¹ NaOH eluent. Small organic ions concentration was determined

using a METROHM 850 pro IC chromatograph with a Metrosep A Supp 16 column. This last column was thermostated at 55 °C and 75 mmol.L⁻¹ Na₂CO₃, 0.75 mmol.L⁻¹ NaOH eluent was used. As the mobile phase from the METROHM chromatograph contains carbonates anions, CO₃²⁻ in the samples had to be analyzed on the DIONEX chromatograph device.

3 Results and Discussion

3.1 Radiolytic gas production

After irradiation, gaseous products are directly analysed by micro-gas-chromatography. Molecular hydrogen H₂ is the main gas produced by water irradiation [4], the resulting yields are expressed in Table 3 along with the formation yield of H₂ for the alpha and gamma irradiation of PCE in different studied mediums and with these same medium without PCE.

Table 3: Hydrogen initial yields values for pure water and PCE 1 g.L⁻¹ solutions in different mediums under alpha and gamma irradiation. PCE2 was used for alpha radiolysis and PCE5 for gamma radiolysis.

Medium	pH	Alpha radiolysis G(H ₂) (×10 ⁻⁷ mol.J ⁻¹)	Gamma radiolysis G(H ₂) (×10 ⁻⁷ mol.J ⁻¹)
H ₂ O (this work)	6.9	0.69 ± 0.05	0.25 ± 0.02
H ₂ O (literature [5])	5.6	0.64 ± 0.06	0.26 ± 0.03
PCE 1 g.L ⁻¹ H ₂ O	8.5	1.34 ± 0.09	1.12 ± 0.05
K ⁺	13.7	0.75 ± 0.05	0.42 ± 0.03
PCE 1 g.L ⁻¹ K ⁺	13.7	0.84 ± 0.08	0.71 ± 0.03
ACW	13.7	0.67 ± 0.04	0.43 ± 0.03
PCE 1 g.L ⁻¹ ACW	13.7	0.90 ± 0.08	0.70 ± 0.04

The irradiation of pure water lead to hydrogen formation yields of G(H₂)=(0.69± 0.05)×10⁻⁷ mol.J⁻¹ and G(H₂)=(0.25 ± 0.02)×10⁻⁷ mol.J⁻¹ for alpha and gamma radiolysis respectively. These yields are consistent with the ones given in the literature in the same radiolytic conditions (Table 3). Moreover, this result shows also a higher formation of H₂ for alpha radiolysis compared to gamma radiolysis pointing out a linear energy transfer (LET) effect. Increasing the LET increases the energy deposition density within the track of the incident particle or the beam in the solution, increases the concentration of radicals, and therefore the probability of radical-radical recombination reactions, producing a higher concentration of molecular species in solution. [6, 7] Comparing H₂ formation with the presence of PCE superplasticizer in the 3 different studied mediums (Table 3) demonstrate a higher production of H₂ with the polymer in solution compared to the blank solutions. Indeed, this

overproduction of H₂ can be explained by hydrogen abstraction reactions on the PCE molecule, H• radicals react with the polymer by taking a hydrogen atom leading to the formation of an organic PCE radical and H₂.

CO₂ has been measured as well for each irradiated solutions described in Table 3. The carbon dioxide production reaches, for a gamma irradiated PCE 1 g.L⁻¹ solution in water, G(CO₂)=(0.44 ± 0.04)×10⁻⁷ mol.J⁻¹. CO₂ can be formed by indirect radiolysis of PCE carboxylate moieties by reaction with a hydroxyl radical HO• leading to the formation of a RCOO• radical (Eq. 1). This radical can then release a CO₂ molecule by electronic rearrangement (Eq. 2).



On the other side, a PCE water solution has also been irradiated by alpha radiolysis but there was no significative formation of CO₂ in the medium, no yield can be given. Less or no carbon dioxide is formed by alpha radiolysis compared to gamma radiolysis. Two hypotheses may explain this result: 1/ a LET effect exists, hydroxyl radical HO• are more disseminated in gamma irradiated solutions and therefore have a higher probability to interact with the PCE molecule to form CO₂ (Eq. 8 and Eq. 9) and 2/ gamma radiolysis favours another way of carboxylate moiety radiolysis like the formation of formate or acetate ions. Formate and acetate formation will be studied in the next part of this paper.

For alkaline medium, in both K⁺ and ACW solutions (with and without PCE) measurements of CO₂ were always under the detection limit, no carbon dioxide formation yields can be given. Either no CO₂ is produced during irradiation or the alkaline medium has an influence on the CO₂ accumulation. It may be possible all CO₂ formed under irradiation is rather dissolved in the pH 13.7 aqueous solutions in the form of CO₃²⁻, so that no CO₂ can be detected by gas chromatography. It could be interesting to quantify CO₃²⁻ ions by ion chromatography to confirm this hypothesis and indirectly quantify the CO₂ formed if it is the case, which will be done in the next part. Another possibility of the influence of the alkaline medium is that at pH 13.7 the hydroxyl radical HO• is mainly in the form of O^{•-} (HO• / O^{•-} pKa = 11.9) probably far less effective to create CO₂ with PCE (Eq. 8 and Eq. 9).

3.2 Carboxylate anions degradation products

After gas measurements, the alpha and gamma irradiated solutions were analyzed by ion chromatography to quantify carbonates and small organic anions coming from the radiolytic degradation of PCE superplasticizer in solution. All systems described in the introduction of the previous part (Table 3) were analyzed by ion chromatography.

Table 5 represents all the radiolytic yields for carbonate, formate and acetate anions obtained from the irradiation of the 3 studied media or solutions, ultrapure water, K⁺ medium and ACW medium, with and without PCE by alpha (α) and gamma (γ) radiolysis. If there is no yield given, either the species is not concentrated enough (very low concentration measured) or its formation does not follow any tendency with the dose.

Table 4: Formation yields of carbonate, formate and acetate ions after alpha (α) and gamma (γ) radiolysis of PCE superplasticizer in various solutions and mediums without PCE. PCE2 was used for alpha radiolysis and PCE5 for gamma radiolysis.

Systems	pH	$G_0(\text{CO}_3^{2-})$ ($\times 10^{-7} \text{ mol.J}^{-1}$)	$G_0(\text{HCOO}^-)$ ($\times 10^{-7} \text{ mol.J}^{-1}$)	$G_0(\text{CH}_3\text{COO}^-)$ ($\times 10^{-7} \text{ mol.J}^{-1}$)
PCE 1 g.L ⁻¹ H ₂ O	8.2	α : -0.24 ± 0.001 γ : -0.42 ± 0.01	α : 0.71 ± 0.04 γ : 1.32 ± 0.05	α : 0.023 ± 0.001 γ : -
H ₂ O	6.9	α : - γ : -	α : - γ : -	α : - γ : -
PCE 1 g.L ⁻¹ K ⁺	13.7	α : 8.85 ± 0.24 γ : 6.50 ± 0.33	α : 0.10 ± 0.01 γ : 1.13 ± 0.07	α : 0.07 ± 0.03 γ : 0.42 ± 0.03
K ⁺	13.7	α : 9.70 ± 0.34 γ : 8.01 ± 0.40	α : 0.039 ± 0.001 γ : -	α : - γ : -
PCE 1 g.L ⁻¹ ACW	13.7	α : 7.50 ± 0.24 γ : -	α : 0.35 ± 0.01 γ : 1.19 ± 0.08	α : 0.08 ± 0.01 γ : 0.47 ± 0.03
ACW	13.7	α : 7.57 ± 0.24 γ : 8.13 ± 0.40	α : 0.017 ± 0.001 γ : -	α : 0.026 ± 0.001 γ : -

In the case of the formation of carbonate ions by the alpha radiolysis of PCE 1 g.L⁻¹ in ultrapure water, its initial formation yield is even negative, $G_0(\text{CO}_3^{2-}) = (-0.24 \pm 0.001) \times 10^{-7} \text{ mol.J}^{-1}$ and $G_0(\text{CO}_3^{2-}) = (-0.42 \pm 0.001) \times 10^{-7} \text{ mol.J}^{-1}$ for alpha and gamma radiolysis respectively. The carbonate ions accumulated in the solution are degraded with the dose. The carbonate ions formation for K⁺ and ACW mediums show very important yields both with and without PCE. The difference of CO₃²⁻ that might come from CO₂ from the PCE radiolytic degradation is too small compared to the dissolution of atmospheric CO₂ and even in favour of the solution without PCE. Indeed, at this pH (pH 13.7), too much atmospheric CO₂ is dissolved in the solutions.

The influence of the medium and pH on the formation of formate ions shows a higher production of HCOO⁻ in the presence of PCE in ultrapure water than in K⁺ and ACW solutions (pH 13.7) both in alpha and gamma radiolysis. When comparing the concentration of formate directly, there is about 50 times more formate formed in ultrapure water in presence of PCE than when irradiating ultrapure water alone, near neutral pH a lot of formate is formed by radiolysis of PCE. The difference is weaker for K⁺ and ACW, with around 5 times more formate formed by radiolysis of PCE at pH 13.7 than without the polymer. The pH seems to have an influence on the formation of formate from PCE. Radicals formed during water radiolysis like H[•] and HO[•], can react with PCE carboxylate moieties to

form formate. But at pH 13.7, these species are mainly in their basic form, aqueous electron e_{aq}^- (H^\bullet / e_{aq}^- $pK_a = 9.77$) and the radical $O^{\bullet-}$ ($HO^\bullet / O^{\bullet-}$ $pK_a = 11.9$), which might be less reactive towards the PCE molecule and explain this weaker formation of formate at pH 13.7.

For the formation of acetate in ACW medium at pH 13.7, the difference of acetate production per joule of energy deposited between solutions with and without PCE is about 3 times higher in presence of PCE in solution. The other results on acetate show low yields and not many differences between solutions of PCE in ultrapure water, K^+ and ACW mediums (pH 13.7), it is hard to conclude on an influence of the medium or pH for the acetate formation.

Moreover, formate and acetate ions formation by alpha and gamma radiolysis of solutions of PCE in K^+ and ACW mediums (pH 13.7) does not show much difference in term of yield according to the composition of the alkaline solutions (except for alpha production of $HCOO^-$). If the solution only contains K^+ ions (K^+ medium) or a mix of K^+ , Na^+ and Ca^{2+} it doesn't seem to affect the formation of formate and acetate ions by degradation of PCE.

A final observation can be made on these results between alpha and gamma radiolysis (Table 5). Indeed, formate and acetate ions formation yields after PCE solution irradiation are always in favor of gamma radiolysis compared to alpha radiolysis. PCE superplasticizer is more degraded in formate and acetate ions by gamma radiolysis highlighting a LET effect. A simple explanation is that the species that lead to the degradation of PCE into formate and acetate ions like $HO^\bullet / O^{\bullet-}$ or H^\bullet / e_{aq}^- (depending on the pH), are more spread in the solution in gamma radiolysis and therefore have a higher probability to interact with the PCE molecule to form formate and acetate ions.

4 Conclusion and future works

In this study, ether polycarboxylate superplasticizer, used in concrete for nuclear waste storage, has been degraded by gamma and alpha radiolysis to investigate the formation of gaseous and soluble organic degradation products which might affect the safety of the storage facility and the radionuclide sorption and migration behaviour in the waste package.

First, a homemade ether polycarboxylate (PCE) has been synthesized to study a pure product and facilitate the understanding of its degradation mechanisms. PCE was characterized by size exclusion chromatography, giving a polydispersity of the polymer between 5.8 and 7.4. This homemade PCE has then been dissolved at a concentration of 1 g.L^{-1} in various aqueous solutions: ultra-pure water (pH 8.5), K^+ medium (pH 13.7) and ACW medium (pH 13.7). Different mediums to get closer and closer to chemical conditions in concrete waste packages.

Alpha and gamma radiolysis of these solutions with a 60.7 MeV helium ion beam and a ^{137}Cs source lead to the formation of gaseous and soluble organic degradation products, which were analyzed by micro-gas chromatography and ion chromatography. The major gas formed was molecular hydrogen H_2 and carbon dioxide CO_2 . The presence of PCE superplasticizer in the 3 different studied mediums

always demonstrates a higher production of H₂ with the polymer in solution compared to the blank solutions without PCE. PCE act as hydrogen atom donor to H• radicals to form more H₂ in the medium. This overproduction of H₂ is however more limited in pH 13.7 solutions due to change in radical composition at this alkalinity. Results also showed higher overall production of H₂ gas after alpha radiolysis than gamma radiolysis highlighting a LET effect occurring in the solution. Carbon dioxide formation was only observed for the gamma radiolysis of PCE in ultrapure water.

In solution, the major species formed were carbonate, formate and acetate anions and small amounts of oxalate and sulfate anions. A higher formation of formate and acetate ions has been observed in the presence of PCE in solution. These species are certainly formed by the degradation of the carboxylate moieties of the PCE polymer. The difference of production of formate in solution containing PCE was 10 times higher when irradiated in water than in K⁺ and ACW medium (pH 13.7). Radicals present in very alkaline solution seem to be less prone to generate formate ions from PCE.

To better understand the degradation mechanisms of PCE leading to the formation of small organic carboxylates in solution, irradiated PCE solutions could be analysed by HPLC-MS or ESI-MS to identify PCE degradation products to see what fragments does the polymer lose after irradiation. Another method to characterize degraded PCE is to analyse the samples by size exclusion chromatography, if there is a change in the mean mass of the polymer and its polydispersity after irradiation.

Acknowledgement

The EURAD-CORI project leading to this application has received funding from the European Union's Horizon 2020 research and innovation programme under grant agreement No 847593.

References

- [1] Taylor, H.F.W. *Cement Chemistry; 2nd ed.; T. Telford: London, 1997; ISBN 978-0-7277-2592-9.*
- [2] Androniuk, I. *Effects of Cement Organic Additives on the Adsorption of Uranyl Ions on Calcium Silicate Hydrate Phases: Experimental Determination and Computational Molecular Modelling*, Thèse de doctorat de l'Université de Nantes, 2017.
- [3] Plank, J.; Pöllmann, K.; Zouaoui, N.; Andres, P.R.; Schaefer, C. *Synthesis and Performance of Methacrylic Ester Based Polycarboxylate Superplasticizers Possessing Hydroxy Terminated Poly(Ethylene Glycol) Side Chains. Cement and Concrete Research* **2008**, 38, 1210–1216, doi:10.1016/j.cemconres.2008.01.007.
- [4] Spinks, J.W.T.; W., R.J.; Spinks, J.W.T.; Woods, R.J. *An Introduction to Radiation Chemistry*,; 3rd ed.; Wiley: New-York, 1990; ISBN 978-0-471-61403-6.

[5] Crumière, F.; Vandendorre, J.; Essehli, R.; Blain, G.; Barbet, J.; Fattahi, M. LET Effects on the Hydrogen Production Induced by the Radiolysis of Pure Water. *Radiation Physics and Chemistry* **2013**, 82, 74–79, doi:10.1016/j.radphyschem.2012.07.010.

[6] Fiegel, V.; Berthon, C.; Costagliola, A.; Blain, G.; Vandendorre, J.; Vermeulen, J.; Saint-Louis, G.; Guerin, L.; Sauvage, T.; Fattahi-Vanani, M.; et al. Alpha Radiolysis of DOTA Ligand in Aqueous Solutions with Helium Ion Beams. *Radiation Physics and Chemistry* **2019**, 165, 108409, doi:10.1016/j.radphyschem.2019.108409.

[7] LaVerne, J.A. Development of Radiation Chemistry Studies of Aqueous Solutions with Heavy Ions. *Nuclear Instruments and Methods in Physics Research Section B: Beam Interactions with Materials and Atoms* **1996**, 107, 302–307, doi:10.1016/0168-583X(95)00793-8.

Preliminary results on the interactions of organic compounds (ISA, EDTA and Polycarboxylate-based additive) on cement paste

M. Grande¹ M. Castellote^{1*}

¹ Institute of Construction Science Eduardo Torroja, IETcc-CSIC, Serrano Galvache 33, 28033, Madrid, Spain.

* Corresponding author: martaca@ietcc.csic.es

Abstract

In this work, preliminary results of interactions of ISA, EDTA and Polycarboxylate-based additive with cement paste (CEM V/A (S-V) 32.5N) in state I are given. More specifically, characterisation of cementitious samples as well as adsorption isotherms in distilled water for the three organic molecules and kinetics for ISA are reported.

1 Experimental work

1.1 Materials

Cement pastes were prepared with CEM V/A (S-V) 32.5N supplied by Tudela Veguin, whose characteristics are given in Table 1.

The **organic molecules** selected were ISA, EDTA and a polycarboxylate-based additive for concrete (POLI). They were purchased as indicated below:

ISA: Isosaccharinic acid-1,4-lactone, by Biosynth Carbosynth[®]. CAS 7397-89-9, C₆H₁₀O₅

EDTA, Ethylenediaminetetraacetic acid, disodium salt, dihydrate (by Scharlau) – CAS 6381-92-6
C₁₀H₁₄N₂O₈·2H₂O.

POLI: SikaPlast[®]-1003 NG. Unknown patented formula

Measurements of these molecules in liquid phase have been carried out by TOC measurements using a XPERT equipment by Hach.

Table 1: Characteristics of the cement V/A (S-V) 32.5N supplied by Tudela Veguin used.
*Physical and Mechanical values are the nominal ones for this cement

Characteristics	Parameter	Various	Value	Range
Chemical	% Fly ash (with respect to the core)	UNE-EN-197-1	27.2	≥ 18 and ≤ 30
	% Slag (with respect to the core)		27.4	≥ 18 and ≤ 30
	% SO ₃		1.2	≤ 3.5
	% CaCO ₃ (with respect to the core)		2.7	≤ 5
	% Cl ⁻		0.01	≤ 0.1
Physical*	Le Chatelier expansion (mm)		0.1	≤ 10
	Setting (min)		Beginning: 250 End: 315	≥ 75
Mechanical*	Compressive strength (MPa)	UNE-EN-196-1	7 days: 27.2	≥ 16
			28 days: 46.3	≥ 32.5 and ≤ 52.5

1.2 Casting of the specimens

Two different types of cement pastes were cast: plain cement paste (C) and cement paste with Fe in this composition (C1-Fe, C2-Fe). FeCl₃ was dissolved into the water that was added to cast the cement pastes. Moreover, two batches of these cement pastes were cast (batches C1 and C2), with the main difference of the atmosphere in which they have been stored. In the case of batch 1 no protective atmosphere was used and it was tested in state I. In the second case, storage and tests were carried out under N₂ atmosphere and were tested in states I and II. The mix details of the different samples are given in Table 2.

Table 2: Mix details of the casted cement pastes

Mix	Casting date	CEM V/A (S-V) 32,5 N	Water	Fe (added as FeCl ₃)	Protective atmosphere	Curing
C1	Febr. 2020	1	0.6*	----	No	12 months in a Ca(OH) ₂ saturated solution.
C1-Fe	Febr. 2020	1	0.45	0.01	No	
C2	May 2021	1	0.45	----	Yes	28 days 100% RH
C2-Fe	June 2021	1	0.45	0.01	Yes	

*Water adjusted to consistency

The aspect of the specimens (batch 1) and the curing procedure are shown in Figure 1.



Figure 1: Batch 1. Aspect of the specimens and curing procedure

1.3 Tests

The interaction between the cement samples prepared in different states of degradation and the three selected organic compounds have been planned in two different liquid media (distilled water (dw) and simulated pore water solution (pw) as follow:

- Adsorption/desorption isotherms
- Kinetics of adsorption
- Natural diffusion test steady state
- Natural diffusion test non steady state
- Electrokinetic tests (multi-regime method)
- Zeta potential measurements

At the moment of the 3rd annual CORI WP Meeting, due to COVID restrictions, a few of these experiments are finished, whose results are given below. The rest of experiments are still on-going.

2 Results

2.1 Characterization

The characterization's results of the samples C1 and C1-Fe are given in Table 3

Table 3: Characterization of samples C1 and C1Fe after 12 months curing in a $\text{Ca}(\text{OH})_2$ saturated solution

Parameter	Various	C1	C1-Fe
Mechanical Strenght (Mpa) 12 months curing	Flexural	2.41	2.68
	Compression	60.5	85.3
Resistivity, 12 months curing ($\text{K}\Omega\cdot\text{cm}$)	$\text{K}\Omega\cdot\text{cm}$	23.81	27.28
BET Surface Area (m^2/g)	Range 1-300 nm	7,86	6,62
Volume pore diameter (1-300 nm) (cm^3/g)		0,043	0,039
Adsorption Average pore diameter (nm) (4V/A by BET)		21,6	23,6
Porosity (% vol)	Range 0.0067-500 μm	19,14	5,74
Bulk Density (g/MI)		1,687	1,767
Average pore diameter μm (4V/A by MIP)		0,016	0,011
Total loss weight (%)	TG (25-1000°C)	21,68	27,09
Free water (%)		9,75	9,95
Total combined water (%)		10,18	15,83
Portlandite, $\text{Ca}(\text{OH})_2$ %		2,92	1,52
Calcite, CaCO_3 %		2,36	2,14

The mix C1-Fe presents better mechanical properties than C1, especially for compression resistance, as expected, due to its lower water:cement ratio. This is in agreement with its lower porosity and higher resistivity and higher bulk density. Free water is similar in both mixes, having C1 smaller percentage of combined water, higher amount of Portlandite and similar amount of Calcite.

The cumulative and differential pore volume by N_2 adsorption (range of pores 1-300 nm) is given in Figure 2, where it can be seen that there aren't significant differences between both samples in these range of pores, having BET areas quite similar. In a higher range of pores, between 0.0067-500 μm , unlike to the nm range, there are important differences in porosity, being much lower that of C1-Fe, in agreement with its smaller water:cement ratio (*Cf.* Figure 3). In both cases, pores are smaller than 0.05 μm , having a maximum at 0.016 and 0.0073 μm for C1 and C1-Fe respectively.

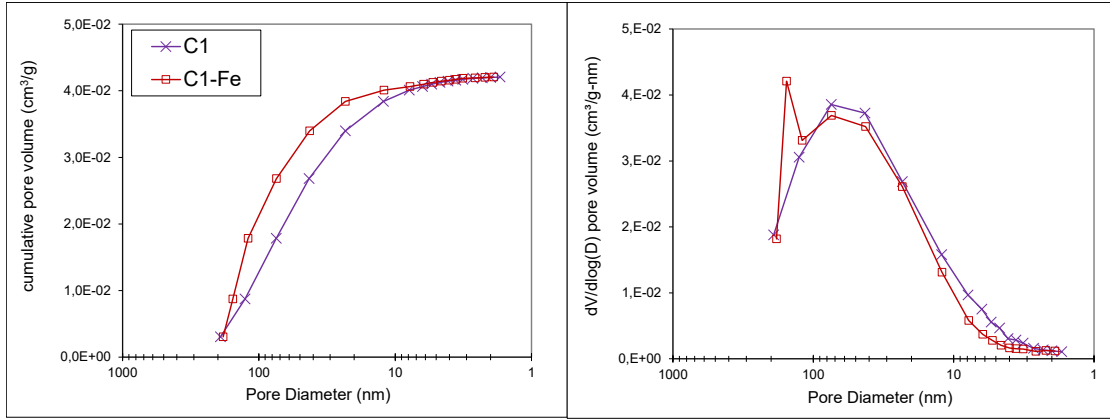


Figure 2: Cumulative and differential pore volume by N_2 adsorption (range of pores 1-300 nm)

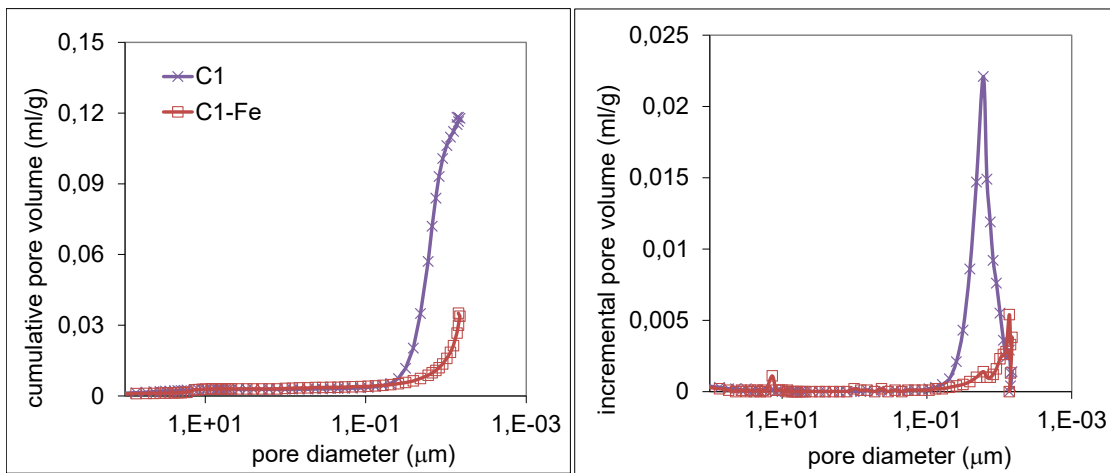


Figure 3: Cumulative and differential pore volume by MIP (range of pores 0.0067-500 μm)

Figure 4 shows the aspect of the samples obtained by backscattered electron (BSE) coupled to a scanning electron microscope at 500 magnifications. Both of the samples present unreacted fly ashes and slags coexisting with others that are being reacted at the moment of the analysis. The pastes seem to be quite compact, specially that containing iron, with lower water:cement ratio, in agreement with the MIP results.

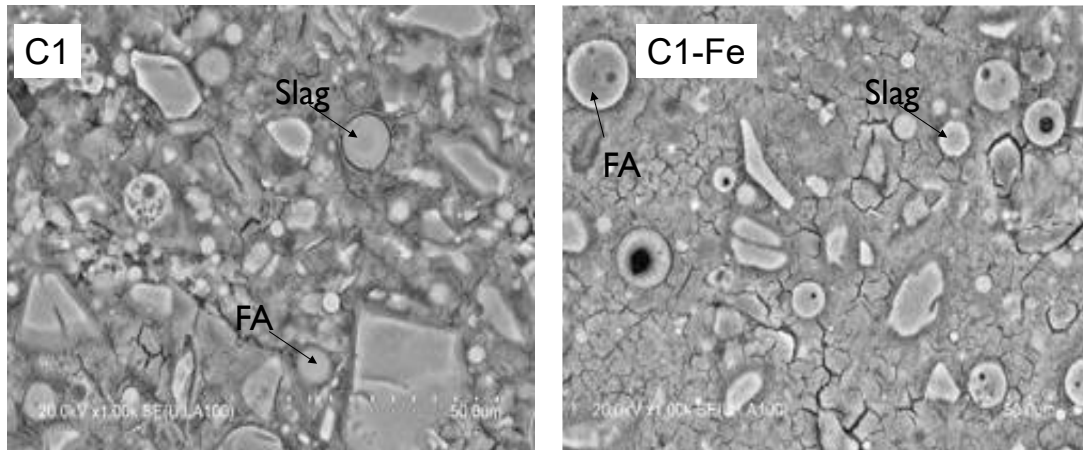


Figure 4: BSE aspect of the specimens C1 and C1-Fe at 500 magnifications

The X-ray diffraction patterns (XRD) were obtained using a Bruker D8 Advance diffractometer with CuK α radiation (40 kV,30 mA). The amount of Ettringite (C₃A.3CaSO₄.32H₂O), that is primarily the product of the hydration reaction between tricalcium aluminate (C3A) and the gypsum, and Calcite (CaCO₃) do not present significant differences in both samples, as can be seen in Figures 5-a and 5-c respectively. However, the amount of Portlandite (Ca(OH)₂) has decreased noticeably and also that of periclase (MgO) in the sample C1-Fe (see Figures 5-b and 5-d respectively). In the sample C1-Fe, with FeCl₃ added during casting, Friedel's salt (3CaO·Al₂O₃·CaCl₂ · 10 H₂O), Volaschioite (Fe₂ H₅ O₇ S_{0.5}), ClFeO, Clinozoisite (Al_{2.79} Ca₂ Fe_{0.21} H O₁₃ Si₃) and Herzynite (Al_{1.94} Fe_{0.76} Mg_{0.3} O₄) can be cited as some of the iron-bearing phases detected. This comparison between phases is not quantitative; it is just a comparison of peak ratios.

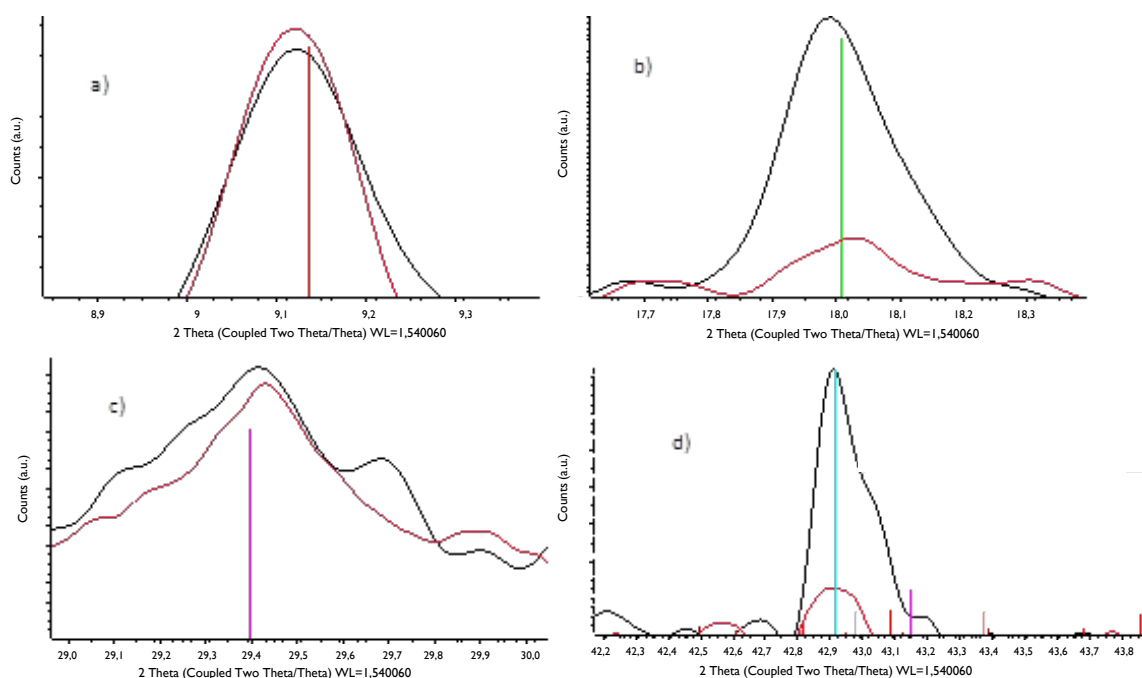


Figure 5: Details of some of the characteristic peaks for a) Ettringite (C₃A.3CaSO₄.32H₂O), b) Portlandite (Ca(OH)₂), c) Calcite (CaCO₃) and d) Periclase (MgO) for C1 (black line) and C1-Fe (red line)

It is remarkable that the Calcite found is not attributed to carbonation of the paste, as even though the samples were neither stored nor manipulated in protective atmosphere, the amount found is attributable to the calcite included in the cement. This is supported for having approximately the same amount in both samples. If carbonation had occurred, it should be higher in the sample C1, with higher gel-porosity.

2.2. Adsorption isotherms on C1

Adsorption isotherms have been carried out at a Solid/Liquid (S/L) ratio of 20g/L for cement paste C1 during 15 days in equilibrium with distilled water (dw). For the adsorption tests, cement paste samples were crushed and sieved. Provided ISA and EDTA are known molecules, it is possible to determine the amount of moles from the total organic carbon (TOC) measurements, that were carried out using the Xpert-TOC/TN analyser by Hach Lange. This is not possible in the case of

polycarboxylate-based additive (POLI) solution as its formula is an industrial secret. Thus, for the sake of comparison, to present all the molecules in the same picture, the isotherms are given in Figure 6 as amount of carbon adsorbed per kg of solid (mg^c/kg) vs. concentration of carbon in the equilibrium solution (mg^c/L).

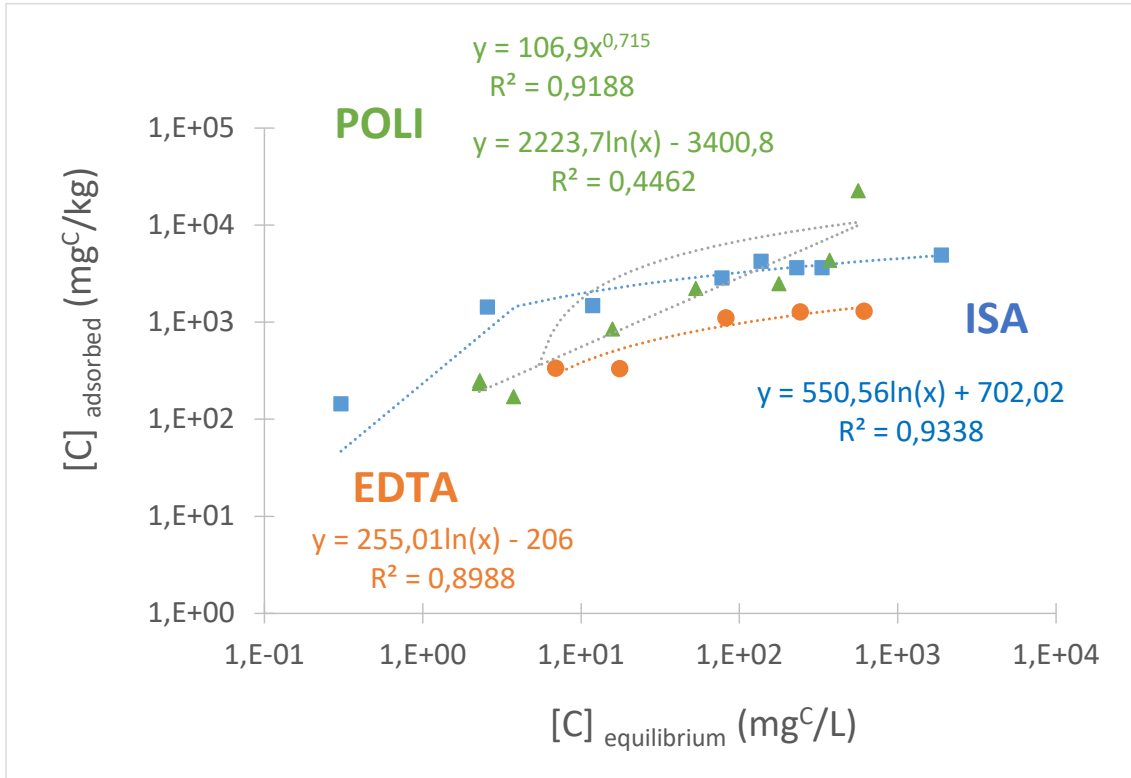


Figure 6: Adsorption isotherms for ISA, EDTA and POLI on cement paste C1 equilibrated with distilled water after 15 days of contact time.

Figure 6 shows a different pattern for the adsorption of POLI in relation to ISA and EDTA, whose best fit corresponds to logarithmic expressions with R² of 0.93 for both of them, while fit of adsorption of POLI to the same equation do not give good results (R² 0.446). Best fit to POLI corresponds to a potential expression (R² of 0.918).

The pH values of the equilibrium solutions at the end of the sorption tests are given in Figure 7, where it can be seen that they are in the range 12±0.5 which, as expected, correspond approximatively to the Portlandite buffer (pH = 12.45 at 25°C). The values of K_d are given in figure 8.

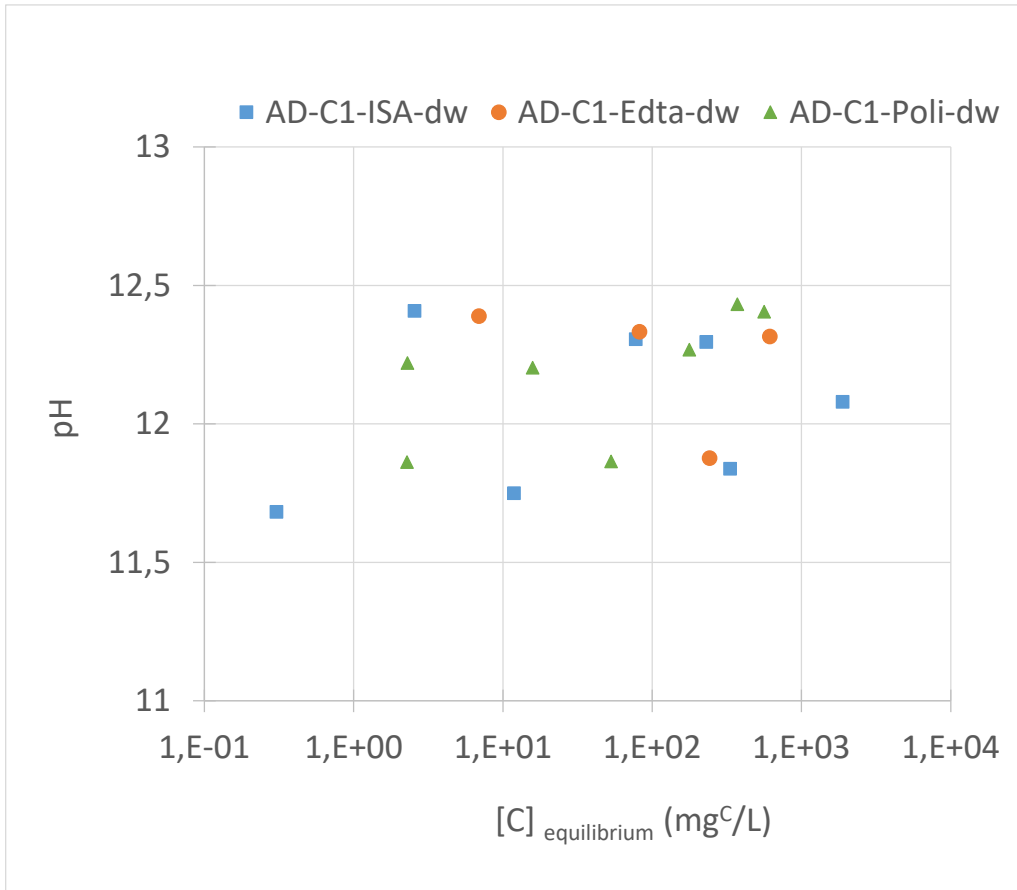


Figure 7: pH of the solutions at the end of the adsorption tests for ISA, EDTA and POLI on cement paste C1 equilibrated with distilled water

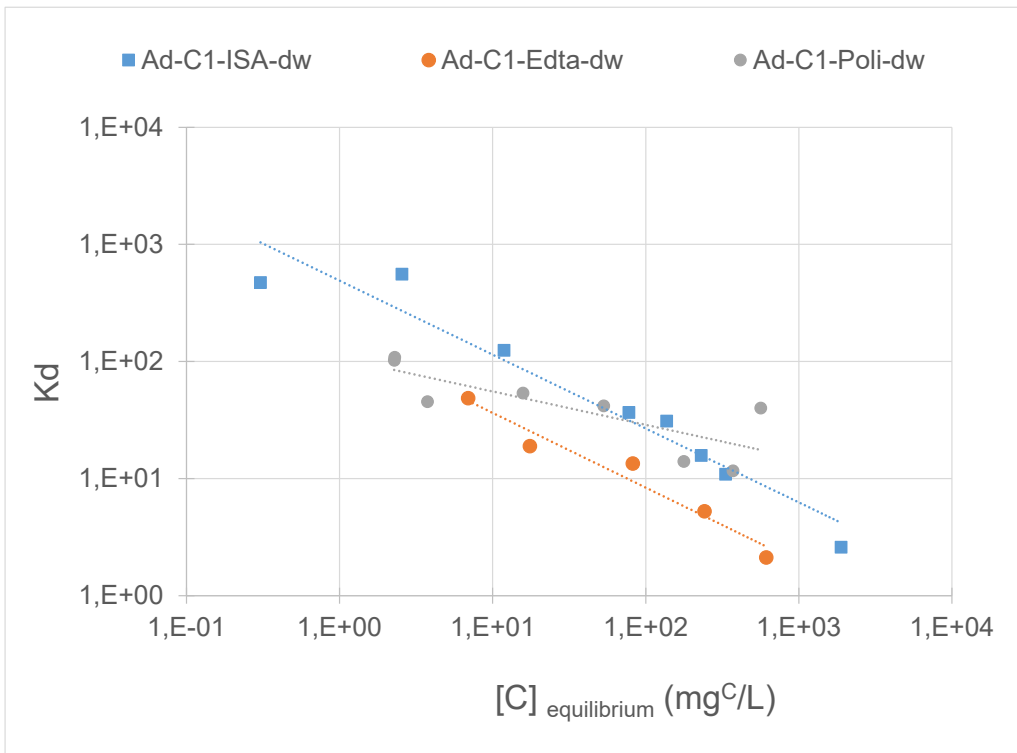


Figure 8: K_d for ISA, EDTA and POLI on cement paste C1 equilibrated with distilled water

According to the results in Figure 6 and Figure 8, ISA has more adsorption affinity for the cement paste than EDTA, for comparable concentration in solution. Both species follow a similar trend-slope of K_d in function of their concentration in solution. POLI exhibits a different trend, with comparable K_d values at concentrations in the equilibrium smaller than 100 mg^C/L, with higher K_d values above this concentration.

In order to compare these results with data in literature [1-3], the values for ISA have been presented together with others in Figure 9, where it can be seen that even though the equilibration media is distilled water, the adsorption values are smaller but with good correspondence.

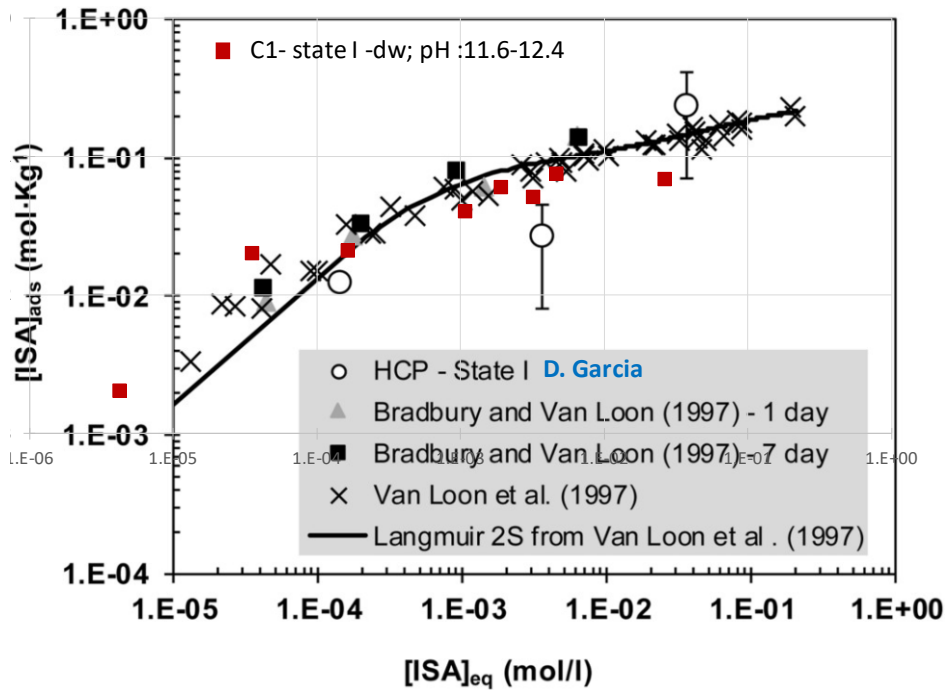


Figure 9: Adsorption isotherms for ISA (this study with data in red) together with data in literature [1-3]

The isotherms have been fitted to 1-site-Langmuir and Freundlich models, as presented in Figure 10 (a-b) and summarized in Table 4.

The Langmuir isotherm is a theoretical model, which is valid for reversible and fast adsorption on a monolayer on a completely homogeneous surface with a finite number of identical and specific adsorption sites and with negligible interaction between the molecules. It is given by equation (1) that, in a linear form, adopts the form of equation (2).

$$q_e = \frac{q_m K_L C_e}{1 + K_L C_e} \quad (1)$$

$$\frac{C_e}{q_e} = \frac{1}{q_m} C_e + \frac{1}{K_L q_m} \quad (2)$$

Where q_e is the adsorbed mass at the equilibrium, corresponding to the concentration at equilibrium C_e . The parameter q_m is a constant that denotes the maximum adsorption capacity, while the constant K_L defines the affinity of the adsorbate for the adsorbent.

The Freundlich model is an empirical equation that assumes no homogeneity in the energy of the surface sites and no limit to the maximum adsorption load and shows an exponential distribution of active centers characteristic of a heterogeneous surface. Mathematical expression for Freundlich model is given by equation (3), which can be linearized to equation (4).

$$q_e = K_f \cdot C_e^{\frac{1}{n}} \quad (3)$$

$$\log q_e = \frac{1}{n} \log C_e + \log K_f \quad (4)$$

The parameters K_f and n characterize the adsorption capacity and intensity, respectively. The parameter n is positive in all the cases, which indicates repulsive interaction between the adsorbate molecules.

In Figure 10 it can be seen that ISA and EDTA isotherms fit quite well to a Langmuir one and worse to a Freundlich one while POLI results only fits to a Freundlich isotherm.

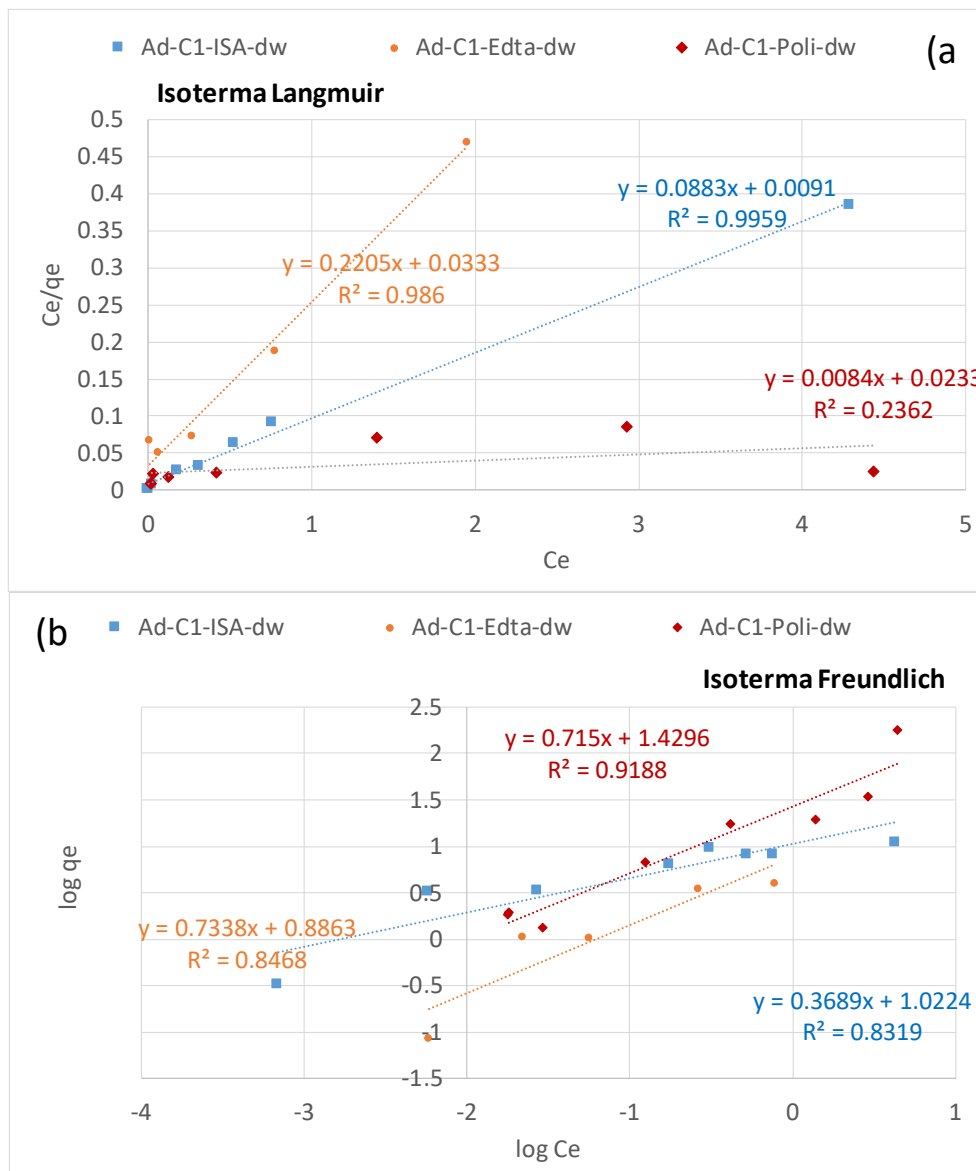


Figure 10: Fitting of the adsorption isotherms on C1 (dw) to 1-site-Langmuir and Freundlich models

Table 4: Fitting of the adsorption isotherms on C1 (dw) to Langmuir (1 site) and Freundlich models.

Isotherm		q_m (g/kg) Maximum amount of adsorption	K_l (L/g) Affinity of the towards the adsorbent	R^2
Langmuir $q_e = \frac{q_m K_l C_e}{1 + K_l C_e}$	ISA	11.32 (0.07mol/Kg)	9.70	0.996
	EDTA	4.53	6.62	0.986
	POLI	4.19	0.36	0.236
		K_f (g kg ⁻¹ (gL ⁻¹) ^{-1/n}) Capacity of adsorption	n Intensity of adsorption	R^2
Freundlich $q_e = K_f \cdot C_e^{\frac{1}{n}}$	ISA	2.78	2.71	0.832
	EDTA	2.43	1.36	0.847
	POLI	4.18	1.40	0.919

Table 4: Fitting of the adsorption isotherms on C1 (dw) to Langmuir (1 site) and Freundlich models.

2.3. Sorption kinetics

ISA in distilled water was analysed for their sorption kinetics on C1 paste. A dissolution of 1g/L of ISA in distilled water was put in contact with the C1 powder and samples were taken and analysed at 0.5, 1, 2, 3, 5 and 24 hours. The results of adsorption have been fitted to the pseudo-first order (Lagergren) given by equation (5) and pseudo-second order (Ho–McKay) (equation 6) models (Figure 11 and Table 5).

$$\frac{dq}{dt} = K_1 (q_e - q) \quad (5)$$

$$\frac{dq}{dt} = K_2 \cdot (q_e - q)^2 \quad (6)$$

where K_1 (min⁻¹) is the first order adsorption kinetic constant, K_2 (mol kg⁻¹ min⁻¹) is the second order adsorption kinetic constant and q_e is the carbon adsorbed at equilibrium.

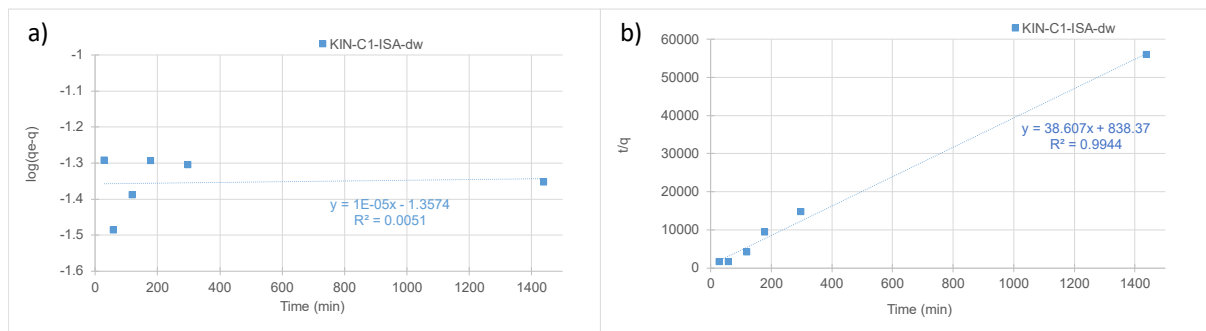


Figure 11: Fitting of the kinetic data of ISA in distilled water on C1 kinetics to a) Lagergren and b) Ho models.

From figure 10 and results in table 5 it is clear that adsorption of ISA in distilled water fits to a pseudo-second order of Ho-McKay, that implies chemisorption or chemical adsorption due to the formation of chemical bonds between adsorbent and adsorbate in a monolayer on the surface [4].

Fitting of the pseudo second model provides a theoretical value for q_e . In this case, a value of 0.026 mol/kg has been obtained, lower than what obtained by the Langmuir isotherm i.e. 0.07 mol/kg.

Table 5: Fitting of the kinetic data of ISA in distilled water on C1 kinetics to Lagergren and Ho models.

Model	q_e (molkg ⁻¹)	K_1 (min ⁻¹)	R ²
<i>pseudo-first order (Lagergren)</i> $\frac{dq}{dt} = K_1 (q_e - q)$	0.257	2.30E-05	0.005
	q_e (molkg ⁻¹)	K_2 (mol kg ⁻¹ min ⁻¹)	R ²
<i>pseudo-second order (Ho–McKay)</i> $\frac{dq}{dt} = K_2 \cdot (q_e - q)^2$	0.026	1.778	0.9944

Table 5: Fitting of the kinetic data of ISA in distilled water on C1 kinetics to Lagergren and Ho models.

3 Conclusions

The preliminary results obtained in this research indicates that ISA has more adsorption affinity than EDTA, following a similar trend of K_d values as a function of the concentration. POLI exhibits a different behaviour, with comparable K_d values for concentrations in the equilibrium solution smaller than 0.1 g^c/L and with higher K_d values above this concentration. This is corroborated by fitting to isotherms, with ISA and EDTA following 1-site-Langmuir model while POLI fits better to a Freundlich isotherm. In the adsorption kinetics on C1 paste, ISA data follows a pseudo-second order, that could imply a chemisorption on the active centers. As mentioned, these results would be completed by further data.

Acknowledgement

The EURAD-CORI project leading to this application has received funding from the European Union’s Horizon 2020 research and innovation programme under grant agreement No 847593.

References

- [1] L. Van Loon, M. Glaus, S. Stallone, A. Laube, Sorption of isosaccharinic acid, a cellulose degradation product, on cement, Environmental science & technology, 31 (1997) 1243-1245.
- [2] M.H. Bradbury, L.R. van Loon, Cementitious near-field sorption data bases for performance assessment of a L/ILW repository in a Palfris marl host rock. CEM-94: update I, June 1997, (1998).
- [3] D. García, P. Henocq, O. Riba, M. López-García, B. Madé, J.-C. Robinet, Adsorption behaviour of isosaccharinic acid onto cementitious materials, Applied Geochemistry, 118 (2020) 104625.
- [4] Y.-S. Ho, Review of second-order models for adsorption systems, Journal of hazardous materials, 136 (2006) 681-689.

Sorption study of selected organic ligands on C-S-H phases and their impact on the retention of plutonium

R. E. Guidone^{1,2*}, B. Lothenbach², A. Tasi¹, X. Gaona¹, M. Altmaier¹, H. Geckeis¹

¹ KIT-INE, Karlsruhe Institute of Technology, Institute for Nuclear Waste Disposal, Hermann-von-Helmholtz-Platz 1, 76344 Eggenstein-Leopoldshafen, Germany

² Empa, Swiss Federal Laboratories for Materials Science and Technology, Laboratory for Concrete and Construction Chemistry, Überlandstrasse 129, 8600 Dübendorf,

* Corresponding author: rosa.guidone@kit.edu

Abstract

Cement is widely used in the context of nuclear waste disposal for construction purposes and for the immobilization of the waste, especially in the case of low and intermediate level wastes. As a product manufactured from limestone and clay, the chemical composition of cement and its "mineralogy" consist mainly of Ca-based phases. The most abundant hydrate, covering two thirds of the bulk composition, is a gel-like poorly structured calcium silicate hydrate (C-S-H, in shorthand notation). In order to improve the workability of the fresh cement, organic chemicals (known as "plasticizer") are generally used. In the context of nuclear waste disposal, additional organics can be present in the disposed waste, *e.g.* decontamination chemicals, degradation products of organic compounds (*e.g.* cellulose-based materials), etc. In order to determine the impact of organic compounds on radionuclide retention by cement (*e.g.* by the formation of aqueous complexes, which can increase radionuclides solubility), the present study investigates the Pu uptake by C-S-H phases via sorption experiments in presence of formate, citrate and gluconate in alkaline conditions. Whilst the low affinity of Pu for formate and citrate does not affect Pu uptake on C-S-H phases, the Pu retention decreases at $[GLU]_{\text{tot}} \geq 10^{-4}$ M, indicating the formation of aqueous Pu-gluconate complexes stable in hyperalkaline pH conditions.

1. Introduction

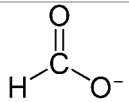
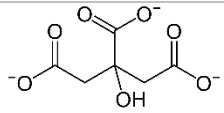
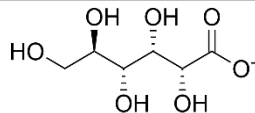
The disposal of radioactive waste in deep geological repositories is widely acknowledge as one of the most favorable disposal options. In the case of low and intermediate level waste (L-ILW), cement is widely used for construction purposes as well as for the conditioning and stabilization of radioactive waste. Cement is a heterogeneous matrix solid material containing different hydrated solid phases.

Calcium-silicate-hydrate (C-S-H) is the main hydrate phase formed during cement hydration. C-S-H phases have a variable Ca:Si molar ratio, which ranges from 0.7 to 1.5 in

synthetic samples, being approximately ≈ 1.8 in hydrated Portland cements (Lothenbach and Nonat 2015). C-S-H consists of ill-crystalline, nanometric particles with a defect tobermorite ($\text{Ca}_4(\text{Si}_6\text{O}_{18}\text{H}_2) \cdot \text{Ca} \cdot 4\text{H}_2\text{O}$) structure consisting of calcium oxide main sheet sandwiched between linear silicate chains in which two silicate tetrahedra are linked to the CaO main layer, and the third position, the bridging tetrahedron can be empty, in a so-called *dreierketten* structure. In between such layers there is an interlayer region where water and different cations can be present, to compensate the negative surface charge of C-S-H. At high Ca concentrations, the charge can be overcompensated leading to an apparent positive surface charge (Krattiger, Lothenbach et al. 2021) (Labbez, Pochard et al. 2011). The presence of calcium near the surface increases also anion sorption on C-S-H (Barbarulo, Peycelon et al. 2007). In addition, C-S-H phases have a high specific surface area ($190\text{-}330 \text{ m}^2/\text{g}$) (Suda, Saeki et al. 2015).

In order to determine the chemical affinity of organics on C-S-H phases the sorption of formate, citrate and gluconate has been investigated in binary systems. The organic ligands investigated in this work are shown in their deprotonated form in Table 1.

Table 1. Chemical formula, structure and acidity constants of selected organic ligands.

Organic ligand	Chemical formula	Structure	pKa
Formate	HCOO^-		3.75
Citrate	$\text{C}_6\text{H}_5\text{O}_7^{3-}$		6.40
Gluconate	$\text{C}_6\text{H}_{11}\text{O}_7^-$		3.86

Although not expected in large amounts in the L-ILW, plutonium can contribute to the long-term risk assessment of such repositories. Furthermore, under the alkaline ($\text{pH} \approx 13.3$) and reducing conditions, Pu(III) and Pu(IV) are expected to control the aqueous chemistry of plutonium. In this context, sorption experiments have been carried out to study the impact of organic ligands on Pu retention by C-S-H phases with Ca:Si=0.8 and 1.4.

2. Methods

2.1. Synthesis C-S-H phases

Sorption experiments with formate, citrate and gluconate were carried out on pre-synthesized C-S-H phases with Ca:Si ratio ranging from 0.8 and 1.4 and an initial solid to liquid

ratio of 55 g·dm⁻³. For each Ca:Si ratio, CaO and SiO₂ (Aerosil 200, Evonik, Essen, Germany) were mixed with high-purity deionized water (resistivity = 18.2MΩcm) generated by a Milli-Q Gradient A10 System (Millipore, Bedford, USA). CaO was produced by heating CaCO₃ at 1000 °C for 12 hours. Afterward, the C-S-H phases were equilibrated for two months in closed PE bottles at 20 °C on horizontal shakers (100 rpm).

2.2. Sorption experiments with organic ligands

Sorption experimental conditions were chosen in order to investigate the physical sorption on C-S-H and to minimize secondary processes such as re-crystallization and precipitation. Formate, citrate and gluconate sorption on C-S-H phases were investigated within $2 \cdot 10^{-5} \text{ M} \leq [\text{L}]_{\text{tot}} \leq 0.2 \text{ M}$. Different volumes of organic ligand solution, Na-formate (Fluka Analytical, Buchs, Switzerland), Na₃-citrate and Na-gluconate (Sigma-Aldrich, St. Louis, Missouri, USA) and NaOH solutions were added to the pre-synthesized C-S-H, such that in all cases the same final solution volume of 50 mL was obtained with a total NaOH concentration of 0.2 M, corresponding to a pH of ≈ 13.2 . Samples were let equilibrate for further 7 days before separation and characterization. Solid and liquid phases were separated by vacuum filtration through 0.45 μm nylon filter in a N₂ filled gloves box. Solid phases were stored in vacuum freeze-dryer for 7 days and stored afterwards in a desiccator over a saturated CaCl₂ solution at a relative humidity of $\approx 35\%$.

The adsorption of organic molecules on C-S-H is described by a distribution coefficient R_d :

$$R_d = \frac{C_{\text{sorb,eq}}}{C_{\text{aq,eq}}} = \frac{C_0 - C_{\text{aq,eq}}}{C_{\text{aq,eq}}} \cdot \frac{V}{m} \left(\frac{\text{dm}^3}{\text{kg}} \right) \quad (1)$$

where $C_{\text{sorb,eq}}$ is the equilibrium concentration of organics sorbed onto solid phase [mol/kg], $C_{\text{aq,eq}}$ is the equilibrium organics aqueous concentration [mol/dm³]. The difference between the initial organics concentration (C_0) and the equilibrium aqueous concentration ($C_{\text{aq,eq}}$) corresponds to the sorbed organics concentration. V is the total solution volume [dm³] and m is dry solid mass of C-S-H phase [kg].

The liquid phases were analyzed for the pH values and concentrations of calcium, silicon, sodium and organics. The pH measurements were carried out on a solution aliquot using Knick pH-meter with a SE 100 pH/Pt 1000 electrode at room temperature. In order to minimize the alkali error (Traynor, Uvegi et al. 2020), the instrument was calibrated with NaOH solutions of known concentration.

The total elemental concentrations of Ca, Na, and Si were measured with an Agilent ICP-OES instrument equipped with an Agilent SPS 4 autosampler. 2 wt.% HNO₃ was used to dilute the samples prior to analysis, applying dilution factors of 10, 100 and 1000.

The TOC analyser (Sievers 5310 C) was used to measure the total organic concentration present in the samples after equilibration. The samples were diluted at least by a factor of 5 (for

the lowest organic concentrations) with 0.1 M HCl solution, and by a factors of 10, 100 and 1000 with 0.01 M HCl at higher organic concentrations.

2.2.2. Sorption experiments with Pu

The uptake of Pu by C-S-H phases was investigated at constant initial Pu concentration (10^{-8} M) and varying: i) the solid to liquid ratio S:L (1-50 g/L), ii) organics concentration (10^{-4} -10-1.5 M) and iii) Ca:Si ratio of the C-S-H phases. Hydroquinone ($C_6H_4(OH)_2$, denoted as HQ) and Sn(II)Cl₂ (both at a concentration of $2 \cdot 10^{-3}$ M) were used as redox buffer. Aliquots of redox buffers and 2 M NaOH solution were inserted to the samples in order to reach the target redox (HQ, $pe+pH \approx 9$; Sn(II), $pe+pH \approx 1$) and alkaline ($pH = 13.2$) conditions. Samples were equilibrated for 2 days before the addition of Pu. A volume of 50 μ L from a diluted Pu(VI) stock solution was added to samples to reach the targeted initial Pu concentration. Samples were equilibrated for three days before the addition of formate, citrate or gluconate to the suspensions. Samples were shaken at ≈ 100 rpm over a period of 90 days.

pH and E_h measurements were performed before the addition of the organic ligands, and at each sampling performed after 7, 14, 60 and 90 days of contact time. E_h values were converted to pe according with $E_h = -RT \ln(10) F^{-1} \log a_{e^-} = RT \ln(10) F^{-1} pe$, where R is the ideal gas constant ($8.31446 \text{ J mol}^{-1} \text{ K}^{-1}$), F is the Faraday constant ($96,485.33 \text{ C mol}^{-1}$), and a_{e^-} is the activity of the electron. Samples were centrifuged at 6000 g for 5 min in order to separate any possible suspended particle; aliquots of 420 μ L withdrawn from the supernatant solution were transferred to a 10 kDa filter (pore diameter size $\approx 2 - 3$ nm, Nanosep®, Pall Life Sciences) and centrifuged at 6000 g for 10 min. An aliquot of the filtrate was then acidified with 2% HNO₃ and measured by SF-ICP-MS in order to get the Pu aqueous concentration.

3. Result and discussion

3.1. Investigation on C-S-H phases and on binary systems with organics

Figure 1 shows the total Ca concentrations for C-S-H phases with Ca:Si ratio of 0.8, 1.0, 1.2 and 1.4 as a function of citrate (a) and gluconate (b) concentrations after 7 days of contact time. In general, Ca concentration increases with the increase of organic concentration indicating a potential for the formation of aqueous Ca-organic complexes and/or a possible partial destabilization of C-S-H. Moreover, for longer equilibration times ($t \geq 7$ days) and higher citrate

concentrations, $\text{Ca}_3(\text{cit})_2 \cdot x\text{H}_2\text{O}(\text{s})$ precipitation is foreseen. The increase of Ca concentration is more pronounced for citrate than for gluconate.

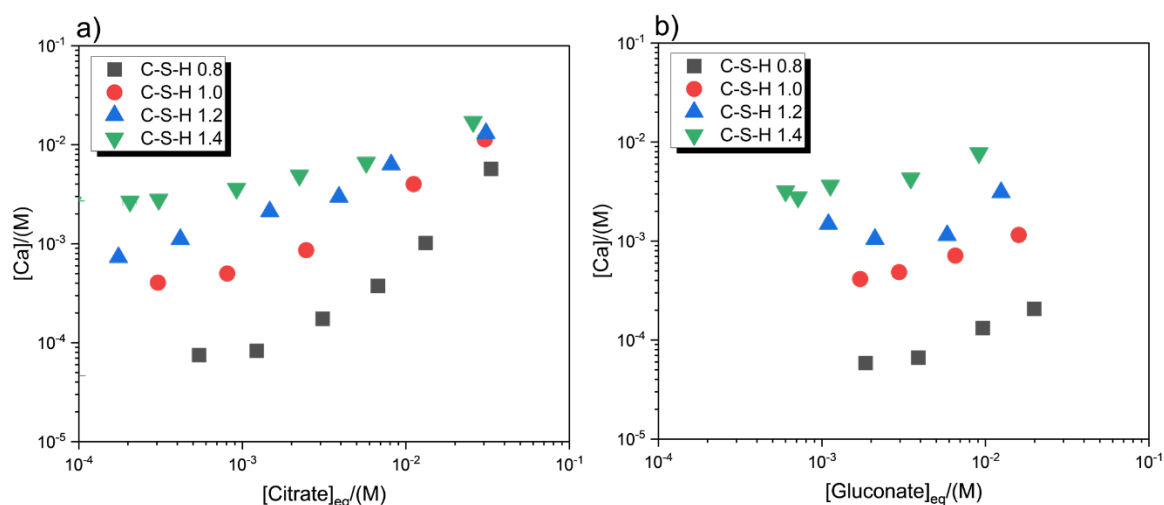


Figure 1. Aqueous Ca concentration as a function of citrate concentration (a) and gluconate concentration (b) for C-S-H phases with Ca:Si ratio ranging from 0.8 to 1.4, after 7 days of contacting time.

In Table 2 the average distribution coefficients, R_d , for formate, citrate and gluconate on C-S-H are reported. Sorption of formate remains relatively constant within the complete range of Ca:Si ratios investigated. In contrast to this, the uptake of citrate and gluconate increases with the Ca:Si ratio of the C-S-H, which is related to the presence of increasing amounts of calcium at the C-S-H surface at high Ca concentrations (Krattiger, Lothenbach et al. 2021) (Labbez, Pochard et al. 2011). The presence of Ca at the surface of C-S-H increases the sorption of inorganic and organic anions (Androniuk, Landesman et al. 2017) (Nalet and Nonat 2016). The high affinity of citrate and gluconate to C-S-H is also related to the functional groups. The citrate structure is characterized by three carboxylic groups (two terminal and one located in the middle of the main chain, see Table 1), which result in high charge density distributed over the entire molecule. It is also known that citrate tends to form strong bidentate complexes with Ca^{2+} ions (Geffroy, Foissy et al. 1999). Gluconate has one carboxylic group and five alcohol groups. The proximity of one alcohol group to the carboxylic group, enhances the acidity of the -OH group such that gluconate can also form bidentate complexes with calcium.

Table 2. Distribution coefficient, R_d , of formate, citrate and gluconate on C-S-H phases with Ca:Si = 0.8-1.4, after 7 days of equilibration time.

<i>Solid phase</i>	<i>Ca:Si</i>	<i>Formate</i> <i>[dm³/kg]</i>	<i>Citrate</i> <i>[dm³/kg]</i>	<i>Gluconate</i> <i>[dm³/kg]</i>
<i>C-S-H 0.8</i>	0.8	3,6±0.9	0.41±0.01	0.30±0.01
<i>C-S-H 1.0</i>	1.0	2.9±0.6	2.45±0.01	1.59±0.01
<i>C-S-H 1.2</i>	1.2	1.4±0.9	10.0±1.9	3.79±0.01
<i>C-S-H 1.4</i>	1.4	4.7±1.2	9.1±0.4	10.1±0.1

3.2. Sorption experiments with Pu

Figure 2 shows the R_d values determined for the uptake of Pu by C-S-H phases with Ca:Si = 0.8 and S:L = 1 g dm⁻³ in the absence and presence of gluconate (left) and citrate (right). Citrate (as well as formate, data not shown) has a negligible impact on the retention of Pu by C-S-H phases, and most of the R_d values determined for both systems fall within the detection limit of the SF-ICP-MS technique. This observation is attributed to (i) the precipitation of Ca₃(cit)₂·xH₂O(s) and consequent decrease of [Citrate]_{aq} remaining in solution (see Figure 3), and (ii) the expectedly weak interaction of An(IV) with citrate in the hyperalkaline conditions investigated in this work, as previously described for the Th(IV) case by Felmy and co-workers (Felmy, Cho et al. 2006). Data collected in the sorption experiments with the C-S-H 0.8-Pu gluconate system show a clear decrease of the distribution coefficient with the increase of gluconate concentration. This observation is attributed to the formation of stable ternary and quaternary Ca(II)-Pu(IV/III)-OH-gluconate complexes. Note that analogous complexes have been reported in the literature for Pu analogues, *i.e.* Th(IV) (Tits, Wieland et al. 2005) and Nd(III)/Cm(III) (Rojo, Gaona et al. 2021).

HQ and Sn(II)-buffered systems show systematic and reproducible differences at log [Gluconate] = -1.5. This finding hints towards (i) a different chemical behavior induced by the redox buffer, expectedly involving the predominance of Pu(IV) and Pu(III) for HQ and Sn(II)

systems, respectively, and (ii) the possibility of a co-adsorption process of Pu(III)_{aq} with GLU triggered by the high surface coverage of the ligand on the solid phase.

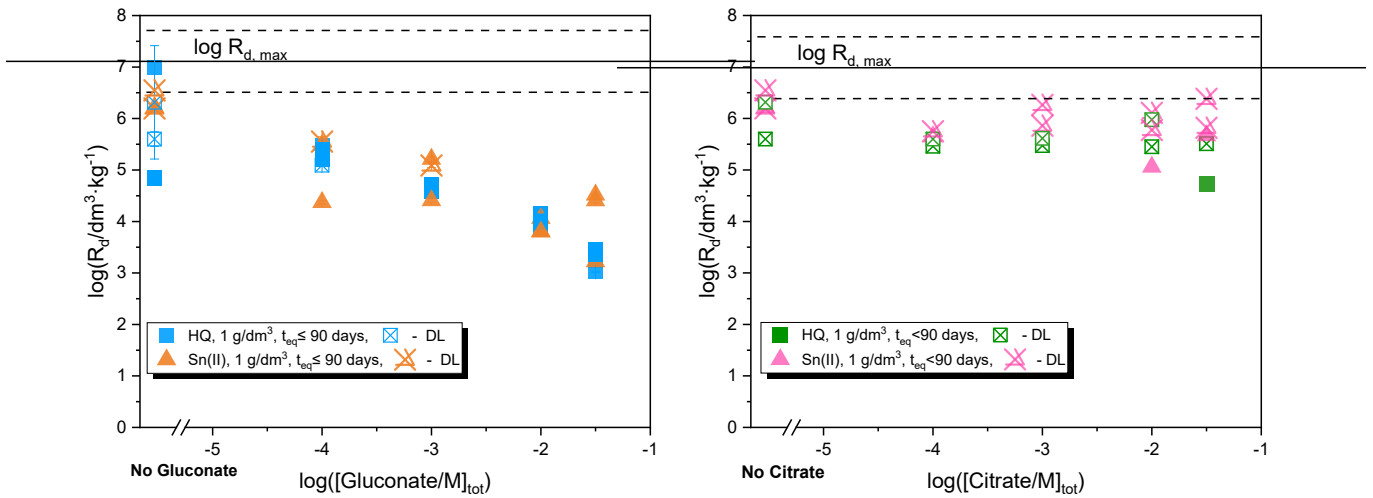


Figure 2. Distribution coefficient $\log(R_d)$ for C-S-H 0.8-Pu-Gluconate (left) and C-S-H 0.8-Pu-citrate (right) as a function of the total ligand concentration. Reported data refer to the cement phases synthesized with the S:L ratio of $1 \text{ g}\cdot\text{dm}^{-3}$ in presence of the two different redox buffered (HQ (■) and Sn(II) (▲)). Solid black lines ($\log R_{d,max}$) correspond to the highest R_d coefficient that can be calculated based on the detection limit of SF-ICP-MS and considered dilutions.

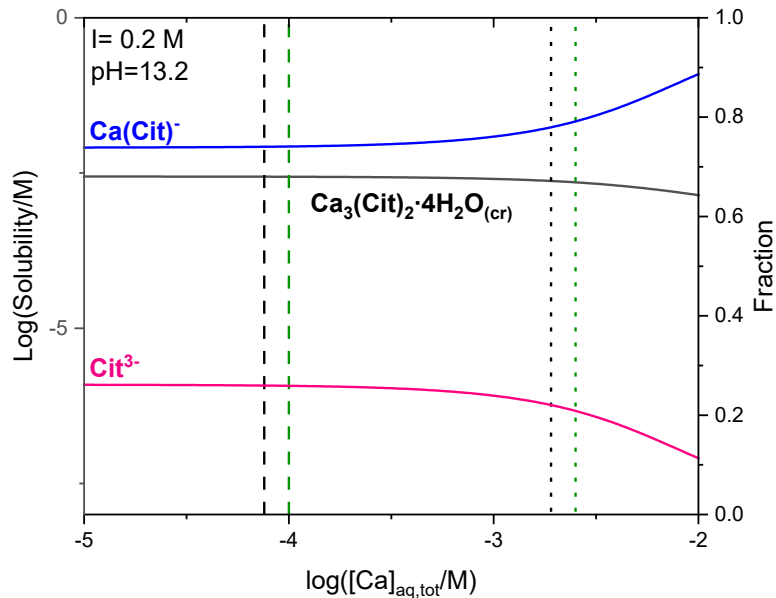


Figure 3. Solubility and fraction diagrams for the Ca-citrate system at $\text{pH}=13.3$ and $-5 \leq \log([Ca^{2+}]_{tot}/M) \leq -1$. Thermodynamic calculation conducted by using SPANA software (Puigdomènech, Colas et al. 2014) and the formation complexes constants reported in ThermoChimie (Giffaut, Grivé et al. 2014). Black and green dashed lines correspond to the total calcium concentration of C-S-H phases with S:L= $1 \text{ g}\cdot\text{dm}^{-3}$ and a Ca:Si ratio of 0.8 and 1.4 respectively. Black and green dotted lines correspond to the total calcium concentration of C-S-H phases with S:L= $25 \text{ g}\cdot\text{dm}^{-3}$ and a Ca:Si ratio of 0.8 and 1.4 respectively.

4. Conclusion

The impact of formate, citrate and gluconate on the uptake of Pu by C-S-H phases with $0.8 \leq \text{Ca:Si} \leq 1.4$ was investigated with a comprehensive characterization of the binary and ternary systems cement-L and cement-RN-L.

Results obtained for the binary systems show that the uptake of formate by C-S-H is independent of the Ca:Si ratio. A strong uptake is observed for citrate and gluconate, with R_d values mostly in the range of $0.1 - 10 \text{ dm}^3 \cdot \text{kg}^{-1}$. The trend to increasing R_d values with increasing Ca/Si ratio in C-S-H phases is attributed to the presence of increasing amounts of calcium at the C-S-H surface at high Ca concentrations, accordingly triggering the stronger interaction with the negatively charged organic ligands.

The uptake of Pu by C-S-H phases remains virtually unaffected in the presence of formate and citrate within the investigated boundary conditions ($\text{pH} = 13.2$ and $10^{-4} \text{ M} \leq [\text{L}] \leq 0.1 \text{ M}$). On the contrary, gluconate decreases the uptake of Pu by C-S-H with Ca/Si = 0.8 and 1.4 by up to 4 orders of magnitude. This observation is in line with previous results reported for Th(IV) and Eu(III), thus supporting the formation of stable ternary or quaternary complexes (Ca-)Pu-OH-GLU in the aqueous phase. The differences observed for the uptake in systems containing HQ or Sn(II) as redox-buffers underpin that the reduction of Pu(IV) to Pu(III) is also feasible in hyperalkaline systems, and highlights the need of undertaking experiments with plutonium beyond the use of redox-stable analogues such as Th(IV) or Eu(III).

Acknowledgement

The EURAD-CORI project leading to this application has received funding from the European Union's Horizon 2020 research and innovation programme under grant agreement No 847593.

References

- Androniuk, I., C. Landesman, P. Henocq and A. G. Kalinichev (2017). "Adsorption of gluconate and uranyl on CSH phases: Combination of wet chemistry experiments and molecular dynamics simulations for the binary systems." Physics and Chemistry of the Earth, Parts A/B/C **99**: 194-203.
- Barbarulo, R., H. Peycelon and S. Leclercq (2007). "Chemical equilibria between C–S–H and ettringite, at 20 and 85 C." Cement and Concrete Research **37**(8): 1176-1181.
- Felmy, A. R., H. Cho, D. A. Dixon, Y. Xia, N. J. Hess and Z. Wang (2006). "The aqueous complexation of thorium with citrate under neutral to basic conditions." Radiochimica Acta **94**(4): 205-212.
- Geffroy, C., A. Foissy, J. Persello and B. Cabane (1999). "Surface complexation of calcite by carboxylates in water." Journal of Colloid and Interface science **211**(1): 45-53.
- Giffaut, E., M. Grivé, P. Blanc, P. Vieillard, E. Colàs, H. Gailhanou, S. Gaboreau, N. Marty, B. Made and L. Duro (2014). "Andra thermodynamic database for performance assessment: ThermoChimie." Applied Geochemistry **49**: 225-236.
- Krattiger, N., B. Lothenbach and S. V. Churakov (2021). "Sorption and electrokinetic properties of ASR product and CSH: A comparative modelling study." Cement and Concrete Research **146**: 106491.
- Labbez, C., I. Pochard, B. Jönsson and A. Nonat (2011). "CSH/solution interface: Experimental and Monte Carlo studies." Cement and Concrete research **41**(2): 161-168.

Lothenbach, B. and A. Nonat (2015). "Calcium silicate hydrates: Solid and liquid phase composition." Cement and Concrete Research **78**: 57-70.

Nalet, C. and A. Nonat (2016). "Ionic complexation and adsorption of small organic molecules on calcium silicate hydrate: Relation with their retarding effect on the hydration of C3S." Cement and Concrete Research **89**: 97-108.

Puigdomènech, I., E. Colas, M. Grive, I. Campos and D. García (2014). "A tool to draw chemical equilibrium diagrams using SIT: Applications to geochemical systems and radionuclide solubility." MRS Online Proceedings Library **1665**(1): 111-116.

Rojo, H., X. Gaona, T. Rabung, R. Polly, M. García-Gutiérrez, T. Missana and M. Altmaier (2021). "Complexation of Nd (III)/Cm (III) with gluconate in alkaline NaCl and CaCl₂ solutions: Solubility, TRLFS and DFT studies." Applied Geochemistry **126**: 104864.

Suda, Y., T. Saeki and T. Saito (2015). "Relation between chemical composition and physical properties of CSH generated from cementitious materials." Journal of Advanced Concrete Technology **13**(5): 275-290.

Tits, J., E. Wieland and M. Bradbury (2005). "The effect of isosaccharinic acid and gluconic acid on the retention of Eu (III), Am (III) and Th (IV) by calcite." Applied Geochemistry **20**(11): 2082-2096.

Ni-63 uptake on CEM I hardened cement paste – preliminary experimental results

Camelia Ichim^{1*}, Crina Bucur¹, Mirela Olteanu¹

¹ Institute for Nuclear Research Pitesti, Romania (RATEN ICN)

* Corresponding author: camelia.ichim@nuclear.ro

Abstract

In the frame of CORI WP of EURAD Programme, RATEN ICN is involved in Task 3 & 4 and we proposed to investigate the effect of organics generated by spent ion exchange resins degradation on Ni (as divalent radionuclide) mobility in cementitious environments. Ni sorption kinetic and isotherms and the effect of organics on Ni sorption will be investigated by batch sorption/desorption tests.

This paper summarises the experiments performed to assess the solubility limit of nickel in cement pore waters, under the relevant conditions anticipated in the near field of a cementitious repository and the preliminary results of the batch tests conducted to evaluate ⁶³Ni uptake on CEM I hardened cement paste.

Preliminary results indicate relatively fast ⁶³Ni sorption kinetic and strong uptake on CEM I hardened cement paste under conditions corresponding to the initial state of HCP degradation. The distribution ratio describing uptake of ⁶³Ni on CEM I HCP was found to be consistent with data obtained under similar experimental conditions and reported in the literature ($R_d = 0.14 \text{ m}^3 \text{ kg}^{-1}$).

The experimental activities are on-going and sorption/desorption isotherms will be derived for CEM I and CEM V HCPs and the corresponding distribution ratios will be assessed. The influence of the solid/liquid ratio in batch type experiments will be evaluated and also the influence of organic molecules on the uptake of ⁶³Ni on cement-based material in different degradation states will be investigated.

1. Introduction

The multi-barrier concept of the near surface disposal facilities and also for the area of geological repositories dedicated for ILW disposal is designed so as to prevent and limit the radionuclide migration and it relies mainly on cement based materials, due to their good mechanical and physical properties. Cementitious materials may also contribute to the containment of radioactivity and limit water ingress into the repository after its closure. Due to their favourable chemical properties, these materials have the potential to retain by sorption, incorporation or precipitation a variety of radionuclides.

For ternary system radionuclide-organics-cement, nickel was selected as divalent radionuclide potentially released in repository by the wastes. Nickel radioactive isotopes are sorbed on cementitious materials by isotopic exchange rather than conventional sorption processes. ⁶³Ni is produced by neutron activation of stable ⁶²Ni isotope that is found in structural materials and irradiated metallic components in a nuclear reactor. In performance assessments, nickel radioisotopes present in LILW to be disposed in a near surface repository are considered to be safety-relevant.

2. Materials and methods

2.1 Hardened Cement Paste Analysis

The Hardened Cement Paste used in these solubility and sorption experiments is based on CEM I 52.5 (OPC, LAFARGE, Val d'Azergues factory), prepared at a water/cement ratio of 0.38 and kept in saturated portlandite water until required for use, in order to avoid carbonation. The powdered HCP material involved in the present study was obtained from this bulk sample by crushing and grinding followed by sieving to collect fraction with particle size less than 63 µm and to obtain and prepare the powdered samples for the degraded states (state II and III) of the cement paste. All operations were performed in a glove box with controlled nitrogen atmosphere.

The HCP samples were characterised by SEM-EDS to gather information on the chemical composition of the material, TGA/DTA to investigate sample weight change and the different compositional trends. To determine the natural nickel content in the samples used for the experiments acid dissolution of CEM I HCP samples was achieved in a closed microwave system and the resulted solutions were analysed by ICP-OES.

The information obtained by SEM-EDS technique on the hardened cement paste composition show that Ca and Si are found to be the major elements in the analysed material (Table 1). The spectrum obtained by SEM/EDS is presented in Figure 1.

Table 1: Major elements in HCP, by EDS

Main oxide content in HCP based on CEM I, State I of degradation [%]	
CaO	43.53 ± 1.3
SiO ₂	16.48 ± 0.8
Al ₂ O ₃	6.41 ± 0.4

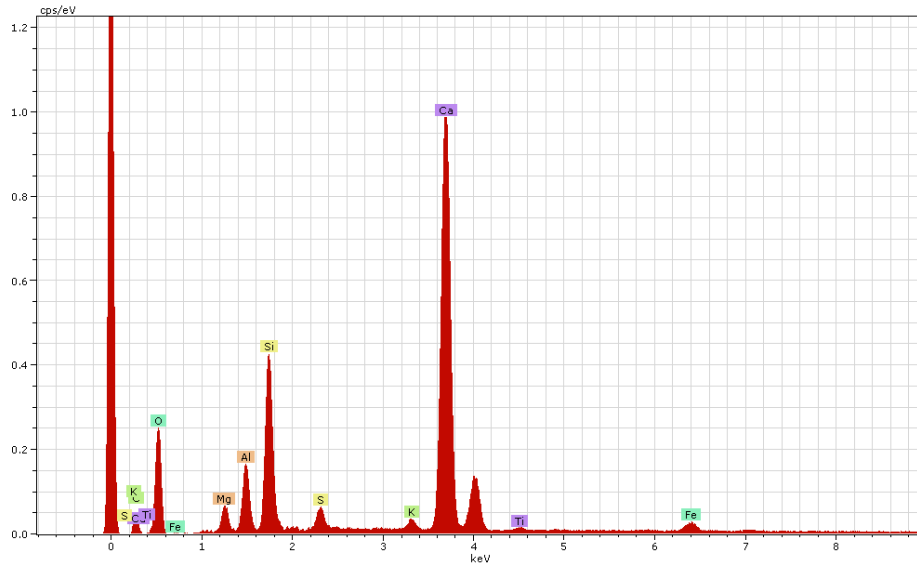


Figure 1: SEM/EDS spectrum for HCP samples analysed

The dehydration kinetic of cement paste at different heating rates was assessed by thermogravimetry. The TGA results presented in Figure 2 show two peaks of mass loss. One peak is around 93°C and it is associated mainly with the loss of pore water, interstitial water or absorbed water and/or calcium sulfoaluminate ($3\text{CaO}\cdot\text{Al}_2\text{O}_3\cdot3\text{CaSO}_4\cdot32\text{H}_2\text{O}$) or ettringite thermal dehydration. The second peak is at approx. 448°C that represents the characteristic temperature for portlandite (CH) dehydration. The TGA results also show that the carbonation of the samples did not occur.

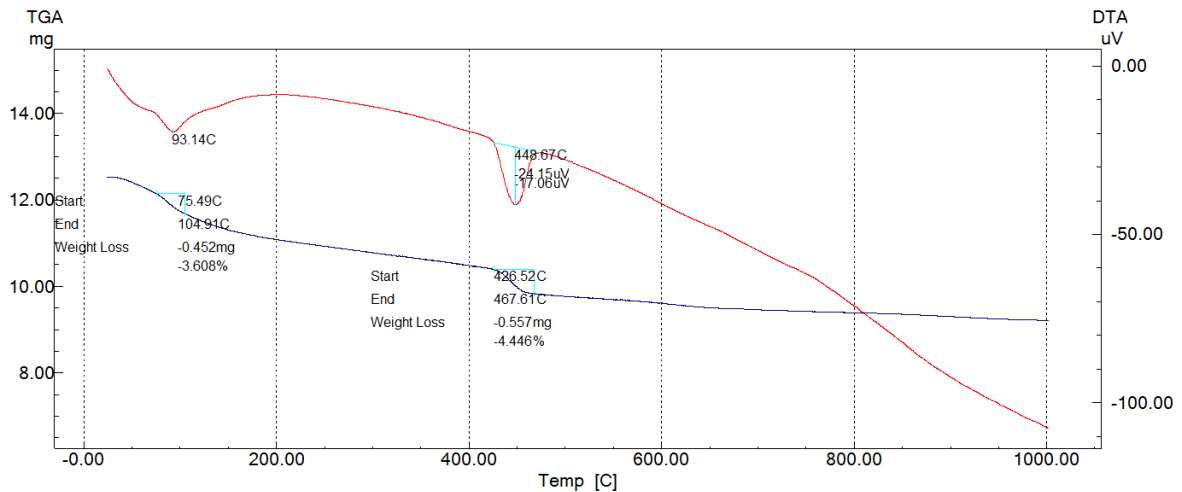


Figure 2: TGA/DTA curves obtained for HCP samples analysed

2.2 ACW preparation and composition

The composition of the solution in equilibrium with HCP was prepared according to the procedure of Wieland et al (2006). Briefly, the composition of a porewater in equilibrium with HCP with respect to the main cement-derived cations at pH 13.3 is summarised in Table 2. The ACW stock

solution was obtained by weighing and dissolving adequate amounts of KOH and NaOH in 2 L of ultrapure water, followed by addition of calcite and portlandite. The solution obtained was shaken for at least 2 week in closed glass bottles and at the end of this period the solution was filtered through 0,22 µm Nylon filters, in nitrogen atmosphere inside a glove box. Finally, to complete the ACW stock solution adequate amounts of Na₂SO₄ and Al₂(SO₄)₃ have been added and the solution was kept until required for use in wet chemistry experiments.

Table 2: Composition of ACW stock solution in equilibrium with HCP

[K]t	[Na]t	[Ca]t	[Al]t	[S]t	[Si]t
0.18 M	0.114 M	1.6 E-03 M	5 E-05 M	2 E-03 M	5 E-05 M

2.3 ⁶³Ni solubility experiment

In the frame of migration studies radionuclide properties in solution are derived by their speciation and solubility. The solubility of nickel in alkaline conditions characteristic for cement-based materials has been reported in a series of studies. From most of these studies it can be concluded that at a pH higher than 12 the concentration of the dissolved nickel is usually less than 10⁻⁶ M. Thus a solubility experiment was conducted to assess Ni solubility limit in ACW in equilibrium with CEM I hardened cement paste (state I). Taking into account the findings of Wieland et al. (2006) upon contacting the HCP with ACW the nickel bound to cement based material could be released into solution. The solubility test was conducted using ⁶³Ni labelled solutions mixed with ACW having the composition of the main cations presented in Table 2, at a pH of 13.3. The solubility test was conducted in nitrogen atmosphere inside a glove box, at room temperature, in centrifuge tubes previously pre-washed. The total nickel concentration in the experiment ranged between 10⁻⁸ M and 10⁻⁵ M. For this concentration range five nickel concentrations have been selected and obtained by preparing stock solution of 10⁻⁴ M NiCl₂ and a stock of ⁶³Ni tracer solution. Appropriate volumes from these stock solutions have been added in ACW. The centrifuge tubes have been intermittently shaken for 7 and 45 days. Since in solubility type experiments, not only Ni-63 concentration is relevant, at the end of each testing period the tubes were centrifuged and aliquots were withdrawn from each solution acidified and analysed for total nickel concentration by ICP-OES (iCAP 6000 series).

2.4 ⁶³Ni sorption experiment

⁶³Ni uptake by HCP based on CEM I (state I) has been assessed by batch sorption experiments. The batch test has been conducted for a solid to liquid ratio (S/L) of 2.5×10⁻² kg L⁻¹ (1 g of 63 µm crushed and sieved HCP in 40 mL ACW), at room temperature, inside a glove box, under nitrogen atmosphere. Sorption experiments were carried out in duplicate in 50 mL polypropylene centrifuge tubes. Before use the centrifuge tubes were prewashed and blank batches were prepared in order to assess nickel concentration in cement pastes. Also ⁶³Ni sorption on centrifuge tubes has been checked. Weighted amounts of dry crushed HCP were equilibrated with ACW prior addition of labelled ⁶³Ni

solutions. For uptake experiments a stock solution using carrier-containing ^{63}Ni radiotracer (NiCl_2 in 0.1 M HCl) has been prepared from a source with the total activity of 3.841×10^6 Bq. The total nickel concentration added in the system have been selected and calculated so that the ^{63}Ni plus carrier concentrations are well below the solubility limit. Nickel concentrations in the system ranged from 10^{-9} M to 10^{-8} M. For sorption kinetic test five concentrations in contacting solutions have been selected in this concentration range.

During the equilibration periods the test tubes have been placed on an orbital shaker at 100 rpm. After equilibration the test tubes have been centrifuged, the supernatant solutions were sampled and the residual activity of ^{63}Ni in the solutions has been measured by LSC counting, using Ultima Gold scintillation cocktail and Canberra Packard Tri-Carb 5110 TR liquid scintillation analyser. The samples counting was performed until the uncertainty of $\% \sigma \leq 0.5$ was achieved.

3. Results

The results of the solubility test carried out to determine nickel solubility limit in ACW are reported in Figure 3, in form of concentration of dissolved Ni in ACW function of the total Ni concentration in the system for 7 and 45 days of equilibration periods.

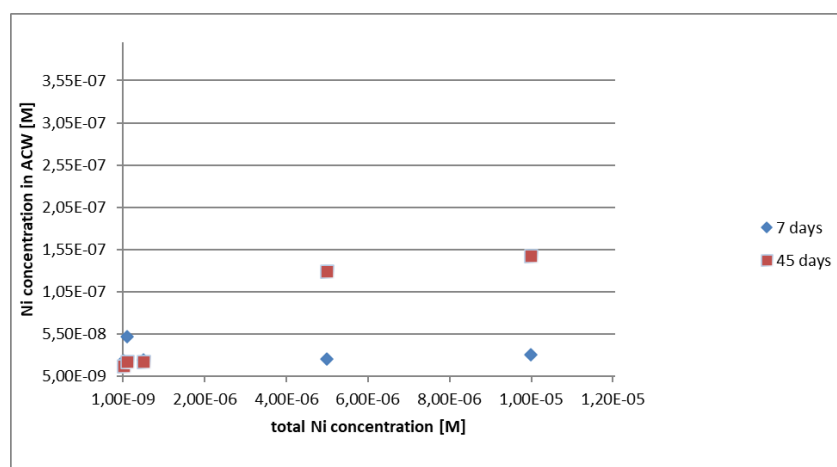


Figure 3: Nickel concentration in solution as a function of the total Ni(II) inventory after 7 and 45 days equilibration times

The observed nickel concentrations at the end of the testing periods, total and in solution, agree well up to a total nickel concentration of about 3×10^{-8} M. Throughout the testing periods it was observed that the measured nickel concentration in solution is lower than the initial nickel concentration introduced in the system, although no visible formation of a precipitate occurred, that can give rise to lower concentrations after the centrifugation and filtration steps.

The mean nickel concentration was considered at that stage a reasonable indication of nickel solubility and for the preliminary sorption tests this value has been selected as solubility limit under the conditions considered and the nickel concentrations in the sorption experiment have been selected an order of magnitude lower than this mean value.

In order to conclude that the concentrations obtained in the solubility test represent true nickel solubility supplementary solubility test will be performed.

The results obtained from the kinetic and ⁶³Ni sorption test on CEM I hardened cement paste have been expressed in terms of percentage uptake, according to the expression given in Eq. 1:

$$A_{ti} = \frac{C_{aq}(t_i) - C_0}{C_0} \times 100 \quad \text{Eq. 1}$$

where: A_{ti} represent the amount of nickel sorbed at time t_i(%), C_{aq}(t_i) is the nickel activity in the aqueous phase at time t_i (Bq/mL), and C₀ is the initial nickel activity in contacting solutions (Bq/mL).

The preliminary results obtained for ⁶³Ni uptake are presented in Figure 4. These results indicate that for initial nickel concentrations in the range of 10⁻⁹M - 10⁻⁸M, nickel is strongly retained on CEM I HCP.

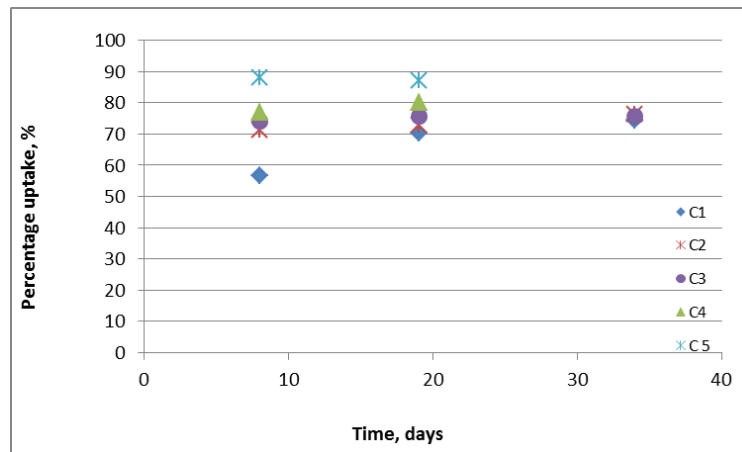


Figure 4: The evolution of ⁶³Ni percentage uptake on CEM I HCP

For each sampling period, the uptake of ⁶³Ni on CEM I HCP has been described in terms of the distribution ratio, R_d, computed according to Eq. 2 and the resulted values are presented in Table 3.

$$R_d = \frac{c_{s,eq}}{c_{l,eq}} = \left(\frac{c_t^0 - c_{l,eq}}{c_{l,eq}} \right) \left(\frac{V}{m_c} \right) \quad [m^3 kg^{-1}] \quad \text{Eq. 2}$$

The definition of the distribution ratio according to Eq. 2 does not suppose a specific sorption process and accounts for the relationship between the Ni retained by the HCP and the concentration of dissolved nickel at each contacting times. The difference between the Ni concentration in the initial solutions contacted with CHP samples (c_t⁰) and the concentration determined in the supernatant solutions (c_{l,eq}) represents the amount of nickel retained on the HCP.

Tabel 3. ⁶³ Ni uptake by CEM I HCP

C1	C2	C3	C4	C5
R d [m³ kg⁻¹]				
0.08	0.11	0.13	0.14	0.27
Mean	0.14			

The distribution ratio values calculated correspond to the mean values deduced from the kinetic test illustrated in Figure 5, by computing the experimental data after 34 days of equilibration. As it was expected the distribution ratio increased during the kinetic test (Figure 5). Supplementary investigations have to be carried out to validate these preliminary results and to gain knowledge on the retention mechanism of ⁶³Ni in cement-based materials.

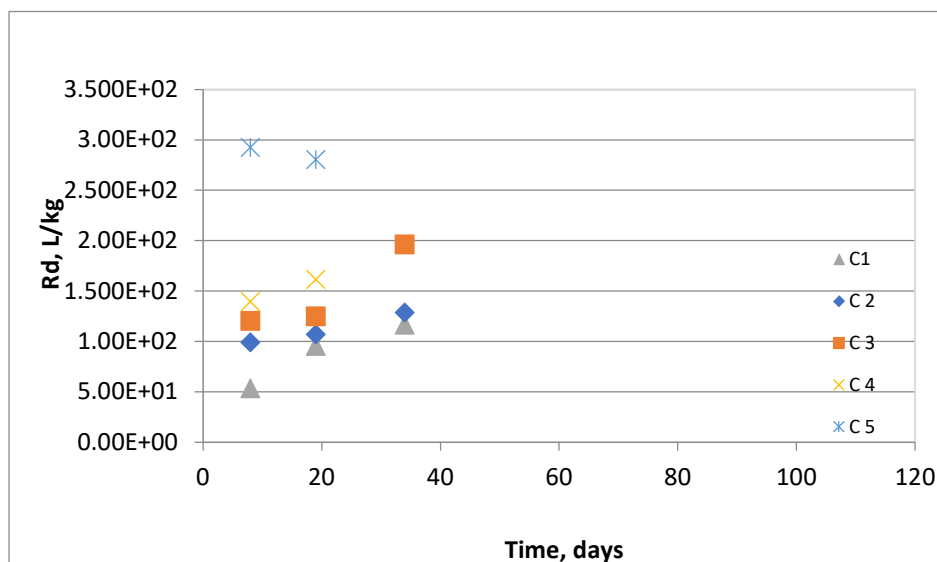


Figure 5: ⁶³Ni uptake kinetic on CEM I HCP (evolution of distribution ratio)

4. Future work

The data presented in this paper represent preliminary experimental data set of the on-going wet chemistry experiments carried out to assess the behaviour of nickel cement-based systems and to understand the uptake mechanism in cementitious matrix.

The following experimental tests are proposed for the next period:

- Solubility tests in presence of organics
- Complete and analyses of the sorption data
- complete the experimental dataset with sorption studies in the presence of FORMIC ACID

Acknowledgement

The EURAD-CORI project leading to this application has received funding from the European Union's Horizon 2020 research and innovation programme under grant agreement No 847593.

References

- Wieland, E. et al. (2006). Experimental evidence for solubility limitation of the aqueous Ni(II) concentration and isotopic exchange of ⁶³Ni in cementitious systems.
- Ochs, M. et al. (2016). Radionuclide and Metal Sorption on Cement and Concrete. Springer International Publishing.

García, D. et al. (2018). The potential role of the degradation products of cement superplasticizers on the mobility of radionuclides. *Applied Geochemistry*, 98, 1-9.

Chemical and physical characteristics of commercial cement superplasticizer based on polymelamine sulphonate

A. Judžentienė*, A. Zdaniauskienė

Center for Physical Sciences and Technology, Department of Organic Chemistry;
Saulėtekio Av. 3, LT-10257 Vilnius, Lithuania

* Corresponding author: asta.judzentiene@ftmc.lt

Abstract

Superplasticizers (SPs) in cement could have impact for the long-term safety of radioactive waste disposal. These organic substances may be leached into groundwater from cementitious material and possibly affect radionuclide migration behaviour. Commercial cement superplasticizer based on polymelamine sulphonate (PMS) Peramin SMF10 (Peramin AB, Sweden) was chosen for the research. Detailed chemical composition of the product SMF10 was done by Wavelength dispersive X-Ray Fluorescence (WD-XRF) spectroscopic method, other physical-chemical properties of the superplasticizer PMS were evaluated by thermo-gravimetric analysis. PMS leaching process in different cement matrixes was investigated as well. In order to evaluate rate of the alkaline degradation of PMS superplasticizer in various aqueous solutions Raman and UV/VIS spectroscopy was applied for analysis. No changes were observed in the hydrolytic solutions with any of the above mentioned methods of analyses.

1.Introduction

Superplasticizers (SPs) are effective organic additives for reducing water content, giving homogeneity and non-segregation of mortar and grout, lowering porosity, increasing mechanical strength and workability, improving resistance to aggressive environments and achieving sufficient fluidity and good plasticity of cement [1–3]. Without these superplasticizers the concrete would contain ~9-11% of water, compared to 7-9% with superplasticizers. According to the market analysts, the sulfonated melamine formaldehyde (PMS) condensates segment held a 31% share of the overall market, which is highest among other types of concrete SPs [4].

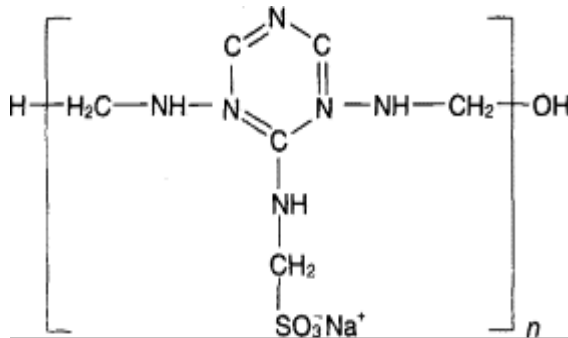
SPs possibly decompose into relatively small molecular weight polymers over the long term, and these organic substances may be leached into groundwater from cementitious materials, and possibly affect radionuclide migration behaviour.

Aim of the present research: i) to investigate chemical and physical characteristics of commercial cement superplasticizer based on polymelamine sulphonate; ii) to evaluate rate of alkaline degradation of PMS superplasticizer in different aqueous solutions.

2. Chemical and physical characteristics of commercial cement superplasticizer based on polymelamine sulphonate.

2.1 Product Peramin ® SMF10 characteristics

Commercial product under the name Peramin ® SMF10 (Peramin AB, Upplands Väsby, Sweden) is based on polymelamine sulphonate (PMS).

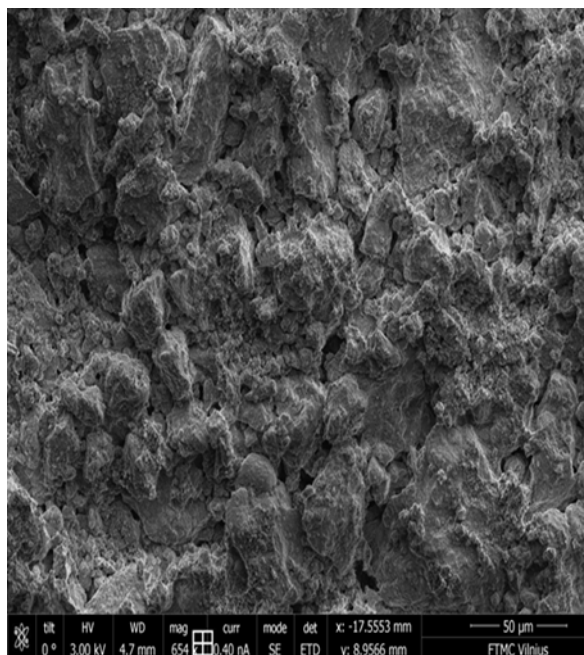


The product is off-white powder or dust with 450-650 kg/m³ density, pH of 5% aqueous solution is around 8.8, and dosage is 0.2-2.0% by weight.

2.1. Characterization of Cementous material by scanning electron microscopy (SEM).

The surface morphology was carried out in a dual beam system FE-SEM-FIB Helios Nanolab 650 (FEI Company), using 2 - 5kV accelerating voltage. Different magnification levels were chosen for this analysis, and the magnification of 650 was shown as the most representative. Thin-plates (150mm×100mm×~3mm) were hardened for 90 days. **Figure 1.** demonstrates clearly how superplasticizer could improve physical, and accordingly mechanical properties of concrete.

a)



b)

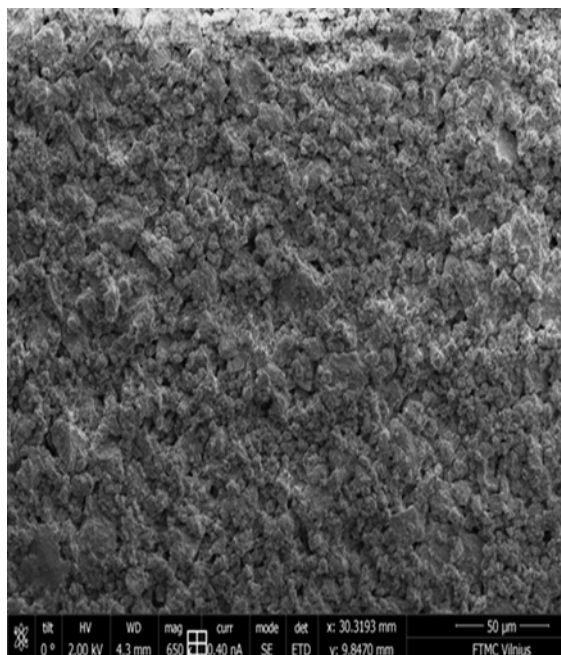


Figure 1: SEM images before leaching, magnification 650 times.

a): samples of cement CI (without superplasticizer)

b): samples of cement CI+2% PMS were prepared with a low amount of tap water (1.2:1, Vol cement: Vol H₂O)

2.2 Detailed chemical composition Peramin ® SMF10

Detailed chemical analysis of the product was performed by Wavelength Dispersive X-Ray Fluorescence (WD-XRF) spectroscopic method, using Axios^{mAX} (Malvern PANalytical) spectrometer equipped with SST-mAX X-ray tube (Rh anode, 4 kW); and results of quantitative analysis were obtained using software Omnian (PANalytical). Major constituent was found polymer of PMS (C₃N₃(NH)₃(CH₂)₃SO₃Na +H₂O) in quantity over 99.8%.

Chemical composition (%) of product Peramin ® SMF10 according to the Product Data Sheet: dry content 93.2 % (93.5± 2), Na₂O+0.658 K₂O 12.0 (< 13), Cl⁻ (as ions) 0.004 (<0.05).

Table 1: Detailed chemical composition of commercial product Peramin SMF10

No.	Compound	Percentage
1.	PMS	99.824
2.	Na ₂ O	0.021
3.	Al ₂ O ₃	0.017
4.	SiO ₂	0.021

5.	P ₂ O ₅	0.054
6.	K ₂ O	0.006
7.	CaO	0.017
8.	Fe ₂ O ₃	0.005
9.	ZnO	0.033
10.	Cl	0.004

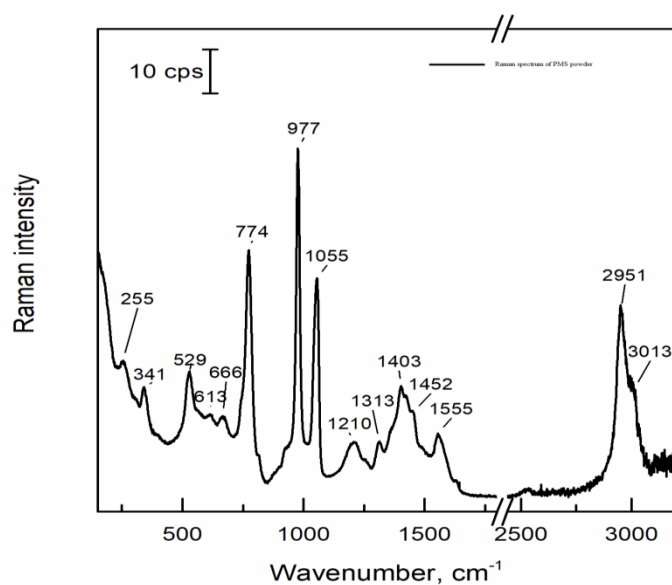


Figure 2: Raman spectrum of polymelamine sulphonate (PMS) powder (commercial product Peramin SMFR 10)

2.3 Thermo-gravimetric analysis of Peramin ® SMF10

Thermogravimetric analysis was performed in the range of 30 - 800°C. Atmosphere - air. Thermal stability of the sample PMS polymer is stable up to 270 °C. The residual ash of the sample may consist of finely divided SiO₂ or metal carbonates / oxides (according to composition table from Elemental analysis).

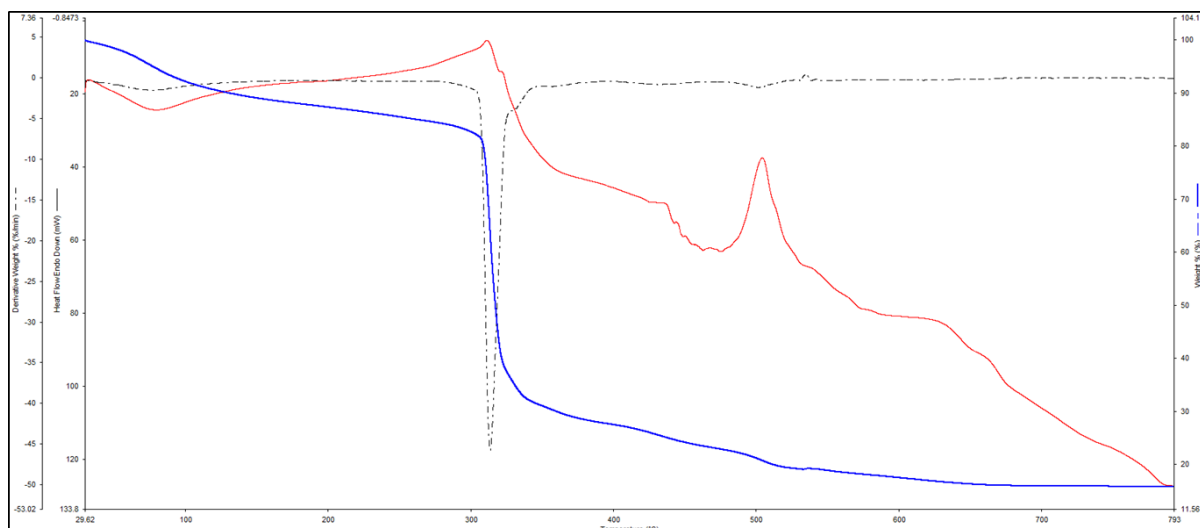


Figure 3: Thermo-gravimetric analysis of Peramin SMF10 (based on PMS)

Three mass losses are observed.

Curves:

- blue (TG) – percentage weight loss (TG);
- dashed black – derivative weight loss (DTG) (% / min);
- red – differential scanning calorimetry (DSC) (heat flow (mW)).

Three mass losses are observed. Thermal processes (red curve - heat flow):

- 1) 36 – 136°C endothermic evaporation of adsorbed H₂O (approx. 7% mass loss);
- 2) 284 – 349 °C exothermic decomposition of polymer / polymer matrix, possibly with formation of monomers and further oxidation of monomers (48% mass loss after evaporation of adsorbed H₂O);
- 3) 473 – 546 °C exothermic complete oxidation of de-polymerization products (final mass 15% of initial sample).

3. Analysis of PMS hydrolytic solutions

Spectroscopic (Raman and UV/Vis) analyses have been undertaken in order to investigate a rate of alkaline degradation of PMS superplasticizer in different aqueous solutions (at room temperature (20±2°C), atmospheric conditions, under natural light, pH=9.9 -12.9, in deionized, tap and synthetic saline water (0.5% NaCl)). Sampling time periods were 0, 3, 7, 15, 21, 28 and 45 days and then the frequency lowered at 6, 8, 10, 12 weeks...up to 7 months. Deionized water has been obtained by Direct – Q 3UV Water purification system (Type 1), conditions 20.0±1.0°C, 18.2 MΩ.cm, pH values have been achieved with 0.5M KOH.

Lambda 25 UV/Vis (Perkin Elmer) spectrometer has been used for spectrophotometric analysis (in a range 200 – 1100 nm) of PMS hydrolytic samples. The identical curves were obtained for just prepared PMS solution and for samples after 7 months of hydrolysis (**Figure 4**).

Raman spectra of different PMS hydrolytic solutions during the time were recorded, using Echelle type spectrometer RamanFlex 400 (Perkin Elmer Inc.) equipped with thermoelectrically cooled (-50 °C) CCD camera and fibber-optic cable for excitation and collection of the Raman spectra. The 785 nm beam of the diode laser was used as the excitation source. The laser power at the samples was restricted at 100mW. The integration time was 300s. The upper curves indicate solutions after 7 months, the lower ones –just made samples (**Figure 5**). The identical curves were obtained for just prepared PMS solution and for samples after 7 months of hydrolysis.

No changes were observed in the hydrolytic solutions with any of the above mentioned spectroscopic methods of analysis.

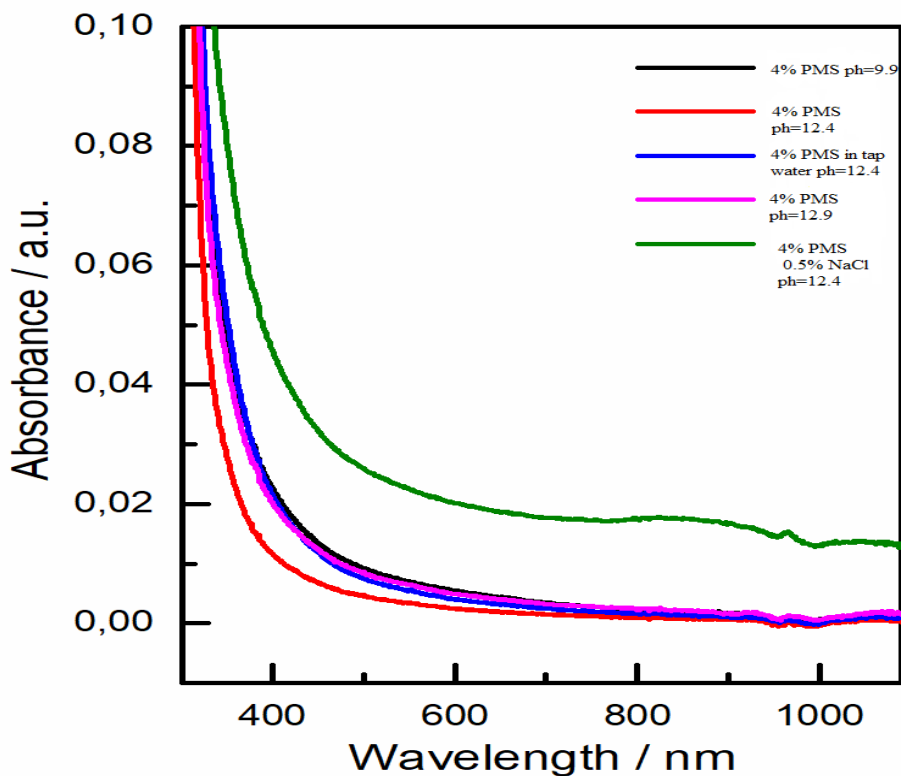


Figure 4: UV/ VIS spectra of different polymelamine sulphonate (PMS) hydrolytic solutions (sampling time: 7 months)

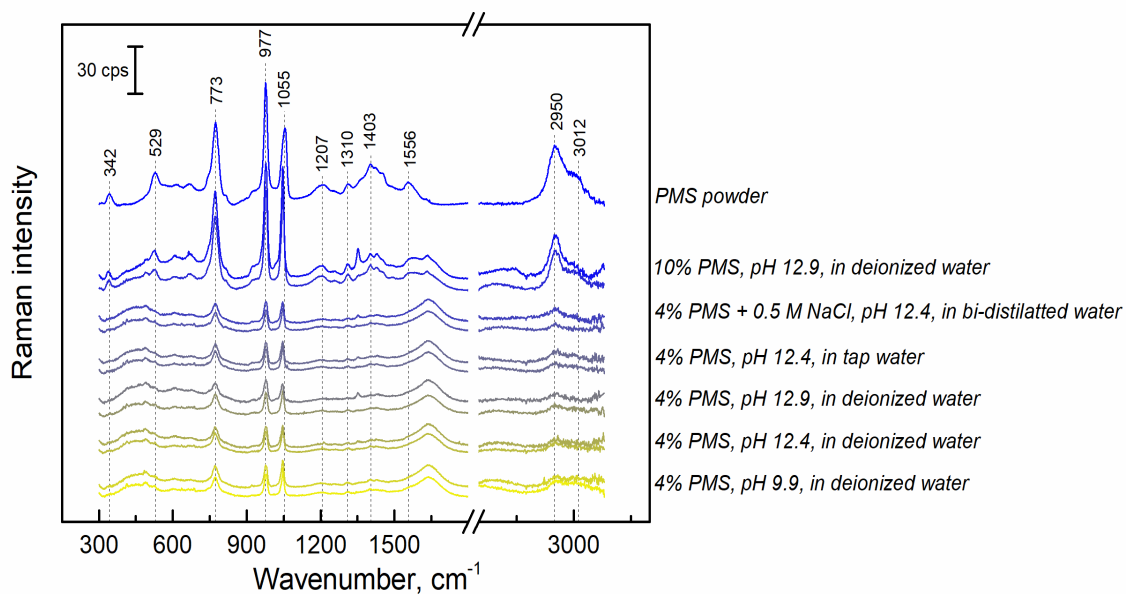


Figure 5. Raman spectra of different polymelamine sulphonate (PMS) hydrolytic solutions (sampling time: 1 day and 7 months)

Acknowledgement

The EURAD-CORI project leading to this application has received funding from the European Union's Horizon 2020 research and innovation programme under grant agreement No 847593.

The Peramin AB for providing product Peramin ® SMF10 (5 kg) free of charge.

References

1. Mollah M. Y. A., Adams W. J., Schennach R. & Cocke D. L. (2000) A review of cement – superplasticizer interactions and their models. *Advances in Cement Research* 12(4), 153.
2. Ramachandran V. S., Malhotra V. M., Jolicoeur C. & Spiratos N. *Superplasticizers: properties and applications in concrete*. (1998) Canada: ISBN-10066017393X.
3. Lahallh S. M., Absl-Halabi M. & Ali A. M. (1988) *Cement and Concrete Research* 18(4), 513.
4. Wood, L. *Concrete Superplasticizers Market -Forecast (2020 -2025)*. Research and Markets.com (2020).

Effect of ISA on the uptake of U(VI) on CEM V HCP

C. Landesman^{1*}, N. Bessagnet¹, V. Baty¹, S. Ribet¹, K. David¹

¹ SUBATECH, UMR 6457, Institut Mines-Télécom Atlantique, CNRS/IN2P3, Nantes Université, 4, Rue Alfred Kastler, La Chantrerie BP 20722, 44307 Nantes cedex 3, France

* Corresponding author: Catherine.landesman@subatech.in2p3.fr

Abstract

Sorption reduction effects due to the presence of complexing substances may have a strong impact on the migration of radionuclides through materials used in nuclear waste repositories.

Subatech contribution to CORI Task 4 aims at understanding the effect of isosaccharinic acid (ISA) on the mobility of uranium(VI) in a CEM V hardened cement paste (HCP) for State II and III cement degradation states. This paper deals with results obtained from wet chemistry experiments (isotherms and kinetics) performed onto U(VI)/HCP binary and U(VI)/ISA/HCP ternary systems for state II.

For U(VI)/HCP system, results confirm high $R_d(U(VI))$ values ($300-70 \text{ m}^3 \text{ kg}^{-1}$) and the progressive saturation of a sorption site. Moreover, desorption experiments support the existence of a reversible surface sorption process for U(VI) for month-long experiments.

For U(VI)/ISA/HCP system, an impact of ISA concentration on U(VI) uptake is reported for the first time on a CEM V HCP at state II. For ISA above a threshold concentration of $2 \cdot 10^{-4} \text{ mol L}^{-1}$, U(VI) uptake is reduced by a factor of 6 and $R_d(U(VI))$ values as low as $1 \text{ m}^3 \text{ kg}^{-1}$ are obtained. Further investigations need to be carried out for a complete understanding of the sorption reduction process but it seems that Calcium ions have an influence on the extent of the phenomenon.

1 Introduction

Cement-based materials are widely used as waste matrices, backfill materials and structural components in current and planned repositories for low, intermediate and high level radioactive waste. Depending on their origins, waste matrices incorporate diverse types of materials such as organic components (cellulose materials, exchange resins, plastic waste, ...) which may affect radionuclides (RN) behaviour due to their complexing properties. In cementitious environments, the alkali degradation of cellulose produces different by-products as isosaccharinic acid (ISA) which, not only, can sorb directly on cement materials but also exhibits strong complexing properties towards radionuclides.

Although radionuclides sorption on hardened cement paste (HCP) is well described in literature, data on ternary (RN-Organic-Cement) systems are very scarce. As an example, the literature dealing with uranium(VI) sorption on HCP and C-S-H phases is extensive and the interactions of RN/materials are very well described [1, 2, 3, 4, 5, 6 for the most recent ones]. But to our knowledge, only one recent review (Ochs *et al* [7]) reports results on the effect of ISA on U(VI) sorption on HCP (from Pointeau *et*

al work, not available in the open literature). This study reports (for a CEM I HCP at state I and III) the existence of a threshold concentration of ISA above which a reduction effect on U(VI) sorption is observed.

In this context, Subatech contribution to CORI Task 4 aims at understanding the effect of isosaccharinic acid on the mobility of uranium(VI) in a CEM V hardened cement paste (HCP) for the two following degradation states (Table 1).

Table 1: Characteristic of the two degradation states used in this study

	Solid	Porewater composition
State II	Presence of Portlandite	No alkaline ions, Ca concentration $\approx 22 \text{ mmol}\cdot\text{L}^{-1}$, pH ≈ 12.5 (saturated lime water = S2 solution)
State III	No Portlandite, Ettingite still present	Corresponding to decalcified C-S-H phases (Ca/Si ≈ 1)

The global experimental methodology is based on transport experiments (diffusion) combined with wet chemistry experiments (batch) either on binary systems such as U(VI)/HCP and ISA/HCP considered as reference systems or on ternary systems U(VI)/ISA/HCP for both degradation states.

This paper reports results on batch experiments for U(VI)/HCP binary system and U(VI)/ISA/HCP ternary system (state II) only.

2 Materials and Methods

Preparation steps, batch experiments and sampling were performed in a glove box (under Argon) in order to prevent any atmospheric carbonation contaminations.

2.1 CEM V Hardened Cement Paste

HCP was provided by CEA/L3MR in December 2014. It was prepared from a CEM V/A (Rombas, Calcia, France), with a water-to-cement ratio (w/c) of 0.4, casted as cylinders (50 mm in height; 50 mm in diameter), cured in a wet chamber (RH > 98%, T= 22°C during 200 days) and finally stored in containers covered with an artificial cement pore water solution ([K] = 291 mmol L⁻¹, [Na] = 79 mmol·L⁻¹, [Ca] = 2.1 mmol·L⁻¹, [SO₄²⁻] = 0.96 mmol·L⁻¹, [Cl] = 0.57 mmol·L⁻¹, pH = 13.5) up to their use (March 2021). For the experiment reported here, one HCP cylinder was grinded (ball grinder) and entirely sieved (< 200 μm).

2.2 Ca(ISA)₂ salt synthesis

Ca(ISA)₂ synthesis has been performed following the CEA (L3MR, Dr R.Dagnélie/Dr N. Macé, personal communication) protocol modified from Whistler and BeMiller [8].

D-Lactose was used as a precursor. The CaO/D-lactose-water mixture, ratio 2:1, was refluxed for 48 hours, then hot-filtered through a Nylon[®] membrane filter (0.8 μm). The filtrate was recovered and reduced, by heating, between 1/10th and 1/20th of the volume, then put in the fridge for crystallization

within 48 hours. The solid was then filtered, rinsed, and dried with a minimum of UP water, then with absolute ethanol, and acetone. The whole purification stage was repeated twice in order to obtain the purified final product which was characterised (as dry powder) by X Ray Diffraction using a Siemens D8 diffractometer running with a Cu anticathode ($\lambda = 1.5406 \text{ \AA}$).

XRD pattern of the synthesized product is presented in Figure 1. $\text{Ca}(\text{ISA})_2$ peak positions have been compared to Poiteau *et al* for identification [9]. This product appears to be pure with just a small amount of unreacted Portlandite which is not an issue for State II experiments.

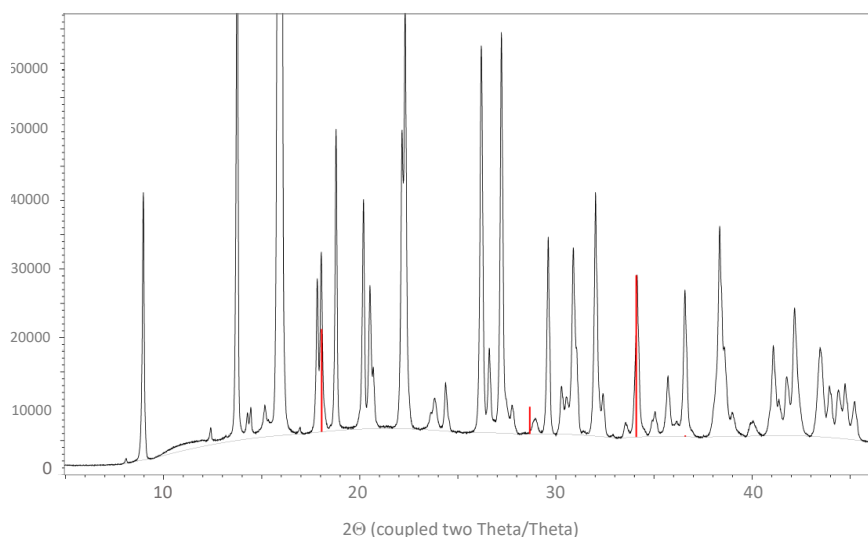


Figure 1: Diffractogram of the synthesized $\text{Ca}(\text{ISA})_2$ salt. (red lines correspond to Portlandite pattern from Crystallography Open Database #1008781)

As a complement, elemental analysis (C, H contents) will be performed in the near future for completing the characterisation of the product.

2.3 Wet chemistry experiments

Sorption/desorption isotherms and time-series (kinetics) have been acquired for U(VI)/HCP binary system and U(VI)/ISA/HCP ternary system (for this report, isotherm only).

Prior to any wet chemistry experiments, an equilibration stage was performed. Appropriate amounts of HCP powder were mixed in 35 mL PPCO Nalgene[®] tubes with 20 mL of S2 solution and agitated during a week. These suspensions were centrifuged (2650g, 15 min) and supernatants were discarded. This stage was repeated twice. Appropriate amounts of U(VI) (binary) system or U(VI) and ISA (ternary system) were then added to S2 solution (total volume 20 mL) in order to obtain the following experimental conditions.

U(VI)/HCP system

Sorption isotherm: $[\text{U}]_0$ from 10^{-8} to $10^{-4} \text{ mol L}^{-1}$, Solid/Liquid ratio = 1 g L^{-1} , duration = 28 days.

Kinetics experiments: sampling time = 3, 7, 14 and 28 days, $[\text{U}]_0 = 3 \cdot 10^{-7}, 3 \cdot 10^{-6}, 1 \cdot 10^{-4} \text{ mol L}^{-1}$, Solid/Liquid ratio = 1 g L^{-1} .

U(VI)/ISA/HCP system

Sorption isotherm: [ISA]₀ from 10⁻⁴ to 2.10⁻² mol L⁻¹, [U]₀ = 1.10⁻⁷ and 1.10⁻⁴ mol L⁻¹, Solid/Liquid ratio = 1 g L⁻¹, duration = 33 days.

Sampling of solutions were performed by weighting. At the end of experiments, suspensions were centrifugated (2650g, 15 min), then supernatants were filtered (Millipore® SFCA, 0.22µm) and sampled for analysis. After removing supernatants, 20 mL of fresh S2 solution (without U(VI) were added to each tube (desorption stage), agitated during 28 days and, at the end, sampled as previously described.

Different analytical techniques have been used: Quadrupolar ICP-MS (ThermoElectron X serie 2) for Uranium (Limit of Quantification (LQ) = 10 ng L⁻¹, Bi as internal standard), TOC meter (Analytik Jena NC2100S) for ISA (Non Purgeable Organic Carbon method, LQ = 1 mgC L⁻¹), Ion Chromatography (Metrohm 850 Professional IC) for Ca (eluant mixture of PDCA 1.3 mM/HNO₃ 8 mM ; LQ = 0.25 mg L⁻¹) and pH values were measured with a microelectrode calibrated at pH 7.00 and 12.45 (IUPAC Standard, Hach).

3 Results/Discussion

At this point of progress in the study, uptake results are expressed and quantified by a solid-liquid distribution ratio (R_d in m³.kg⁻¹), defined by:

$$R_d = \frac{[X]_{solid}}{[X]_{solution}} = \left(\frac{[X]_0}{[X]_{solution}} - 1 \right) \frac{V}{m}$$

where $[X]_{solid}$ [mol kg⁻¹] is the concentration of the sorbed species per mass of HCP, $[X]_{solution}$ [mol L⁻¹] is the concentration of the species X in solution at equilibrium, $[X]_0$ [mol L⁻¹] is the initial concentration of the species X introduced in the suspension, V [L] is the volume of solution and m [kg] is the dry mass of HCP.

If the sorption process is found to be reversible, R_d becomes K_d (solid-liquid distribution coefficient). The higher the R_d (K_d) value, the higher the uptake.

U(VI)/HCP system

Uptake results are presented in Figure 2. R_d (U(VI)) values range from 300 to 70 m³ kg⁻¹ for U(VI) concentrations in solution (at equilibrium) from 4.10⁻¹¹ to 2.10⁻⁶ mol L⁻¹. These high R_d values are consistent (even if higher) with what is known about U(VI) uptake on HCP in literature data [1, 4 and references therein]. R_d values are constant up to $[U]_{eq} = 4.10^{-9}$ mol L⁻¹ ($[U]_{init} = 3.10^{-6}$ mol L⁻¹) which corresponds to the linear part of the isotherm ($[U(VI)]_{solid} = f([U(VI)]_{solution})$). Beyond this point, R_d values decrease indicating the progressive saturation of a sorption site.

Moreover, desorption experiment shows that sorption and desorption isotherms exhibit similar R_d values which indicates that U(VI) uptake seems to be reversible. This is confirmed by kinetics experiments dealing with the evolution of R_d (U(VI)) vs time (Figure 3). Taking into account uncertainties, U(VI) uptake shows a reversible behaviour up to, at least 28 days of sorption. This suggests that, for these (rather) short-term experiments, U(VI) uptake is dominated by a surface sorption process.

U(VI) uptake by cementitious materials has been already explained in terms of inner-sphere complexation on the surfaces of the cement particles [1, 10]. In addition, C-S-H phases are described as the uptake-controlling phases for U(VI) immobilization.

In particular, Tits *et al* have demonstrated from TRLFS studies that U(VI) complexes can be either sorbed as inner-sphere complexes on C-S-H surface silanol sites or incorporated into C-S-H interlayers [3]. Moreover, Macé *et al* have shown from EXAFS data that U(VI) is taken up as $\text{UO}_2(\text{OH})_4^{2-}$ type species by C-S-H surface [2]. Androniuk *et al* have also shown, by performing Molecular dynamics (MD) simulations, that U(VI) can sorb on several sites onto C-S-H surface (as mono- or bidentate species) and that a competition with calcium for these sorption sites should be expected [11].

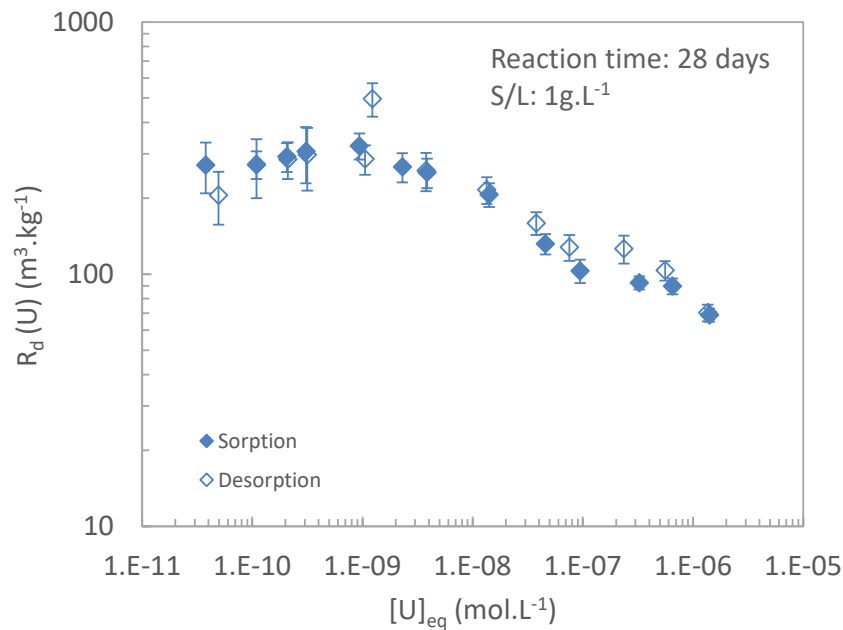


Figure 2: U(VI) sorption and desorption isotherms on HCP State II (Uranium initial concentration ranging from 10^{-8} to 10^{-4} mol L $^{-1}$)

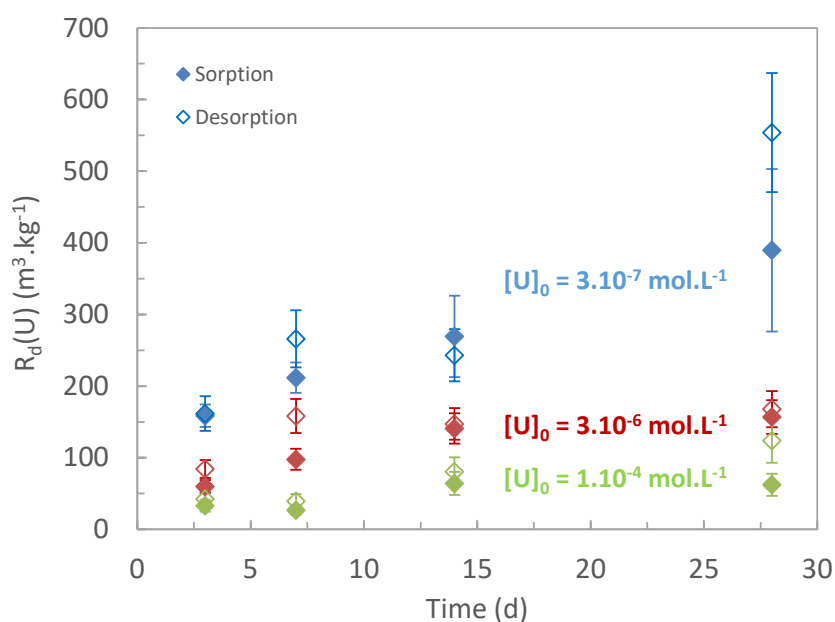


Figure 3: Evolution of the R_d values as a function of time and U(VI) initial concentration

More recent MD simulations have shown that, in presence of calcium (in alkaline solutions), a strong interaction between U(VI) hydroxyl species and Ca^{2+} exists suggesting the formation of a stable Ca-uranyl complex at aqueous C-S-H interfaces [12]. The stabilisation by Ca^{2+} ions, in alkaline solutions, have been observed for other actinides and is thus expected for U(VI) complexes. Nevertheless, this has not been identified yet [13, 14].

Finally, a surface sorption mechanism, based on U(VI) complexes sorption on C-S-H surface, is supported by the results from reversibility experiments (desorption isotherm and kinetics). This process seems to be the dominant uptake process during the first weeks of sorption (up to, at least, 1 month). Nevertheless, these results stay still consistent with the existence of an incorporation process of U(VI) species that may develop over the long term.

U(VI)/ISA/HCP system

Uptake isotherms of uranium in presence of ISA are reported Figure 4.

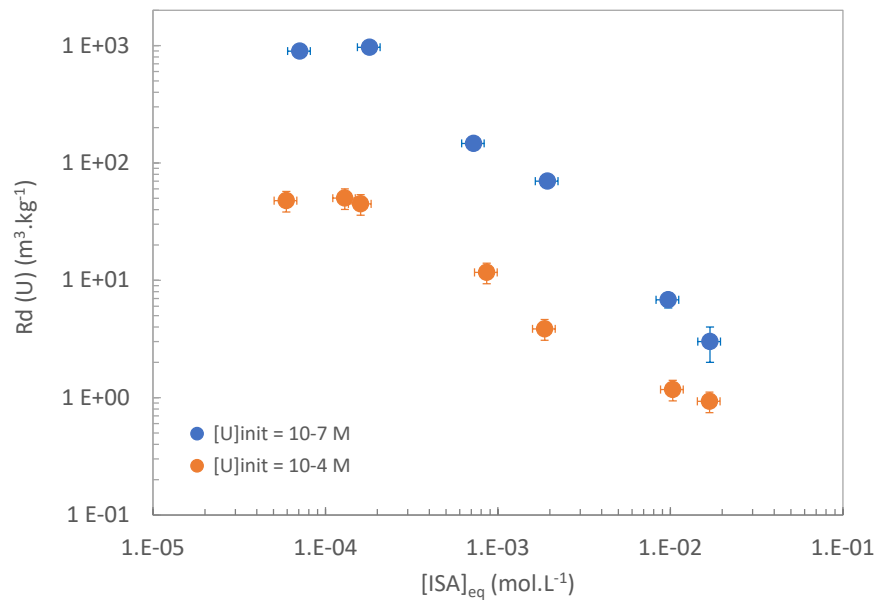


Figure 4: U(VI) sorption isotherms in presence of ISA ($[U(VI)]_0 = 10^{-7}$ and 10^{-4} mol.L⁻¹ ; sorption time: 33 days)

$R_d(U(VI))$ values range are from 1000 to 3 m³ kg⁻¹ and from 50 to 0.9 m³ kg⁻¹ for initial U(VI) concentrations of 10^{-7} and 10^{-4} mol L⁻¹ respectively. ISA concentrations at equilibrium in solution range from 6.10^{-5} to 2.10^{-2} mol L⁻¹. It is then noticeable that $R_d(U(VI))$ values are globally lower than in an ISA-free system.

For both U(VI) initial concentrations, the presence of ISA has a strong impact on uranium behaviour. In fact, for ISA concentrations above $2 \cdot 10^{-4}$ mol.L⁻¹, $R_d(VI)$ values decrease almost linearly by a factor of 333 or 55 depending on initial U(VI) concentrations (10^{-7} and 10^{-4} mol L⁻¹ respectively).

This behaviour is similar to what has been observed by Pointeau *et al* (reported in [7]) for a CEM I HCP (State I and III). The threshold concentration of ISA reported in our study is lower than the value reported by Ochs *et al* for state I ($\approx 10^{-3}$ mol L⁻¹) but in the same order of magnitude.

In the presence of ISA, PhreeqC calculations indicate that uranium speciation would be dominated (> 97%) by uranium-ISA complex $\text{UO}_2(\text{OH})_4(\text{HISA})^{3-}$. Thus, Ochs *et al* interpret the sorption reduction (at state I) by the predominance of this complex which may exhibit a lower affinity than U(VI) hydroxyl complexes, for cement particles surface due to its higher negative charge [7].

Moreover, using the same CEM V HCP as in the present study, Garcia *et al* report that ISA uptake is higher at State II compared to State I [15]. Similar trends have been reported for the uptake of gluconate complexes on C-S-H phases [16, 11] and have been explained by the formation of calcium bridging surface complexes [12]. The presence of these complexes, by weakening Ca binding to the surface, could ease the Ca^{2+} substitution by Ca-uranyl complexes.

Assuming that ISA and gluconate behaviours are close, the stabilisation of Ca-uranyl complexes on cement surface could explain why the sorption reduction in presence of ISA appears to be lower for state II than for state I.

4 Conclusion/Future work

Subatech contribution deals with the effect of ISA on U(VI) uptake on a CEM V HCP for State II and III conditions. This study relates progress obtained for State II only.

For U(VI)/HCP binary system, desorption experiments strongly support a sorption surface mechanism as the dominant uptake process at least for the first week of the solid-liquid interaction.

For U(VI)/ISA/HCP ternary system, experiments show the existence of a threshold concentration of ISA at 2.10^{-4} mol L⁻¹ above which U(VI) uptake strongly decreases. This gives R_d values as low as 0.9 m³ kg⁻¹ which are low values for actinide elements. Nevertheless, it seems that the sorption reduction is limited by the presence of Ca^{2+} ions which play a major role in uptake mechanisms.

Desorption experiments on U(VI)/ISA/HCP ternary system and sorption/desorption experiments on ISA/HCP binary system are in progress in order to complete the set of data for State II conditions.

Future works will be focused on State III conditions, taking into account the decalcification of C-S-H phases and its impact on either U(VI) and ISA uptakes.

In parallel, diffusion experiments on binary and ternary systems have been launched (both states) in order to acquire data on the limiting process of U(VI) transport (uptake or diffusion) in presence of ISA.

Acknowledgement

The EURAD-CORI project leading to this application has received funding from the European Union's Horizon 2020 research and innovation programme under grant agreement No 847593.

References

- [1] Pointeau I., Landesman C., Giffaut E., Reiller P. (2004) Reproducibility of the uptake of U(VI) onto degraded cement pastes and calcium silicate hydrate phases. *Radiochimica Acta*, 92, 645-650
- [2] Macé, N., Wieland, E., Dähn, R., Tits, J., Scheinost, A. C. (2013) EXAFS investigation on U(VI) immobilization in hardened cement paste : influence of experimental conditions on speciation. *Radiochimica Acta* 101, 379–389.
- [3] Tits, J., Walther, C., Stumpf, T., Macé, N., Wieland, E. (2015) A luminescence line-narrowing spectroscopic study of the U(VI) interaction with cementitious materials and titanium dioxide. *Dalton Transactions* 44, 966–976.

- [4] Wieland E., Macé N., Dähn R., Kunz D., Tits J. (2010) Macro- and micro-scale studies on U(VI) immobilization in hardened cement paste. *Journal of Radioanalytical and Nuclear Chemistry*, 286(3), 793-800
- [5] Gaona, X., Kulik, D.A., Macé, N., Wieland, E. (2012) Aqueous-solid solution thermodynamic model of U(VI) uptake in C-S-H phases. *Applied Geochemistry* 27, 81–95.
- [6] Tits J., Geipel G., Macé N., Eilzer M., Wieland E (2011) Determination of Uranium(VI) sorbed species in calcium silicate hydrate phases: A laser-induced luminescence spectroscopy and batch sorption study. *Journal of Colloid and Interface Science*, 359, 248-256
- [7] Ochs M., Vriens B., Tachi Y. (2018) Retention of Uranium in cement systems: effect of cement degradation and complexing ligands. *Progress in Nuclear Science and Technology*, 5, 208-212
- [8] Whisler R. L. and BeMiller J.N. (1963) in Wolfrom M.L. and BeMiller J.N. Eds, *Methods in Carbohydrate Chemistry*, Academic Press New York, vol 2: Reactions of Carbohydrates, 447-479
- [9] Pointeau I., Hainos D., Coreau N., Reiller P. (2006) Effect of organics on selenite uptake by cementitious materials. *Waste Management*, 26, 733-740
- [10] Sutton M., Warwick P., Hall A. (2003) Uranium(VI) interactions with OPC/PFA grout. *Journal of Environmental Monitoring*, 5, 922.
- [11] Androniuk I., Landesman C., Henocq P., Kalinichev A.G. (2017) Adsorption of gluconate and uranyl on C-S-H phases: Combination of wet chemistry experiments and molecular dynamics simulations for the binary systems. *Physics and Chemistry of the Earth*, 99, 194-203
- [12] Androniuk I., Kalinichev A.G. (2020) Molecular dynamics simulation of the interaction of Uranium(VI) with the C-S-H phase of cement in the presence of gluconate. *Applied Geochemistry*, 113, 104496
- [13] Altmaier, M., Neck, V., Fanghänel, T. (2008) Solubility of Zr(IV), Th(IV) and Pu(IV) hydrous oxides in CaCl₂ solutions and the formation of ternary Ca-M(IV)-OH complexes. *Radiochimica Acta*, 96 (9-11), 541-550.
- [14] Fellhauer, D., Altmaier, M., Gaona, X., Lützenkirchen, J., Fanghänel, T. (2016) Np(V) solubility, speciation and solid phase formation in alkaline CaCl₂ solutions. Part II: Thermodynamics and implications for source term estimations of nuclear waste disposal. *Radiochimica Acta*, 104 (6), 381-397
- [15] Garcia D., Henocq P., Riba O., Lopez-Garcia M., Madé B., Robinet J-C. (2020) Adsorption behaviour of isosaccharinic acid onto cementitious materials. *Applied Geochemistry*, 118, 104625
- [16] Nalet, C., Nonat, A. (2016) Ionic complexation and adsorption of small organic molecules on calcium silicate hydrate: relation with their retarding effect on the hydration of C3S. *Cement and Concrete Research* 89, 97-108.

Investigations on the Interaction of U(VI) with C-S-H in the Presence of EDTA

E. Maragkou¹, I. Pashalidis^{1*}

¹ Department of Chemistry, University of Cyprus, P.O. Box 20537, Cy-1678 Nicosia, (Cyprus)

* Corresponding author: pspasch@ucy.ac.cy

Abstract

The interaction of EDTA with calcium silicate hydrate (C-S-H) and its impact on the sorption of U(VI) by C-S-H in the presence of varying EDTA concentrations has been investigated under ambient conditions and N₂ atmosphere. The characterization of the solid phase was carried out by FTIR, XRD and TGA measurements and the uranium concentration in solution was analyzed by alpha-spectroscopy. In solutions of increased EDTA concentration ([EDTA] > 0.1 M) calcium is complexed and extensively extracted from C-S-H, which results in the dissolution of the Ca(OH)₂ phase and deterioration of C-S-H. Hence, solutions of lower EDTA concentrations (0.0000 < [EDTA] ≤ 0.0100 M) and U(VI) have been used to investigate the sorption of U(VI) by C-S-H and the desorption of U(VI) from C-S-H, which was coprecipitated with U(VI) (C-S-H/U). Under N₂ atmosphere, the presence of EDTA in solution results in lower sorption efficiency (e.g. lower K_d values) due to stabilization of U(VI) in solution in the form of EDTA complexes. However, lower desorption efficiency (e.g. higher K_d values) are observed when EDTA solutions are contacted with the C-S-H/U phase, because of the formation of ternary C-S-H/U(VI)/EDTA surfaces complexes, which stabilize U(VI) onto the C-S-H phase. On the other hand, under ambient atmosphere the U(VI) carbonate complexes govern the U(VI) chemistry in solution, resulting generally in lower K_d values.

1. Introduction

Generally, low- and intermediate-level radioactive waste is solidified in cementitious matrices prior underground geological disposal [Grambow, 2016]. Calcium silicate hydrate (C-S-H) phases are the main component of cementitious matrices and consist of Ca–O sheets linked on each side to silicate chains [Richardson, 2008]. Cementitious matrices immobilize radionuclides through their sorption and incorporation into the C-S-H phases. The effective incorporation of radionuclides (including lanthanides and actinides) is related to high recrystallization rate of C-S-H and occurs by substitution of Ca ions in the interlayers and the Ca–O layer present in the C-S-H phases [Tits, et al., 2015].

Uranium, as a primary nuclear fuel, is an important component of nuclear waste and under highly alkaline conditions, which are characteristic for cementitious matrices is expected to exist predominantly in the hexavalent oxidation state (U(VI)) and in the form of the hydrolyzed uranyl species, UO₂(OH)_n⁽ⁿ⁻²⁾⁻ and [Hongbin and Yuxiang, 2005]. The chemistry of uranium in cementitious environment is of particular interest not only because of the abundant presence of uranium in nuclear

and radioactive wastes, but also because U(VI) could act as an analogue for other hexavalent actinides such as Pu(VI) [Pashalidis et al., 1993]. There are several studies on the U(VI) interaction with C-S-H and include classical sorption experiments and spectroscopic studies to better understand and describe the U(VI)-C-S-H system [Tits et al., 2015; Zhang and Wang, 2017; Atkins and Glasser, 1992; Hongbin and Yuxiang, 2005; Wang et al., 2020; Ochs et al., 2018; Macé et al., 2013; Tits et al., 2011]. There are also investigations on ternary U(VI)-C-S-H organic ligand systems [Androniuk et al., 2017, Pointeau et al., 2008] indicating the significant impact of the organic ligand on the chemical behavior of U(VI) in such systems. However, there is still need for further studies on the effect of EDTA on the sorption of U(VI) on C-S-H.

EDTA (ethylene diamine tetraacetic acid) is a chelating agent that has been widely used as a decontamination agent in nuclear facilities and therefore is found at relatively increased levels in nuclear/radioactive wastes. As a hexadentate ligand, EDTA forms very stable complexes with calcium and polyvalent metal ions (e.g., actinides and lanthanides) and therefore strongly affects their stability in the aqueous phase and their leaching from cementitious and geological matrices. Generally, investigations regarding the U(VI) sorption by cementitious matrices and the impact of organic complexing molecules are fundamental in order to evaluate the long-term performance assessment and assess the safety of nuclear waste disposal facilities. This is because cement is a main part of the engineered barrier, which contains and isolates the radionuclides from the biosphere and organic molecules are abundant in the nuclear waste and in the environment [du Bois de Maquillé, 2013]. This study deals with the impact of EDTA on the interaction of U(VI) with the cementitious matrix and C-S-H was selected as the cementitious phase to study the U(VI) (de)sorption in the presence of EDTA at varying concentrations. The impact of EDTA on the C-S-H stability was investigated by determining the calcium concentration in solution and performing XRD, TGA, and FTIR measurements of the related solid phases. Moreover, sorption and desorption studies were performed in aqueous EDTA solution containing uranium ($[U(VI)] = 5 \times 10^{-5}$ M) in contact with C-S-H and aqueous EDTA solutions in contact with EDTA C-S-H/U(VI), respectively, at various EDTA concentrations (0, 0.0001, 0.001 and 0.01 M). In addition, to study the effect of carbonate, the experiments were performed under N₂- and ambient atmosphere.

2 Materials and Methods

2.1 Materials and Characterization Methods

In all experiments, analytical grade reagents and de-ionized water were used. The ²³²U-tracer solution, which was added for the uranium quantification, was obtained from NPL (National Physical Laboratory, Teddington, UK). EDTA solutions of different concentration (0.0001, 0.001, 0.01 and 0.1 M) have been prepared by dissolution of disodium EDTA dihydrate (C₁₀H₁₄N₂O₈ · 2Na · 2H₂O, Aldrich) in de-ionized water.

Solid calcium-silicate-hydrate (C-S-H) has been synthesized according to Maddalena et al. [Maddalena et al., 2019] at a C:S ratio of 1.27 and the solid product has been characterized by FTIR spectroscopy (FTIR, FTIR-ATP 8900, IR Prestige-2, Shimadzu, Europa GmbH, Duisburg, Germany) and X-Ray diffraction Shimadzu XRD-6000 Series). The preparation of C-S-H was carried out by mixing 12.02 g Ludox (50%, Aldrich) with 8.52 g CaO (Aldrich) in 35 mL de-ionized water under N₂. The product was cast in cubes and left for one month under water-vapour saturated N₂-atmo-sphere. Finally, the C-S-H cubes have kept overnight in dried-aceton to remove excess water and then dried under vacuum at 70 °C for 24 h.

2.2 The Impact of EDTA on the C-S-H stability and EDTA sorption by C-S-H

The effect and sorption of EDTA on the C-S-H solid was investigated by contacting a certain amount of the solid (0.2 g) with 20 mL aqueous solution of EDTA (0, 0.0001, 0.001, 0.01 and 0.1 M). After 30 days contact time, the calcium concentration in solution was determined by flame-photometry and after solid–liquid phase separation the solids have been analyzed by X-ray diffraction, thermogravimetric analysis and FTIR as described elsewhere [Maragkou and Pashalidis, 2021a, Maragkou and Pashalidis, 2021b].

2.3. Sorption and Desorption Experiments

Sorption and desorption experiments were performed in batch-type experiments using 0.2 g C-S-H in 20 mL aqueous solution of EDTA (0, 0.0001, 0.001 and 0.01 M) and pH 11, as described elsewhere [Maragkou and Pashalidis, 2021a, Maragkou and Pashalidis, 2021b]. For the sorption experiments the U(VI) concentration in solution was 5×10^{-5} M and for the desorption experiments the C-S-H used was co-precipitated with uranium at a U(VI)/Ca(II) ratio of 1/10000, using the same amounts of U(VI) and C-S-H solid as in the sorption experiments. The experiments were performed under N₂ atmosphere and ambient conditions to explore the effect of carbonate on the sorption efficiency of U(VI). After 30 days contact time, aliquots of the solution have been obtained, filtrated using membrane filters (pore size: 450 nm) and the uranium concentration in solution was determined by alpha-spectroscopy as described elsewhere [Kiliari and Pashalidis, 2010]. Prior electrodeposition the sample-electrolyte mixture was traced with the U-232 isotope to account for any uranium losses during electrodeposition and alpha-particle counting. It has to be noted that, assuming UO₂(OH)₂ as solubility-limiting solid phase and only hydrolysis reactions one would expect solid phase precipitation particularly under N₂-atmosphere and in the absence of EDTA, because the U(VI) concentration used is about two orders of magnitude higher than the calculated solubility. However, we haven't observed any precipitation also in reference systems (without CSH) and this is most probably attributed to the higher solubility of freshly precipitated UO₂(OH)₂ and partial contamination of the solutions with atmospheric CO₂ during sample preparation.

The (de)sorption efficiency was quantified in terms of the partition coefficient, K_d . The partition coefficient, K_d (L/kg), is here defined as the ratio of the quantity of the radionuclide adsorbed per mass of dry C-S-H (C_{ads}) to the amount of the radionuclide remaining in solution (C_{aq}).

$$K_d = C_{ads} / C_{aq} \text{ (L/kg)} \quad (1)$$

3 Results and Discussion

3.1 The Impact of EDTA on the C-S-H stability and EDTA sorption by C-S-H

Figure 1 presents the powder X-ray diffractograms of C-S-H in contact with aqueous solutions of varying EDTA concentration. The diffractogram corresponding to the C-S-H sample in contact with de-ionized water (0.00 M EDTA) is a characteristic for C-S-H and has a disordered layered structure similar to tobermorite [Grangeon et al., 2013]. The diffractograms of C-S-H in contact with EDTA solutions up to 0.01 M do not change significantly indicating that the C-S-H phase remains to a large extent stable in the respective solutions. However, the diffractogram of the sample in contact with 0.1 M EDTA changes significantly indicating the deterioration of the C-S-H phase. This is attributed to the calcium ion complexation by EDTA [Crea et al., 2003] and following dissolution of the Ca(OH)₂ phase. The dissolution of the Ca(OH)₂ phase is extensive, and the remaining solid phase consists mainly of amorphous silica as indicated by the dominating broad peak at $2\theta = 30^\circ$ in the diffractogram

corresponding to 0.1 M EDTA. Hence, (de)sorption experiments have been performed with EDTA solutions with concentrations ≤ 0.01 M [Maragkou and Pashalidis, 2021a].

Figure 2 shows the IR spectrum of C-S-H solids in contact with aqueous solutions of varying EDTA concentration. The broad peak at 3450 cm^{-1} is associated with the O–H stretching vibration, the band at 1636 cm^{-1} in the spectra of both samples corresponds to the bending vibration of the coordinated water, the strong peak at 1430 cm^{-1} is associated with the bending mode of the Ca-OH vibration and the peak at 964 cm^{-1} could be attributed to the antisymmetric stretching vibration of Si–O–Si and the stretching vibration of O–Si–O [Guan et al., 2013].

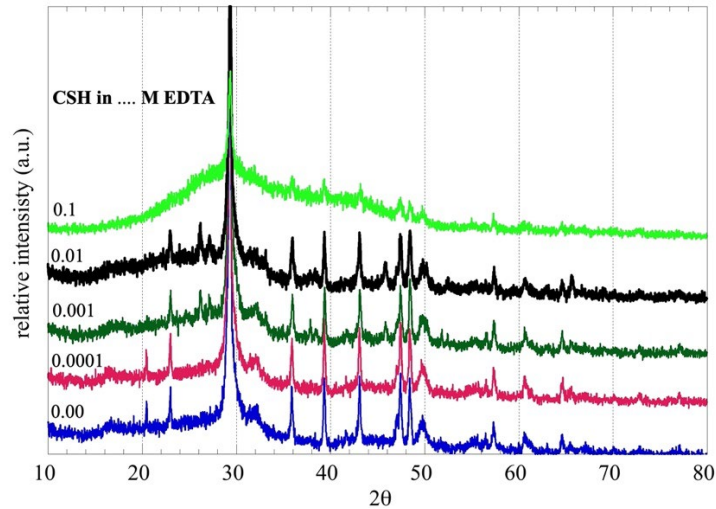


Figure 1: *p*-X-ray diffractograms of C-S-H in contact with aqueous solutions of varying EDTA concentration.

The FTIR spectra in Figure 2 indicate that the strong peak at 1430 cm^{-1} associated with bending mode of the Ca-OH vibration [Guan et al., 2013] almost disappears in the spectra of C-S-H in contact with 0.1 M EDTA because of the extensive dissolution of the $\text{Ca}(\text{OH})_2$ phase. Moreover, the intensity of the band at 1636 cm^{-1} associated with bending mode of water molecules declines with increasing EDTA concentration indicating lower water content of C-S-H in contact with EDTA solutions. This can be attributed that the sorption/incorporation of EDTA molecules into the C-S-H phase, which retards the effectiveness of the C-S-H hydration [Nalet and Nonat, 2016].

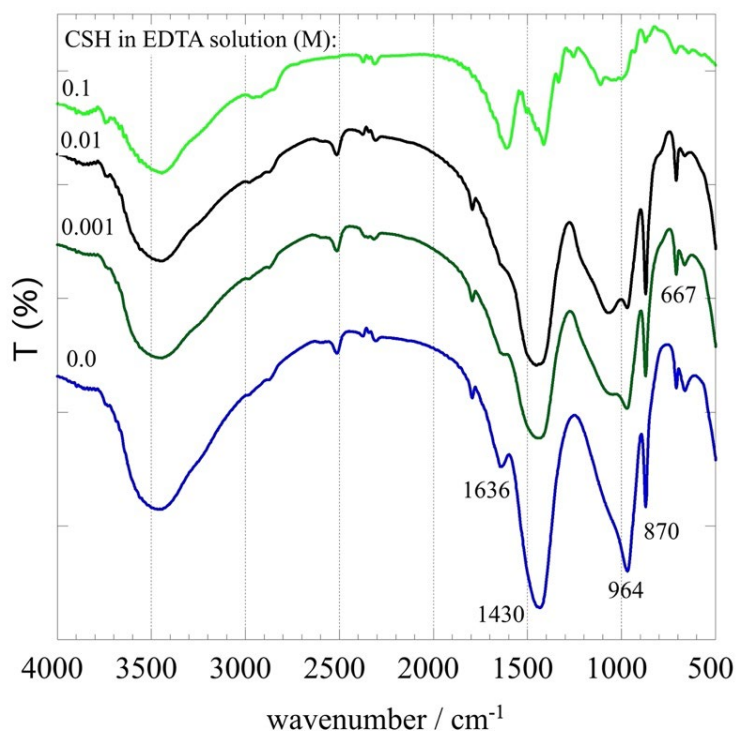


Figure 2: FTIR(KBr) spectra of C-S-H solids in contact with aqueous solutions of varying EDTA concentration.

Thermogravimetric investigations have shown that the C-S-H in contact with 0.001 M EDTA solutions presents the lowest water content followed by C-S-H in contact with 0.01 M EDTA solution. On the other hand, C-S-H samples in contact with 0.0001 M EDTA and aqueous solution don't differ significantly with one another [Maragkou and Pashalidis, 2021a]. Furthermore, calcium concentration measurements in solution have shown that the lowest calcium ion concentration is observed in 0.001 M EDTA solutions [Maragkou and Pashalidis, 2021a] indicating that EDTA forms surface complexes with the adsorbed counter calcium ions, which compensate the negative surface charge of the C-S-H surface [Nalet and Nonat, 2016; Song et al., 2020].

3.2. Sorption and Desorption Experiments

Figure 3 shows the K_d values determined after contacting for 30 days under N_2 atmosphere at pH 11 C-S-H with aqueous solutions of varying EDTA concentration and constant uranium concentration ($[U(VI)] = 5 \times 10^{-5}$ M), which are denoted as sorption, and C-S-H/U(VI) at a U(VI)/Ca(II) ratio of 1/10000 with aqueous solutions of varying EDTA concentration, which are denoted as desorption. From the data shown in Figure 3 it is obvious that the K_d values obtained from the sorption experiment are generally lower than the corresponding K_d values associated with desorption experiments. It is also evident the highest difference is observed for the 0.001 EDTA system. The lower K_d values for the sorption system are ascribed to the stabilization of U(VI) in solution due to the formation of U(VI)-EDTA complexes [Bhat and Krishnamurthy, 1964], whereas the higher K_d values for the desorption system are attributed to the formation of ternary C-S-H/U(VI)/EDTA complexes [Maragkou and Pashalidis, 2021a, Maragkou and Pashalidis, 2021b]. This behavior seems to be similar for both metal ions (e.g. Ca^{2+} and UO_2^{2+}) and is pronounced in the 0.001 M EDTA system.

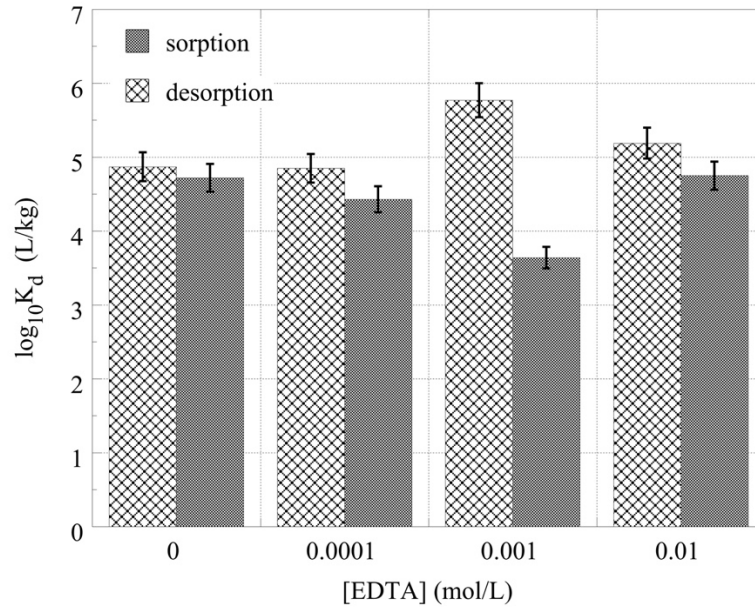


Figure 3: K_d values determined for the U(VI) sorption by C-S-H and desorption by C-S-H/U(VI) after contacting the solid phase with aqueous solutions of varying EDTA concentration and constant uranium concentration ($[U(VI)]_0 = 5 \times 10^{-5} M$) for 30 days under N_2 atmosphere and pH 11.

Figure 4 shows the K_d values determined after contacting for 30 days under ambient atmosphere at pH 11 C-S-H with aqueous solutions of varying EDTA concentration and constant uranium concentration ($[U(VI)] = 5 \times 10^{-5} M$), which are denoted as sorption, and C-S-H/U(VI) at a U(VI)/Ca(II) ratio of 1/10000 with aqueous solutions of varying EDTA concentration, which are denoted as desorption. From the data shown in Figure 4 it is obvious that the K_d values obtained from the sorption and desorption experiment are generally lower than the corresponding K_d values associated with the experiments under N_2 atmosphere. It also evident there is no general trend related to the EDTA concentration [Maragkou and Pashalidis, 2021a, Maragkou and Pashalidis, 2021b]. This behavior has been attributed to the formation of very stable carbonate complexes of U(VI) [Pashalidis et al., 1997; Pashalidis et al., 1993], which in the presence of calcium ions results in the formation of ternary Ca(II)/U(VI)-carbonato complexes ($Ca_n UO_2(CO_3)_3^{(4-2n)-}$) [Shang and Reiller, 2020; Shang et al., 2020].

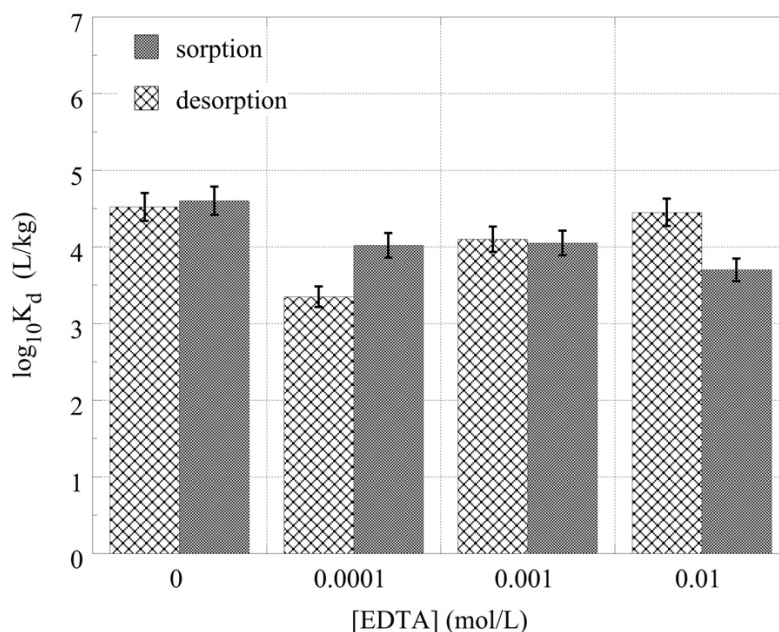


Figure 4: K_d values determined for the U(VI) sorption by C-S-H and desorption by C-S-H/U(VI) after contacting the solid phase with aqueous solutions of varying EDTA concentration and constant uranium concentration ($[U(VI)]_o = 5 \times 10^{-5} M$) for 30 days under ambient atmosphere and pH 11.

4 Conclusions and Future Work

The interaction of EDTA with C-S-H at increased concentrations ($[EDTA] > 0.01 M$) results in degradation of the solid phase, because of the extensive dissolution of $Ca(OH)_2$. On the other hand, at lower EDTA concentrations ($[EDTA] \leq 0.01 M$), the organic ligand is sorbed by the solid phase in the form of $Ca(II)$ -EDTA surface complexes. The incorporation of EDTA in the C-S-H matrix is corroborated by FTIR spectroscopic and XRD measurements.

Under N_2 atmosphere, the presence of EDTA in solution results in lower sorption efficiency (e.g. lower K_d values) due to stabilization of U(VI) in solution in the form of EDTA complexes and in lower desorption efficiency (e.g. higher K_d values) when EDTA solutions are contacted with the C-S-H/U phase, because of ternary C-S-H/U(VI)/EDTA surfaces complexes, which stabilize U(VI) onto the C-S-H phase. Under ambient atmosphere the U(VI) carbonate complexes govern the U(VI) chemistry in solution, resulting generally in lower K_d values.

Further studies involving solid NMR and sophisticated spectroscopic methods (e.g., Raman, XPS, EXAFS), as well as thermodynamic calculations could give detailed information on the sorption process at the molecular level and improve our knowledge regarding the effect of EDTA on the U(VI) interaction with C-S-H.

Acknowledgement

The EURAD-CORI project leading to this application has received funding from the European Union's Horizon 2020 research and innovation programme under grant agreement No 847593.

References

- Androniuk, I.; Landesman, C.; Henocq, P.; Kalinichev, G.A. Adsorption of gluconate and uranyl on C-S-H phases: Combination of wet chemistry experiments and molecular dynamics simulations for the binary systems. *Phys. Chem. Earth*. 2017, 99, 194–203.
- Atkins, M.; Glasser, F.P. Application of portland cement-based materials to radioactive waste immobilization. *Waste Manage.* 1992, 12, 105–131.
- Bhat, T.R.; Krishnamurthy, M. Studies on EDTA complexes—II uranyl-EDTA system. *J. Inorg. Nucl. Chem.* 1964, 26, 587–594.
- Crea, F.; De Stefano, C.; Gianguzza, A.; Piazzese, D.; Sammartano, S. Speciation of poly-amino carboxylic compounds in seawater. *Chem. Speciat. Bioavailab.* 2003, 15, 75–86.
- Du Bois de Maquillé, L.; Renaudin, L.; Goutelard, F.; Jardy, A.; Vial, J.; Thiébaud, D. Determination of ethylenediaminetetraacetic acid in nuclear waste by high-performance liquid chromatography coupled with electrospray mass spectrometry. *J. Chromatogr. A*. 2013, 1276, 20–25.
- Grambow, B. Geological disposal of radioactive waste in clay. *Elements*, 2016, 12, 239–245.
- Grangeon, S.; Claret, F.; Linard, Y.; Chiaberge, C. X-ray diffraction: a powerful tool to probe and understand the structure of nanocrystalline calcium silicate hydrates. *Acta Crystallographica*, 2013, B69, 465–473.
- Guan, W.; Ji, F.; Chen, Q.; Peng, Y.; Ling, P. Synthesis and Enhanced Phosphate Recovery Property of Porous Calcium Silicate Hydrate Using Polyethyleneglycol as Pore-Generation Agent. *Materials*. 2013, 6, 2846–2861.
- Hongbin, T.; Yuxiang, L. The existence state of uranium(VI) in portland cement matrix material immobilization body. *Uranium Min. Metall.* 2005, 38, 86–90.
- Kiliari, T.; Pashalidis, I. Simplified alpha-spectroscopic analysis of uranium in natural waters after its separation by cation-exchange. *Radiat. Meas.* 2010, 45, 966–968.
- Macé, N.; Wieland, E.; Dähn, R.; Tits, J.; Scheinost, A.C. EXAFS investigation on U(VI) immobilization in hardened cement paste: influence of experimental conditions on speciation. *Radiochim. Acta*. 2013, 101, 379–389.
- Maddalena, R.; Li K.; Chater, A.P.; Michalik, S.; Hamilton A. Direct synthesis of a solid calcium-silicate-hydrate (C-S-H). *Constr. Build. Mater.* 2019, 223, 554–565.
- Marangou, E.; Pashalidis, I. Investigations on the Interaction of EDTA with Calcium Silicate Hydrate and Its Impact on the U(VI) Sorption. *Coatings* 2021a, 11, 1037.
- Marangou, E.; Pashalidis, I. The effect of EDTA on the desorption of uranium from calcium silicate hydrate matrices. *J. Radioanal Nucl Chem.* 2021b, <https://doi.org/10.1007/s10967-021-08089-w>.
- Nalet, C.; Nonat, A. Ionic complexation and adsorption of small organic molecules on calcium silicate hydrate: Relation with their retarding effect on the hydration. *Cem. Concr. Res.* 2016, 89, 97–108.
- Ochs, M.; Vriens, B.; Tachi, Y. Retention of uranium in cement systems: effects of cement degradation and complexing ligands. *Prog. Nucl. Sci. Technol.* 2018, 5, 208–212.
- Pashalidis, I.; Czerwinski, K.R.; Fanghaenel T.; Kim, I.J. Solid-Liquid Phase Equilibria of Pu(VI) and U(VI) in Aqueous Carbonate Systems. Determination of the Carbonate Stability Constants. *Radiochim. Acta* 1997, 76, 55–62.
- Pashalidis, I.; Runde, W.; Kim, I.J. A study of solid-liquid phase equilibria of Pu (VI) and U (VI) in aqueous carbonate systems. *Radiochimica Acta*, 1993, 61, 141–146.
- Pointeau, I.; Coreau, N.; Reiller, P. E. Uptake of anionic radionuclides onto degraded cement pastes and competing effect of organic ligands. *Radiochim. Acta* 2008, 96, 367–374.
- Richardson, I.G. The calcium silicate hydrates. *Cem. Concr. Res.* 2008, 38, 137–158.
- Shang, C.; Reiller, P.E. Determination of formation constants and specific ion interaction coefficients for $\text{Ca}_n\text{UO}_2(\text{CO}_3)_3^{(4-2n)-}$ complexes in NaCl solution by time-resolved laser-induced luminescence spectroscopy. *Dalton Trans.*, 2020, 49, 466–481.
- Shang, C.; Reiller, P.E.; Vercouter, T. Spectroluminescence measurements of the stability constants of $\text{Ca}_n\text{UO}_2(\text{CO}_3)_3^{(4-2n)-}$ complexes in NaClO₄ medium and the investigation of interaction effects. *Dalton Trans.*, 2020, 49, 15443–15460.
- Song, Z.; Cai, H.; Liu, Q.; Liu, X.; Pu, Q.; Zang, Y.; Xu, N. Numerical Simulation of Adsorption of Organic Inhibitors on C-S-H Gel. *Crystals*. 2020, 10, 742.

- Tits, J.; Geipel, G.; Macé, N.; Eilzer, M.; Wieland, E. Determination of uranium(VI) sorbed species in calcium silicate hydrate phases: A laser-induced luminescence spectroscopy and batch sorption study. *J. Colloid Interface Sci.* 2011, 359, 248–256.
- Tits, J.; Stumpf, T.; Rabung, T.; Wieland, E.; Fanghänel, T. Uptake of Cm(III) and Eu(III) by calcium silicate hydrates: A solution chemistry and time-resolved laser fluorescence spectroscopy Study. *Environ. Sci. Technol.* 2003, 37, 3568–3573.
- Tits, J.; Walther, C.; Stumpf, T.; Mace, N.; Wieland, E. A luminescence line-narrowing spectroscopic study of the uranium(VI) interaction with cementitious materials and titanium dioxide. *Dalton Trans.* 2015, 44, 966–976.
- Wang, F.; Chen, G.; Ji, L.; Yuan, Z. Preparation and mechanical properties of cemented uranium tailing backfill based on alkali-activated slag. *Adv. Mater. Sci. Eng.* 2020, 2020, 1–7.
- Zhang, W.; Wang, J. Leaching performance of uranium from the cement solidified matrices containing spent radioactive organic solvent. *Ann. Nucl. Energy*, 2017, 101, 31–35, doi:10.1016/j.anucene.2016.09.055.

Analysis of superplasticizers adsorption on cement minerals.

T. Missana*, M. García-Gutiérrez, O. Almendros Ginestá.

CIEMAT – Physical Chemistry of Actinides and Fission Products
Avenida Complutense 40, 28040 MADRID (Spain)

* Corresponding author: tiziana.missana@ciemat.es

Abstract

One of the objectives of CIEMAT in CORI was to analyse the possible roles of superplasticizers on the mobility of different radionuclides (RN) in cement. In this context, it is important to analyse the extent of the adsorption of these organic additives because adsorption: 1) can modify the surface properties of the solids and their overall interactions with RN; 2) can limit the organic concentration in the pore water and the formation of aqueous complexes, which can render RN more mobile.

To carry out this study two different commercial superplasticizers were selected: a melamine based (SIKAMENT™ 200 R, Sika, Spain) and a polycarboxylate ester (PCE, Master Glenium SKY 886, BASF), which were previously characterised. Their adsorption was analysed in different minerals (CSH phases, ettringite, portlandite) and cement (CEM V, fresh and degraded to State II) in their equilibrium waters, using batch sorption experiments and electrophoretic measurements. The concentration of the organic in the aqueous phases was determined measuring the total organic carbon, TOC and/or by UV-Vis spectroscopy.

Introduction

The presence of organics in radioactive waste repositories is of concern as organics may form very stable complexes with radionuclides (RN) in the aqueous phase and limit their retention on the surrounding solids. In low-level waste repositories (as for example the Spanish *El Cabril*), cementitious materials are used for stabilization and containment of the waste. One of the characteristics of these materials is that they generate an hyperalkaline chemical environment which is generally favourable to RN retention. However, large quantities of organic materials are present in these repository (papers, tissues, plastics, rubber, etc.) which can degrade under alkaline hydrolysis and/or radiolysis. The degradation products of these materials may form complexes with RN and affect their transport in the system. Furthermore, different (organic) additives are added to cement, which role on RN migration is not yet fully understood. In particular, the addition of plasticizers/superplasticizers to cement is a quite common procedure, to improve the workability of cement reducing the water/ cement ratio (w/c).

In this work, we analysed the adsorption of two different superplasticizers (SPs), on different cement materials. The study of the interactions of SP with the different cementitious materials provide fundamental information on the possible role on RN migration in the system. Organic adsorption in the solid phases can be in fact very relevant in limiting the organic concentration in solution and/or

modifying the surface properties. Furthermore, very few studies available to assess the potential role of these additives on RN migration (García et al., 2018).

Materials and methods

Superplasticizers

Two different commercial products were used for the experiments: the first one is based on modified melamine (SIKAMENT™ 200 R, Sika, Spain); the second product is the Master Glenium SKY 886 (BASF), Master Glenium SKY (MG) is an innovative superplasticizer based on latest generation of polycarboxylate ether (PCE) polymers. SIKA is a dark brown product, with a density of approximately 1.15 kg·L⁻¹ and a pH of approximately 8. The recommended dose for cement preparation y between 1% and 1.5% in cement weight. MG is a milky product with a pH of 5.6 and a density of 1.02 kg·L⁻¹. This is used as unique additive in a percentage of approximately 0.5 – 2.0 % on cement weight depending on the type of concrete. In the experiments, we tried to maintain the concentration of both superplasticizers in concentrations nearest as possible to the real ones (1-10% of solid weight). The SIKA had a dry residue of 363±6 g·L⁻¹ with a TOC of approximately 153.8 g·L⁻¹ (42 %). TheMG, contained a dry residue of approximately 228±1 g·L⁻¹ and a TOC of 117 g·L⁻¹ (51%).

Solids & contact solutions

The analysed solids were: (1) CSH phases at different Ca/Si ratios, in equilibrium with their synthesis water; (2) Portlandite in 20 mM Ca(OH)₂, pH=12.4; (3) Ettringite in synthetic equilibrium water (pH=10.5) and (4) CEM V (fresh and degraded) in synthetic waters (pH 13.2 and 12.3). All these materials were previously characterised by X-ray diffraction and FT-IR spectroscopy. All the data related to solid and water characterisation are detailed elsewhere (Missana et al., 2022).

ζ-potential measurements

The electrokinetic potential (or ζ-potential) is the value most readily accessible from experiments to determine the sign and magnitude of the surface charge of a solid under different experimental conditions. To evaluate the effects of the presence of the SPs on the surface charge of the solids, their ζ-potential was measured by laser Doppler electrophoresis using a Malvern Zeta-Master equipment with a He-Ne laser (633 nm).

Sorption tests

Sorption tests were carried out using a *batch sorption* method. The superplasticizers were added at the desired concentration in the solid suspended in its equilibrium water at the solid to liquid ratio of 10 g·L⁻¹; the contact time was 7 days. The solid phase was separated from the liquid by centrifuging (9500·g) for 30 min. The concentration of the superplasticizer in the liquid phase was estimated by TOC measurements and/or UV-Vis spectroscopy. The distribution ratios, R_d , were determined by means of the usual formula:

$$R_d = \frac{C_{ini} - C_{fin}}{C_{fin}} \cdot \frac{V}{m},$$

being C_{ini} and C_{fin} the initial and final SPs concentrations and m/V the solid to liquid ratio. Calibration curves were carried out, before the determination of SPs concentration by UV-Vis.

In all the cases, the reference for C_{ini} in each system was taken by diluting the SP in the appropriate equilibrium water.

Results and Discussion

Figure 1 shows the ζ -potential of the solids analysed as a function of the SPs concentration ($\text{g}\cdot\text{L}^{-1}$). Figure 1a and 1b, shows the results obtained on two different CSH (0.8 and 1.4) with MG and SIKA, respectively. As can be seen in the Figure, the initial potential of the two different CSH is negative (-15 mV) in the case of the CSH (0.8) and positive (+8 mV) for CSH (1.4). Independently of the initial charge, the presence of MG brings the potential to slightly negative values (-5 mV to -10 mV), whereas the presence of SIKA to a more negative value (around -25 mV).

A similar behaviour is observed also in the case of portlandite (Figure 1c) and ettringite (Figure 1d) with initial ζ -potentials of (+18 mV) and (-11 mV) respectively, that in the presence of MG and SIKA tends to similar values (-5 mV and -25 mV) to those observed in the case of the CSH gels, even upon the addition of small SP concentrations. The same is observed in the case of the cement (CEM V), which initial charge change from negative to positive, depending on the degradation state (fresh \sim -25 mV and degraded \sim +25 mV). So, the final charge of the system is always dominated by the presence of the SPs.

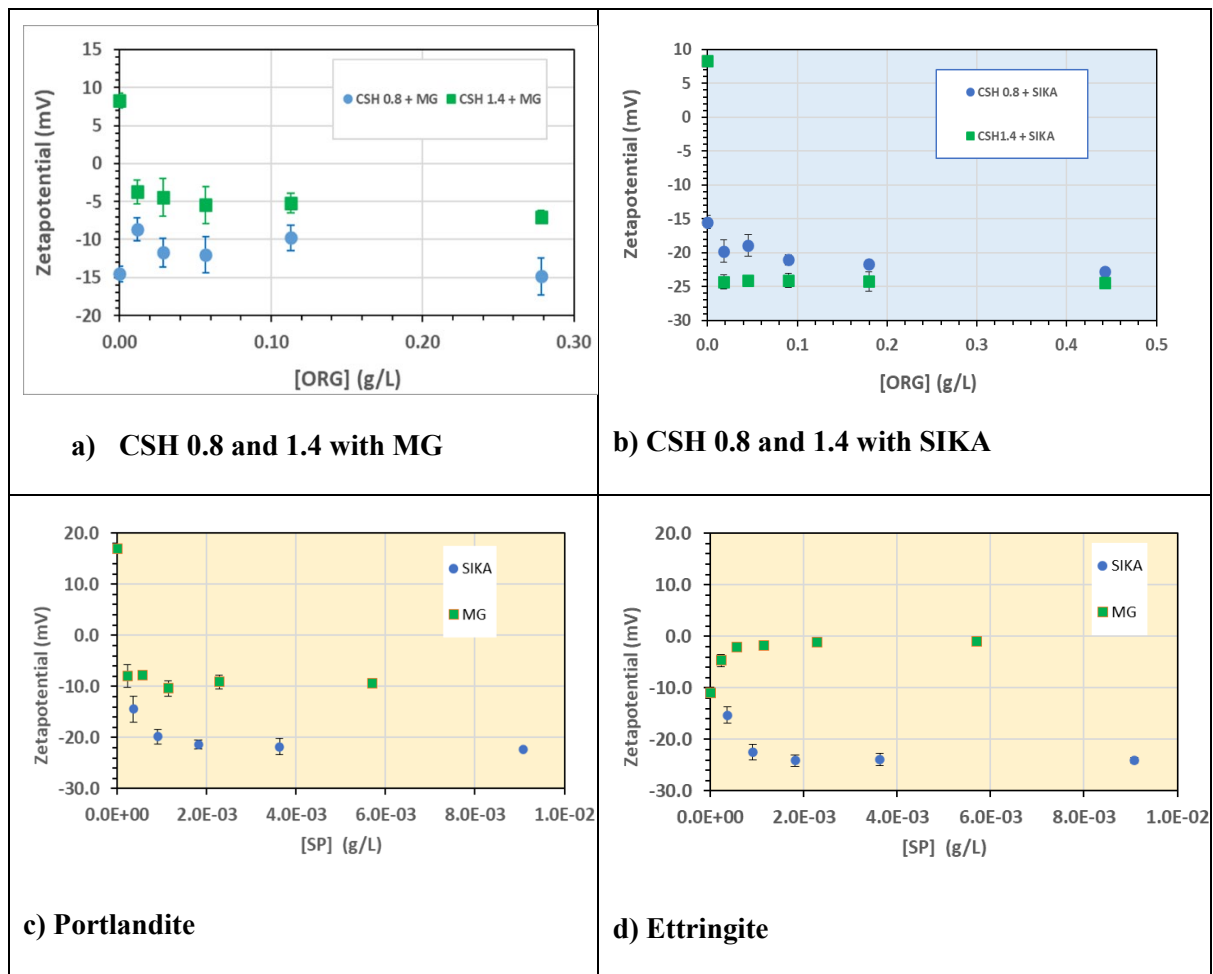


Figure 1: ζ -potential measurements as a function of the SP concentration in different solids.

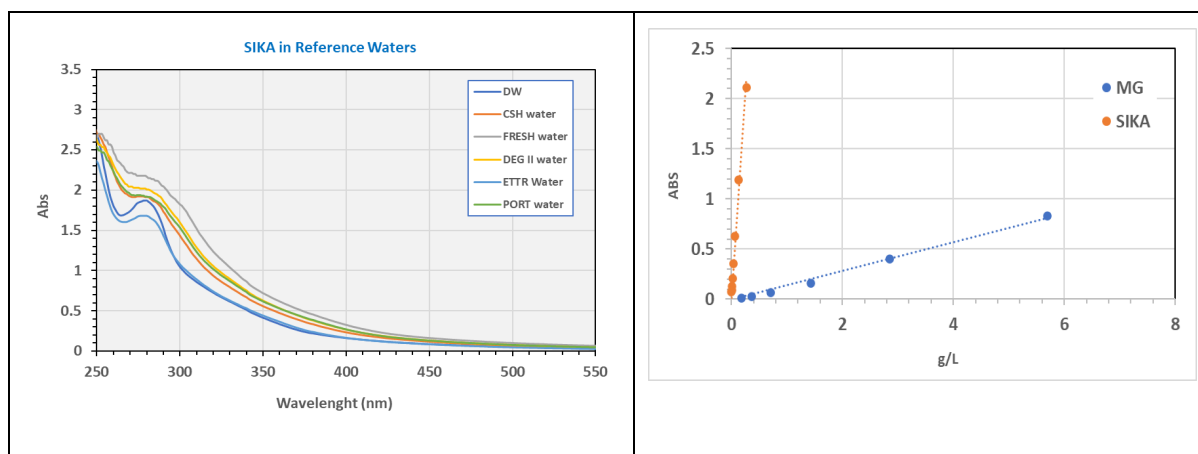


Figure 2: Left: UV-Vis spectra of the SIKA superplasticizer in different waters; Right: Calibration curves for SIKA and MG.

To determine the actual extent of the adsorption of the SPs in the different solids analysed, batch sorption experiments were carried out. In these tests, we preferred the use of techniques that can identify the presence of the organic in a “selective” way. In fact, even if the SPs (and their diluted samples) were perfectly characterised in terms of TOC content, working at low concentrations, sometimes TOC measurements gave uncertain results. We attributed them to possible incidental contamination of unknown organics from (some) plastic vessels, probably due to the high pH of the tests. For this reason, in principle, we relied more on the results obtained by UV-Vis spectroscopy.

The calibration curves used to determine the concentration of the two different SPs by UV-Vis were obtained for each system in its equilibrium water: both SPs present a clear adsorption peak around 278-280 nm. However, as can be seen in Figure 2 (left) in which the spectra of SIKA obtained in different aqueous solutions are shown, some differences were observed depending on the initial water (deionized water, DW, or other equilibrium waters). Minor effects were observed in the case of MG.

An example of the obtained calibration curves is shown in Figure 2 (right), where it can be clearly observed that the effective extinction coefficient (ϵ), related to the slope of the calibration curves, is much higher for SIKA than MG. This characteristic limited the use of UV-Vis to relatively high concentrations of MG but was adequate for the targeted concentration of SIKA.

A summary of the R_d values obtained for MG and SIKA in the different materials, under the specified experimental conditions is given in Table 1. In the CSH phases, both the adsorption of MG and SIKA depends on the Ca/Si ratio. In general, more adsorption is observed for CSH (1.4) than in CSH (0.8) with a factor of 1.7 in the case of MG, and a factor 4.4 in the case of SIKA. This can be related to a lesser interaction of the SPs, which initially possess negative charge, with the negatively charged solids.

The R_d values measured at very high concentrations (10 % of solid weight) for MG are smaller than those measured for the lower SP concentration (1 % of solid weight), possibly indicating that saturation of adsorption sites may occur under these conditions.

Table 1: R_d values determined for MG and SIKA in different solids

MG (1 g·L⁻¹) – 10 % solid weight		
Solid	R_d (mL·g⁻¹)	Technique
CSH (0.8)	48.3±6	UV-Vis
CSH (0.8)	49.6±5	TOC
MG (0.11 g·L⁻¹) – 1 % solid weight		
CSH (0.8)	253±33	TOC
CSH (1.2)	343±38	TOC
CSH (1.4)	429±54	TOC
Portlandite	n.d	TOC
Ettringite	n.d	TOC
CEM V fresh	< 10	TOC
CEM V deg II	< 10	TOC
SIKA (0.3 g·L⁻¹) – 3 % solid weight		
CSH (0.8)	122±10	UV-Vis
CSH (1.2)	285±28	UV-Vis
CSH (1.4)	535±59	UV-Vis
Portlandite	86±9	UV-Vis
Ettringite	66±7	UV-Vis
CEM V (fresh)	30±2	UV-Vis
CEM V (deg II)	51±6	UV-Vis
SIKA (0.18 g·L⁻¹) – 2 % solid weight		
CSH (0.8)	143±19	TOC
CSH (1.2)	237±26	TOC
n.d.=not determined		

Adsorption of the SPs is higher in the CSH gels than in other studied material, in agreement with the higher surface area of the gels in respect to the cement or other cement minerals as portlandite or ettringite. No striking differences are observed between the two SP concerning their adsorption in the different solids with the unique exception of CEM V (both fresh and degraded) where MG adsorption is negligible.

Conclusions

The sorption behaviour of two different SPs on cementitious materials has been investigated. The addition of MG and SIKA to the different solids, independently on their initial surface charge, brings the zetapotential to values near -5 mV and -25 mV, respectively. This may mean that the surface charge

acquired by the solid may be not directly associated to the adsorption of the SP, but to the physical coverage of the surface and the shielding of the original charge.

Nevertheless, batch sorption experiments showed that the SPs can be retained at the surface of the cementitious materials. The highest adsorption is observed for both SPs in the CSH phases, especially in the CSH (1.4), which presented the highest Ca/Si ratio and initial positive surface charge.

Considering the relatively small concentration of the SPs that must be added to the cement, and the non-negligible adsorption of these organics in the main cement mineral phases, a reduced concentration in the porewater can be expected, which would limit the possible aqueous complexation of radionuclides.

Acknowledgement

The EURAD-CORI project leading to this application has received funding from the European Union's Horizon 2020 research and innovation programme under grant agreement No 847593.

References

- García D., Grivé M., Duro L., Brassiness S., de Pablo J. (2018) The potential role of the degradation products of cement superplasticizers on the mobility of radionuclides. *Applied Geochemistry*, <https://doi.org/10.1016/j.apgeochem.2018.09.004>.
- Missana T., García-Gutierrez M., Almedros Ginestá O. Fernandez A.M, Mingarro M., Gil P. (2022). Characterization of the materials used in the CORI project. CIEMAT Technical Interim Report CIEMAT/2G120/2022-1.

Radiolytic and hydrolytic degradation of PolyCarboxylate as superplasticizer

M. Štok^{1*}, T. Gajšt¹, E. Heath¹, D. Heath¹, S. Rupnik¹, V. Radulović¹, E. Žagar², D. Pahovnik²

¹ Jožef Stefan Institute, Jamova cesta 39, 1000 Ljubljana, Slovenia

² National Institute of Chemistry Slovenia, Hajdrihova ulica 19, 1000 Ljubljana, Slovenia

* Corresponding author: marko.strok@ijs.si

Abstract

Radiolytic and hydrolytic degradation of commercial polycarboxylate superplasticizers intended for use as an additive to concrete for radioactive waste disposal purposes were investigated. Samples of as received and lyophilized superplasticizer were subjected to gamma irradiation in a nuclear reactor up to an accumulated dose of 3.2 MGy. In addition, hydrolysis experiments in 0.1 mol L⁻¹ NaOH were performed to investigate the degradation of the superplasticizer under alkaline conditions. Original and degraded samples were then characterized using FTIR, NMR and SEC. Results show that the predominant reaction during radiolytic degradation under experimental conditions is crosslinking of the superplasticizer backbone, which leads to gelation of liquid samples at doses of 0.6 – 0.8 MGy. After prolonged irradiation up to 3.2 MGy, a fraction of the superplasticizer sample reverted to a liquid as polyethylene glycol chains cleave off the polymer backbone. A similar process occurs during 3 days hydrolysis in 0.1 mol L⁻¹ NaOH, where the cleavage of ester bonds was identified from the FTIR spectra. In addition, SEC analysis confirmed the presence of lower molecular weight compounds, again most probably polyethylene glycol cleaved off the backbone of the superplasticizer.

1 Introduction

Polycarboxylate superplasticizers (PCEs) are used as admixtures to concrete to increase concrete fluidity without adding excess water, resulting in increased workability and higher concrete strength and durability. Typical PCEs are comb-shaped polymers with several nonionic pendant chains of polyethylene glycols (PEG) attached to an anionic backbone (Figure 1) (Chen et al., 2018; Ilg and Plank, 2019; Li et al., 2019; Plank et al., 2008; Xiang et al., 2020).

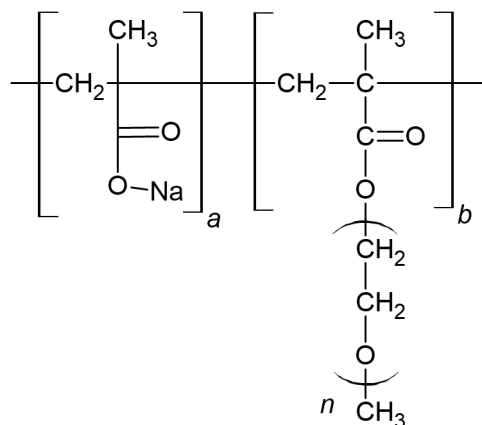


Figure 1: Structure of typical PCEs.

When PCEs are used as admixtures in concrete to stabilize and immobilize radioactive waste, they are subjected to possible radiolytic and hydrolytic degradation. Degradation products, especially low molecular products, can influence the mobility of radionuclides contained in concrete and affect the radionuclide retention performance of the radwaste repository. In addition, the formation of gaseous degradation products can compromise its integrity. This study aims to characterize degradation products of commercial PCEs subjected to gamma irradiation in nuclear reactors and hydrolysis in alkaline conditions to elucidate how this might affect the long-term disposal of radionuclides.

2 Materials and methods

2.1 Studied PCEs

A commercial PCE Cementol Hiperplast 210 (CH210) from TKK company was used for radiolytic and hydrolytic studies. It is intended to be used in the Slovenian radwaste disposal programme. Unfortunately, little information about its actual chemical structure is available, except that it is polycarboxylate-based. CH210 is supplied as brown-yellowish liquid with a density of (1.06 ± 0.02) kg/L and a pH of 5 ± 1 at 20°C.

2.2 Gamma irradiation

Gamma irradiation was conducted in the TRIGA Mark II nuclear reactor when it was not in operation. The source of gamma rays were uranium fuel elements used during reactor operation. Aliquots of CH210 were transferred to 20 mL glass vials capped with a septum under ambient atmosphere and irradiated in a triangular irradiation channel at room temperature. The samples were inserted in the channel 30 min after shutdown, where they remained until the next scheduled operation of the reactor, where they were then removed and replaced 30 min after the reactor was shut down. During the shutdown, the dose rate decreased exponentially by approximately 15 kGy/h 20 min. Samples were irradiated up to 3.2 MGy, and aliquots were taken at different dose intervals for analyses. The final received dose was 1.1 MGy.

2.3 Alkaline hydrolysis

20 mL of 0.1 M NaOH was added to 1 mL of CH210 non-irradiated and irradiated (1.1 MGy) and left to hydrolyze for three days under a nitrogen atmosphere. Afterwards, the samples were lyophilized

and characterized using FTIR, NMR and SEC. Summary of irradiation and hydrolysis conditions are summarized in Table 1.

Table 1: Irradiation and hydrolysis conditions used in degradation studies of sample CH210

Treatment	Gamma irradiation	Irradiation atmosphere	Hydrolysis contact time	Hydrolysis atmosphere
No treatment	/	/	/	/
Irradiation	1.1 MGy	Ambient air	/	/
Hydrolysis	/	/	3 days	N ₂
Irradiation + hydrolysis	1.1 MGy	Ambient air	3 days	N ₂

2.3 Characterization of PCEs

Lyophilized powdered samples were analyzed using FTIR spectrometer (Perkin-Elmer Spectrum 400 FT-IR spectrometer).

¹H nuclear magnetic resonance (NMR) spectroscopy was used to identify the general structure of the PCEs and possible differences between irradiated, not irradiated and hydrolysed samples using a Bruker Avance 400 with a BBO probe.

SEC-MALS measurements were conducted with liquid chromatograph with UV, RI (Perkin Elmer, Hewlett Packard), and ELS 2100 detectors (Polymer Laboratories) to determine the molecular weight averages (M_n , M_w) of separated compounds and to identify difference between irradiated, not irradiated and hydrolysed samples.

3 Results and discussion

3.1 Radiolytic degradation

Visual changes of the liquid CH210 samples have been observed during irradiation. Gelation of the sample has occurred between 0.6-0.8 MGy of irradiation dose. In addition, overpressure in irradiation vials has been observed before samples turned into the gel. However, analysis of these gases was not possible in this experimental setup. At irradiation dose of 3.2 MGy, part of sample turned back from a gel into a liquid.

Analysis of its FTIR spectrum revealed the presence of O-H functional groups, ether functional groups, carboxylate functional groups, as well as C-H stretching from sp³ hybridized carbons (Figure 2). However, there is no significant difference between the irradiated sample (1.1 MGy dose) and the non-irradiated sample.

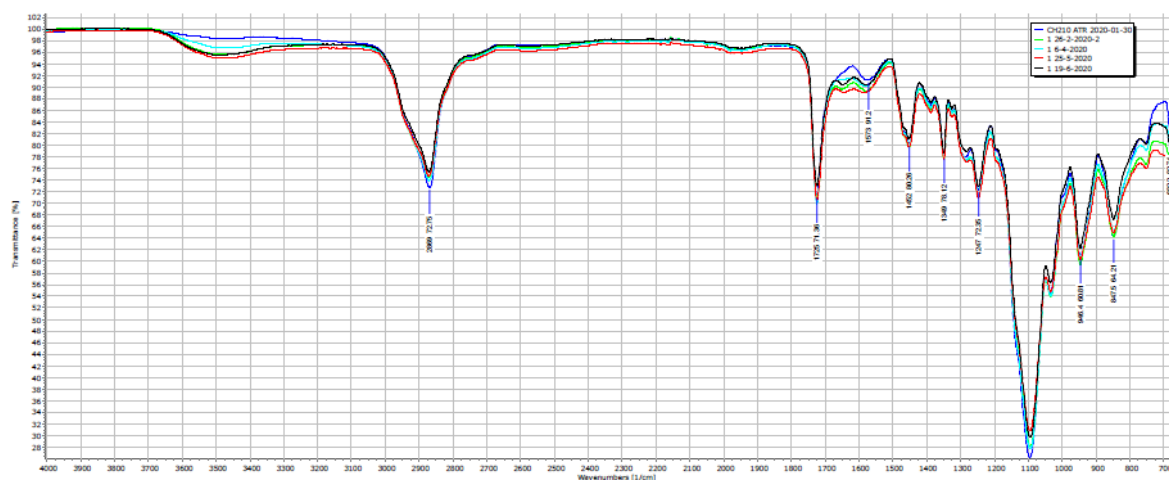


Figure 2: FTIR spectra comparing original and irradiated CH210 PCEs sample.

Table 2: FTIR vibrational band assignments from Figure 2

Wavenumber (cm ⁻¹)	Band assignment
3100 – 2700	O-H
1726	C=O
1422	C-O-H
1247	C-O

NMR results confirm the presence of polycarboxylate superplasticizer, but more information about the structure is difficult to obtain. Again, there are no significant differences between the irradiated and non-irradiated samples in the NMR spectra (Fig 3).

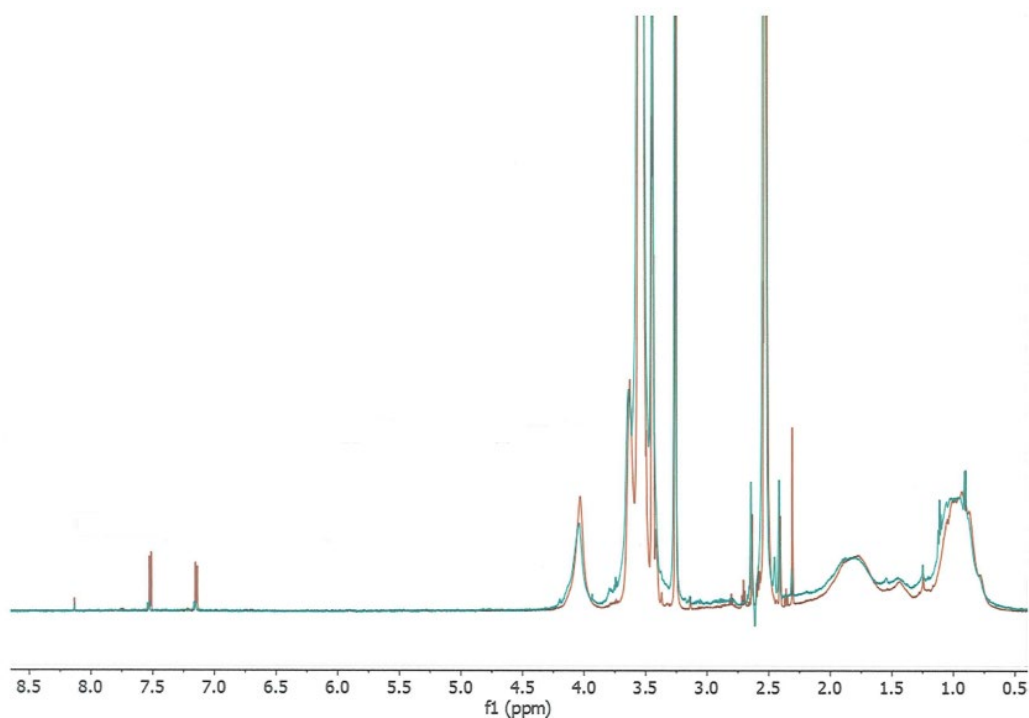


Figure 3: NMR results comparing original and irradiated CH210 PCEs sample. Red – original, blue – irradiated CH210 PCEs sample.

Table 3: NMR band assignments from Figure 3

δ (ppm)	Band assignment
0.7 – 1.3	R-CH ₃
1.4 – 1.7	R ₃ CH
2.1 – 2.6	R-CO ₂ -R
3 – 3.8	R-O-R

Size exclusion chromatography analysis revealed that no significant amount of low molecular weight compounds was formed during irradiation (Fig. 4). Irradiation-induced changes revealed an increase in molecular weight (Table 4), which is consistent with visual observation of gelation of the irradiated sample. In addition, only 47 % of the sample remained soluble, and the results for the irradiated sample correspond only to the soluble part. It can be assumed that the molecular weight of the insoluble part is even larger.

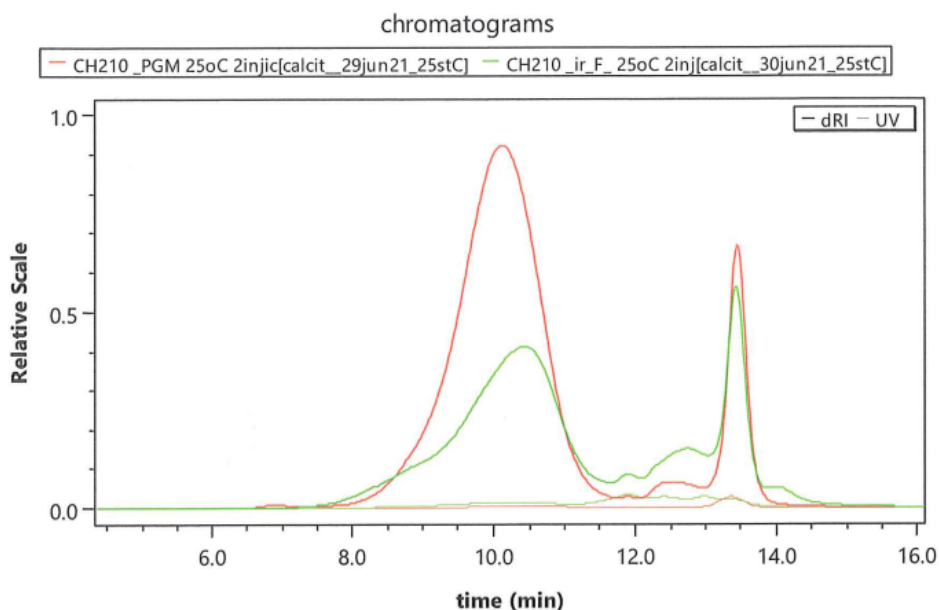


Figure 4: SEC chromatograms for original and irradiated CH210 PCEs sample.

Table 4: Molecular weight of not irradiated and irradiated sample CH210

Sample	M_w	M_n	M_w/M_n
CH210	63000	30500	2.069
CH210 irradiated	125400	22600	5.561

A similar analysis of the fraction of sample, which turned back into the liquid form after irradiation (3.2 MGy) and results show that only PEG sidechains are present in this sample as there remains only peak between 12-13 min of elution time, indicating that PEG sidechains were cleaved off the backbone.

3.2 Hydrolytic degradation

As expected, hydrolysis induced cleavage of ester bonds and cleavage of PEG sidechains from the backbone of the PCEs. Results showed that the PEG side chains equivalent to approximately 20 repeating units were separated from the PCE backbone. These appear as visible peaks at 12-13 min elution time (Fig. 6). In addition, the C=O stretch (1700 cm^{-1}) disappears from the FTIR spectra (Fig. 5).

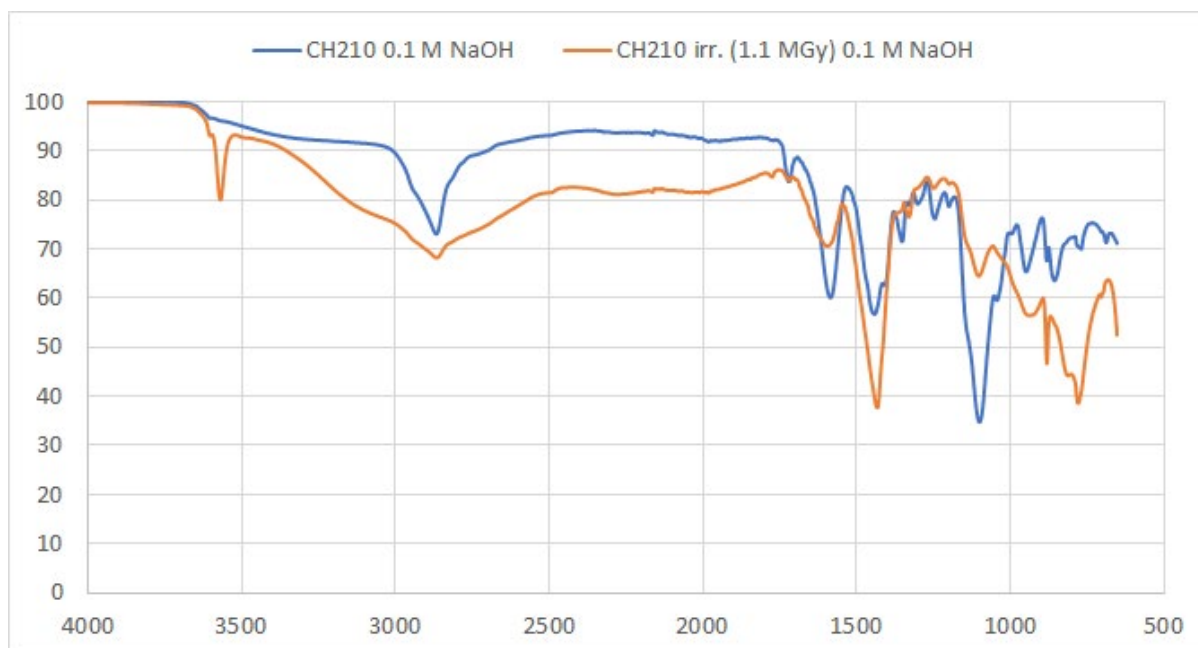


Figure 5: FTIR spectra of original and irradiated CH210 PCEs sample after hydrolysis in 0.1 M NaOH.

Table 5: FTIR vibrational band assignments from Figure 5

Wavenumber (cm ⁻¹)	Band assignment
3100 – 2700	O-H
1583	COO ⁻
1432	C-O-H

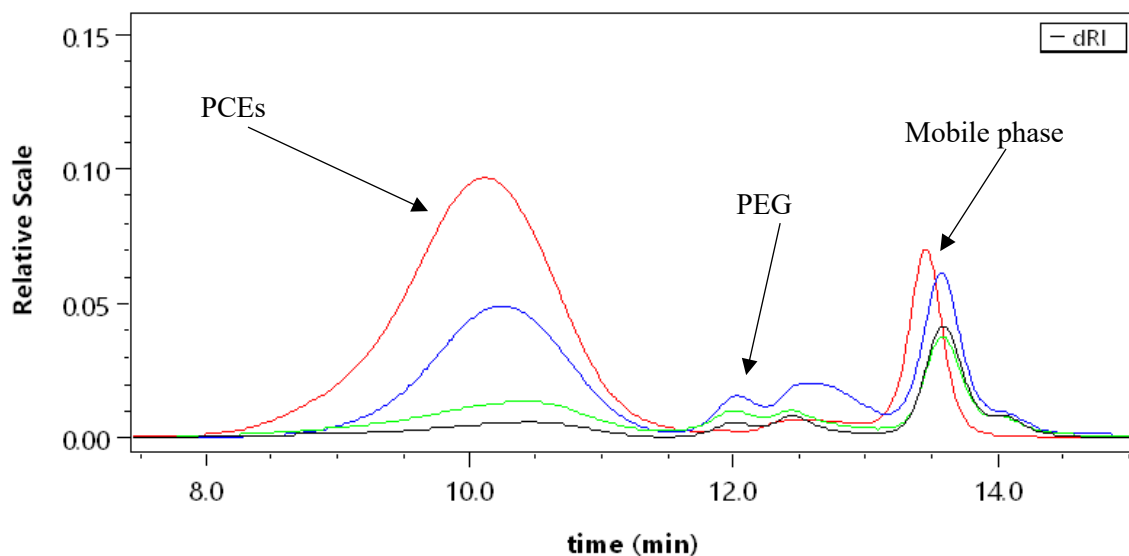


Figure 6: SEC chromatogram of original and irradiated CH210 PCEs sample after hydrolysis. Red – original, blue – original hydrolyzed in 0.1 M NaOH, green – insoluble fraction of irradiated to 1.1. MGy and hydrolyzed in 0.1 M NaOH, black – soluble and insoluble fraction of irradiated to 1.1. MGy and hydrolyzed in 0.1 M NaOH.

3 Conclusions

Results indicate that backbone crosslinking is the main process during irradiation of investigated commercial PCEs, with gelation occurring at 0.6 – 0.8 MGy of gamma irradiation dose. The result is a notable increase in the molecular weight of the sample. However, irradiation conditions are not fully representative of the actual conditions in cement as the concentration of SP would be much lower. In addition, cement particles would probably reduce the possibility that large amounts of PCEs could come into contact for crosslinking. At irradiation doses of 3.2 MGy, cleavage of PEG sidechains occurs, a process that is also dominant during 0.1 mol L⁻¹ NaOH hydrolysis. PEG seems to be the major degradation product of irradiation and hydrolysis of PCEs sample investigated. In order to improve our understanding of PCEs behaviour during radiolysis, it would be needed to design experiment, which would better mimic actual conditions during radwaste storage. This would probably prevent crosslinking of PCEs and may rather promote formation of different radiolytic products as found during this study. Nevertheless, formation of PEG seems to be dominant process in alkaline conditions in cementitious environment.

Acknowledgement

The EURAD-CORI project leading to this application has received funding from the European Union's Horizon 2020 research and innovation programme under grant agreement No 847593. The support by the Slovenian Research Agency (Programme P1-0143 and P2-0075) is acknowledged.

References

- Chen, G., Lei, J., Du, Y., Du, X., Chen, X., 2018. A polycarboxylate as a superplasticizer for montmorillonite clay in cement: Adsorption and tolerance studies. *Arab. J. Chem., SI: Nanochemistry for Materials* 11, 747–755. <https://doi.org/10.1016/j.arabjc.2017.12.027>
- Ilg, M., Plank, J., 2019. Synthesis and Properties of a Polycarboxylate Superplasticizer with a Jellyfish-Like Structure Comprising Hyperbranched Polyglycerols. *Ind. Eng. Chem. Res.* 58, 12913–12926. <https://doi.org/10.1021/acs.iecr.9b02077>
- Li, S., Pang, H., Zhang, J., Meng, Y., Huang, J., Lin, X., Liao, B., 2019. Synthesis and performance of a novel amphoteric polycarboxylate superplasticizer with hydrolysable ester group. *Colloids Surf. Physicochem. Eng. Asp.* 564, 78–88. <https://doi.org/10.1016/j.colsurfa.2018.11.043>
- Plank, J., Pöllmann, K., Zouaoui, N., Andres, P.R., Schaefer, C., 2008. Synthesis and performance of methacrylic ester based polycarboxylate superplasticizers possessing hydroxy terminated poly(ethylene glycol) side chains. *Cem. Concr. Res.* 38, 1210–1216. <https://doi.org/10.1016/j.cemconres.2008.01.007>
- Xiang, S., Gao, Y., Shi, C., 2020. Progresses in Synthesis of Polycarboxylate Superplasticizer [WWW Document]. *Adv. Civ. Eng.* <https://doi.org/10.1155/2020/8810443>

Impact of the degradation products of UP2 on the uptake of Ni(II), Ln(III) and Pu(III/IV): solubility and sorption studies

P. Szabo, A. Tasi, X. Gaona*, M. Altmaier, H. Geckeis

Karlsruhe Institute of Technology, Institute for Nuclear Waste Disposal, Karlsruhe (Germany)

* Corresponding author: xavier.gaona@kit.edu

Abstract

Solubility and sorption experiments with proxy ligands representative for the degradation of a polyacrylonitrile-based filter aid (UP2) were performed to assess the impact of these degradation products on the retention of Ni(II), Nd(III)/Eu(III) and Pu(III/IV) in cementitious systems relevant for the disposal of low and intermediate level radioactive waste (LILW). The impact of glutarate (GTA), α -hydroxy-isobutarate (HIBA) and 3-hydroxy-butyrate (HBA) on the solubility of Ca(II), Nd(III) and Pu(IV) is negligible at $[L]_{tot} \leq 0.1$ M, whereas a slight increase in the $[Ni]_{aq}$ is observed at $[L]_{tot} > 10^{-2}$ M. The latter observation is likely related to the formation of weak Ni(II)-OH-L complexes. Consistently with solubility experiments, the uptake of Ni(II), Eu(III) and Pu(III/IV) by hardened cement paste (HCP) in degradation stage II is only weakly affected by the presence of GTA, HIBA and HBA. These results will be further complemented with on-going experiments using complex UP2 degradation leachates simulating close-to-real systems under repository conditions.

1 Introduction

The filter aid UP2 (consisting mainly of polyacrylonitrile, PAN) is widely used in nuclear power plants as support material for ion exchange resins and for particle removal. Significant amounts of used UP2 are accordingly disposed of in underground repositories for low and intermediate level nuclear waste (LILW), e.g. in SFR (Sweden). The degradation of PAN in the hyperalkaline conditions defined by cementitious systems may result in organic degradation products affecting the retention of radionuclides, and thus is of particular interest in the context of nuclear waste disposal (Duro et al., 2012; Keith-Roach et al., 2021). Previous studies have hinted that degradation leachates of UP2 may decrease the uptake of radionuclides by cement, although the main degradation products as well as their overall impact on sorption remain ill-defined (Litmanovich and Platé, 2000; Duro et al., 2012). This work aims at investigating the impact of the degradation products of UP2 on the solubility and sorption of selected radionuclides in cementitious systems under alkaline, reducing conditions. The ligands glutarate (GTA, C₅H₇O₄), α -hydroxy-isobutarate (HIBA, C₄H₇O₃) and 3-hydroxy-butyrate (HBA, C₄H₇O₃), identified within Task 2 of this project (Tasi et al., 2021a), have been systematically used as UP2 fragments which likely form during degradation. GTA represents the bulk chain of the generated polymer fragments, whereas HIBA and HBA emulate the effect of the end groups.

2 Experimental

All experiments were conducted in gloveboxes under Ar atmosphere with $T = (22 \pm 2) \text{ }^\circ\text{C}$. Solubility experiments were performed from undersaturation conditions, *i.e.* equilibrating the well-defined solid phases $\text{Ca}(\text{OH})_2(\text{cr})$, $\beta\text{-Ni}(\text{OH})_2(\text{cr})$, $\text{Nd}(\text{OH})_3(\text{s})$ and $\text{PuO}_2(\text{ncr, hyd})$ with cement pore water both in the absence and in the presence of the proxy ligands GTA, HIBA and HBA. $\text{Ca}(\text{OH})_2(\text{cr})$ and $\text{Ni}(\text{OH})_2(\text{cr})$ are commercially available, $\text{Nd}(\text{OH})_3(\text{s})$ was prepared by hydration of $\text{Nd}_2\text{O}_3(\text{cr})$, whereas the $\text{PuO}_2(\text{ncr, hyd})$ used in this work was synthesized in a previous study, with an isotopic composition of 99.4 wt.% ^{242}Pu , 0.58 wt.% ^{239}Pu , 0.005 wt.% ^{238}Pu and 0.005 wt.% ^{241}Pu . Experiments were conducted in pore water solutions corresponding to cement CEM I in the degradation stage II (*i.e.* $\text{pH} \approx 12.5$ and $[\text{Ca}] \approx 0.02 \text{ M}$) containing $10^{-6} \text{ M} \leq [\text{L}] \leq 0.1 \text{ M}$. In experiments involving Pu, reducing conditions are maintained by hydroquinone or Sn(II). Redox conditions were not controlled for the rest of radionuclides / elements.

Sorption experiments were performed with a hardened cement paste (HCP) CEM I 42,5 N BV/SR/LA type provided as a monolith by the Swedish Nuclear Fuel and Waste Management Company (SKB). The HCP monolith was milled and sieved to a particle size of $<100 \text{ }\mu\text{m}$ as described in Tasi et al. (2021b), then stored under Ar atmosphere until use in the sorption experiments. A detailed characterization of this material was provided in Tasi et al. (2021b). The sorption study was conducted using the isotopes ^{63}Ni , ^{152}Eu and ^{242}Pu , which were quantified after sorption and phase separation by means of liquid scintillation counting (LSC), gamma spectrometry and inductively coupled plasma mass spectrometry (ICP-MS), respectively.

3 Results and discussion

3.1 Solubility experiments

The solubility of Ca(II), Nd(III) or Pu(IV) in cement pore water solutions with $10^{-6} \text{ M} \leq [\text{L}]_{\text{tot}} \leq 0.1 \text{ M}$ ($\text{L} = \text{GTA, HIBA, HBA}$) is not affected by these proxy ligands, as shown in Figure 1 for the Pu-HBA system with Sn(II) as reducing chemical. The three investigated proxy ligands promote a slight increase in the solubility of Ni(II) at $[\text{L}]_{\text{tot}} > 10^{-2} \text{ M}$ (data not shown), suggesting the possible formation of stable ternary complexes Ni-OH-L in the hyperalkaline conditions investigated in this work. These observations can be rationalized as follows: Nd(III) and Pu(IV) are characterized by very strong hydrolysis (dominated by $\text{Pu}(\text{OH})_4(\text{aq})$ and $\text{Nd}(\text{OH})_3(\text{aq})$ under the conditions of this study), which outcompete any possible complexation with the investigated proxy ligands. In the case of Nd(III), different observations may apply at lower pH values in the degradation stage III of cement, for which a weaker hydrolysis is expected. On the other side, Ca^{2+} has a significantly larger ionic radius than Ni^{2+} ($r_{\text{Ca}^{2+}} = 1.00 \text{ \AA}$, $r_{\text{Ni}^{2+}} = 0.69 \text{ \AA}$, in both cases for coordination numbers of 6) (Shannon, 1976), which results in much weaker ionic interactions between Ca^{2+} and the proxy ligands as compared with Ni^{2+} . The stronger interaction with Ln(III) and An(III/IV) reported for other polyhydroxocarboxylic acids like iso-saccharinic or gluconic acids is related to the presence of multiple alcohol functional groups in those ligands, which allow the formation of chelate complexes outcompeting hydrolysis even in hyperalkaline conditions (Gaona et al., 2008; Hummel et al., 2005; Tits et al., 2005; Vercammen et al., 2001, among others).

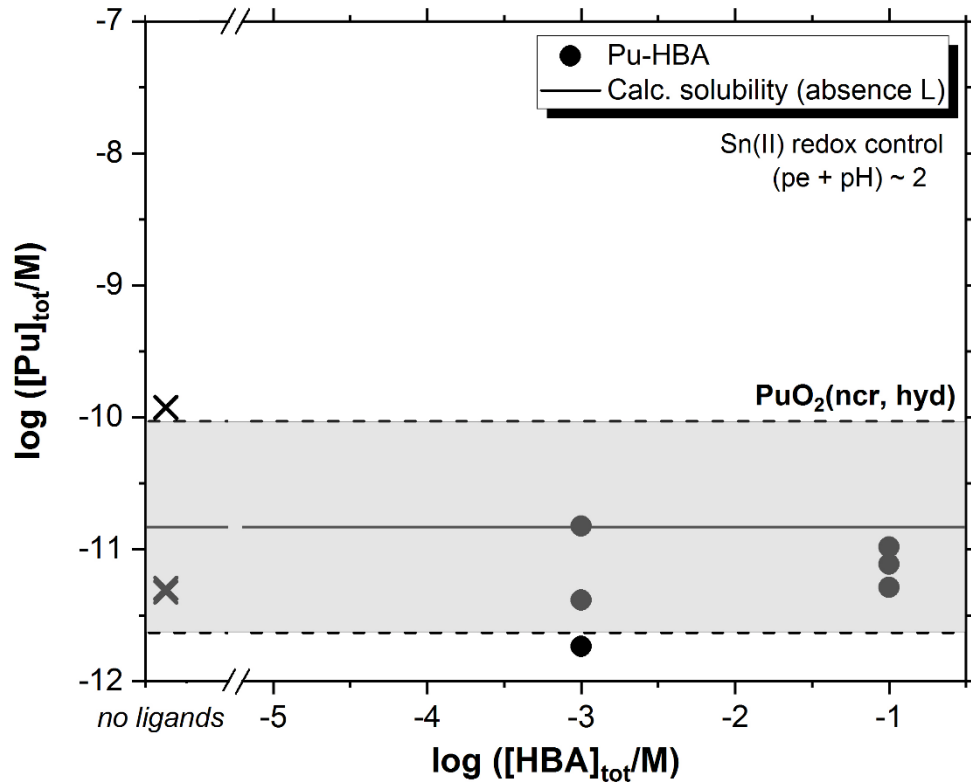


Figure 1: Solubility of $PuO_2(ncr, hyd)$ in equilibrium with cement pore water at $pH = 12.5$ with $[HGA]_{tot} = 10^{-3}$ and $0.1 M$. Redox conditions buffered by $Sn(II)$ ($pe + pH \approx 2$). Cross symbols show the concentration of Pu determined in the absence of proxy ligands. Black solid and dashed lines in the figure represent the calculated solubility of $PuO_2(ncr, hyd)$ and corresponding uncertainty at $pH = 12.5$ in ligand-free systems (Grenthe et al., 2020; Neck et al., 2007).

3.2 Sorption experiments

The uptake of $Ni(II)$, $Eu(III)$ and $Pu(III/IV)$ by HCP is only weakly affected by GTA, HIBA or HBA. A minor decrease in the $\log R_d$ values (with $R_d = [RN]_{solid} / [RN]_{aq}$, in $L \cdot kg^{-1}$) is observed for $Ni(II)$ and $Pu(IV)$ only at $[L]_{tot} > 10^{-2} M$, as shown in Figure 2 for the $Ni(II)$ -HBA system. The slight decrease in the uptake of $Ni(II)$ in the presence of proxy ligands is consistent with the weak complexation observed for these system in the solubility experiments (see discussion in Section 3.1). These results support that the degradation products of UP2 are expected to have a weak effect on the retention / mobilization processes of key radionuclides in the context of cement-based repositories for LILW.

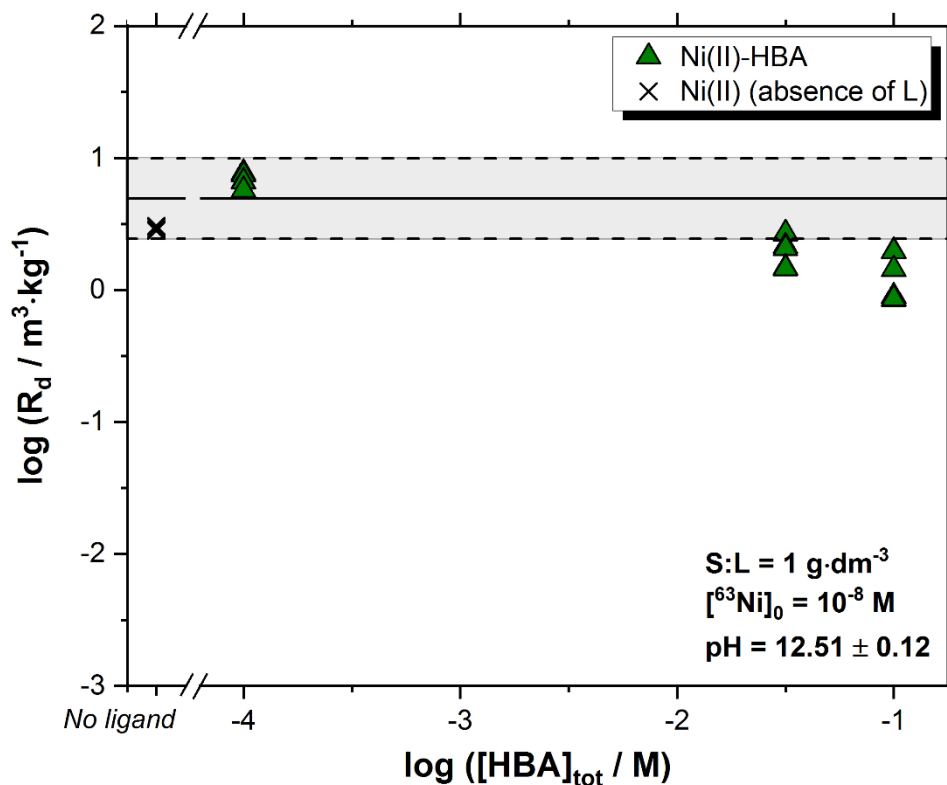


Figure 2: Uptake of Ni(II) by HCP expressed as $\log R_d$ values (with R_d in $\text{m}^3 \cdot \text{kg}^{-1}$) as a function of $\log [\text{HBA}]$. Cross symbols show the $\log R_d$ values determined in the absence of HBA.

4 Summary and conclusions

The impact of the degradation products of the UP2 filter-aid on the uptake of Ni(II), Eu(III) and Pu(IV) by HCP CEM I in the degradation stage II was investigated by a combined solubility and sorption study. On the basis of ¹H NMR results conducted within Task 2 of this project, the ligands GTA, HIBA and HBA were proposed as proxy degradation products of UP2 degradation products and were used throughout these experiments.

The solubility of Ca(II), Nd(III) and Pu(IV) remains unaffected at $[\text{L}]_{\text{tot}} \leq 0.1 \text{ M}$, with L = GTA, HIBA or HBA. The solubility of Ni(II) increases slightly at $[\text{L}]_{\text{tot}} > 10^{-2} \text{ M}$, although $[\text{Ni}]_{\text{aq}}$ remains within the uncertainty of the solubility equilibrium in the absence of L, *i.e.* $\beta\text{-Ni}(\text{OH})_2(\text{cr}) \rightleftharpoons \text{Ni}(\text{OH})_2(\text{aq})$. This observation suggests the possible formation of weak Ni-OH-L complexes under the investigated hyperalkaline conditions, which however require further experimental confirmation. In line with solubility data, the uptake of the investigated radionuclides remains mostly unaffected in the presence of GTA, HIBA and HBA. At the highest concentrations of GTA, HIBA and HBA considered in this work ($[\text{L}]_{\text{tot}} = 0.1 \text{ M}$), a decrease of $\leq 1 \log R_d$ -units is observed for Ni(II) and Pu(IV) indicating slightly weaker sorption at high ligand concentrations.

The results obtained with the identified proxy ligands indicate a weak impact on the solubility and sorption of key radionuclides and metal ions in cementitious systems relevant in the context of repositories for LILW. On-going studies within Task 4 are dedicated to assess the impact of UP2

complex degradation leachates simulating close-to-real systems under repository conditions on the solubility and sorption of Ni(II), Eu(III) and Pu(IV).

Acknowledgement

A. Maier and S. Hedström at SKB are thanked for discussions and feedback. The EURAD-CORI project leading to this application has received funding from the European Union's Horizon 2020 research and innovation programme under grant agreement No 847593. SKB is likewise acknowledged for financially supporting this work.

References

- Duro, L., Grive, M., Gaona, X., Bruno, J., Andersson, T., Boren, H., Dario, M., Allard, B., Hagberg, J., Källström, K. (2012). Study of the effect of the fibre mass UP2 degradation products on radionuclide mobilization, SKB Technical Report R-12-15.
- Gaona, X., Montoya, V., Colàs, E., Grivé, M., Duro, L. (2008). Review of the complexation of tetravalent actinides by ISA and gluconate under alkaline to hyperalkaline conditions, *Journal of Contaminant Hydrology*, 102, 217–227.
- Grenthe, I., Gaona, X., Plyasunov, A.V., Rao, L., Runde, W.H., Grambow, B., Konings, R.J.M., Smith, A.L., Moore, E.E. (2020). Second Update on the Chemical Thermodynamics of Uranium, Neptunium, Plutonium, Americium and Technetium. OECD Nuclear Energy Agency, Boulogne-Billancourt, France.
- Hummel, W., Anderegg, G., Rao, L., Puigdomènech, I. and Tochiyama, O. (2005). *Chemical Thermodynamics Vol. 9. Chemical Thermodynamics of Compounds and Complexes of U, Np, Pu, Am, Tc, Se, Ni and Zr with Selected Organic Ligands*. Elsevier, North Holland, Amsterdam.
- Keith-Roach, M., Lindgren, M., Källström, K. (2021). Assessment of complexing agent concentrations for the post-closure safety assessment in PSAR SFR, SKB Technical Report R-20-04.
- Litmanovich, A. D., Platé, N. A. (2000). Alkaline hydrolysis of polyacrylonitrile. On the reaction mechanism, *Macromolecular Chemistry and Physics*, 201, 2176–2180.
- Neck, V., Altmaier, M., Fanghänel, T. (2007). Solubility of plutonium hydroxides/hydrous oxides under reducing conditions and in the presence of oxygen. *C. R. Chim.* 10, 959-977.
- Shannon, R.D. (1976). Revised Effective Ionic Radii and Systematic Studies of Interatomic Distances in Halides and Chalcogenid, *Acta Crystallographica*, A32, 751-767.
- Tasi, A., Szabo, P., Gaona, X., Altmaier, M. and Geckeis, H. (2021a). Contribution by KIT-INE to CORI Task 2, in: Ricard, D., Vandenborre, J. (Eds.), *Eurad European Joint Programme on Radioactive waste management, Milestone DMS97 – CORI Technical Report -Task 2 Hydrolytic/radiolytic degradation of organics: description of first results on hydrolytic and radiolytic organic degradation and identification of released species*.
- Tasi, A., Gaona, X., Rabung, T., Fellhauer, D., Rothe, J., Dardenne, K., Lutzenkirchen, J., Grive, M., Colas, E., Bruno, J., Källstrom, K., Altmaier, M. and Geckeis, H. (2021b). Plutonium retention in the isosaccharinate - cement system. *Appl. Geochem.* 126.
- Tits, J., Wieland, E. and Bradbury, M.H. (2005). The effect of isosaccharinic acid and gluconic acid on the retention of Eu(III), Am(III) and Th(IV) by calcite. *Appl. Geochem.* 20, 2082-2096.
- Vercammen, K., Glaus, M.A. and Van Loon, L.R. (2001). Complexation of Th(IV) and Eu(III) by alpha-isosaccharinic acid under alkaline conditions. *Radiochim. Acta* 89, 393-401.

The stability of α -isosaccharinate under highly alkaline, reducing conditions

Jan Tits^{*}, Dominik Kunz, Typhaine Guillemot⁺, Erich Wieland

Laboratory for Waste Management, Paul Scherrer Institut, Villigen-PSI, (Switzerland)

* Corresponding author: jan.tits@psi.ch

⁺Present address: National Cooperative for the Disposal of Radioactive Waste, Nagra, Wettingen, Switzerland

Abstract

α -isosaccharinate (ISA) is an important degradation product of cellulose under alkaline, anaerobic conditions. From the existing scientific literature, it is inferred that this hydroxycarboxylate is stable in homogeneous alkaline solutions under anaerobic conditions. In the present study, the stability of α -ISA is investigated under reducing conditions in heterogeneous systems consisting of an alkaline solution in the presence of portlandite and with or without zero-valent iron powder as potential catalysts for degradation reactions. α -ISA solutions were heated in autoclaves or gas-tight reactors at 90°C for periods of up to 120 days in the presence of portlandite and with or without iron powder. The concentrations of α -ISA and organic degradation products in both liquid and gas phases were measured at regular time intervals. The results confirm that α -ISA is stable also in these heterogeneous systems. The observed decrease of the α -ISA concentration in the presence of zero-valent iron is likely due to a sorption and/or co-precipitation process involving iron corrosion products growing on the surface of the zero-valent iron particles.

1 Introduction

In many countries, low- and intermediate-level radioactive waste (L/ILW) is planned to be stored in deep geological repositories (DGR). Prior to storage, this type of waste is typically solidified in a cement matrix and, after disposal, caverns and access tunnels will be backfilled with cementitious materials, thus establishing highly alkaline conditions in the near-field of the repository. L/ILW may contain significant amounts of organic materials (e.g., cellulose-based materials used for laboratory purposes, for cleaning and for protective clothing in operational areas of nuclear facilities) that can degrade over time possibly resulting in the formation of organic ligands forming strong complexes with radionuclides (e.g., Wieland, 2014) or gaseous degradation products including CO₂ and CH₄ (Wiborgh et al., 1986). The complexing properties of cellulose degradation products and the resulting impact on radionuclide mobility are well documented in the literature (e.g., Gaona et al., 2008; Van Loon et al., 1999b; Wieland, 2014). Further decomposition to CO₂ can enhance the degradation of the cementitious engineered barrier through carbonation processes. The lower pH resulting from these CO₂-induced degradation processes causes increased microbial activity and accelerates corrosion reactions eventually leading to gas pressure build-up in the repository. Under the highly alkaline, anaerobic conditions typical for

DGRs for L/ILW situated in clay-type host rocks, cellulose degradation is expected to mainly occur through abiotic processes, as such an environment is unfavourable for microbial activity (i.e. pH > 11 and limited availability of free water) (Small, 2019; Small et al., 2008). Abiotic cellulose degradation processes under anaerobic, high pH conditions result in the formation of mainly α -isosaccharinic acid (α -ISA) and β -isosaccharinic acid (β -ISA) as well as a series of low molecular weight (LMW) carboxylic acids (CAs) in smaller amounts (e.g., Glaus et al., 1999). Thermodynamic calculations predict that, under repository conditions, these organic compounds are unstable and decompose to produce $\text{CO}_2(\text{aq})$, HCO_3^- , CO_3^{2-} and CH_4 (Wieland and Hummel, 2015). In real systems under repository conditions, however, the organic compounds may be metastable as their abiotic degradation occurs so slowly that it cannot be quantified under laboratory conditions at ambient temperatures. Nonetheless, this does not mean that further degradation and formation of gaseous products cannot take place during the safety relevant period of a DGR operation; i.e., hundreds of thousands of years. Furthermore, the presence of solids such as zero-valent iron (Fe(0)) or magnetite is known to catalyse decomposition reactions of LMW organic compounds (e.g., McCollom and Seewald, 2003a, b). Finally, Glaus and Van Loon (2009) found indications that α -ISA might be unstable in the presence of solid portlandite. The authors suggested that the reasons for the observed decomposition may be the presence of traces of oxygen, but an experimental proof for this suggestion could not be given.

In the present study, the α -ISA stability has been investigated under alkaline, reducing conditions in the presence of portlandite, *with or without* Fe(0) powder as a possible catalyst, and at a temperature of 90°C to accelerate potential degradation reactions. During cellulose degradation, two diastereomers (α -ISA and β -ISA) form in equal quantities (Glaus et al., 1999; Van Loon et al., 1999a). α -ISA was chosen because this diastereomer has stronger radionuclide complexing capabilities compared to β -ISA (Van Loon et al., 1999b). The study focusses on the identification and quantification of possible aqueous and gaseous degradation products of α -ISA. Therefore, the experiments were carried out in gas-tight containers; either in simple autoclaves where only the liquid phase can be analysed at the end of the experiment, or in custom-made gas-tight pressure reactors, which allow samplings from both the liquid and the gas phases without opening the reactor.

2. Materials and methods

Materials

All solutions used throughout this study were prepared in glove boxes under a controlled N_2 atmosphere (O_2 and $\text{CO}_2 < 0.1$ ppm), using analytical grade chemicals ("Emsure®", Merck, Germany) and ultrapure (deionised, de-carbonated) water (Milli-Q® water; 18.2 M Ω cm resistivity) generated by a Milli-Q gradient A10 purification system (Millipore, USA). The MilliQ water was degassed by boiling for one hour prior to its storage in the glove box for further use. CaO was obtained by heating $\text{CaCO}_3(\text{s})$ at a temperature of 900°C for ~12 hours. The Fe(0) powder was purchased from Merck, Darmstadt, Germany. According to the manufacturer, its purity is > 99% and its maximal particle diameter is 60 μm . The specific surface area of the Fe(0) powder was determined with the help of a seven-point Brunauer-Emmett-Teller (BET) N_2 adsorption isotherm to yield a value of 0.075 $\text{m}^2 \text{g}^{-1}$.

α -ISA stability experiments were performed in the presence of an artificial cement pore water (ACW) simulating the chemical conditions prevailing during the first phase of the cement degradation. The ACW contains 0.18 M KOH, 0.114 M NaOH and $1.6 \cdot 10^{-3}$ M $\text{Ca}(\text{OH})_2$ (saturated w.r.t. portlandite).

α -ISA was added to all experiments in the form of α -D-isosaccharino-1,4-lactone (α -ISA lactone). Under high pH conditions, the α -ISA lactone ring reacts with OH⁻ to form the open chain α -ISA. Note that the amount of OH⁻ consumed during this reaction (1 mole OH⁻ for each mole of α -ISA lactone) had no influence on the pH of 13.3 in ACW. α -ISA lactone was synthesised applying the procedure of Whistler and BeMiller (1963), which was slightly modified by Vercammen et al. (2000). Speciation calculations carried out with Medusa (Puigdomenech, 2014) using the thermodynamic data for the Ca – ISA system reviewed in Hummel et al. (2005) reveal that the dominant aqueous α -ISA species in ACW at pH 13.3. is the negatively charged α -ISA⁻ ligand.

Analytical methods

Total and individual dissolved carbon compounds formed during the anoxic and alkaline degradation of cellulose were identified and quantified by a total organic carbon (TOC) analyser and by high performance ion exchange chromatography coupled with mass spectrometry (HPIEC-MS), respectively. These analyses cannot be performed on highly alkaline solutions. Therefore, the solution samples were neutralised prior to analysis using H-cartridges (OnGuard cartridge, Dionex, USA) allowing treatment of up to 12 mL of ACW with a pH of 13.3 in one run.

A HPIEC measurement procedure was put in place to enable optimal identification and quantification of α -ISA and a series of LMW CAs including formic acid (FA), acetic acid (AA), glycolic acid (GA), propionic acid (PA), lactic acid (LA), valeric acid (VA), malonic acid (MA), oxalic acid (OA) and butyric acid (BA). For this purpose an ICS-5000 ion chromatography (IC) system (Dionex/Thermo Fisher, USA) coupled to a MSQTM Plus mass spectrometer (MS) (Thermo Fisher, Sunnyvale, CA, USA), operating in the negative electrospray ionisation (ESI) mode, was used. Optimal cone voltage for scanning both α -ISA and the CAs was found to be in the range between 30 – 50 V. A tiny co-elution between ISA and LA was observed in the spectra of the MS in the selected ion monitoring (SIM) mode. For a reliable quantification of both compounds but also for a more stable signal of α -ISA, the high concentrations of α -ISA were measured with conductivity detection, which was switched off after 7.4 min elution time. The MS source directly took over afterwards for scanning LA at its specific mass fragments, as well as the subsequently eluted CAs. Tests with ACW solutions containing a mixture of known concentrations of ISA and the CAs listed above, in the proportions expected in a cellulose degradation experiment (ISA/CA = ~30/1), showed that the HPIEC measurements resulted in concentrations in agreement with the injected concentrations with uncertainties in the range between 1% and 8%. Thus, recovery obtained by the HPIEC-MS analysis was complete for all individual compounds indicating that none of the organic compounds was lost during the analysis, in particular during pre-treatment with the H-cartridge.

Total dissolved organic carbon in solution (non-purgeable organic carbon, NPOC) was measured with a Shimadzu TOC-L analyser (Kyoto, Japan). Tests with ACW solutions containing mixtures of known concentrations of ISA and the CAs listed above revealed uncertainties on the NPOC measurements varying between ~5% (at the lowest TOC concentration of 11 ppm) and < 1% (at the highest TOC concentration of 65 ppm). NPOC analysis of pure ACW solutions revealed a non-negligible contamination with non-purgeable organic carbon of 2.5 ± 0.3 ppm. HPIEC-MS analysis of the blanks revealed the presence of ~0.38 ppm FA and ~1.04 ppm AA together with very small amounts of OA, LA and PA. Approximately 30% of the contamination could not be identified and probably consisted of organic compounds other than CAs. All NPOC measurements of the samples from the degradation experiments in ACW were therefore corrected for this NPOC background.

For the analysis of the gaseous compounds that could potentially be formed during α -ISA degradation under reducing conditions in the presence of Fe(0), a gas chromatograph coupled to a mass spectrometer (GC-MS) was used, consisting of a TRACE™ GC Ultra gas chromatograph (GC) coupled to an ISQ MS (Thermo Fisher Scientific Inc., Waltham, MA, USA) with electron ionisation (EI). The analytical procedures applied were developed in the framework of a previous project and described elsewhere (Cvetković et al., 2018). The GC-MS analyses included the following gaseous compounds: hydrogen (H₂), methane (CH₄), ethane (C₂H₆), ethene (C₂H₄), propane (C₃H₈), propene (C₃H₆) and butane (C₄H₁₀). Uncertainties on the reported gaseous hydrocarbon concentrations were estimated to be $\leq 20\%$ (Cvetković et al., 2018).

The limits of detection (LOD) and the limits of quantification (LOQ) of the different analytical methods were calculated from the measurement of five blank replicates following the procedure described by Keith et al. (1983) and Barwick and Prichard (2011). The uncertainties on the reported aqueous CA concentrations and gaseous hydrocarbon concentrations were conservatively estimated to be 10% and 20%, respectively based upon the experience gained during the test experiments with HPIEC-MS and NPOC measurements described above, and the typical uncertainties obtained with the GC-MS equipment reported by Cvetkovic et al. (2018).

Set-up of the stability experiments

A first type of α -ISA stability tests was performed in autoclaves (volume = 50 mL) equipped with teflon inlets at a temperature of 90°C in ACW in the presence of portlandite, *with or without* Fe(0). In a glove box, the required amounts of portlandite and Fe(0) powder were weighted and transferred into the autoclaves. A volume of 40 mL of ACW was added as well as an aliquot of a 0.02 M α -ISA solution (e.g. 0.0324 g of α -ISA lactone dissolved in 10 mL ACW). The autoclaves were tightly closed, transferred to an oven located in the inert atmosphere glovebox and maintained at a temperature of 90°C for up to 120 days. At the end of the stability test, the autoclaves were cooled down to room temperature and opened outside the glove box to sample the solutions. In parallel, blank experiments were set-up to quantify the organic contaminants present in solution under the various experimental conditions considered. The concentrations of the CAs in the α -ISA solutions were corrected by the concentrations determined in their respective blank experiments.

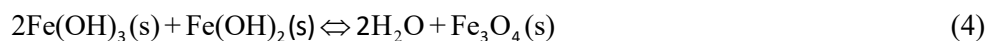
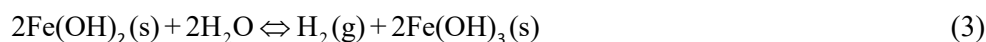
During the stability tests the internal pressure in the autoclaves rose due to the increase of the temperature from 25°C to 90°C (water vapour), and due to H₂ production caused by the anoxic corrosion of the Fe(0) powder. The H₂ partial pressure in the autoclaves was estimated by assuming that the mass of iron powder corroded during the degradation experiment depends on the corrosion rate, R_c ($m \cdot a^{-1}$), the surface area of the iron particles, A (m^2), and the duration of the experiment, t (a). Assuming further that surface area of the Fe(0) particles is large enough to avoid the corrosion reaction causing a significant surface area reduction during the experiment, the moles of Fe(0) (n_{Fe}) that are corroded as a function of time can be calculated as follows:

$$n_{Fe} = \frac{R_c \cdot t \cdot A \cdot \rho}{M_{Fe}} \quad [\text{moles}] \quad (1)$$

with M_{Fe} = the molar mass of Fe = 0.055845 kg mol⁻¹ and ρ = density of Fe = 7855 kg m³.

The anoxic corrosion of Fe(0) proceeds in several steps (e.g., Jelinek and Neufeld, 1982; Linnenbom, 1958; Reardon, 2005; Senior et al., 2017): in an initial, fast step, metallic Fe is oxidised to iron(II)

hydroxides (eq. 2) which in a second, slower step known as the Shikorr reaction, are transformed to magnetite (eqs. 3 (slow reaction) and 4 (fast reaction)):



The Shikorr reaction is only relevant at temperatures above 80°C (Linnenbom, 1958; Reardon, 2005; Smart et al., 2017) but can be catalysed by the presence of Fe(0) (Reardon, 2005). Under the experimental conditions described above, it is, thus, very likely, that the dominant Fe corrosion product formed, will be magnetite.

Combination of reactions (2), (3) and (4) gives the overall reaction for anoxic corrosion of iron:



Eq. 5 reveals that for the corrosion of three moles of Fe, four moles of H₂ are produced. Taking into account this stoichiometry and applying the ideal gas law, the H₂ partial pressure can be calculated from the value of n_{Fe}.

The contribution of the vapour pressure to the total pressure in the autoclaves can be estimated using the Antoine equation (e.g., P.J. Linstrom and Mallard, 2022):

$$\log_{10}(\text{P}) = A - \left(\frac{B}{T + C} \right) \quad (6)$$

In this equation, A, B and C are constants which take the following values in the temperature range between 344 K and 373 K: A=5.08354, B=1663.125, C=-45.622. Application of the Antoine equation for H₂O at a temperature of 90°C gives a vapour pressure of 0.69 bar.

The α-ISA stability was further investigated in custom-made, 500 mL, gas-tight stirred pressure reactors (Versoclave Type 3E, Büchi, Uster, Switzerland) in those experimental conditions under which a clear decrease of the initial α-ISA concentration was observed in the autoclave experiments. The reactor walls and lid are made of 0.8 cm thick CrNiMoTi steel, which is in direct contact with the reacting medium. The pressure reactors used in the stability experiments were washed with 0.1 M HCl to dissolve any possible precipitates (portlandite or iron corrosion products) from previous experiments. Subsequently, the reactors were thoroughly rinsed with MilliQ water and dried. Note that the acid treatment may have caused corrosion of the stainless steel surface and influence the degradation of α-ISA.

The required amounts of portlandite and Fe(0) powder were weighted and transferred into the reactor. After closing tightly, the gas phase in the reactor was slowly evacuated and replaced by N₂ gas while the iron powder was retained at the bottom of the reactor by a strong magnet. The portlandite powder was too heavy to be stirred up during this evacuation procedure. In the glove box, a stainless steel cylinder was evacuated and filled with 400 mL ACW solution containing 5·10⁻⁴ M α-ISA. The cylinder was then connected to the evacuated reactor and the α-ISA solution was transferred into the reactor by the existing vacuum. The final pressure in the reactor was adjusted to 3.0 bar with N₂ gas (at

T = 25°C) and the temperature was increased to 90°C resulting in a starting pressure of ~3.6 bar. Both the solution and the gas phase were sampled at regular time intervals without opening the reactor by taking advantage of the existing overpressure. After each sampling, the pressure in the reactor was restored by adding the required amount of N₂. At the end of each experiment, the reactor was opened and samples of the remaining solution were analysed for their cation composition and pH.

3. Results and discussion

In a first step, the stability of α -ISA was tested at 90°C in a series of preliminary experiments in the autoclaves in presence and absence of portlandite and Fe(0) powder. In these experiments, an ACW solution containing 100 μ M α -ISA and two ACW suspensions containing the same α -ISA concentration and either 100 g L⁻¹ portlandite or 100 g L⁻¹ portlandite + 25 g L⁻¹ Fe(0) powder, respectively, were let react for 75 days. In parallel, a series of blank autoclaves was set-up with the same contents (i.e. ACW solution and ACW suspensions) as the autoclaves described above, but without α -ISA and let to react over the same period. At the end of the experiments, the supernatant solutions were analysed for the α -ISA and CA concentrations. The results of these experiments are summarised in Table 1 together with the LOD and LOQ of the organic compounds detected in the solutions and suspensions.

No α -ISA was detected in the blanks, as expected, while significant amounts of FA, AA, OA and GA were measured. The CA concentrations determined in the solutions and suspensions containing α -ISA were thus corrected for these background concentrations. During the reaction period of 75 days, the α -ISA concentration remained constant in the ACW solution and the suspension containing ACW and portlandite, indicating that the presence of the latter solid does not cause any α -ISA degradation. In the presence of portlandite and Fe(0) powder, however, a significant decrease of the α -ISA concentration was observed along with a slight increase in the CA concentrations. The increase in the CA concentrations was, however, not proportional to the decrease of α -ISA concentration and might be due to organic contamination of the iron powder. As a result of the observations made in these preliminary test experiments, further studies focused only on the stability of α -ISA in ACW at 90°C in the presence of portlandite and Fe(0) powder. The stability of α -ISA was investigated in the autoclaves and in the custom-made gas-tight Versoclave pressure reactors as function of the reaction time and amount of Fe(0) powder. The starting α -ISA concentration in these experiments was 5 · 10⁻⁴ M.

The stability tests in the autoclaves showed that, in the presence of portlandite and Fe(0) powder, the α -ISA concentration decreased with progressing reaction time during the first 30 days and then remained constant (Figure 1a). It was also observed that the α -ISA concentration dropped significantly with the presence of increasing amounts of Fe(0) (Figure 1b). NPOC concentrations and the sum of the concentrations of all analysed organic compounds ($[\alpha\text{-ISA}] + \Sigma[\text{CA}]$), denoted as $\Sigma(\text{C})$, both expressed in terms of α -ISA concentrations (i.e., normalized to the concentration of α -ISA which contains 6 carbon atoms), showed the same behaviour as the α -ISA concentration in the experiments and were of the same order of magnitude as the latter (Figure 1a and 1b). This observation indicates that the decrease in α -ISA concentration is not accompanied by an increase of the aqueous concentrations of other LMW organic compounds. This finding suggests that the decrease of the $[\alpha\text{-ISA}]$ is not the result of a degradation process but rather a process involving sorption on, or co-precipitation with iron corrosion products. It should be noted that the composition of the gas phase could not be analysed in these experiments.

Table 1: α -ISA and CA concentrations determined with HPIEC in blank (ACW) and α -ISA solutions, both in presence and absence of 100 g L⁻¹ portlandite (portl.) and/or 25 g L⁻¹ Fe(0) powder (Fe(0)). The CA concentrations in the α -ISA solutions are corrected for the respective CA concentrations found as contaminants in the blanks.

Blanks	[α -ISA] μ M	[FA] μ M	[AA] μ M	[OA] μ M	[GA] μ M
LOD	0.7	2.2	1.6	0.3	0.1
LOQ	2	5.5	4.2	0.7	0.2
ACW	0	10.7 \pm 2.5	23.5 \pm 5.9	2.1 \pm 0.5	0.1 \pm 0.03
ACW+portl.	0	-	-	-	-
ACW+portl.+Fe(0)	0	21.5 \pm 5.4	33.6 \pm 8.5	2.1 \pm 0.5	0.1 \pm 0.03
α-ISA					
Start	103 \pm 26	0.60 \pm 0.15	0.7 \pm 0.2	0.0	0
ACW	103 \pm 26	1.7 \pm 0.4	2.1 \pm 0.5	0.30 \pm 0.07	1.03 \pm 0.26
ACW+portl.	97 \pm 24	5.0 \pm 1.3	3.2 \pm 0.8	3.6 \pm 0.9	0.30 \pm 0.08
ACW+portl.+Fe(0)	40 \pm 10	18.6 \pm 4.6	18.0 \pm 4.5	10.6 \pm 2.6	3.8 \pm 0.9

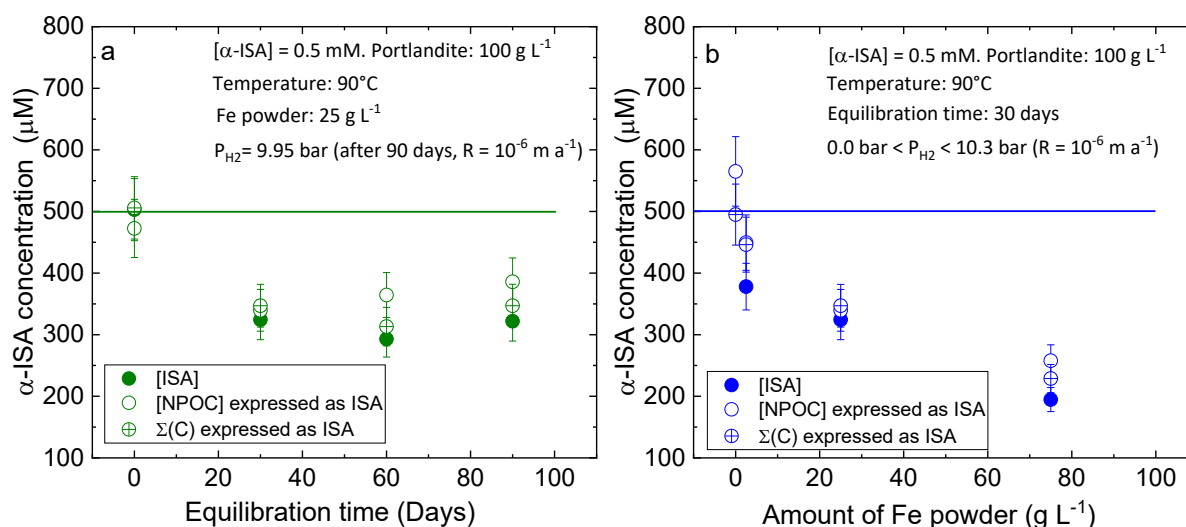


Figure 1: α -ISA stability in ACW at pH = 13.3 at 90°C in the presence of portlandite and Fe(0) powder measured in autoclaves. a) α -ISA concentration in ACW as function of equilibration time in the presence of 100 g L⁻¹ portlandite and 25 g L⁻¹ Fe(0) powder. b) Influence of the presence of increasing amounts of iron powder on the α -ISA concentration in ACW after an equilibration time of 30 days. H₂ partial pressures reported in the figures were calculated assuming a short term iron corrosion rate of 10⁻⁶ m a⁻¹ (Diomidis, 2014, Figure 3.18, corrosion rate in 0.1 M NaOH at 80°C), an initial specific surface area (σ) of the iron powder of 0.075 m² g⁻¹ and a decreasing iron surface with progressing corrosion.

In order to obtain an overview of the organic compounds present both in solution and in the gas phase, α -ISA stability experiments at 90°C in ACW in the presence of portlandite and Fe(0)-powder were repeated in gas-tight Versoclave reactors. The results of experiments in which the stability of a $5 \cdot 10^{-4}$ M α -ISA solution was tested as a function of time in the presence of two different portlandite concentrations and 2 different concentrations of Fe(0) powder are shown in Figure 2. The starting pressure in these experiments was set to 3 bar N₂ at 25°C. The temperature increased from 25°C to 90°C during the first two hours of the experiment, which caused a pressure rise to a value of ~3.6 bar. The pressure in the reactor continued to increase during the first 30 to 60 days due to the formation of H₂ gas caused by anoxic corrosion of the iron powder (Figure 2a, b). After this initial phase, the pressure and H₂ concentration in the gas phase remained constant throughout the experiments (Figure 2a, b). In the reactor with the highest iron powder concentration (25 g L⁻¹), the reactor pressure increased much stronger. In this experiment, the pressure had to be reduced twice manually to prevent the pressure from exceeding the maximum allowed value of 8 bars (the maximum pressure given by the manufacturer is 10 bar. In practice, however, the rupture disks often breaks already at a pressure of ~8 bar). Correcting for this loss of pressure, the maximum pressure in the reactor was ~10.0 bar. Subtracting the starting pressure of 3 bar and the vapour pressure at 90°C of 0.69 bar gives a maximum H₂ partial pressure of ~6.3 bar meaning 5.2 mmol H₂ produced per g iron powder over 90 days. This is somewhat higher than the H₂ production calculated for similar iron powder suspensions (25 g L⁻¹ iron powder in ACW) in the autoclaves (9.95 bar = 3.3 mmol H₂ per g iron powder after 90 days reaction time; Figure 1). Note however, that the corrosion rate of 10^{-6} m a⁻¹ used in these calculations is only an approximate value taken from the literature (Diomidis, 2014) and derived from short term corrosion experiments under conditions not fully comparable to the present experiments. The surface area of the steel parts of the reactor vessel was estimated to be ~0.0428 m² (assuming the vessel is a cylinder with a known volume of 0.649 L and a height of 0.136 m). This approximately 5% of the surface area of the iron powder in the corrosion experiment (0.75 m²) and, thus, its contribution to H₂ production from corrosion can be neglected.

Analysis of the solutions shows that the α -ISA concentration decreased only slightly with time in the reactors with a Fe(0) powder concentration of 2.5 g L⁻¹. A much more significant decrease of the α -ISA concentration was observed in the presence of 25 g L⁻¹ iron powder (Figure 2c). $\Sigma(C)$ is identical to the α -ISA concentration, meaning that no LMW CAs were formed during the observation period (Figure 2d). NPOC concentrations were approximately 100 μ M higher than $\Sigma(C)$, as exemplified in Figure 2d for the experiment with 25 g L⁻¹ Fe(0) powder, suggesting the presence of impurities originating from the reactor. After correction for their concentrations in the blanks, the concentrations of gaseous hydrocarbons were negligible in all experiments.

Both types of experiments show that α -ISA concentrations in ageing alkaline cement pore water solutions decrease only in the presence Fe(0) powder. The presence of solid portlandite does not cause any significant decrease in the α -ISA concentration in contrast to earlier reported observations (Glaus and Van Loon). This observation thus supports the assumption made by the latter authors that the decrease of α -ISA concentration might be due to oxidation reactions caused by traces of O₂ sorbed on the portlandite surfaces. A detailed examination of the aged α -ISA solutions and the corresponding gas phases in the present experiments did not lead to the detection of significant amounts of LMW organic degradation products. This observation suggests that the decrease in α -ISA concentration observed in the present experiments is not caused by abiotic degradation processes but rather by a sorption process involving the metallic Fe(0) or newly formed iron corrosion products.

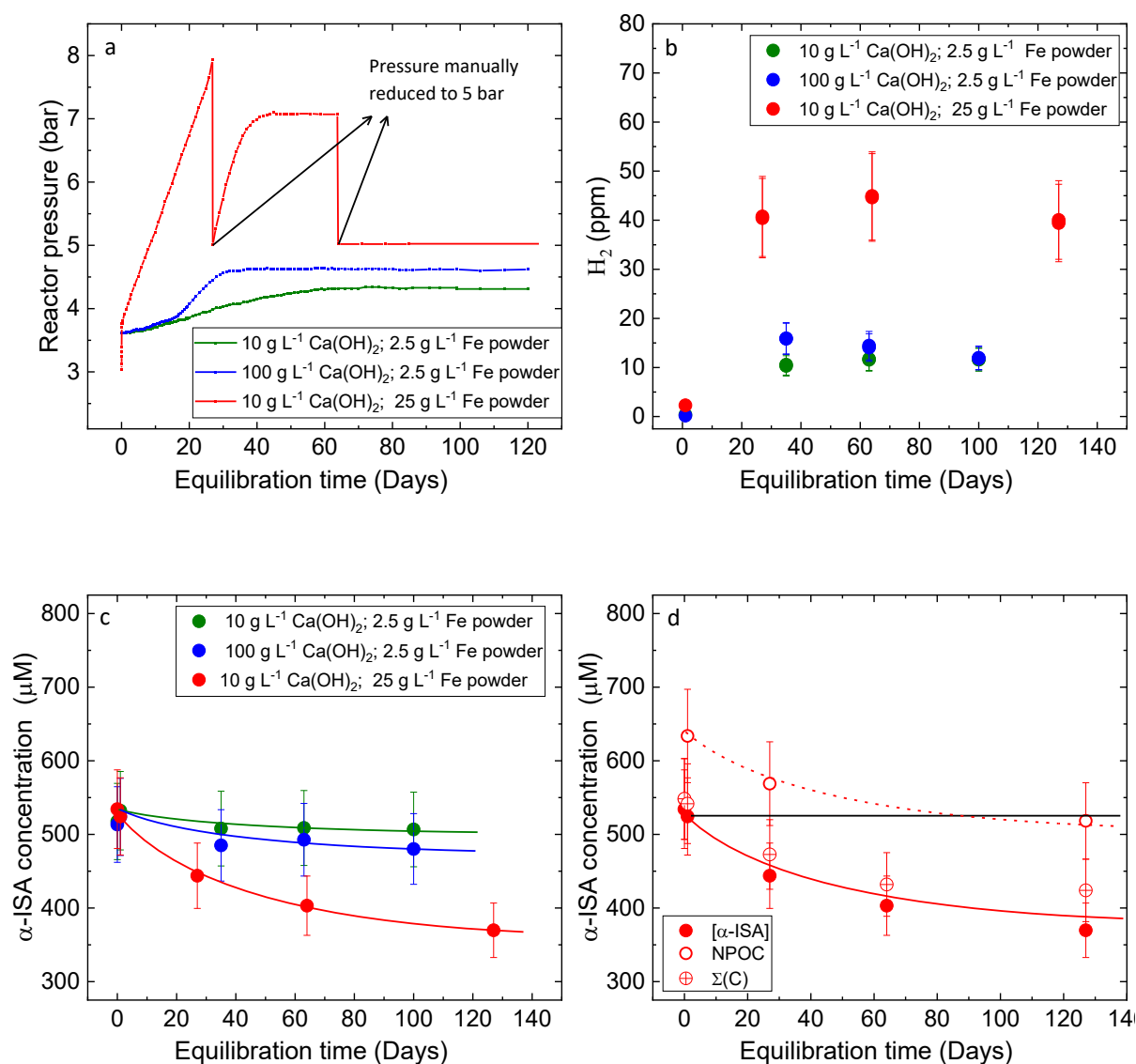


Figure 2: *α-ISA stability in ACW at pH = 13.3 at 90°C in the presence of portlandite and Fe(0) powder measured in gas-tight pressure reactors under N₂ atmosphere. The starting pressure was 3.0 bar. a) Evolution of the gas pressure with time. b) Evolution of the H₂ concentration in the gas phase with time. c) Effect of the amount of portlandite and Fe(0) powder on the evolution of the α-ISA aqueous concentration with time. d) Evolution of the α-ISA concentration, NPOC and Σ(C) in the aqueous phase as a function of time in the presence of 10 g L⁻¹ portlandite and 25 g L⁻¹ Fe(0) powder.*

Indeed, the decrease of the α-ISA concentration with increasing amounts of iron powder indicates that the latter material plays a key role in the fate of α-ISA. The slow decrease in α-ISA concentration with time (Figure 1a and 2c) may be explained by sorption onto increasing amounts of iron corrosion products rather than by the metallic Fe(0). The flattening of the curve representing the evolution of the α-ISA concentration with time (Figure 1a and 2c) might be explained by a slow-down of the formation of the iron corrosion products due to passivation. The dominant iron corrosion product expected in the present experiments (ACW, anoxic conditions, T = 80°C) is magnetite (see discussion above). The surface charge of this mineral is negative under alkaline conditions (e.g., Sun et al., 1998) making the sorption of the negatively charged α-ISA⁻ anion unlikely. However, sorption of Ca²⁺ present in the ACW

might induce a reversal of the magnetite surface charge, which would greatly improve the affinity of the mineral surface for α -ISA. Alternatively, the formation of α -ISA-containing iron corrosion products by co-precipitation on the surface of the Fe(0) particles could be another process accounting for the removal of α -ISA from solution. Indeed, there are many indications in the recent literature that gluconate (an organic ligand with a structure similar to ISA), and ISA have a high affinity for trivalent cations (trivalent actinides (An(III)), lanthanides (Ln(III)) and also Fe(III)) and that the presence of Ca further enhances the stability of Fe(III), An(III)- and Ln(III)- complexes with these organic ligands (Bechtold et al., 2002; Böszörményi et al., 2019; Rojo et al., 2021; Tasi et al., 2021). Co-precipitation between Ca(II), α -ISA and Fe(III) thus offers a possible further potential explanation for the decrease in α -ISA concentration in solution in the presence of Fe(0) particles.

4 Conclusions

α -ISA is stable in ACW at pH = 13.3 under reducing conditions and a temperature of 90°C over a period of up to 120 days, both in absence and in presence of portlandite and Fe(0) powder. This conclusion is based on the absence of detectable concentrations of organic degradation products in both solution and gas phase. The decrease of the α -ISA concentration with time and with increasing amounts of Fe(0) powder might be explained by a sorption and/or co-precipitation process involving iron or its corrosion products growing on the surface of the Fe particles.

Acknowledgement

The EURAD-CORI project leading to this application has received funding from the European Union's Horizon 2020 research and innovation programme under grant agreement No 847593.

References

- Barwick, V., Prichard, E., 2011. Eurachem Guide: Terminology in Analytical Measurement—Introduction to VIM 3. Eurachem. Available at: www.eurachem.org. Accessed October 23, 2017.
- Bechtold, T., Burtscher, E., Turcanu, A., 2002. Ca²⁺-Fe³⁺-D-gluconate-complexes in alkaline solution. Complex stabilities and electrochemical properties. J. Chem. Soc., Dalton Trans., 2683-2688.
- Böszörményi, É., Iado, J., Dudás, C., Kutus, B., Szabados, M., Varga, G., Pálkó, I., Sipos, P., 2019. The structure and composition of solid complexes comprising of Nd(III), Ca(II) and D-gluconate isolated from solutions relevant to radioactive waste disposal. Pure Appl. Chem. 92, 1709-1715.
- Cvetković, B.Z., Rothardt, J., Büttler, A., Kunz, D., Schlotterbeck, G., Wieland, E., 2018. Formation of low-molecular-weight organic compounds during anoxic corrosion of zero-valent iron. Environ. Eng. Sci. 35, 447-461.
- Diomidis, N., 2014. Scientific basis for the production of gas due to corrosion in a deep geological repository. Nagra Arbeitsbericht NAB 14-21, Nagra, Wettingen, Switzerland.
- Gaona, X., Montoya, V., Colàs, E., Grivé, M., Duro, L., 2008. Review of the complexation of tetravalent actinides by ISA and gluconate under alkaline to hyperalkaline conditions. J. Contam. Hydrol. 102, 217-227.
- Glaus, M.A., Van Loon, L.R., 2009. Chemical Reactivity of α -Isosaccharinic Acid in Heterogeneous Alkaline Systems. PSI Report Nr. 08-01, Paul Scherrer Institut, Villigen, Switzerland.
- Glaus, M.A., Van Loon, L.R., Achatz, S., Chodura, A., Fischer, K., 1999. Degradation of cellulosic materials under the alkaline conditions of a cementitious repository for low and intermediate level waste. Part I: Identification of degradation products. Anal. Chim. Acta 398, 111-122.

- Hummel, W., Anderegg, G., Puigdomenech, I., Rao, L., Tochiyama, O., 2005. Chemical thermodynamics of compounds and complexes of U, Np, Pu, Am, Tc, Se, Ni, and Zr with selected organic ligands. Elsevier, Amsterdam, The Netherlands.
- Jelinek, J., Neufeld, P., 1982. Kinetics of Hydrogen Formation from Mild Steel in Water under Anaerobic Conditions. *Corros. Sci.* 38, 98-104.
- Keith, L.H., Crummett, W., Deegan, J., Libby, R.A., Taylor, J.K., Wentler, G., 1983. Principles of Environmental Analysis. *Anal. Chem.* 55, 2210-2218.
- Linnenbom, V.J., 1958. The Reaction between iron and water in the absence of oxygen. *J. Electrochem. Soc.* 105, 322-324.
- McCullom, T.M., Seewald, J.S., 2003a. Experimental constraints on the hydrothermal reactivity of organic acids and acid anions: I. Formic acid and formate. *Geochim. Cosmochim. Acta* 67, 3625 - 3644.
- McCullom, T.M., Seewald, J.S., 2003b. Experimental study of the hydrothermal reactivity of organic acids and acid anions: II. Acetic acid, acetate, and valeric acid. *Geochim. Cosmochim. Acta* 67, 3645-3664.
- P.J. Linstrom, P.J., Mallard, W.G., 2022. NIST Chemistry WebBook, NIST Standard Reference Database Number 69. National Institute of Standards and Technology, Gaithersburg MD, 20899 (retrieved February 2, 2022).
- Puigdomenech, I., 2014. MEDUSA, make equilibrium diagrams using sophisticated algorithms, 2 ed. Royal Institute of Technology, School of Chemical Science and Engineering, Stockholm, Sweden.
- Reardon, E.J., 2005. Zerovalent irons: styles of corrosion and inorganic control on hydrogen pressure buildup. *Environmental Science & Technology* 39, 7311-7317.
- Rojo, H., Gaona, D., Rabung, T., Polly, R., Garcia-Gutiérrez, M., Missana, T., Altmaier, M., 2021. Complexation of Nd(III)/Cm(III) with gluconate in alkaline NaCl and CaCl₂ solutions: Solubility, TRLFS and DFT studies. *Applied Geochem.* 126, 104864.
- Senior, N., Newman, R., Wang, S., Diomidis, N., 2017. Understanding and quantifying the anoxic corrosion of carbon steel in a Swiss L/ILW repository environment. *Corr. Eng. Sci. Techn.* 52, 78-83.
- Small, J., 2019. Final Synthesis report for WP1. MIND project deliverable D1.9. Horizon 2020 Project, European Union, Euratom.
- Small, J., Nykyri, M., Helin, M., Hovi, U., Sarlin, T., M., I., 2008. Experimental and modelling investigations of the biogeochemistry of gas production from low and intermediate level radioactive waste. *Applied Geochem.* 23, 1383-1418.
- Smart, N.R., Rance, A.P., Nixon, D.J., Fennell, P.A.H., Reddey, B., Kursten, B., 2017. Summary of studies on the anaerobic corrosion of carbon steel in alkaline media in support of the Belgian supercontainer concept. *Corrosion Engineering, Science and Technology* 52, 217-226.
- Sun, Z.X., Su, F.W., Forsling, W., Samskog, P.O., 1998. Surface characteristics of magnetite in aqueous suspension. *J. Colloid Interf. Sci.* 197, 151-159.
- Tasi, A., Gaona, X., Rabung, T., Fellhauer, D., Rothe, J., Dardenne, K., Lützenkirchen, J., Grivé, M., Colàs, E., Bruno, J., Källström, K., Altmaier, M., Geckeis, H., 2021. Plutonium retention in the isosaccharinate - cement system. *Applied Geochemistry* 126, 104862.
- Van Loon, L.R., Glaus, M.A., Laube, A., Stallone, S., 1999a. Degradation of cellulosic materials under the alkaline conditions of a cementitious repository for low- and intermediate-level radioactive waste. II. Degradation kinetics. *J. Environmental Polymer Degradation* 7, 41-51.
- Van Loon, L.R., Glaus, M.A., Laube, A., Stallone, S., 1999b. Degradation of Cellulosic Materials under the Alkaline Conditions of a Cementitious Repository for Low- and Intermediate Level Radioactive Waste. Part III: Effect of Degradation Products on the Sorption of Radionuclides on Feldspar. *Radiochim. Acta.* 86, 183-199.
- Vercammen, K., 2000. Complexation of Calcium, Thorium and Europium by α -Isosaccharinic Acid under Alkaline Conditions., Dissertation N° 13466, ETH, Zürich, Switzerland.
- Whistler, R.L., BeMiller, J.N., 1963. α -D-isosaccharino-1,4-lactone, action of lime water on lactose, in: M.L. Wolfrom, M.L., J.N. Miller, J.N. (Eds.), *Methods in Carbohydrate Chemistry*. Academic Press, N.Y., USA.

- Wiborgh, M., Höglund, L.O., Pers, K., 1986. Gas Formation in a L/ILW Repository and Gas Transport in the Host Rock, Nagra Technical Report, NTB 85-17, Nagra, Wettingen, Switzerland.
- Wieland, E., 2014. Sorption data base for the cementitious near field of L/ILW and ILW repositories for provisional safety analysis for SGT-E2, Nagra Technical Report. Nagra, Wettingen, Switzerland.
- Wieland, E., Hummel, W., 2015. Formation and stability of ¹⁴C-containing organic compounds in alkaline iron-water systems: preliminary assessment based on a literature survey and thermodynamic modelling. Mineral. Mag. 79, 1275-1286.

The effect of gamma irradiation on cementitious materials with superplasticizers – The Czech contribution

R. Vašíček^{1*}, Z. Hlaváč², P. Večerník³, B. Drtinová⁴, M. Vlk⁴, M. Kučerová¹

¹ Czech Technical University in Prague, Faculty of Civil Engineering, Thákurova 7, 166 29 Prague 6 (Czech Republic)

² Research Centre Řež, s.r.o.; Hlavní 130, Řež, 250 68 Husinec (Czech Republic)

³ ÚJV Řež, a. s., Hlavní 130, Řež, 25068 Husinec (Czech Republic)

⁴ Czech Technical University in Prague, Faculty of Nuclear Sciences and Physical Engineering, Břehová 7, 115 19 Prague 1 (Czech Republic)

* Corresponding author: radek.vasicek@cvut.cz

Abstract

Within Task 3 of EURAD WP3 CORI, the ‘Czech team’ studies the influence of the degradation of organic concrete additives (plasticizers) and organic radioactive waste (e.g. ion exchange resins (IER), sorbents) fixed in the cement matrix on the migration of radionuclides in the cement/concrete environment. Samples are subjected to gradual degradation (radiolysis, hydrolysis, temperature). The main physical properties of the cementitious materials, such as strength, elasticity and, more rarely, hydraulic conductivity, are regularly tested/ monitored to control the evolution of the macroscopic behaviour of the samples. FNSPE CTU and ÚJV Řež have started a study of organic substances behaviour (formate, acetate, EDTA, adipate, and phthalate) in presence of cementitious materials (hydrated cement paste CEM I, witness sample of concrete from L/ILW repository containing CEM III and CSH, both irradiated and fresh) in portlandite water or NaOH solution. FCE CTU is responsible for macroscopic testing. This contribution describes materials, sample preparation / manufacture, and tests performed before and after irradiation of cementitious samples (CEM I paste and “Richard”); status as of autumn 2021. The results of the EURAD WP3 CORI project are applicable not only in the case of the L/ILW Richard repository safety assessment and its possible lifetime extension, but the data obtained will also be used for safety assessment and calculations related to other radioactive waste repositories in the Czech Republic, including the decommissioning waste section in the planned deep repository (concrete containers, structural parts, and fillings).

1 Introduction

The objective of EURAD WP3 CORI is to evaluate the influence of the degradation of organic concrete additives (plasticizers) and organic radioactive waste (e.g., ion exchange resins, sorbents) fixed in the cement matrix on the migration of radionuclides in the cement/concrete environment.

For the Czech Republic, as a "third party of SÚRAO", the departments of two faculties of the Czech Technical University in Prague (Department of Nuclear Chemistry; Faculty of Nuclear Sciences and Physical Engineering (FNSPE CTU) and Centre of Experimental Geotechnics of Faculty of Civil Engineering (FCE CTU)) and ÚJV Řež, a.s. are participating. Research Centre Řež, s.r.o. participates

separately, as a direct member of the consortium. All four participating research groups together with SURAO form the ‘Czech team’.

As planned, CORI Task 3 tests the interaction of organic and cementitious materials by means of sorption experiments. The experiments in Task 3 correspond closely to those in Task 4, which differ only in the presence of radionuclides. Task 3 work also includes tests on the mechanical and transport properties of the samples (pristine and exposed to the degradation procedures "radiolysis" and "temperature"). The connection with Task 2 is realized by the study of the sorption behaviour of degradation products identified in Task 2 in presence of cementitious materials. The studied cementitious materials were mixed with additives in order to improve their properties, i.e. plasticizers, and substances of an organic nature, which may be part of the deposited radioactive waste, such as ion exchangers or sorbents. The study of the sorption of model organic molecules already known as degradation products of more complex organic substances is being carried out as another part of the research.

The greatest attention has so far been paid to the characterization of cementitious materials. Three different types of materials were chosen as representatives of the cement matrices: newly prepared hydrated CEM I cement paste, with or without the addition of plasticizers, witness samples of structural concrete from the Richard repository (15 years old) and pure CSH phase.

This contribution describes materials, sample preparation / manufacture, and tests performed before and after irradiation of cementitious samples (CEM I paste and “Richard” concrete); status as of autumn 2021. Due to the situation of the COVID-19 pandemic, the work on the study of the behaviour of degradation products in the presence of cementitious materials is the most delayed.

2 Materials and samples

In the current course of work, cement matrices and plasticizers are the materials used most. Three different types of materials were selected as representatives of cementitious matrices. This is CEM I fresh hydrated cement paste with or without the addition of ISOLA BV and CX ISOPLAST 531 plasticizers, which was chosen without the addition of plasticizers as a reference material in WP3 CORI, as well as samples of structural concrete from the L/ILW Richard repository (15 years old witness samples), which are used due to the connection of the project with the safety assessment of this repository, and the phase of pure cement CSH, as a representative of a more homogeneous material.

Super/plasticizers, ISOLA BV and CX ISOPLAST 531, were obtained from the concrete plant (CEMEX Czech Republic, s.r.o.) where the concrete mixtures for the treatment and processing of radioactive wastes, which is carried out in ÚJV, are produced (more details can be found in our contribution regarding CORI Task 2 – Večerník et. al., under preparation).

In addition to plasticizers and their degradation products, sorbents and IER’s degradation products and model degradation products are also planned to be studied. However, the identification of degradation products for sorbents and ion exchangers is still ongoing in Task 2. From the group of model molecules, which are (readily) available, these substances are studied at present: EDTA, in the form of disodium salt, Chelaton 3 (Lachema), p.a.; phthalic acid, manufactured by Sigma-Aldrich, with purity $\geq 99.5\%$; adipic acid, manufactured by Sigma-Aldrich, purity $\geq 99.5\%$; formic acid salts – sodium formate (PENTA s.r.o.) and its form $\text{H}^{14}\text{COONa}$ (manufactured by PerkinElmer); acetic acid salts – sodium acetate (PENTA s.r.o.) and its labelled form $\text{CH}_3^{14}\text{COONa}$ (manufactured

by PerkinElmer). The main working concentrations, $5 \cdot 10^{-5}$ and $5 \cdot 10^{-3} \text{ mol} \cdot \text{L}^{-1}$ were selected based on Van Loon & Hummel (1995). The ratio of solid to liquid phase L/S in all sorption experiments has been equal to 100, 250, 500 and $800 \text{ L} \cdot \text{kg}^{-1}$. On average, during the sorption tests, CEM I paste contains 5.34 % moisture, Richard concrete 3.26 % while CSH with Ca/Si = 1 has 64 % water. Most of the parameters under which the sorption experiments take place are common to CORI Tasks 3 and 4.

2.1 Richard concrete samples (CEM III)

These are samples of concretes from the Richard LLW/ILW repository, which were prepared during the reconstruction of the chambers in 2006. SÚRAO delivered two 15 cm cubes of structural concrete on January 13, 2020 (Figure 1; hereafter referred to as "Richard concrete" or "CEM III"). The samples were stored underground at Richard repository until sampling in 1/2020. According to the available information (source SÚRAO; recipe No. 377), the structural concrete is C 30/37 XA2 concrete (with a compressive strength after 28 days of 30 MPa), which was used as concrete for the final floors and walls of the chamber segments. Its formulation (quantity per 1 m^3 of mixture) is given in Table 1. The binder used was CEM III/B 32.5 blast furnace cement. Sample S3P was casted on 5 May 2006 while S3/5R1 on 13 April 2006.

The structural concrete samples supplied were first drilled (2/2020) - four cores of approximately 43 mm diameter were obtained from each cube (Figure 1). Three cores (A, B, both from S3P and E from S3/5R1) were cut into 43 mm high cylinders and used for compressive strength testing (samples A2-4, B2-B4 and E2-4). Cores C, D (both from S3P) and G, H (both from S3/5R1) were transferred to the UJV and core F (from S3/5R1) was retained in the FCE CTU laboratory for hydraulic conductivity test. Parts of the cubes were also given to the co-researchers to prepare crushed material for further testing. The remainder of the material is stored in the FCE CTU sample warehouse at the Josef Underground Laboratory.



Figure 1: Two cubes of structural concrete from the Richard LLW/ILW repository (left) and cores drilled from S3P (right).

Table 1: Recipe for "Richard structural concrete"; No. 377 (source SÚRAO)

	Origin	Quantity
Cement	CEM III/B 32.5 SV	400 kg

Aggregates	0/4 mm Dobříň	895 kg
	8/16 mm Dobkovičky	640 kg
	11/22 mm Dobkovičky	350 kg
Plasticizer	Stachement ML	4 kg
Water		165 kg

2.2 Cement paste samples (CEM I)

The main part of the experimental work on cementitious materials is carried out on samples of cement pastes prepared at the beginning of the CORI project. Portland cement CEM I 42.5 R, CEMEX Prachovice; 4/2020 (hereafter referred to as "CEM I") was used for the mixes.

The CEM I samples were first made without plasticizer - as a reference and then as mixtures with plasticizers. Two types of plasticizers with a slightly different influence on the properties of the concrete mix (see Figure 2) were used. Figure 2 presents relative influence (beneficial from 0) of particular plasticizer on behaviour of cement mix, according to the producer (not directly related to/ measured on the CEM I samples). Samples of different sizes and shapes for the tests (pristine material and after hydrolytic and radiolytic degradation) are, depending on the plasticizer used, labelled C-x (reference without plasticizer) and CLA-x or CST-x (IsoLA/ IsoplaST). For more information on plasticizers, see contribution to CORI Task 2 – Večerník et. al., under prep.). The preparation steps of CEM I (+ plasticizers) samples included (Figure 3):

- filling of moulds in layers; compaction on the compaction table;
- storage in a humid environment for 24 h; unmoulding and storage in water;
- after 26 days cutting and marking the samples;
- initial tests (compressive strength) after 28 days.
- Detailed information on fresh mortar samples is provided in Table 2.

Three types of samples were made from fresh mortars:

- cubes of 50 mm edge length;
- cylinders of two sizes (with height/ diameter 50/50 mm and 84/42 mm) and
- discs with height/ diameter 8/50 mm).

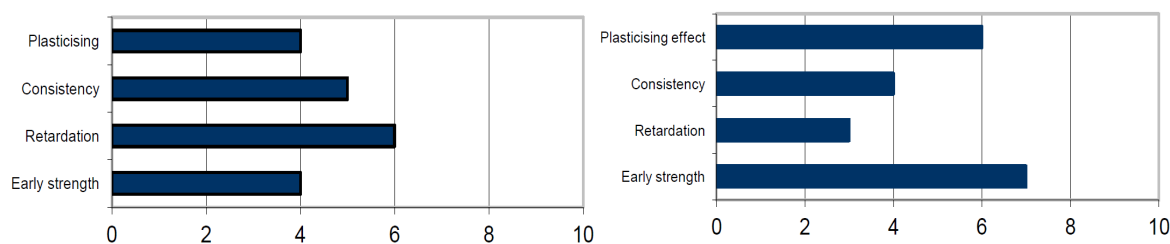


Figure 2: Relative influence (beneficial) on the properties of the concrete mix using ISOLA BV (left) CX ISOPLAST 531 (right) (0 – the least, 10 – the most); data by producer.



Figure 3: Preparation of CEM I paste samples.

Table 2: Fresh cement paste sample data

Material	Date of mixing	Plasticizer /cement	Water reduction	Real w/c	Marking
CEM I (42.5)	27 July 2020	0.0 %	0 %	0.40	C-xxx
CEM I + Isoplast	28 July 2020	1.0 %	30 %	0.28	CST-xxx
CEM I + Isola	29 July; 3 Aug 2020	1.0 %	20 %	0.32	CLA2-xxx

2.3 CORI reference material

The Czech team prepared a reference material (hydrated cement paste) for all CORI partners. After discussion, a recipe for the preparation of cement paste from Czech cement CEM I (CEM I 42.5 R, CEMEX Prachovice) with a water in the water/cement ratio $w/c = 0.45$ was chosen. The result of cement binder mineralogical analysis and its comparison to results of analysed two reference binders are shown in Table 3, and the comparison to certificate values is also shown. Reference cement binders were produced by Verein der Deutschen Zementindustrie, Germany. The measured data are in a good agreement with reference values and confirmed there is no deviation of CEM I 42.5 R, CEMEX Prachovice to standard CEM I binder.

The mixing and filling of cylindrical moulds took place in the laboratories of ÚJV on 14 April 2021. The filled moulds were placed in a box with a humid atmosphere (100% relative humidity). After 5 days (April 19, 2021), the samples were removed from the moulds and were kept under humid

atmosphere in the closed box. On April 22, 2021 (i.e. 8 days after preparation), the samples were cut to the defined size (cylinders with a diameter of 50 mm and a height of 100 or 50 mm). The samples thus prepared were further stored in a humid environment in a closed box. After 33 days of maturation, the samples were sent to CORI partners who were interested in obtaining this type of samples (CIEMAT, ANDRA, CEA, AMPHOS21, RATEN, CSIC, JSI, SCK-CEN).

A sample of CEM I raw cement (CEM I 42.5 R, CEMEX Prachovice) was also sent to CORI partners who were interested (BRGM, CIEMAT, KIT / EMPA, RATEN, CSIC).

Table 3: Reference material - raw CEM I binder analysis

	Cemex Prachovice, CEM I 42.5R	Referenzement VDZ100 (2015-03, CEM I 42.5R)	Reference material VDZ100a (05-2019, CEM I 42.5R)	Referenzement VDZ100 (2015-03, CEM I 42.5R) certificate values	Reference material VDZ100a (05-2019, CEM I 42.5R) certificate values
Alite (M3)	58.0±0.2	58.0±0.2	57.4±0.2	59.0±0.6	59.0
Belite	10.2±0.2	13.0±0.2	12.8±0.2	14.1±0.5	14.1
Brownmillerite	11.2±0.1	10.1±0.1	10.4±0.1	6.9±0.5	6.9
C3A (cub)	4.9±0.1	5.5±0.1	5.1±0.2	5.9±0.3	5.9
C3A (ort)	1.0±0.1	2.4±0.1	2.3±0.2	2.3±0.3	2.3
C3A (sum)	5.9	7.9	7.4	8.3±0.3	8.3
Quartz	0.1±0.0	0.2±0.0	0.1±0.0	0.2±0.1	0.2
Calcite	6.2±0.1	4.8±0.1	4.4±0.1	4.4±0.1	4.4
Gypsum	1.1±0.1	0.2±0.1	0.1±0.1	0.2±0.1	0.2
Bassanite	1.8±0.1	1.4±0.1	1.4±0.1	1.8±0.3	1.8
Anhydrite		2.2±0.1	2.5±0.1	2.6±0.3	2.6
Portlandite	1.9±0.1	1.6±0.1	1.6±0.1	2.0±0.3	1.1
Lime	0.1±0.0	0.1±0.0	0.5±0.0	0.3±0.1	0.3
Periclase	1.9±0.1	0.1±0.0	0.8±0.0	0.1±0.1	0.1
Arcanite	0.9±0.0	0.3±0.1	0.5±0.1	0.3±0.1	0.3
Aphthitalite	0.8±0.1	0.2±0.1	0.1±0.1	0.2±0.1	0.2

2.4 Synthetic CSH phase

CSH phase samples were prepared in the laboratory of the FNSPE CTU according to the procedure of Atkins et al. (1992). Sorption experiments will be carried out in a glove box in N₂ atmosphere. More details can be found in our contribution to CORI Task 4 this research has not been initialized yet.

3 Test plan and methods

3.1 Experimental plan

In addition to sorption experiments, Task 3 also includes tests of mechanical and transport properties of cementitious samples (non-degraded and exposed to degradation procedures "radiolysis"). Testing and use of cementitious samples then consist of both macro-mechanical and transport tests and chemical analyses:

- determination of compressive strength on cylinders (Richard concrete),
- determination of compressive strength by punches on thin discs (CEM Ipastes),
- determination of hydraulic conductivity (CEM I pastes),
- characterization of changes in organic materials, thus, plasticizers,
- interaction/transport of model or identified degradation products (from Task 2) with/through selected cement samples (by sorption/diffusion experiments).

Irradiation details

The irradiation parameters of the hardened cement pastes containing CEM I and Richard concrete samples were as follows:

- requested dose rate of gamma radiation for HCP or concrete $3 \text{ kGy}\cdot\text{h}^{-1}$,
- requested final dose of gamma radiation for HCP or concrete 7 MGy,
- irradiation in an aerobic atmosphere (attendance of oxygen and CO_2),
- no thermal regulation (dependent on outer temperature, in range $12 \div 20 \text{ }^\circ\text{C}$),
- irradiation cell equipped with air conditioning (especially due to ozone O_3).

The HCP samples and Richard concrete samples (Figure 4) were irradiated from September to December 2021. The average dose rate was $3.0 \text{ kGy}\cdot\text{h}^{-1}$, and the samples gained 7 MGy total dose.



Figure 4: HCP and Richard concrete samples in front of the irradiator (left) and dosimetry measurement in the radiation chamber during door closing (right).

3.3 Test methods

Non-destructive testing via the ultrasonic pulse method

The time of the flight of ultrasonic pulses (US) was determined using ultrasonic instrument a PUNDIT PL 200 ultrasonic instrument from the Swiss company Proceq. The short sinus signal of 150 kHz frequency was generated by the ultrasonic instrument and sent through the transducer to the tested sample.

Destructive strength tests

Two types of destructive tests are performed: uniaxial strength test on cylinders and a ‘punch test’ on thin discs. The determination of compressive strength on cylinders ($h/d = 1$) is based on EN 196-1 and EN 1926. At least three samples are tested in one set. The size of 50 mm in diameter and 50 mm in

height is used for fresh mortar samples and 42/42 mm for Richard concrete. Specimens of this size and shape are used because of the following:

- limited availability of source specimens (15 cm cubes) of Richard concrete;
- the equivalence of the diameter of 50-mm specimens and thin specimens (discs) for punch tests for cement pastes;
- 50 mm is a suitable diameter for further tests in the UJV and CVR

The determination of compressive strength with punches on thin specimens follows the test procedure which has been used, e.g. in the CEBAMA project (Vehmas et al., 2020); the specimen is crushed with coaxial punches with a diameter of 7.98 mm. Thin samples, 50 mm in diameter, 8 mm thick are used to maximise the surface area/volume ratio of the sample. They are used only for cement pastes due to the presence of coarse aggregate in the Richard concrete making the evaluation of the results problematic. At least eight discs are tested in one set.

The compressive force at failure can be evaluated; in addition, the relationship to compressive strength can be empirically determined by testing on 50/50 mm cylinders. The evolution of the parameter over time due to interaction/ degradation can be observed by following the evolution of the directly measured quantities (failure force) without introducing further uncertainties due to the use of empirical relationships for the conversion to stress (compressive strength). The deformation values of the specimens can also be deduced from the quantities measured by the testing device (press) (direct measurement is problematic on 8 mm thin specimens). From the ratio of the force increment and the corresponding deformation from the linear part of the test record, the 'rigidity' (kN mm^{-1}) is quantified. It should be pointed out here that this is only an indicative value, although, according to the available results, it helps to give an idea of the evolution of the material. The values of maximum load (kN) and rigidity (kN mm^{-1}) are used for comparison due to the use of non-standard specimen sizes and shapes (especially discs). A potential recalculation to and further use of the well-known terms and values of 'compressive strength' and 'modulus of elasticity' would be problematic and misleading, among other things, due to the necessary introduction of additional uncertainties into the results. Thus, the output of the punch tests here is a pair of values for compressive strength (kN) at failure and 'rigidity' (kN mm^{-1}) which allows evaluation of the parameters in time/ before and after degradation/ irradiation.



Figure 5: A punch test on CEM I HCP discs

Leaching experiments

Leaching experiments are performed in batch reactors, where demineralised water is used as the leaching solution. The studied cementitious materials are crushed and milled. A solid/liquid ratio

(sample weight to solution volume) $S / L = 1/10 \text{ g mL}^{-1}$ is applied. The leaching of the materials is done under common laboratory conditions. In the leachates the presence of organic compounds is determined as the content of total organic carbon (TOC); other parameters determined consisted of the pH, conductivity, main cation, and anion concentrations.

Sorption experiments

Currently, experiments are being carried out in connection with the experiments from CORI Task 4, under the same conditions. First experiments studying the sorption of selected degradation products on hydrated CEM I cement paste and concrete sample containing CEM III were performed and evaluated. Simple organic compounds (formate and acetate) labelled with the radioactive isotope ^{14}C were used for these experiments that overlap in Tasks 3 and 4. The experiments were carried out in a solution of portlandite water (saturated $\text{Ca}(\text{OH})_2$ solution) in an aerobic environment (under normal laboratory conditions) and in an anaerobic environment (in a glove box with an inert atmosphere of argon).

Regarding other model organic molecules, the focus is mainly on EDTA (Figure 6), which is determined chromatographically on the column C-18 (isocratic elution, $1 \text{ mL} \cdot \text{min}^{-1}$, using $0.03 \text{ mol} \cdot \text{l}^{-1}$ acetate buffer, pH 4, prepared according to Bergers & de Groot, 1994). In the concentration range $5 \cdot 10^{-5} \text{ mol} \cdot \text{l}^{-1}$ and lower, a linear calibration curve $y = 231756x$ was obtained, with EDTA eluted at 4 min.

HPLC determination is now optimized for adipate and phthalate.

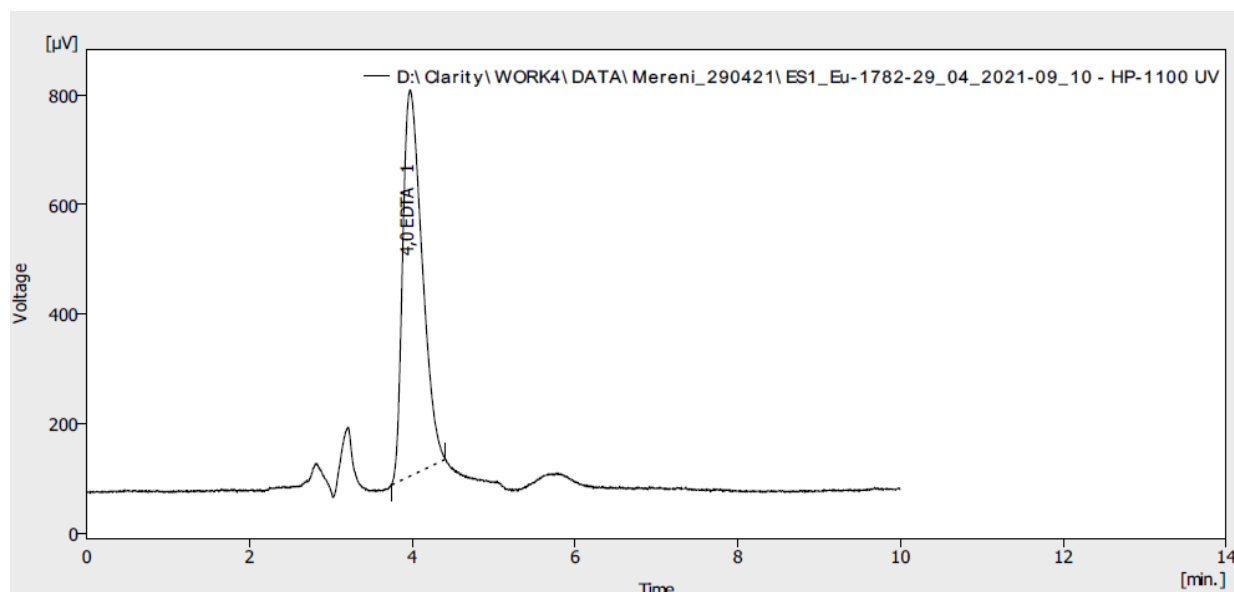


Figure 6: EDTA chromatogram, Bergers & de Groot method (1994).

4 Results

4.1 Compressive strength and rigidity

Compressive tests on cylinders – cement pastes

Cylindrical samples (50/50 mm) made from CEM I cement pastes (C-xxx, CLA2-xxx, CST-xxx) were tested as part of the initial characterization. At least six samples were in each set. The mean values range from 56.4 MPa (C) and 76.1 MPa (CST) to 89.2 MPa (CLA2) of uniaxial strength (Figure 7).

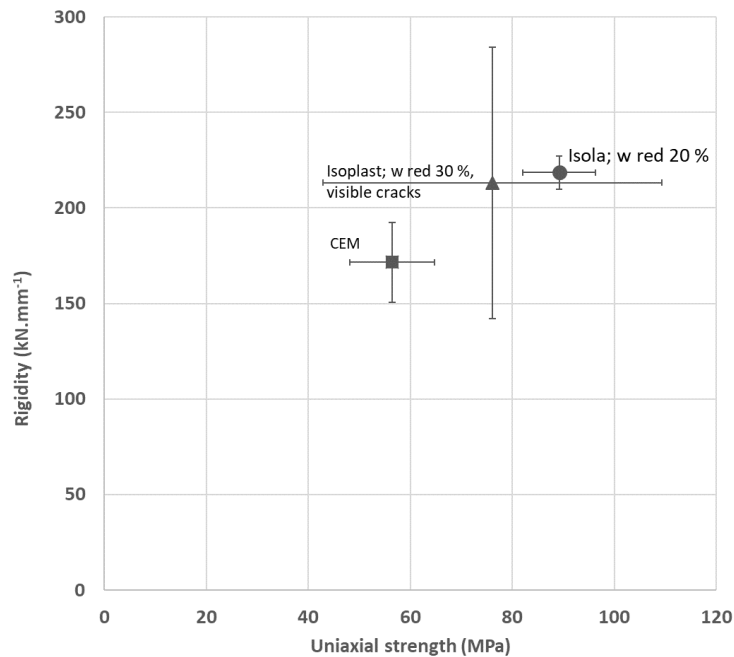


Figure 7: Rigidity and compressive strength on 50/50 mm cylinders made of fresh CEM I cement pastes; initial characterization; mean values of 6-8 samples

In cement pastes, in some cases, visible cracks appeared after hardening. This is evident in the strength test results due to the higher variance of the results - the effect is greatest for the mixture with the Isoplast plasticizer. The lowest average strength (and rigidity) is recorded for the reference material (CEM I), which corresponds to the highest amount of water content during mixing and consequently the lowest bulk density.

Compressive tests on cylinders - Richard concrete

Three cylindrical samples before and four after irradiation were tested. Figure 8 shows the mean values of uniaxial strength and rigidity. The mean value of the uniaxial strength (on 42 mm cylinder) is approximately 62 MPa. The large spread of results is due to the low number of available (and the tested) samples and a high content of large aggregates in relation to sample size. The minor decrease of the mean value after irradiation is, if any, negligible and probably not caused by influence of irradiation (7 MGy) on the material structure (see the section on non-destructive testing).

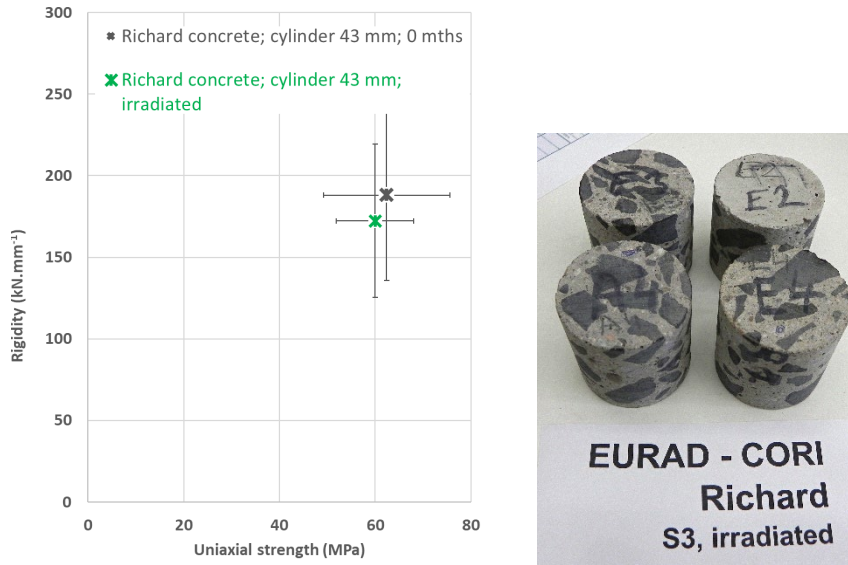


Figure 8: Rigidity and compressive strength of cylinders; input and post-irradiation data for Richard concrete (mean values of 3 and 4 samples) – left; samples after irradiation

Compressive tests with punches on thin specimens of cement pastes

Tests were performed on thin CEM I paste samples before and after irradiation for each material (C, CLA2, CST). Each set contained eight discs. Figure 9 shows the load at failure vs. the dry density of the samples (after irradiation). There is a clear dependence of dry density on water reduction during mixing.

Figure 10 shows the mean values of the load at failure and rigidity (initial in black; irradiated in green). The mean values of the load are between 4.4 to 7.1 kN, where the lower values correspond to CEM I (C-xxx) samples (without superplasticizers, i.e. samples with lowest density). There is no clear nor systematic shift after irradiation.

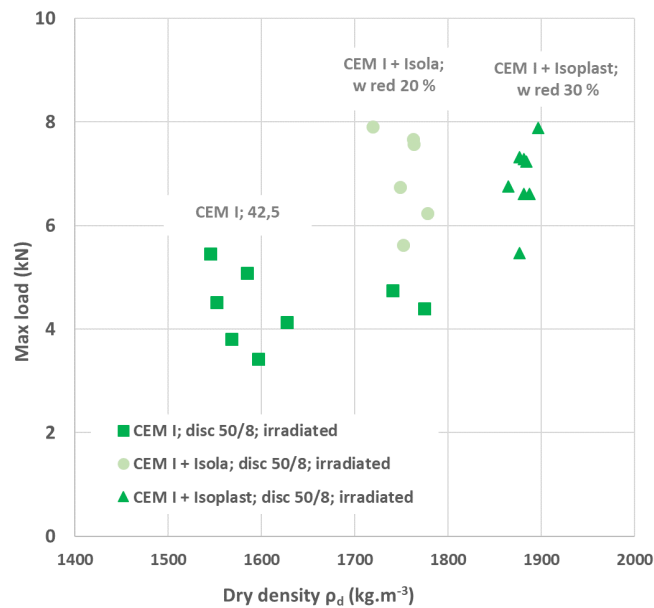


Figure 9: The load at the failure vs. dry density of the thin CEM I paste specimens; post-irradiation

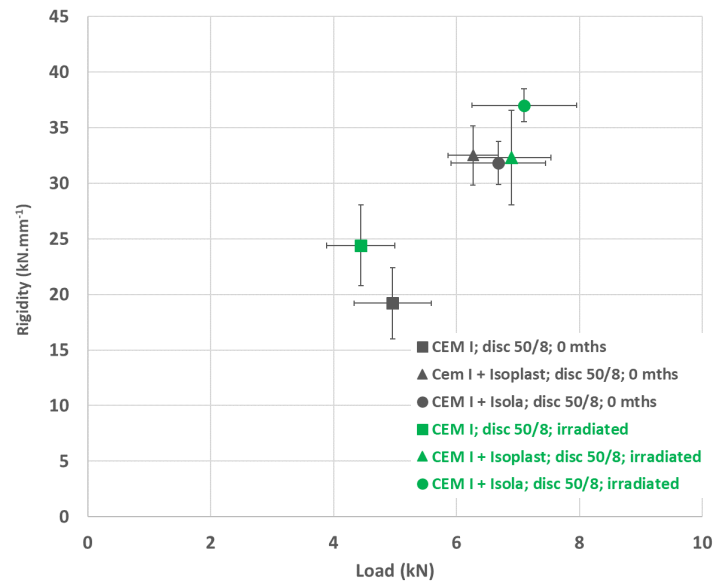


Figure 10: Rigidity vs. force in failure of thin CEM I paste specimens; initial (black) and post-irradiation (green); average values of 8 samples

4.2 Non-destructive testing using the ultrasonic pulse method

The time of flight depends on density and elastic properties of the material of the tested sample. In general, a higher rate of ultrasonic signal means better quality of the test material. The decrease in the propagation rate of the signal may be caused by local and global disturbances in the structure of the test material, such as cracks or microcracks. However, in case of absorbent porous material of concrete type, the time of flight can be also influenced by the current humidity of the test body, as the signal partially passes through water or air in the pores. The measurement method is shown in Figure 11 and Figure 12. Table 4 shows the bulk density, ultrasonic velocity, and dynamic E-modulus of three different types of hardened cement paste discs CEM I, CEM I + Isola BV and CEM I + CX Isoplast 531 before and after irradiation of 7 MGy at a dose rate of 3 kGy.h⁻¹. Figure 13 shows the dynamic E modulus of the 3 hardened cement pastes before and after irradiation. Figure 14 shows the percentage changes of two monitored parameters (density and ultrasonic velocity) for the three types of samples before and after irradiation.



Figure 11: Measurement of the Richard concrete sample using the ultrasonic pulse method (by Pundit PL200).

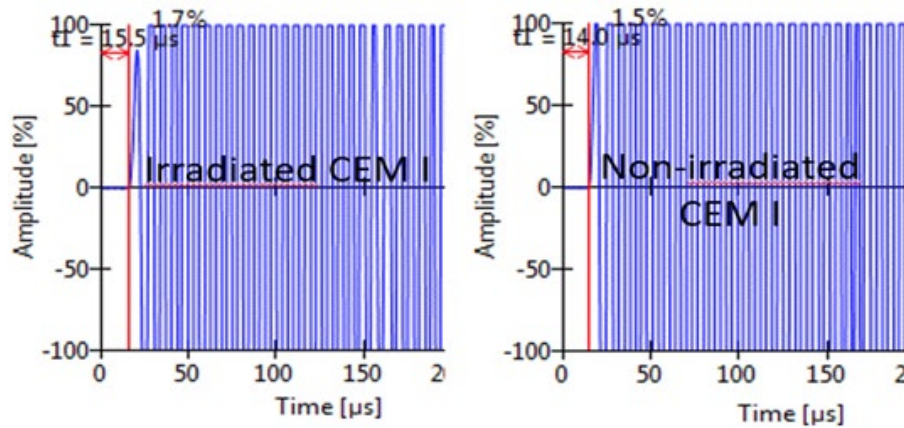


Figure 12: Record of the measurement of HCP CEM I discs by the ultrasonic pulse method.

Table 4: Bulk density, ultrasonic velocity, and dynamic E-modulus of hardened cement pastes (CEM I) before and after gamma irradiation (7 MGy)

Hardened Cement Paste	Density ($\text{g}\cdot\text{cm}^{-3}$)		US velocity ($\text{km}\cdot\text{s}^{-1}$)		Dyn. E-modulus (GPa)	
	Reference	Irradiated	Reference	Irradiated	Reference	Irradiated
CEM I	2.0 ± 0.0	1.7 ± 0.1	3.9 ± 0.1	3.6 ± 0.2	31 ± 2	23 ± 3
CEM I + Isola	2.1 ± 0.0	1.9 ± 0.0	3.9 ± 0.2	3.8 ± 0.0	31 ± 4	28 ± 1
CEM I + Isoplast	2.2 ± 0.0	2.0 ± 0.0	4.2 ± 0.1	4.1 ± 0.1	39 ± 2	34 ± 2

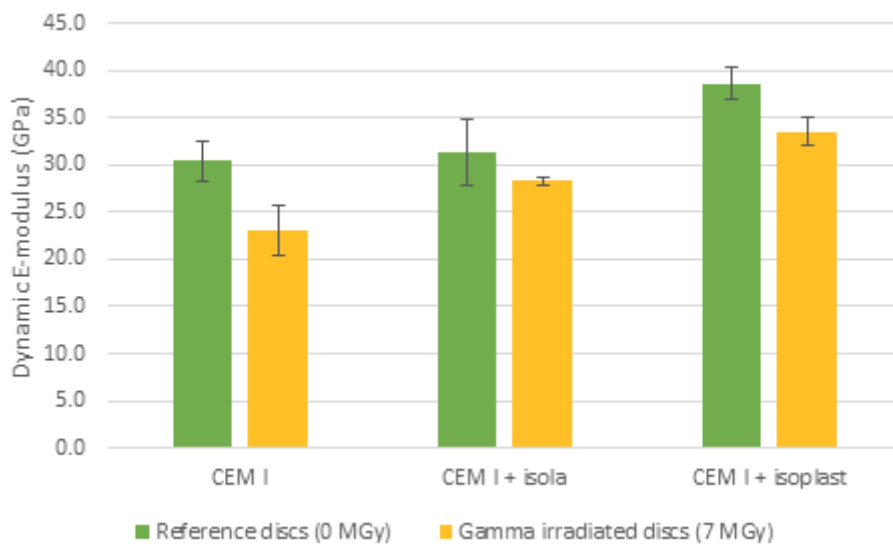


Figure 13: Dynamic E-modulus of CEM I HCP discs determined by the ultrasonic pulse method.

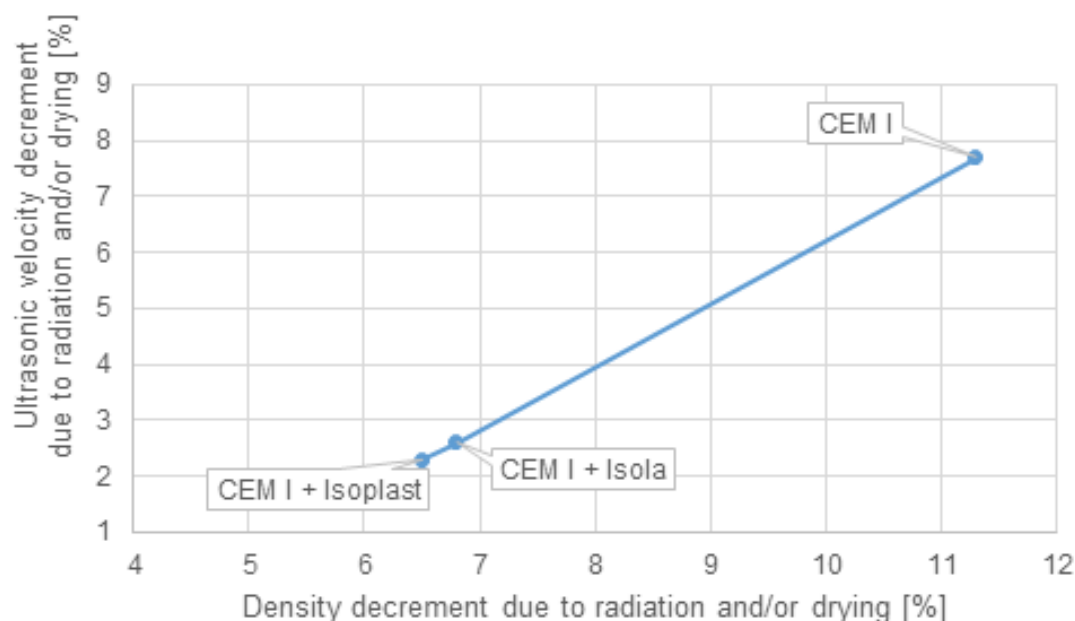


Figure 14: Dependence of density decrease (%) and ultrasonic velocity decrease (%) of hardened cement pastes due to 7 MGy gamma irradiation and/or drying caused by air conditioning.

From the results listed above, several conclusions can be drawn:

- 1) Reference samples from CEM I have lower density (bulk density) than samples with an admixture of superplasticizers (Isola or Isoplast). The CEM I paste contains more pores filled with water, which partially evaporates during irradiation as a result of active air ventilation and partially decomposes by radiolysis into hydrogen and oxygen. Due to this fact, it is possible to observe the greatest reduction in flight time (Figure 12), also in specific density or ultrasonic speed (Table 4 or Figure 14) as well as in dynamic E-modulus (Figure 13).
- 2) Samples with Isoplast superplasticizer show the highest density of the material, highest speed of ultrasonic signal, and the highest E-modulus from all tested samples. This fact is also valid before and after irradiation. It can be said that CEM I + Isoplast forms the group of samples of the highest quality among the three measured hardened cement pastes.
- 3) By visualizing the data, it is clear that the decrease in the ultrasonic velocity in all samples is not caused by damage to the material, e.g., by cracks or some other change in the structure of the hardened cement paste, but due to loss of water by radiolysis or evaporation caused by irradiation and ventilation. The values of velocity decrement and density decrement due to radiation correlate very well with each other (see Figure 14). The positive dependence of the E-modulus and water content is described, for example, in Zhang et al. (2020) or Kazmierczak et al. (2019). On the other hand, the only known authors who reported a decrease in mechanical strength parameters due to lower gamma doses (< 600 kGy) are Vodak et al. (2011). All other authors publish concrete damage thresholds for gamma radiation between 100 and 300 MGy (e.g., Hilsdorf et al. 1987, Kaplan 1989, or Kontani et al. 2013).

4.2 Sorption

During sorption experiments with labelled acetate and formate, it was found that the different environments have no effect on the sorption of acetate on the pure CEM I paste and the R_d for pure CEM III paste is nearly the same. In the case of formate, a slightly higher sorption on the CEM I cement

paste was observed under normal laboratory conditions (Table 5). These values will serve as a reference for comparing the effect of the presence of organic substances (plasticizers and organic degradation products) on the migration (sorption) of tracers on CEM I cement paste.

Table 5: Values of acetate and formate distribution ratios R_d ($\text{ml}\cdot\text{g}^{-1}$) on pure CEM I and CEM III pastes

Organics	Cementitious material	Conditions	$R_d \pm U(y)$ ($\text{ml}\cdot\text{g}^{-1}$)
$\text{H}^{14}\text{COONa}$	CEM I	Aerobic (lab)	2.2 ± 0.1
		Anaerobic (box)	1.8 ± 0.1
$\text{CH}_3^{14}\text{COONa}$		Aerobic (lab)	0.4 ± 0.2
		Anaerobic (box)	0.4 ± 0.1
	CEM III	Aerobic (lab)	0.3 ± 0.1

New set of pure cement paste and cement paste with ISOLA plasticizer (with the same composition as described in the text above) were prepared for comparison of sorption/interaction of ^{14}C -formate tracer behaviour with these materials at laboratory conditions. Comparison of the data shown in **Table 5** and Figure 16 reveals that the different values of R_d are observed for pure cement paste. This is probably caused by material differences prepared at different casting campaigns. This possible material variability and its influence on R_d uncertainties will be evaluated.

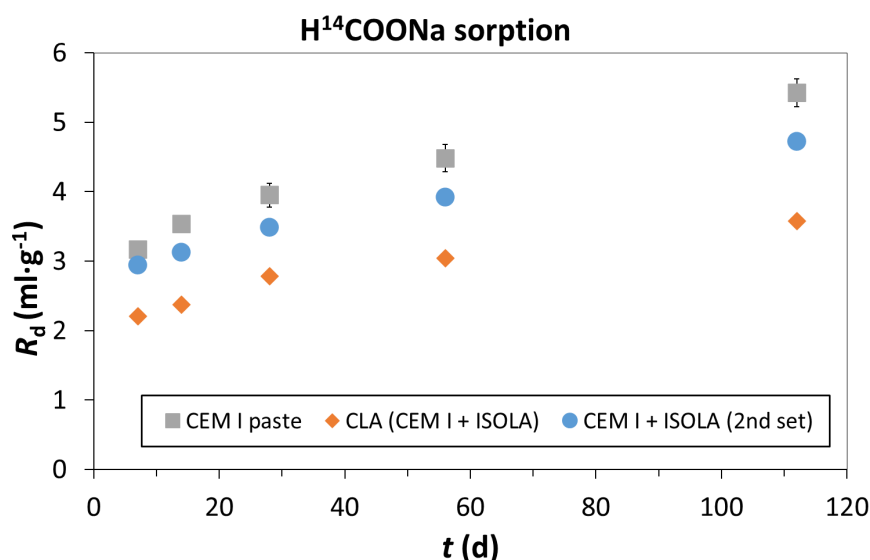


Figure 15: Formate tracer sorption on new set of pure CEM I paste and mixtures with ISOLA plasticizer- long-term kinetics test at laboratory conditions (ongoing up to 6 months)

5 Conclusions

As part of the EURAD WP3 CORI research, samples of organic materials (plasticizers and sorbents), hydrated cement pastes with or without the addition of organic plasticizers, concrete from the L/ILW

repository Richard and pure CSH phases were obtained or prepared. These samples were subjected to degradation procedures (radiolysis, hydrolysis, and temperature).

Samples of CORI reference cementitious material (hydrated CEM I paste) were prepared and subsequently distributed to all interested CORI partners. This material will serve as a common unifying parameter in the overall evaluation of the results achieved by the project participants at the end of the project.

The interaction of simple organic molecules (formate, acetate) with the cementitious materials showed a low distribution ratio, where the acetate R_d values ($0.4 \text{ ml}\cdot\text{g}^{-1}$) are approximately 5 times lower than formate R_d values ($2.2 \text{ ml}\cdot\text{g}^{-1}$).

Destructive strength tests showed uniaxial strength between 56 and 89 MPa for CEM I (+ ISOLA/ISOPLAST superplasticisers) pastes (50 mm cylinders) and approx. 60 MPa for Richard concrete (42 mm cylinders). The tests (both on cylinders and discs) did not reveal a clear macroscopic effect of gamma irradiation (7 MGy) neither on Richard concrete nor on CEM I (+ superplasticisers) pastes.

The non-destructive test results show that exposure to gamma irradiation caused drying and radiolysis of water in hardened cement paste. Part of the drying was caused by air conditioning in the gamma irradiation chamber.

6 Future work

6.1 Strength and hydraulic conductivity test

The sampling of cement pastes from degradation procedures after 12 months occurred in late 2021. The “monitoring” of macroscopic behaviour will continue in these samples. According to the plan, the hydraulic conductivity of the cement paste samples will also be included; the initial characterisation of the number of samples was almost finished.

6.2 Nondestructive testing using the ultrasonic pulse method

Recently, ultrasonic pulse measurement was employed in EURAD WP16 MAGIC, where concrete samples from the Bukov repository are being non-destructively tested. Methodology determined in CORI will be employed there.

6.3 Leaching

Comparison of leachate solution from experiments with pure CEM I cement paste, cement paste with Isola and Isoplast plasticizers and Richard concrete samples is planned – mainly concentrations of dominant elements (Ca, Mg, Na, K, Al, Si,...), pH of the leachate, total organic carbon concentration.

6.4 Sorption

Sorption and diffusion experiments (under the same conditions as in Task 4) with fresh CEM I and Richard concrete, degraded CEM I and Richard concrete, and CSH (reduced plan) have been implemented. The main attention has been paid to the study of EDTA sorption behavior, a slightly reduced range of experiments has been performed with adipate, phtalate, and is planned for degradation products identified in Task 2. The continuation and evaluation of these experiments is ongoing.

Acknowledgement

The EURAD-CORI project leading to this application has received funding from the European Union's Horizon 2020 research and innovation programme under grant agreement no. 847593. The output was created also with the financial participation of SÚRAO (Czech Radioactive Waste Repository Authority) (SO2020-017). This contribution is partially a result of European Regional Development Fund-Project "Centre for Advanced Applied Sciences" (Grant No. CZ.02.1.01/0.0/0.0/16_019/0000778).

References

- Atkins M., Glasser F.P. & Kindness A. (1992). Cement hydrate phases: Solubility at 25 °C. *Cem. Concr. Res.* 22, 241–246.
- Bergers P.J.M. & de Groot A.C. (1994). The analysis of EDTA in water by HPLC, *Water Research* 28, 639-642.
- Hilsdorf H., Kropp J. & Koch H (1978) The effects of nuclear radiation on the mechanical properties of concrete, *ACI SP-55*, 223-251.
- Kaplan M.F. (1989). *Concrete Radiation Shielding: Nuclear Physics, Concrete Properties, Design and Construction*. John Wiley & Sons: NY.
- Kazmierczak, C. d. S., Boaro, J. K. B., Lunardi, M. P., Kulakowski, M. P., & Mancio, M. (2019). Influence of the moisture content on the dynamic modulus of elasticity of concrete made with recycled aggregate. *Ambiente Construído*, 19(2), 79–89. <https://doi.org/10.1590/s1678-86212019000200309>.
- Kontani O., Sawada S., Maruyama I., Takizawa M. & Sato O. (2013) Evaluation of irradiation effects on concrete structure - gamma ray irradiation tests on cement paste, *Proceedings of the ASME 2013 Power Conference*, Power2013-98099.
- Van Loon L. & Hummel W. (1995). The radiolytic and chemical degradation of organic ion exchange resins under alkaline conditions: effect on radionuclide speciation (PSI--95-13). Switzerland.
- Večerník P., Kozempel J., Vlk M., Hlaváč Z., Hybášková M. & Drtinová B., An effect of radiolysis and hydrolysis on superplasticizers and organic sorbents – The Czech contribution. S&T 3rd Annual Workshop EURAD WP CORI. under preparation.
- Vehmas T., Montoya V., Alonso M.C., Vašíček R., Rastrick E., Gaboreau S., Večerník P., Leivo M., et al. (2020). Characterization of Cebama low pH reference concrete and assessment of its alteration with representative waters in radioactive waste repositories. *Applied Geochemistry*, 121 ISSN 0883-2927.
- Vodák F., Vydra V., Trtík K. & Kapičková O. (2011) Effect of gamma irradiation on properties of hardened cement paste, *Mater Struct*, 44, 514, 101-107.
- Zhang G., Li C., Wei H., Wang M., Yang Z. & Gu Y (2020) Influence of Humidity on the Elastic Modulus and Axis Compressive Strength of Concrete in a Water Environment. *Materials* 13(24) 5696. 10.3390/ma13245696

An effect of radiolysis and hydrolysis on superplasticizers and organic sorbents – The Czech contribution

P. Večerník^{*1}, J. Kozempel², M. Vlk², Z. Hlaváč³, M. Hybášková¹, B. Drtinová²

¹ÚJV Řež, a. s.; Hlavní 130, Řež, 25068 Husinec (Czech Republic)

²Czech Technical University in Prague, Faculty of Nuclear Sciences and Physical Engineering; Břehová 7, 115 19 Prague 1 (Czech Republic)

³Research Centre Řež, s.r.o.; Hlavní 130, Řež, 250 68 Husinec (Czech Republic)

* Corresponding author: petr.vecernik@ujv.cz

Abstract

The contribution of the “Czech Team” (Czech technical University in Prague; ÚJV Řež, a. s.; Research Centre Řež, s.r.o.) in the WP3 CORI of EURAD project aims to verify the impact of the degradation of organic compounds used as concrete additives (plasticisers) and organic radioactive wastes (ion exchangers and sorbents) fixed in the cement matrix on the migration of radionuclides in the cement/concrete environment. WP3 CORI is divided into 4 sub-Tasks, of which Tasks 2-4 are dedicated to the experimental research works. The content of Task 2 is to identify products that arise from organic matter present in radioactive waste storage sites during degradation processes, such as radiolysis or hydrolysis, in a highly alkaline environment that is characteristic for cement matrices.

For experimental works two types of plasticizers (ISOLA BV and CX ISOPLAST 531) and AMERLITE MB20 ion exchange resin and PAN (polyacrylonitrile) sorbents were selected. The results of Task 2 will be applied in Task 3, which is focused on studies of the migration behaviour of degradation products identified in Task 2 and also model ones in the presence of cementitious materials, and in Task 4, which is studying the behaviour of selected radionuclides in the systems defined in Task 3.

1 Introduction

The aim of WP3 CORI is to verify the influence of the degradation of organic concrete additives (plasticizers) and organic radioactive wastes (e. g. ion exchangers, sorbents) fixed in the cement matrix on the migration of radionuclides in the cement/concrete environment.

The following organic materials were selected by the Czech team for the research within Task 2: (super)plasticizers ISOLA BV and CX ISOPLAST 531 as a representatives of organic substances present directly in the concretes applied in radioactive waste management, sorbents based on polyacrylonitrile – PAN (pure PAN, AMP-PAN and KNiFC-PAN) and ion exchange resin AMBERLITE MB20, which are or can be part of stored RAW.

The results of the EURAD WP3 CORI project will support the L/ILW repository Richard safety assessment, calculations and possible lifetime extension. The data obtained will also be applicable for safety assessment and calculations related to other radioactive waste repositories in the Czech Republic (concrete containers, structures and fillings).

2 Materials and samples

2.1 (Super)Plasticizers

Two types of (super)plasticizers, ISOLA BV and CX ISOPLAST 531, were obtained from the concrete plant (CEMEX Czech Republic, s.r.o.) where the concrete mixtures for radioactive wastes treatment and processing, which is carried out in ÚJV, are produced. Approximately 1 liter of material from each was obtained from the stocks of plasticizers used by the concrete plant.

ISOLA BV (hereinafter "ISOLA") is a lignosulfonate based plasticizer for summer season use with a good plasticizing and homogenizing effect and a slightly retarding effect dependent on cement and meets the requirements of EN 934-2 standards. Parameters according to the manufacturer:

- pH: 4.5 ± 1.0
- density (20 °C): $1.17 \pm 0.03 \text{ g}\cdot\text{cm}^{-3}$
- Cl content: $\leq 0.10 \text{ mol. \%}$
- Na₂O equivalent: $\leq 2.50 \text{ mol. \%}$
- colour and condition: brown liquid
- recommended dosage: 0.2–1.5 mol. % by weight of cement

The influence on the properties of the concrete mixture declared by the manufacturer is shown in Figure 1.

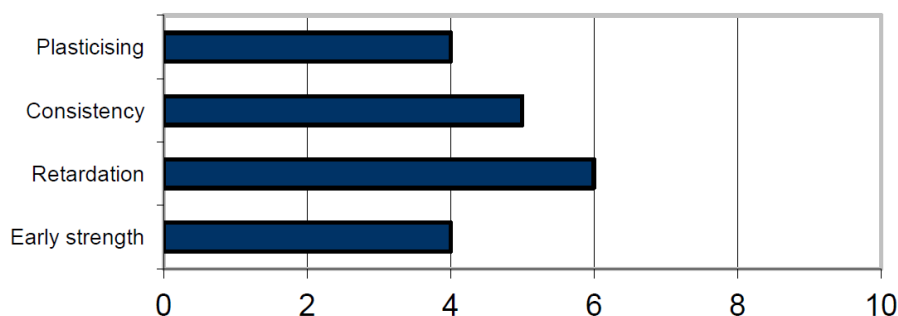


Figure 1: Influence on the properties of the concrete mix when using ISOLA BV (0 – the least, 10 – the most)

CX ISOPLAST 531 (hereinafter "ISOPLAST") is a superplasticizer for winter use based on polycarboxylic ether and lignosulfonate with a strong plasticizing and homogenizing effect, with accelerated onset depending on cement and extended retention of workability, meets the requirements of EN 934- 2 standards. Parameters according to the manufacturer:

- density (20 ° C): $1.03 \pm 0.03 \text{ g}\cdot\text{cm}^{-3}$
- Cl content: $\leq 0.10 \text{ mol. \%}$
- Na₂O equivalent: $\leq 1.50 \text{ mol. \%}$
- colour and condition: brown liquid
- recommended dosage: 0.2–2.0 mol. % by weight of cement
- pH value: manufacturer does not state; determined in the laboratory: 2.7

The influence on the properties of the concrete mixture declared by the manufacturer is shown in Figure 2.

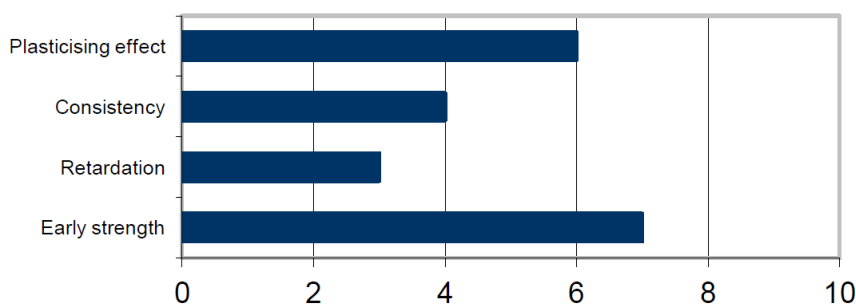


Figure 2: Influence on the properties of the concrete mix when using CX ISOPLAST 531 (0 – the least, 10 – the most)

2.2 Sorbents and ion exchange resins

Two types of materials are studied: commercially available ion exchange resin AMBERLITE MB20 and laboratory prepared polyacrylonitrile (PAN) sorbents. In the case of this group of substances, they are also referred to in the text by the collective name "sorbents".

Parameters of AMBERLITE resin according to the manufacturer:

- skeleton: styrene-DVB
- type: mixed
- ionic form: H⁺/OH⁻
- bulk density: 730 g·L⁻¹
- maximum temperature: 60 °C

Parameters of polyacrylonitrile (PAN) sorbents:

- polyacrylonitrile resins
- prepared in the laboratory of the FNSPE CTU
- PAN (pH = 6.24), AMP-PAN (pH = 0.41), KNiFC-PAN (pH = 6.32)
- sphere size: 0.3–0.8 mm

2.3 Samples for radiolysis and hydrolysis degradation studies

Samples for the radiolytic and hydrolytic degradation studies were prepared in an almost identical manner in the laboratories of the Department of Nuclear Chemistry, FNSPE CTU and ÚJV. The biggest difference was the use of different irradiation ampoules, the selection of which was very limited due to the planned high doses during irradiation (up to 12 MGy) and the impossibility of using vials/ampoules made of organic materials. Thin-walled glass ampoules with a volume of 10 mL were used by the FNSPE, sealed by melting of the glass in flame (Figure 3). There was concern that this type of ampoules would not become too brittle when exposed to high doses, which would certainly lead to loss of the sample. Another unknown was the increase of the pressure inside the ampoules due to gaseous radiolysis products. However, it turned out that the ampoules can withstand all applied doses. However, the ampoules must be opened very carefully and therefore were frozen before opening. The advantage of using these ampoules is that the sample remains intact until its analysis and cannot be contaminated with any cap material. Alternatively, it was possible to irradiate the samples in thick-walled glass vials/vessels of larger volume (20 or 50 mL), from which samples could be taken sequentially. However, these vials/vessels are often closed with a plastic cap (e. g. polypropylene), which is unsuitable for use in the irradiation facility, because radiation degrades the plastic and could

contaminate the sample. In ÚJV the use of thick-walled glass crimp vials with a volume of 20 mL with aluminum caps with a combined silicone/teflon seal was chosen as a variant solution (Figure 3). These crimp vials have been successfully used for irradiation in other projects solved by ÚJV, but at lower total doses. The use of different sample vials was therefore chosen as a compromise due to the ambiguities described above with their resistance to exposure to the planned dose of up to 12 MGy.

For PAN materials which have to be filled into the thin-walled glass ampoules (volume of 10 mL) with the thin input neck the following procedure was applied: sorbent with original solution was infilled into the ampoule by plastic pipette, then the solution was removed by syringe with stainless steel needle. After the control of the sorbent weight, the original solution was added in the volume (mL) amount corresponding to the value of the half of the wet sorbent weight (g). This procedure was repeated even with the addition of strongly alkaline or strongly acidic solutions (for studies of hydrolysis). The use of wet sorbents was preferred in this case instead of using the dried materials in order to avoid osmotic shock which could damage the dry sorbent material and distort the experimental results. It should be noted that sorbents, although having the same skeleton and bead size, are also significantly different in moisture content. Drying to constant weight at 60 °C showed that PAN contained 89.7% of water, AMP-PAN half the content (48.2%) and the least moisture was in the KNiFC-PAN sorbent (2.7%).

The complexity of sample preparation was reflected not only in the above discussed issue of ampoule material selection, but it was also necessary to solve a process of labeling of samples that will not be degraded by radiation (using a marker) in combination with browning of the glass. Finally, metal “dog tags” with embossed identification of each sample were used. The samples were prepared in laboratory under common conditions in air atmosphere, but after sealing or closing of the ampoules, they become closed systems and the oxygen content that could react with the studied substances was thus limited.



Figure 3 : Sealing of glass ampoules (left) and a crimp vial (right) with samples for radiolysis and hydrolysis

The most problematic step during the preparation of samples was alkalization of several organic substances with too low original pH values. These were samples of both plasticizers and AMP-PAN, whose initial pH is even 0.41. The original plan to use the solutions must have been changed because the addition of 0.1 mol·L⁻¹ NaOH and especially Ca(OH)₂, the maximum concentration of which in relation to the solubility limit is approximately 0.02 mol·L⁻¹ under laboratory conditions, was not sufficient to achieve the required pH value. Therefore, the pH of the plasticizers, which are in the form

of solutions, was adjusted to pH value about 12.5 by the addition of solid NaOH or Ca(OH)₂. For example, in the case of ISOPLAST with a starting pH = 2.7, the resulting NaOH solution contained 0.31 mol·L⁻¹ (0.174 g solid NaOH was added to 14 mL of ISOPLAST) and the achieved pH was 12.4. In the case of Ca(OH)₂, a slightly different approach was chosen due to its limited solubility. Excess solid Ca(OH)₂ was mixed with plasticizer, the dispersion system was stirred with a magnetic stirrer for 24 hours, and the undissolved part of Ca(OH)₂ was separated by centrifugation before pipetting an appropriate volume of solution into ampoules. The pH on these samples reached approximately the value of 12.

In case of sorbent materials (PAN, AMBERLITE) the procedure with addition of solutions of NaOH and Ca(OH)₂ solutions was applied. In case of strongly acid AMP-PAN, the degradation was observed immediately after the addition of alkaline solution (yellow sorbent beads discolor immediately to white and after a few days the beads disintegrate into smaller particles) and this set was thus excluded from the study of radiolytic degradation. The samples were prepared for study of the hydrolysis in alkaline environment only.

The list of samples prepared for radiolysis and/or hydrolysis at different initial conditions is described in Table 1.

Table 1: Samples of materials prepared for radiolytic and/or hydrolytic degradation studies

material	conditioning
ISOLA BV	original solution
	dried
	with addition of solid Ca(OH) ₂
	with addition of 0.1 mol·L ⁻¹ NaOH
	with addition of solid NaOH
CX ISOPLAST 531	original solution
	with addition of solid Ca(OH) ₂
	with addition of solid NaOH
AMBERLITE MB20	original, wet
	dried
	original, with addition of 0.02 mol·L ⁻¹ Ca(OH) ₂
	original, with addition of 0.1 mol·L ⁻¹ NaOH
PAN, AMP-PAN, KNiFC-PAN	original, in original solution
	original, with addition of 0.02 mol·L ⁻¹ Ca(OH) ₂
	original, with addition of 0.1 mol·L ⁻¹ NaOH
	original, with addition of 0.1 mol·L ⁻¹ HNO ₃

3 Test plan and methods

3.1 Experimental plan - radiolysis

Samples of plasticizers and sorbent materials were prepared as described in chapter 2.3. Sampling after the irradiation was planned at reached doses of 0.5; 1; 2; 4 and 8 MGy in the case of plasticizers and at reached doses of 1; 2; 4; 8 and 12 MGy in the case of sorbents. Specifications of irradiation procedure are described in chapter 3.3.

3.2 Experimental plan - hydrolysis

Samples of plasticizers and sorbent materials were prepared as described in chapter 2.3. Ampoules with samples for hydrolysis experiments are placed in the laboratory under common laboratory conditions. In addition, the samples of ISOLA plasticizer are degraded by hydrolysis in alkaline conditions at increased temperature of 60 °C. The sampling of the materials is continuous with focus on main sampling campaign at the longest possible period of time according to project schedule.

3.3 Irradiation

Parameters of irradiation

- Irradiation of cement-based materials as well as organic compounds
- Requested dose rate of gamma radiation for liquid organic samples 1–1.5 kGy · h⁻¹ (for hardened cement pastes or concrete 3 kGy·h⁻¹)
- Requested final dose of gamma radiation for liquid organic samples 0.5–12 MGy (for hardened cement pastes or concrete 7 MGy)
- Irradiation in aerobic atmosphere (attendance of oxygen and CO₂)
- Irradiation cell equipped by air-conditioning (especially because of ozone O₃)
- No thermal regulation (dependent on outer temperature, in range 12–20 °C)

Irradiation experiment specification

Liquid organic samples have been irradiated since July 2020 until January 2022. Single sets of samples have been taken out of the irradiator after 0.5, 1.0, 2.0, 4.0, 8.0 and 12 MGy as shown in Table 2. Average dose rate between July 2020 and December 2020 was 1.25 kGy·h⁻¹, samples gained 4 MGy. Samples were moved on a side of irradiator within the period from January 2021 to June 2021, so that the dose rate sank to 0.5 kGy·h⁻¹ and gained 2 MGy more. Cumulative dose of 8 MGy was reached in beginning of August 2021 thanks to dose rate 1.75 kGy·h⁻¹. Final dose 12 MGy was reached in the end of October 2021. Four additional campaigns were performed in 2021.

Table 2: Average doses and dose rates of irradiation of liquid organic samples

Dose\month	VII.20	VIII.20	IX.20	X.20	XI.20	XII.20	I.21	II.21	III.21	IV.21	V.21	VI.21	VII.21	VIII.21	IX.21	X.21	XI.21	XII.21		
0.5 MGy	1.5 kGy/h																			
1.0 MGy	1.5 kGy/h																			
2.0 MGy	1.5 kGy/h																			
4.0 MGy	1.5 kGy/h																			
8.0 MGy	1.5 kGy/h				0.5 kGy/h				1.75 kGy/h											
12.0 MGy	1.5 kGy/h				0.5 kGy/h				1.75 kGy/h											
4.0 MGy													1.75 kGy/h							
4.0 MGy																	1.75 kGy/h			

3.4 Analytical methods

For characterisation of organic compounds presented in the samples after radiolysis and hydrolysis following analytical methods and techniques are planned/were used: HRMS (high resolution mass spectrometry), FT-IR (Fourier-transform infrared spectroscopy), HPLC (high performance liquid chromatography), UV/VIS (ultraviolet–visible) spectroscopy, refractometry, TGA (thermogravimetric analysis).

Infrared spectroscopy

IR spectra are measured on a NICOLET iS50 FT-IR spectrometer in the mid-infrared region, the range of the spectrum is 4000 to 400 cm⁻¹. The ATR, diamond crystal measurement technique is used. The spectra are processed in the OMNIC 9 programme.

Mass spectrometry

The mass spectrum is measured on an Exactive Plus Orbitrap mass spectrometer with ESI ionization technique (voltage 4.5 kV, resolution 100,000 @ 1 Hz, capillary temperature 300 °C, probe temperature 30–40 °C). The XcaliburTM 2.1 SW program is used for evaluation.

Liquid chromatography

The high-performance liquid chromatography apparatus consists of two pumps SDS20 and 30 connected by a dynamic mixer and an AS1000 automatic injector with a Reprisil C18 column (5 × 250 mm, 5 µm). The device is equipped with UV/VIS detection with variable wavelength. The analyzes are performed at a wavelength of 254 nm and the flow rate of the mobile phase was set to 1.0 ml·min⁻¹ (pressure 70 bar).

Thermogravimetry

Thermogravimetric analysis with evolved gas analysis by mass spectrometry was performed on SetSys Evolution’s apparatus. The weight of the measured samples was approximately 10 mg. Thermal

degradations of plasticizer were studied under an argon atmosphere (flow of 60 mL·min⁻¹) in α -Al₂O₃ crucible. The heating rate was set to 10 °C·min⁻¹ in the temperature range of 30–600 °C. Gases that evolved during heating were analysed with quadrupole mass spectrometer QMG 700 (Pfeiffer Vacuum, DEU) connected to a thermal analyser through SuperSonic System (Setaram, FRA). In mass spectrometry the different fragments of various molecular weight were observed. Evaluation was focused mainly on specific fragments corresponding to carbon dioxide, formate and acetate as expected dominant degradation products.

4 Results

4.1 ISOLA plasticizer

Basic characterizations of the ISOLA plasticizer using liquid chromatography with mass spectrometry were performed. The input forms for these basic characterizations were original ISOLA plasticizer (Figure 4), dried plasticizer and sample conditioned by Ca(OH)₂ and hydrolysed. The samples were diluted 1000x with a water/methanol mixture in a ratio of 1:1, at higher dilutions the signals were not intense enough. The measurements were performed in positive mode. Higher signal intensities in the initial parts of the spectrum can be observed in the affected samples (drying, addition of calcium hydroxide), which indicates the detection of a larger amount of lower molecular weight substances (that means expected degradation products), but the obtained data must be further evaluated in more detail.

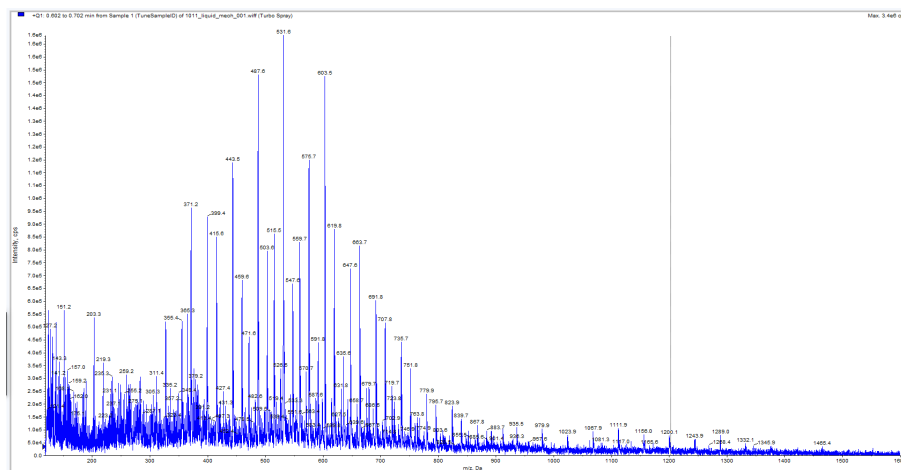


Figure 4: Mass spectrum of original ISOLA plasticizer

The results of simultaneously performed thermogravimetry (TG) and differential thermal analysis (DTA) supplemented with mass spectrometry (MS) identification of evolved gases and substances can be used for comparison of original and degraded materials. These methods are used for characterization of different mixtures of cements and plasticizers or leachates (Angelescu et al., 2016; Gad et al., 2018; Guérandel et al., 2011; Sun et al., 2014; Yilmaz et al., 1993), in general could be applied for comparison of plasticizers at initial conditions and in degraded states directly. The initial idea was to compare the initial and degraded ISOLA superplasticizer as a real material and defined chemical substance – calcium lignosulfonate because ISOLA is a lignosulfonate-based plasticizer. The first comparison of the ISOLA

plasticizer and powdered calcium salt of liginosulfonic acid (CAS No.: 8061-52-7, ROTH) can be seen in following figures. The comparison of TG/DTA and MS of original ISOLA and calcium liginosulfonate is presented in Figure 5. A lot of low molecular weight compound were detected by mass spectrometry analysis during thermal treatment of TG/DTA analysis. It is expected that these low molecular weight compounds (carbonates, acetate, formate etc.) are produced during the superplasticizer degradation. For initial comparison of original, dried/powdered and hydrolysed ISOLA (with Ca(OH)₂ addition; for one year at 60 °C) by thermogravimetric analysis TG/DTA and MS records are presented in Figure 6 and selected signals for CO₂, formate/formic acid, acetate/acetic acid are in detail showed in Figure 7. As can be seen for the carbon dioxide, its release is observed in the range of 200–500 °C for all three studied samples, but for the hydrolysed sample the release of CO₂ was perceptible also at 100–130 °C (see Figure 7). That can be caused by degradation of ISOLA during hydrolysis at temperature 60 °C. When comparing the analysis of formate fragments during the thermal analysis, it can be observed, that the release occurred in the two temperature intervals, 60–180 and 300–420 °C. Original ISOLA released formate in both temperature intervals, while hydrolysed material only at the lower temperatures, but dried material only in higher temperature interval (see Figure 7). That means, the drying process and the hydrolysis (at 60 °C in alkaline conditions in the presence of Ca(OH)₂) causes the changes of the ISOLA plasticizer. When comparing the analysis of acetate fragments during the thermal analysis, it can be observed, that the main release occurred in the temperature interval 250–500 °C. As can be seen in the Figure 7, there is a significant decrease in the MS intensity signal for hydrolysed sample in comparison to original or dried ISOLA samples. That could be explained as the degradation of plasticizer in alkaline conditions in the presence of Ca(OH)₂ at 60 °C. For following comparison with other samples obtained data needed to be evaluated in detail.

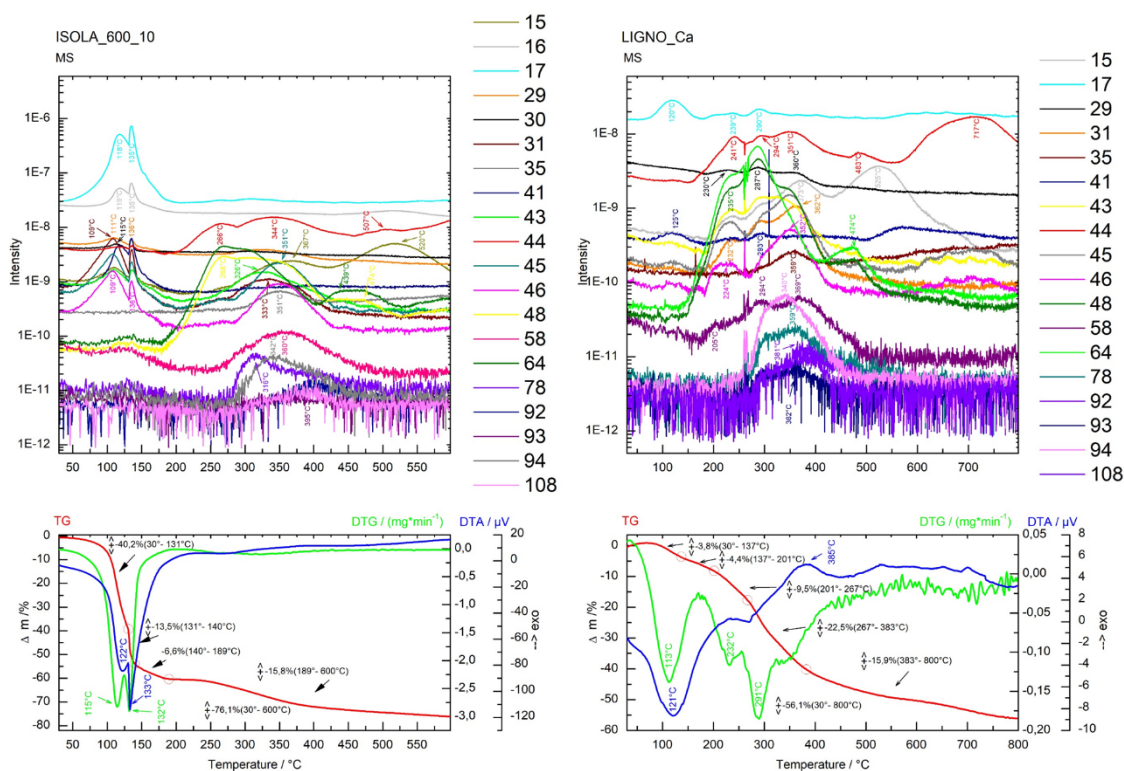


Figure 5: The comparison of TG/DTA and MS of original ISOLA plasticizer (left) and calcium liginosulfonate (right). Mass spectra for different low molecular weight compounds (15-108) recorded during TG/DTA are shown in upper figures.

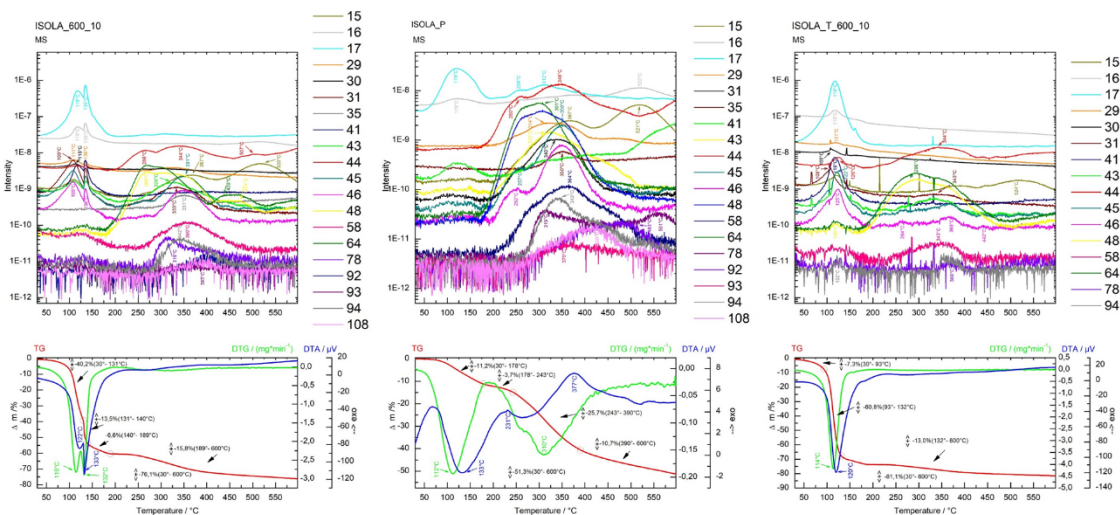


Figure 6: Comparison of ISOLA plasticizer as original (left), dried/powdered (middle) and hydrolysed at 60 °C (right) materials by TG/DTA and MS analysis. Mass spectra for different low molecular weight compounds (15-108) recorded during TG/DTA are shown in upper figures.

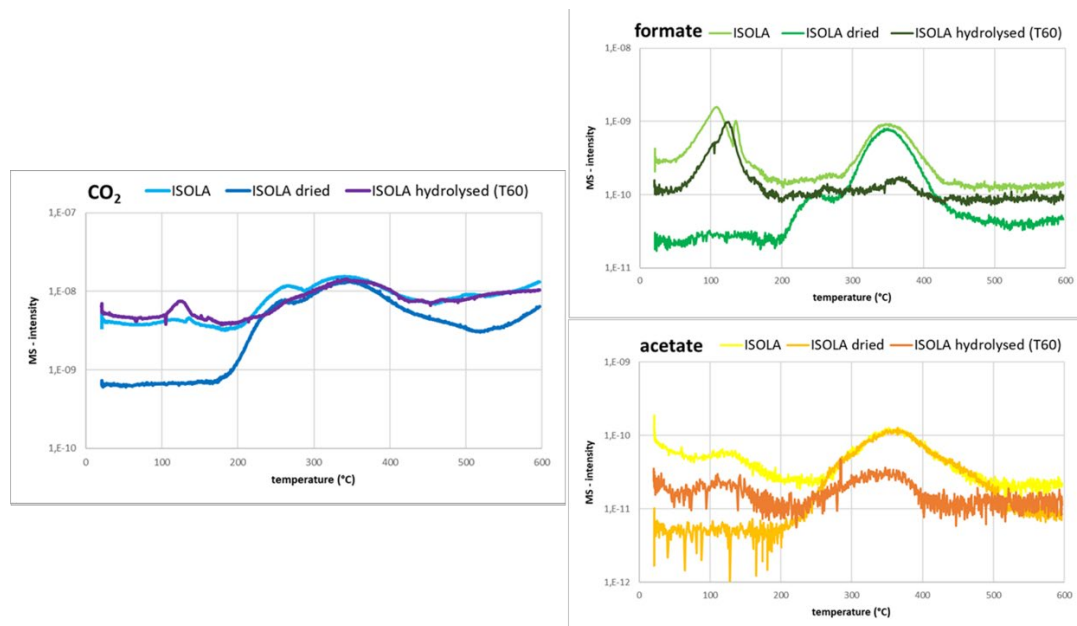


Figure 7: Comparison of original, dried and hydrolysed ISOLA by thermogravimetric analysis; selected signals for CO₂, formate/formic acid and acetate/acetic acid

We are expecting that these TG/DTA and MS analyses will help reveal the formation of degradation products, and by detailed evaluation of the data it will be possible to compare the extent to which the degradation of the superplasticizer material occurs and to identify the chemical composition of the

degradation products. The confirmation of degradation products composition will be combined using other methods.

4.2 CX ISOPLAST 531 plasticizer

Basic characterizations of the CX ISOPLAST 531 plasticizer using liquid chromatography with mass spectrometry were performed. The input forms for these basic characterizations were untreated plasticizer CX ISOPLAST 531 (Figure 8). The samples were diluted 1000x with a water/methanol mixture in a ratio of 1: 1, at higher dilutions the signals were not intense enough. The measurements were performed in positive mode. In the affected samples (drying, addition of calcium hydroxide) it is possible to observe higher signal intensities in the initial parts of the spectrum, which indicates the detection of a larger amount of substances with lower molecular weight (i.e. expected degradation products). Several additional peaks were also observed which may indicate “cross-linked” products of hydrolyzed and irradiated product of the plasticizers. Gel-like products together with significant turbidity increase/ cross-linking was observed, both under irradiation and hydrolysis conditions.

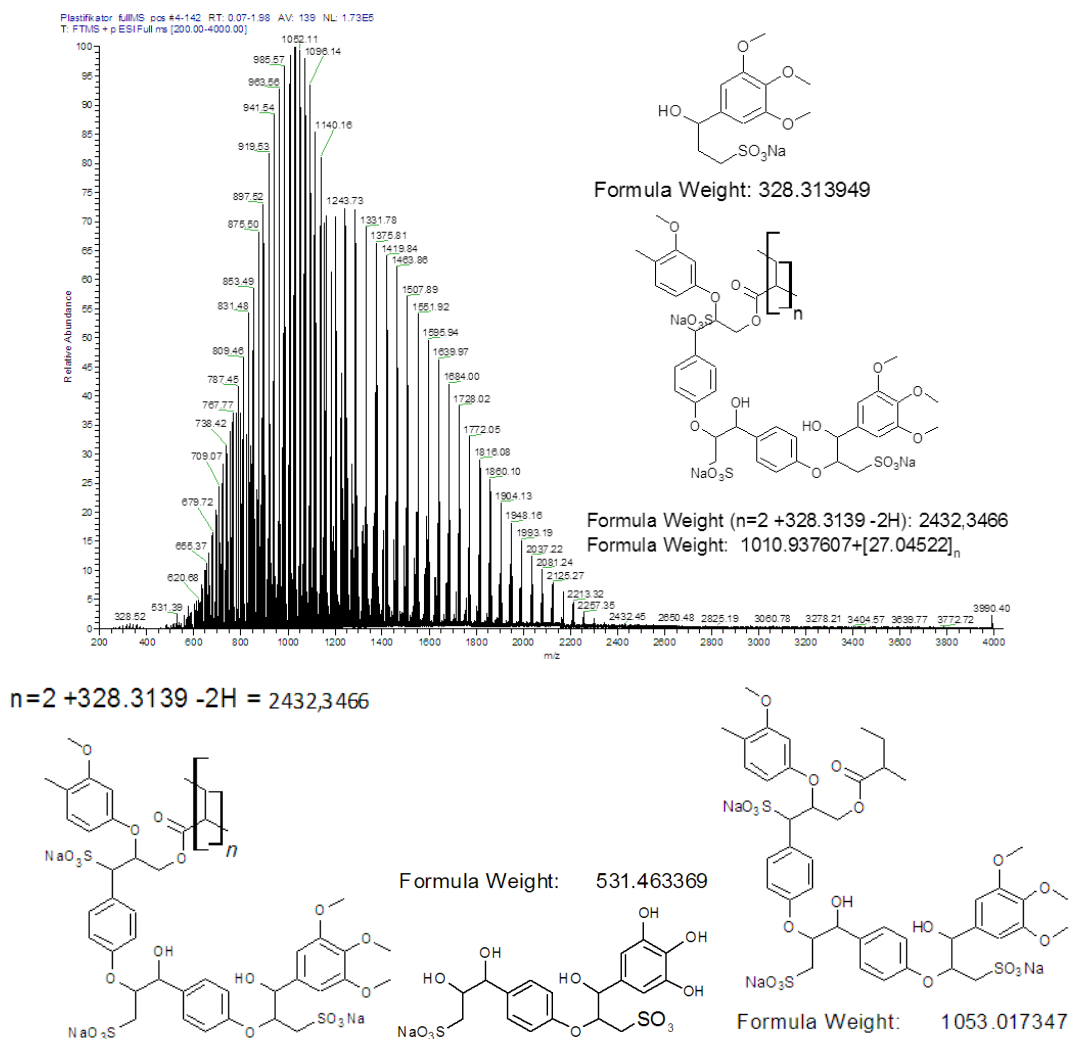


Figure 8: HR mass spectrum of CX ISOPLAST 531 superplasticizer with some of the identified fragments.

4.3 AMBERLITE resin

AMBERLITE ion exchange resin was irradiated according to experimental irradiation plan, samples are still under analysis and evaluation. In addition, the degradation process by digestion using solutions of hydrogen peroxide and iron/copper sulphate was tested to compare the released degradation products. The degradation procedure according to the literature (Walling et al., 2021) was tested and should result to total degradation (with production of CO₂ and H₂O) or release of organic molecules (such as formic, oxalic, acetic acids etc.).

4.4 PAN sorbents

Basic conditions of hydrolysis were studied in 0.1 mol·L⁻¹ solution of sodium hydroxide. The progress of the hydrolysis was monitored with MS and FT-IR spectra. In HRMS spectra were identified fragments of intramolecular cyclisation which corresponds to the transformation of nitrile groups to amide and imine products. Aliquot 100 µL was poured into 1 mL of methanol and measured on ESI. In both ionisation modes were identified products of hydrolysis with lower molecular weight. As a product of hydrolysis 2-hydroxypentanedionic acid (MW 148.03 Da) was identified as [M+H]⁺ at m/z 149.1325 Da. Also, intramolecular fragment of hydrolysis was observed at m/z 338.3413 Da in positive mode of ionisation. The basic/acidic hydrolysis proceeds via intermediates (-C=N) and amide (-CONH₂) and leads to the formation of a carboxyl functional group (-COOH). The presence of intermediates in the reaction mixture is manifested by characteristic vibration bands in the infrared spectrum of the examined samples. The hydrolysed samples show a characteristic decrease in the intensity of the band around 1455 cm⁻¹, which can be assigned to the nitrile functional group in polyacrylonitrile. This is also related to the decrease in the valence vibration intensity of the nitrile group at 2250 cm⁻¹. The bands around 1565 cm⁻¹ correspond to the vibrations -COO⁻ or alternatively -CONH₂. The wide intense band at the wavelength of 1637 cm⁻¹ corresponds to the vibrations of the intermediate with the functional group -C=NH.

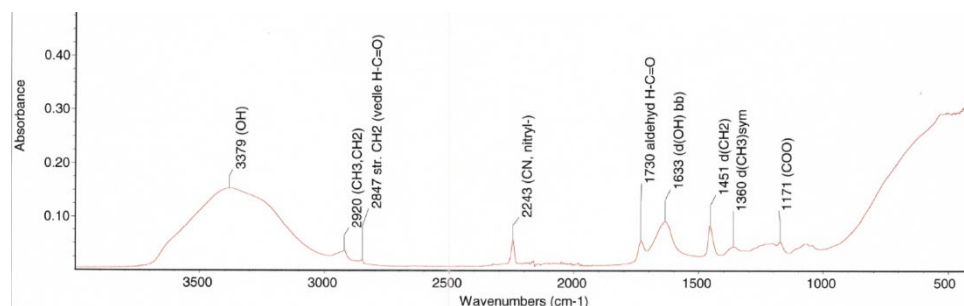


Figure 9: FT-IR spectrum showing characteristic functional groups of HNO₃ hydrolysed PAN sample.

5 Conclusion

The results obtained so far confirmed the degradation processes (by radiolysis and hydrolysis) on studied materials occurred.

Mass spectrometry analyses and thermogravimetric analyses of ISOLA plasticizer confirmed the degradation processes on studied samples after the hydrolysis, when samples were exposed to the alkaline environment and temperature of 60 °C.

CX ISOPLAST 531 superplasticizer degrades under hydrolysis and radiolysis conditions resulting in both low-molecular fragments as well as high-molecular condensation products.

PAN based sorbents degrade both under hydrolysis and radiolysis conditions resulting in water soluble low molecular weight organic acids.

6 Future work

Future experimental works will follow the project proposal and will be focused mainly on detailed evaluation of recently obtained data, further characterization of the irradiated and hydrolysed systems and comparison of degradation effects (radiolysis, hydrolysis) on studied materials.

Contribution is being prepared for the RADCHEM 2022 conference, in which some aspects of our work will be further discussed.

Acknowledgement

The EURAD-CORI project leading to this application has received funding from the European Union's Horizon 2020 research and innovation programme under grant agreement No 847593. The output was created also with the financial participation of SÚRAO - Czech Radioactive Waste Repository Authority (SO2020-017 and SO2020-014). *This contribution is partially a result of European Regional Development Fund-Project "Centre for Advanced Applied Sciences" (Grant No. CZ.02.1.01/0.0/0.0/16_019/0000778).*

References

Angelescu N., Stanciu D., Aguiar J. L., Abdelgader H. S., Bratu V. (2016): Role of superplasticizer additives upon hydration process of cement pastes. The Scientific Bulletin of Valahia University – Materials and Mechanics – Nr. 11

Gad E. A. M., Habib A. O., Mousa M. M. (2018): Understanding the mechanism of decomposition reactions of neat and superplasticized ordinary Portland cement pastes using thermal analysis. Epitoanyag-Journal of Silicate Based & Composite Materials 70.3

Guérandel C., Vernex-Loiset L., Krie, G., De Lanève M., Guillot X., Pierre C., Muller J. F. (2011): A new method to analyze copolymer based superplasticizer traces in cement leachates. *Talanta*, 84(1), 133-140

Sun G., Wang L., Weng L. T., Zhang J., L. Z., Chen G. (2014): Determination of adsorption mechanism of polycarboxylate-ether based superplasticizers using crystallization, thermal and mass spectrometry methods. *Rsc Advances*, 4(49), 25479-25485

Walling S., Um W., Corkhill C. L., Hyatt N. C. (2021): Fenton and Fenton-like wet oxidation for degradation and destruction of organic radioactive wastes, *Materials Degradation*, 5 (1). 50

Yilmaz V. T., Odaba M., Icbudak H., Ölmez H. (1993): The degradation of cement superplasticizers in a high alkaline solution. *Cement and concrete research*, 23(1), 152-156

INE Scientific Working Documents
ISSN 2701-262X
www.kit.edu